SYNTHESIS AND STUDY OF NEW LATE METAL COMPLEXES FEATURING *N*-PHOSPHINOAMIDINATE LIGANDS

by

Colin M. Kelly

Submitted in partial fulfilment of the requirements
for the degree of Doctor of Philosophy

at

Dalhousie University
Halifax, Nova Scotia
November 2017

Table of Contents

List of Tables ..... **v**

List of Figures ..... **vi**

List of Schemes ..... **ix**

Abstract ..... **xii**

List of Abbreviations and Symbols Used ..... **xiii**

Acknowledgments ..... **xiv**

Chapter 1 Introduction **1**

1.1 The Role of Ligand Design in Tuning Organometallic Reactivity 1

1.2 Neutral Phosphine Ligands 2

1.3 Neutral P,N-Ligands 7

1.4 Anionic N,N-, P-P-, and P,N-Ligands 11
1.4.1 Bis(phosphino)borate Ligation 12
1.4.2 Monoanionic N,N-donor Ligands 16
1.4.3 Monoanionic P,N-donor Ligands 23

1.5 Thesis Research Overview 26

Chapter 2 Synthesis, Structural Characterization, and Reactivity of Cp*Ru(*N*-Phosphinoamidinate) Complexes **30**

2.1 Introduction 30

2.2 Results and Discussion 33
2.2.1 Synthesis and Characterization of Cp*Ru(κ^2-P~N) species 33
2.2.2 Probing the Reactivity of **2-2a** and **2-2b** 36

2.3 Conclusions 41

2.4 Statement of Contributions 42

2.5 Experimental Details 42

Chapter 3 Synthesis and Reactivity of a Neutral, Three-Coordinate Platinum(II) Complex Featuring Terminal Amido Ligation **53**

3.1 Introduction 53

3.2 Results and Discussion 58
3.2.1 Synthesis and Characterization of Platinum Amido Species 58
3.2.2 Probing the Reactivity of **3-1** 65
3.2.3 Computational Studies 70

3.3 Conclusions 73

3.4 Statement of Contributions 73

3.5 Experimental Details 74

Chapter 4 Dehydrogenative B-H/C(sp^3)-H Benzylic Borylation Within the Coordination Sphere of Platinum(II) 82

4.1 Introduction 82

4.2 Results and Discussion 86
4.2.1 Synthesis and Characterization of (κ^2-P,N)M(η^3-benzyl) Complexes 86
4.2.2 Probing the Reactivity of (κ^2-P,N)M(η^3-benzyl) Complexes 91
4.2.3 Computational Mechanistic Studies 96

4.3 Conclusions 101

4.4 Statement of Contributions 101

4.5 Experimental Details 102

Chapter 5 A Manganese Pre-Catalyst for the Mild Reduction of Amides, Ketones, Aldehydes, and Esters 119

5.1 Introduction 119

5.2 Results and Discussion 122
5.2.1 Synthesis and Characterization of (κ^2-P,N)Mn(N($SiMe_3$)$_2$) (**5-1**) 122
5.2.2 Catalytic Reduction of Tertiary Amides Employing **5-1** 124
5.2.3 Catalytic Reduction of Ketones and Aldehydes Employing **5-1** 127
5.2.4 Catalytic Reduction of Esters Employing **5-1** 129

5.3 Conclusions 129

5.4 Statement of Contributions 130

5.5 Experimental Details 130

Chapter 6 Conclusion 138

References 142

Appendix A Crystallographic Experimental Details 153

Appendix B NMR Spectra of Organic Products 189

Appendix C Copyright Agreements 203

List of Tables

Table 2-1. Crystallographic solution and Refinement Data for **2-2a**, **2-2b**, **2-3** and **2-4**. **50**

Table 2-2. Selected interatomic distances (Å) and angles (º) for **2-2a**, **2-2b**, **2-3** and **2-4**. **52**

Table 4-1. Selected interatomic distances for **4-1**, **4-4**, **4-5, 4-7,** and **4-8** **95**

List of Figures

Figure 1-1. General example of an N-phosphinoamindinate ligand with a recently reported Cr complex **2**

Figure 1-2. Examples of common tertiary phosphine ligands **3**

Figure 1-3. Examples of well-known catalysts supported by monodenate phosphine ligands **4**

Figure 1-4. Examples of popular bidentate phosphine ligands **6**

Figure 1-5. Phosphinooxazoline (PHOX) motif and mor-DalPhos **8**

Figure 1-6. Comparison of Pd-ligand interactions showing Buchwald's biarylmonophosphine ligand and Hartwig's JosiPhos variant **9**

Figure 1-7. General bis(phosphino)borate (BP_2^-) ligand motif, a phenyl substituted example, general nacnac motif, and a general amidinate motif **12**

Figure 1-8. Resonance structures of the of (bis)phosphino borate ligands showing a ylide resonance contributor **15**

Figure 1-9. Three-coordinate copper(I) complex supported by a (bis)phosphino borate ligand **16**

Figure 1-10. General depiction of nacnac ligands and examples of low-coordinate Fe and Rh complexes supported by nacnac ligation **17**

Figure 1-11. General motif of the amidinate ligand family and possible metal binding modes **21**

Figure 1-12. Examples of monoanionic P,N-ligands **24**

Figure 1-13. A neutral N-phosphinoamidine and deprotonation to give the lithium salt of an anionic N-phosphinoamidinate **26**

Figure 1-14. Fe and Co pre-catalysts supported by *N*-phosphinoamidinates **28**

Figure 2-1. Previously studied $[Cp^*RuL_2]^+X^-$ and $Cp^*Ru(\kappa^2\text{-}L{\sim}X)$ complexes, and the new Cp*Ru(*N*-phosphinoamidinate) complexes featured herein **32**

Figure 2-2. Crystallographically determined structures of **2-2a** and **2-2b** **36**

Figure 2-3. Crystallographically determined structures of **2-3** and **2-4** **38**

Figure 2-4. ^{1}H NMR spectrum of **2-2a** **44**

Figure 2-5. ^{1}H NMR spectrum of **2-2b** **46**

Figure 3-1. Three-coordinate Pt(II) complex featuring a weak agostic interaction **54**

Figure 3-2. Previously reported three-coordinate Pt(II) complexes **55**

Figure 3-3. Crystallographically determined structures of **3-2** **55**

Figure 3-4. Proposed metalation product **3-4** **60**

Figure 3-5 Crystallographically determined structures of **3-1** **62**

Figure 3-6. T-shaped three-coordinate LPd(aryl)(amido) species **63**

Figure 3-7. Variable-temperature ^{1}H NMR data for **3-1** **65**

Figure 3-8. Crystallographically determined structures of **3-5** **66**

Figure 3-9. Crystallographically determined structures of **3-6** **68**

Figure 3-10. Crystallographically determined structures of **3-7** **69**

Figure 3-11. ^{13}C DeptQ 135 NMR spectrum of **3-7** **69**

Figure 3-12. HOMO and LUMO orbitals for **3-1** **71**

Figure 3-13. Transition-state structures for **3-6** and **3-7** **72**

Figure 3-14. HOMO and LUMO orbitals for **3-1** **71**

Figure 4-1. Crystallographically determined structures of **4-2** and **4-3** **88**

Figure 4-2. Crystallographically determined structure of **4-1** **89**

Figure 4-3. Crystallographically determined structure of **4-4** **90**

Figure 4-4. Crystallographically determined structure of **4-5** **90**

Figure 4-5. Crystallographically determined structure of **4-6** **92**

Figure 4-6. Crystallographically determined structure of (κ^2-P,N)Pt(NH_2(1-Ad))(η^1-benzyl) **93**

Figure 4-7. Crystallographically determined structures of **4-7** and **4-8** **95**

Figure 4-8. DFT structures for **4-1(HBPin)**, B-H activation **TS1**, and C-H activation **TS2.** **99**

Figure 4-9. Concentration of **4-7** vs. Time (10 equiv HBpin, 300 K) **112**

Figure 4-10. Concentration of **4-7** vs. Time (15 equiv HBpin, 300 K) **113**

Figure 4-11. Concentration of **4-7** vs. Time (20 equiv HBpin, 300 K) **113**

Figure 4-12. Concentration of **4-7** vs. Time (25 equiv HBpin, 300 K) **114**

Figure 4-13. Concentration of **4-7** vs. Time (30 equiv HBpin, 300 K) **114**

Figure 4-14. Determination of rate constant for the reaction of **4-1** with HBpin **115**

Figure 4-15. Concentration of **4-7** vs. Time (20 equiv HBpin, 310 K) **115**

Figure 4-16. Concentration of **4-7** vs. Time (20 equiv HBpin, 315 K) **116**

Figure 4-17. Concentration of **4-7** vs. Time (20 equiv HBpin, 325 K) **116**

Figure 4-18. Eyring analysis based on the temperature dependence of the reaction of **4-1** with HBPin to give **4-7** **117**

Figure 5-1. Recently reported manganese homogenous catalysts **120**

Figure 5-2. Crystallographically determined structure of **5-1** **123**

Figure 5-3. Catalytic reduction of tertiary amides to tertiary amines employing **5-1** **125**

Figure 5-4. Catalytic reduction of ketones and aldehydes employing **5-1** **128**

Figure 5-5. Catalytic reduction of esters employing **5-1** **129**

List of Schemes

Scheme 1-1. Proposed mechanism for the catalytic hydrogenation of propene utilizing $RhCl(PPh_3)_3$ **4**

Scheme 1-2. Allylic substitution reaction in which nucleophilic attack occurs at the carbon atom bound *trans* to phosphorous **8**

Scheme 1-3. General reaction scheme for the monoarylation of ammonia **10**

Scheme 1-4. General reaction scheme for the monoarylation of hydrazine and acetone **11**

Scheme 1-5. Benzene C-H activation mediated by $\{Ph_2B(CH_2PPh_2)_2\}Pt(Me)(THF)$ **13**

Scheme 1-6. Proposed mechanisms for benzene C-H activation by zwitterionic (bis)phosphino borate complexes and a cationic SiP_2 complex **14**

Scheme 1-7. Reaction scheme for Rh(I) mediated C-C bond activation of cyclobutanones **16**

Scheme 1-8. Bifunctional activation of H_2 by a nacnac supported Ru complex **17**

Scheme 1-9. C-H bond activation mediated by (nacnac)Pt complexes **19**

Scheme 1-10. Proposed catalytic cycle for alkane transfer dehydrogenation mediated by (nacnac)Pt **20**

Scheme 1-11. Ru amidinate mediated redox isomerization of an allylic alcohol to the corresponding saturated ketone **22**

Scheme 1-12. Ru mediated allylic substitution redox catalysis **22**

Scheme 1-13. Zwitterionic P,N-supported Ru species that quickly decomposes by double geminal C-H bond activation to produce a carbene hydride complex **24**

Scheme 1-14. Deprotonation of a PHOX ligated Ru complex to generate the anionic PHOX ligand in *situ.* **25**

Scheme 1-15. Anionic-P,N-ligated Ir catalyzed alkylation of anilines by alcohols **25**

Scheme 1-16. General reaction scheme for the (N-phosphinoamidine)Cr catalyzed oligomerization of ethylene to selectively form 1-hexene and 1-octene **27**

Scheme 1-17. Isomerization and terminal hydroboration of 4-octene with **1-3** **28**

Scheme 2-1. Simplified transfer hydrogenation between alcohols and ketones with Noyori's (η^6-*p*-cymene) Ru(κ^2-N~N) catalyst **30**

Scheme 2-2. *In situ* formation of a Cp*Ru(κ^2-P~N) invoked by Ikariya for the isomerisation of allylic alcohols **32**

Scheme 2-3. Synthesis of Cp*Ru(*N*-phosphinoamidinate) complexes, **2-2a** and **2-2b** **35**

Scheme 2-4. Reactivity of Cp*Ru(*N*-phosphinoamidinate) complexes, **2-2a** and **2-2b** with two-electron (L) donors **37**

Scheme 2-3. Reactivity of the Cp*Ru(*N*-phosphinoamidinate) complex **2-2a** with ammonia borane and loss of dihydrogen from the resulting product **2-5** **40**

Scheme 2-4. Examples of unsuccessful reaction attempts with **2-2a** and **2-2b** **41**

Scheme 3-1. Potential hydroamination mechanism utilizing a three-coordinate Pt amido species **57**

Scheme 3-2. Proposed mechanism for the intermolecular migratory insertion of ethylene into a Pd-N bond **58**

Scheme 3-3. Synthesis of the dichloride dimer **3-2** **59**

Scheme 3-4. Proposed reaction scheme for the reaction of **3-2** with two equivalents of 2,6 dimethyl anilide **61**

Scheme 3-5. Synthesis of three-coordinate Pt(II) amido complex, **3-1** **62**

Scheme 3-6. Synthesis of **3-5**, **3-6**, and **3-7** from **3-1** **70**

Scheme 4-1. Theoretical activation of an E-H bond to give (κ^2-P,N)M(ER_n) **83**

Scheme 4-2. Theoretical *in situ* dissociation to form (κ^2-P,N)M(η^1-benzyl) **83**

Scheme 4-3. Prototypical metal-catalyzed benzylic (poly)borylation of toluene **84**

Scheme 4-4. Mechanism for the benzylic borylation of toluene with HBPin **85**

Scheme 4-5. Generalized benzylic borylation of toluene **86**

Scheme 4-6. Synthesis of the (κ^2-P,N)Pt(η^3-benzyl) complex **4-1** **87**

Scheme 4-7. Synthetic protocol for the isolation of chloride dimers **4-2**/**4-3** followed by treatment with BnMgCl to yield (η^3-benzyl)metal complexes **4-4** and **4-5** **88**

Scheme 4-8. Synthesis of **4-6** **91**

Scheme 4-9. Synthesis of **4-7** and **4-8** **94**

Scheme 4-10. Plausible mechanisms of benzylic borylation considered by DFT **98**

Scheme 4-11. Proposed B-H activation and C-H activation *en route* to **4-7** **100**

Scheme 5-1. Synthesis of [(κ^2-P,N)Mn(N($SiMe_3$)$_2$)], **5-1** **123**

Abstract

N-Phosphinoamidine/amidinate (P,N) ligands have recently been shown to be highly effective for the selective chromium-catalyzed tri-/tetramerization of ethylene. Since this initial report, a joint collaboration between the Chevron-Phillips Chemical Company (CPChem) and the Stradiotto/Turculet research groups at Dalhousie University has reported on the iron-catalyzed hydrosilyation of carbonyl compounds and the cobalt-catalyzed hydroboration of alkenes using (P,N)M($N(SiMe_3)_2$) complexes (M = Fe, Co).

These monoanionic, bidentate P,N-chelating ligands offer a mix of hard and soft donors and the anionic charge promotes tight binding to facilitate the isolation of unusual low-coordinate late metal complexes. The propensity of such species to exhibit unusual bonding motifs, unprecedented reactivity, and their applications in catalysis is the focus of this work. Futhermore, the chemistry of monoanionic P,N-ligands in general is surprisingly underexplored.

Encouraged by the exceptional reactivity of the first-row transition metal complexes mentioned above, the initial goals of this thesis were to explore the synthesis and reactivity of low-coordinate second and third-row transition metal complexes. Coordinatively unsaturated Cp*RuL_n complexes have a well-established track record of exhibiting new and unusual metal-centered reactivity with diverse applications in organic synthesis. As such, considerable focus continues to be directed toward developing new and isolable classes of such complexes and exploring their stoichiometric reactivity. In this regard, the synthesis and reactivity of 16-electron Cp*Ru(II) (Cp* = η^5-C_5Me_5) complexes supported by *N*-phosphinoamidinates is detailed herein.

Intrigued by the ability of related (nacnac)Pt species in supporting low-coordinate reactive complexes, structurally and electronically unique low-coordinate Pt(II) complexes supported by *N*-phosphinoamidinate ligands were developed in pursuit of unusual bonding motifs and reactivity. The synthesis and reactivity of an isolable, three-coordinate, neutral, 14-electron Pt(II) species along with the synthesis and reactivity of a Pt(II)-η^3-benzyl complex that undergoes an unprecedented benzylic borylation reaction is also detailed herein.

Within the spirit of moving toward the use of relatively abundant and inexpensive metals in catalysis, and building on the previous advances in this area by the CPChem/Turculet/Stradiotto team, this thesis also examines the development of the manganese complex (P,N)Mn($N(SiMe_3)_2$). The remarkable ability of this complex to reduce amides, ketones, aldehydes, and esters under mild conditions is described herein.

List of Abbreviations and Symbols Used:

Anal. Calcd. = analysis calculated
AB = Ammonia borane
Ad = adamantyl
Ar = aryl group
Bn = benzyl
COD = 1,5-cyclooctadiene
COSY = homonuclear correlation spectroscopy
Cp = cyclopentadienyl
Cp* = pentamethylcyclopentadienyl
CPChem = Cheveron-Phillips Chemical Company
Cy = cyclohexyl
DFT = Density Functional Theory
d = doublet
DEPT = Distortionless Enhancement by Polarisation Transfer
DCE = Dichloroethane
E = main group element
EXSY = Exchange Spectroscopy
Fc = Ferrocene
HBPin = pinacol borane
HBCat = caetchol borane
HMBC = heteronuclear multiple-bond correlation spectroscopy
HSQC = heteronuclear single-quantum correlation spectroscopy
IR = infrared
$^{n}J_{XX}$ = n bond coupling constant between atom X and atom X`
L = two-electron donor ligand
M = generic transition metal *or* mol/L
m = multiplet
Mes = 2,4,6-trimethylphenyl
NMR = nuclear magnetic resonance spectroscopy
OAc = acetoxy group
ORTEP = Oak Ridge Thermal Ellipsoid Plot
OTf = trifluoromethyl sulfonate or triflate
PDI = Pyridinediimine
PHOX = phosphinooxazoline
ppm = parts per million
Pr = propyl
s = singlet
THF = tetrahydrofuran
Ts = tosyl group
Tp = trispyrazolylborate
δ = chemical shift
X = anion *or* anionic ligand

Acknowledgements

First, and most importantly, I have to thank my excellent supervisors and advisors Dr. Mark Stradiotto and Dr. Laura Turculet. Their support, guidance, and care in instructing my studies over the past six years has been instrumental in my success. Furthermore, they stood by me with patience and kept faith in my abilities even when I faltered and started to lose faith in myself. For that I will be forever grateful. Furthermore, you both live busy lives and have a lot of students to manage, but you consistently make each one of us feel like you have time for us and you care about our work, which is maybe the most important quality for a supervisor to have.

I would also like to thank my supervisory committee (past and present) for keeping me on track and taking the time to follow my work throughout this journey. I would also like to thank Norm Schepp for helping me conduct the kinetic experiments, I would have been lost without your help. Additionally, I'd like to thank Dr. Mike Lumsden who has always been very helpful with various NMR experiments and Drs. Robert McDonald and Mike Ferguson from the University of Alberta for X-ray crystallography experiments reported in this thesis. A special thank you to Giselle Andrews as well and perhaps an apology for how many times she had to email me reminders about registration, etc. Furthermore I would like to thank the Chevron-Phillips Chemical Company for the opportunity to work on such interesting chemistry.

I also owe a big thank you to the Turculet and Stradiotto group members (past and present). You guys made working the lab enjoyable and I'll never forget the fun and good laughs we all had together and having you there to lean on when the chemistry just wasn't working. It was an unforgettable five years.

Lastly I'd like to thank my friends, family, and my incredible parents Mike and Lillian for always having my back – without the support I've received from all of you I would of never had a fraction of the success I have had in my life. Thank you all.

I'd also like to acknowledge a quote from a song I'd to listen to when times were tough and I felt like the weight of grad school was just too much. "Does it feel that your life's become a catastrophe? Oh it has to be for you to grow boy." – Take the Long Way Home, Supertramp.

CHAPTER 1: Introduction

1.1 The Role of Ligand Design in Tuning Organometallic Reactivity

The field of organometallic chemistry has attracted significant interest over the past fifty years due in part to the established utility of organometallic species in developing new reactivity that has been shown to have real-world applications in synthesis and catalysis. The development of homogeneous transition metal catalysts has figured most prominently in this regard, as demonstrated by the awarding of the 2001, 2005, and 2010 Nobel Prizes in Chemistry for advancements in the fields of asymmetric catalysis,[1] olefin metathesis,[2] and palladium mediated coupling reactions,[3] respectively. Although these three examples represent tremendous accomplishments in their respective fields, many synthetic challenges still remain, for which organometallic catalysts may play an important role in solving.

A systematic approach to developing new structure, bonding, and reactivity in the field of organometallic chemistry often begins with the synthesis of ancillary ligands that can stabilize reactive metal centers. If a complex shows unusual structural features or novel stoichiometric reactivity, this can often be tuned and optimized so that it may be applied in a catalytic fashion. The design of the ancillary ligand plays a key role in this process, as it allows the direct tuning of the properties of the final complex by means of the denticity, donor ability, as well as the steric and electronic features of the ligand. As many homogeneous catalysts currently in use are based on electron-rich late transition metals, typically the most desirable characteristics to target in designing a new metal complex for potential catalytic applications include a relatively low coordination number,

to allow substrate binding while ensuring the metal center is electron rich to facilitate key mechanistic steps such as oxidative addition.

In this regard, the focus of the research detailed in this document centers around the synthesis and study of reactive late metal complexes that are supported by *N*-phosphinoamidine/amidinate ligands (Figure 1-1).

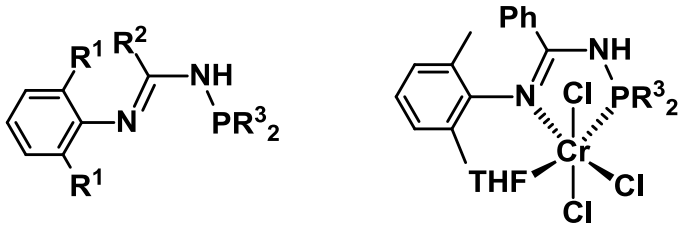

Figure 1-1. General example of an *N*-phosphinoamidine pro-ligand with a recently reported Cr complex.[4]

These neutral or monoanionic, bidentate P,N-chelating ligands are anticipated to lead to highly reactive, low-coordinate late metal complexes that may have applications in catalysis. To better place these ligands in the context of organometallic chemistry and ligand design, a brief overview of chemically similar ligands and the reactivity of their respective late metal complexes is detailed herein.

1.2 Neutral Phosphine Ligands

Neutral tertiary phosphines (PR_3, R = alkyl or aryl; Figure 1-2), represent an important, heavily studied, and widely used ligand class in organometallic chemistry. Phosphine ligands are L-type donors (neutral two-electron donor) that can be described as both σ-donors and π-acceptors.

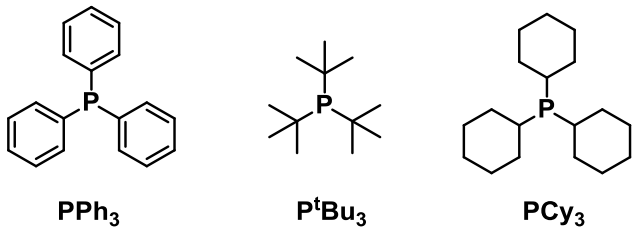

Figure 1-2. Examples of common tertiary phosphine ligands.

In previous studies, Tolman was able to quantify the relative donor strength and steric features of a series of mono- and bidentate neutral phosphines.[5] Tolman observed that different substituents on phosphine ligands significantly affected donor strength. Experimentally, he established the relative donor strength by measuring the change in υ_{CO} for a series of $LNi(CO)_3$ complexes, where L represents a phosphine ligand. As an example, alkyl substituted phosphines proved to be much better σ-donors than aryl phosphines due to the greater s-character of sp^2-hybridized orbitals of aryl substituents. He also developed a 3-D space filling model now known as the Tolman cone angle that quantified the steric pressure the ligand delivered to the metal coordination sphere; the respective angles for the phosphines depicted in Figure 1-2 are as follows, 182° ($P\textit{t}Bu_3$) > 170° (PCy_3) > 145° (PPh_3). These studies enabled researchers to mindfully select phosphine ligands based on the characteristics they desired. The availability and predictability of the behavior of a wide variety of phosphine ligands makes it relatively easy to tune complexes to fit a particular steric or electronic profile.

Many transition metal complexes supported by monodentate phosphines have proven to be efficient catalysts (Figure 1-3). A pioneering and popular example of this is $RhCl(PPh_3)_3$, also known as Wilkinson's catalyst (**A**, Figure 1-3). This complex earned fame as one of the first homogenous catalysts reported for the hydrogenation of olefins and led to an explosion of interest in this area.[6] The mechanism of catalytic hydrogen

employing $RhCl(PPh_3)_3$ relies on dissociation of one the phosphine ligands to give a catalytically active species (Scheme 1-1). In this regard, thoughtful ligand selection is essential, as the phosphine has to be relatively labile while still able to donate sufficient electron density to the metal to facilitate the oxidative addition of H_2 in the subsequent step of the mechanism.

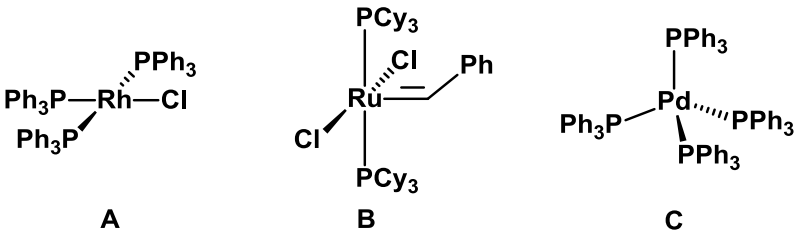

Figure 1-3. Examples of well-known catalysts supported by monodenate phosphine ligands: Wilkinson's catalyst (**A**),[6] first generation Grubbs catalyst (**B**) used for olefin metathesis,[7] and $Pd(PPh_3)_4$ (**C**) is commonly used in a variety of cross-coupling reactions.[8]

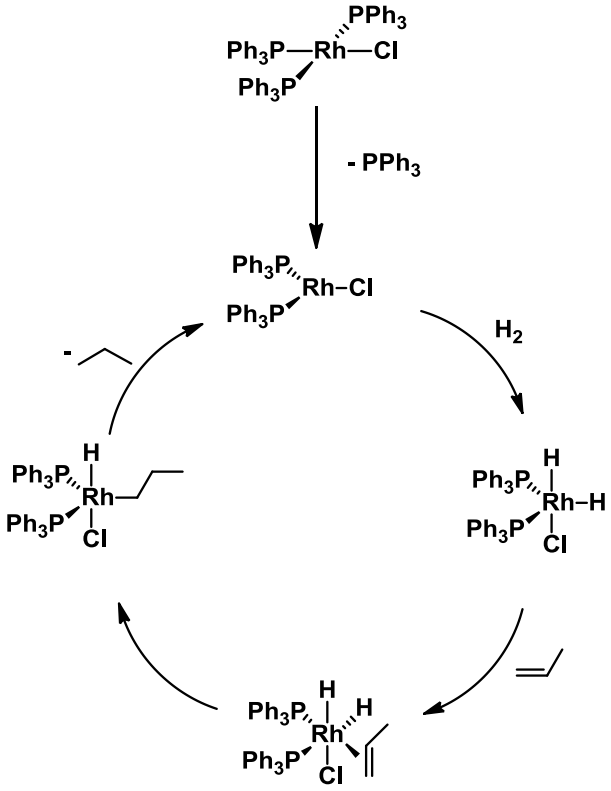

Scheme 1-1. Simplified mechanism for the catalytic hydrogenation of propene utilizing $RhCl(PPh_3)_3$.

To complement monodentate phosphine ligands, bidentate phosphines also represent a popular ligand class in organometallic chemistry (Figure 1-4). As we shift from monodentate to bidentate ligands, additional stability is afforded to the complex by virtue of the chelate effect. The chelate effect refers to the enhanced ability of a multidentate ligand to bind to a metal compared to two monodentate ligands of equivalent donor strength. This phenomenon, in a thermodynamic sense, is dependent on the entropy of reaction. Basically, one could envision that two moles of a monodentate ligand is equal to one mole of a bidentate ligand in a chemical reaction; this means that less entropy is lost when the chelate complex is formed compared to the formation of a complex with two moles of a monodentate ligand. It can also be considered from a kinetic perspective. Assuming the rate constant for the binding of one equivalent of a monodentate ligand and one moiety or end of a bidentate ligand is equivalent, the rate for the binding of a second monodentate ligand intermolecularly is less than the rate for binding of the second end of a bidentate ligand intramolecularly. This can be rationalized by envisioning the binding of the second end of the bidentate ligand as a directed substitution rather than a random one. In a similar fashion, the rate to reattach a "lost" ligand is greater if it is tethered to a moiety that is still binding to the metal center. The additional thermodynamic stability conveyed by the chelate effect can be crucial in supporting reactive intermediates and low-coordinate complexes.

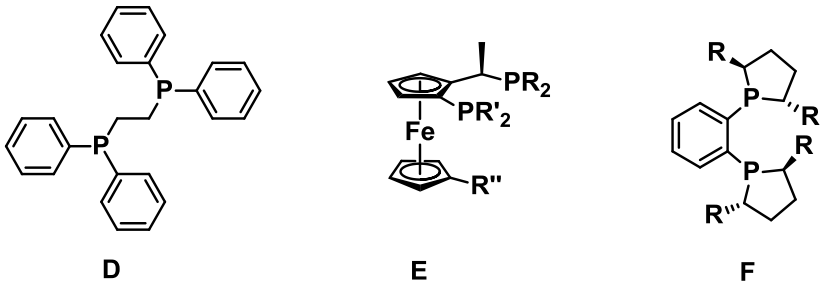

Figure 1-4. Examples of popular bidentate bisphosphines: 1,2-bis(diphenylphosphino)ethane or dppe (**D**), JosiPhos (**E**)[9], and DuPhos (**F**).[10]

Many phosphine ligands have had chiral moieties incorporated into their design to enable their potential use in asymmetric catalysis. Examples of such ligands include both JosiPhos and DuPhos (**E** and **F**, Figure 1-4). The name JosiPhos truly represents a family of ligands that can be tuned in a modular fashion, by altering the substitution at the R, R' and R" positions, in order to fit a desired electronic, steric, and chiral profile. Ligands within this family have proven to be adept in many areas of catalysis that include, but are not limited to: enantioselective hydrogenation, hydroboration, and hydroformylation; cross-coupling reactions, and reductive amination.[9] In this regard, JosiPhos is an excellent example of a ligand family that can be strategically varied to synthesize catalyst complexes that accommodate a wide range of reactivity, while keeping the general ligand motif constant. DuPhos, developed by DuPont, is also an example of a privileged ligand family that relies on chiral (bis)phospholanes to confer asymmetric reactivity. Although the DuPhos family also has a number of varied applications, it is most widely known for its utility in industrial relevant Rh-mediated asymmetric hydrogenations.[10] The subsequent success of the DuPhos ligand family has also led to a wealth of interest in designing ligands that exploit the chiral phospholane motif.[11]

In summary, neutral mono- and bidentate phosphines have an array of applications in organometallic synthesis and catalysis. At a fundamental level, the

relative ease with which such ligands can be tuned reliably enables researchers to make educated ligand choices to suit their specific reactivity applications. Modular phosphine ligand families, including JosiPhos, also instill an appreciation of the subtleties of ligand design for optimization of a specific reaction or catalytic system.

1.3 Neutral P,N-Ligands

As a complement to neutral bidentate P,P-donor ligands, neutral bidentate P,N-ligands featuring a relatively soft P donor and hard N donor have shown to be of particular utility in tuning metal reactivity. Due to the π-accepting nature of phosphines, such ligands can stabilize metals in low oxidation states, while the harder N-donor can act as a strong σ-donor to support metals in higher oxidation states. The ability of a P,N-ligand to stabilize metal centers in both high and low oxidation states is of particular importance to catalytic cycles that employ oxidative addition and reductive elimination steps. As an aside to its electronic properties, hemilability arising from N-dechelation to open up an additional reactive site at the metal presents an interesting opportunity for catalysis, whereby highly reactive, catalytically active species may be accessed reversibly during the course of a reaction.[12,13] Additionally, P,N ligands can convey some degree of regiocontrol by means of the *trans* effect, which can result in a relatively more labile site positioned *trans* to the P donor.[14] An example of a reaction that could exploit this phenomenon is allylic substitution, where nucleophilic attack will preferentially take place at the carbon bound *trans* to phosphorus (Scheme 1-2). Overall, P,N ligands represent an intermediate in electron donating ability compared to P,P- and N,N-bidentate ligands.

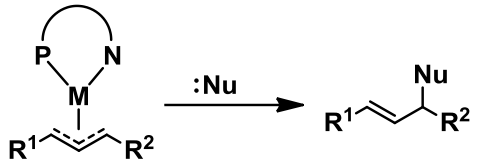

Scheme 1-2. General depiction of an allylic substitution reaction in which nucleophilic attack occurs at the carbon atom bound *trans* to phosphorus.

Interest in P,N-ligands has increased significantly over the past few decades. Prominent examples of P,N ligands that have sparked interest in their utility and subsequently played a key role in advancing late metal catalysis include phosphinooxazolines (PHOX) and Mor-DalPhos (Figure 1-5).

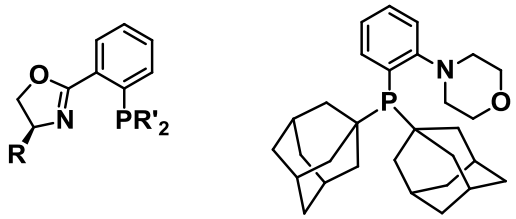

G **H**

Figure 1-5. Phosphinooxazoline (PHOX) motif (**G**)[15] and Mor-DalPhos (**H**).[16]

PHOX ligands (**G**, Figure 1-5) represent a modular class of chiral P,N-ligands that have showed utility as ancillary ligands in a variety of catalytic systems.[15] The general ligand motif has seen a significant amount of variation at the R and R' positions, indicated in Figure 1-5. Additionally, researchers have also explored replacing the phenylene backbone with other rigid groups based on ferrocene or substituted phenyl rings. Initially, the PHOX ligand class was designed by Pfaltz and co-workers to support late metal complexes that catalyzed enantioselective allylic substitutions.[17] PHOX complexes of palladium, tungsten, iridium, and platinum have all been shown to successfully mediate such allylic substitution reactions. Beyond allylic substitution, PHOX ligands have shown propensity toward asymmetric hydrogenation, intermolecular

asymmetric Heck reactions, hydrosilylation of ketones and alkene/CO copolymerization among others.[14,15] In many cases, the catalytic activity of P,N complexes outperformed analogous complexes supported by P,P- and/or N,N-ligation, suggesting that the mixed donor set is key to the increased reactivity observed. This versatility, along with the modularity of the ligand, has cemented its reputation as a staple in asymmetric catalysis and a leading example with respect to neutral P,N ligands.

The relatively recent development of the DalPhos ligand family (**H**), more specifically Mor-DalPhos, has also led to significant advancements in the field of catalysis.[16] Developed by the Stradiotto group, these ligands were initially designed to address challenges in Pd-catalyzed C-N and C-C cross coupling reactions. Beginning with C-N cross coupling reactions, Stradiotto proposed that a neutral P,N ligand motif could offer an intermediate electronic environment with respect to other prominent ligands in the field (Figure 1-6).[16] Building on this proposal, Stradiotto and co-workers synthesized a number of phenylene bridged P,N ligands to screen in the monoarylation of ammonia (Scheme 1-3).[18] The initial screen showed that the ligand variant containing an *ortho*-morpholino group, Mor-DalPhos, gave exceptional results.

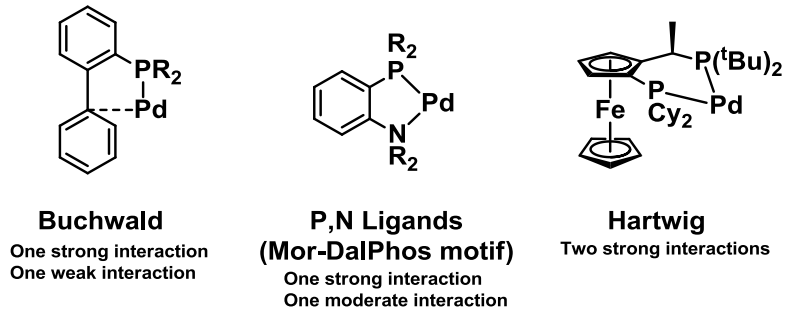

Figure 1-6. Comparison of Pd-ligand interactions showing Buchwald's biarylmonophosphine ligand and Hartwig's JosiPhos variant; both have proven to be successful in C-N cross coupling.[16]

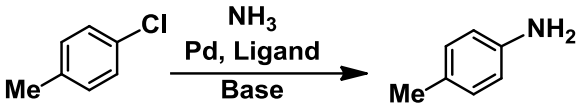

Scheme 1-3. General reaction scheme for the Pd-catalyzed monoarylation of ammonia.

Further studies showed that Mor-DalPhos could accommodate a broad scope of substrates while giving exceptional chemoselectivity, even in the presence of other amine moieties.[18] Encouraged by these results, Stradiotto and co-workers sought to extend their cross-coupling system to other challenging coupling partners. In this regard, the monoarylation of hydrazine was successfully targeted (Scheme 1-4), based on the high value of aryl hydrazines in the synthesis of nitrogen heterocycles.[19] Prior to this work, no examples of palladium cross-coupling of aryl electrophiles with hydrazines had been reported. In a similar manner, Stradiotto and co-workers also wanted to extend the utility of the DalPhos ligands to the challenging monoarylation of acetone (Scheme 1-4).[20] Again, Mor-DalPhos proved to be an exceptional ligand in mediating this cross-coupling reaction. Initial results showed good to excellent yields over a broad substrate scope. Not unlike the monoarylation of hydrazine, this was the first reported example of selective mono-α-arylation of acetone in the literature. In addition to palladium cross-coupling, Mor-DalPhos has proven to be an effective ligand in the stereo- and regioselective hydroamination of internal alkynes.[21] This work has since been expanded upon by Zhang and co-workers who continue to utilize the Mor-DalPhos ligand motif in a variety of gold-mediated transformations.[22]

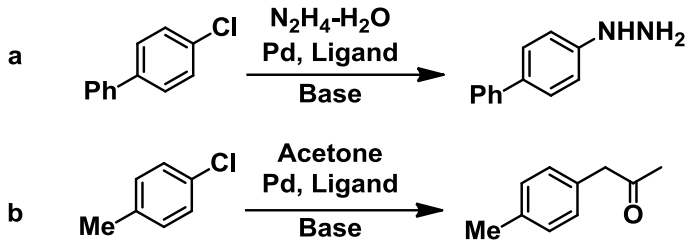

Scheme 1-4. General reaction scheme for the monoarylation of hydrazine (a) and acetone (b).

In the last several years, the DalPhos ligand family has continued to lead to unprecedented reactivity in the field of catalysis. Of these recent developments, the most notable discovery has been the PAd-DalPhos ligand and its application in challenging nickel-mediated amine arylation reactions under mild conditions.[23]

The success of both the PHOX and DalPhos ligand families further demonstrates how ligand design can enable researchers to improve upon existing catalytic reactions, and also to develop entirely new catalytic processes. Furthermore, since the inception and subsequent success of neutral P,N-ligands, it has become clear that they offer a unique electronic environment relative to P,P- and N,N-donor bidentate analogues, and as a result such ligands play an important role in advancing the field of late transition metal catalysis.

1.4 Anionic P,P-, N,N-, and P,N-Ligands

In many catalytic processes, the active catalyst species features a cationic late metal center that is balanced by an outer sphere anion such as triflate ($OSO_2CF_3^-$) or BX_4^- (X = F, Ph, C_6F_5). Such cationic species, especially when coordinatively unsaturated, are considered to possess enhanced electrophilicity, which typically leads to enhanced reactivity. While such complexes can be very active catalysts, there are also drawbacks associated with the generation of charge-separated species, including poor

solubility in nonpolar solvents, poor tolerance of polar or coordinating functional groups in potential substrates, and possible counterion effects that can complicate and/or diminish reactivity. An alternative strategy to synthesizing such charge separated complexes is to incorporate the negative charge within the ancillary ligand framework. In contrast to the neutral ligands discussed thus far, appropriately designed anionic ancillary ligands can support the formation of highly reactive low-coordinate late metal complexes, while avoiding the need for an accompanying counteranion. One can also envision that anionic ligands bind more tightly to formally cationic late metal fragments, thereby preventing degradation pathways that may be initiated by ancillary ligand dissociation. Examples of monoanionic P,P-ligands are relatively few in comparison to the many neutral counterparts. However, (bis)phosphino borates (**I**, **J**), developed by the Peters group, have proven to be a promising example that will be detailed herein (Figure 1-7).[24] As a complement to this, monoanionic N,N-ligands such as diketiminates (nacnac, **K**)[25] and amidinates (**L**)[26] have become well-known in the organometallic literature, and will also be highlighted.

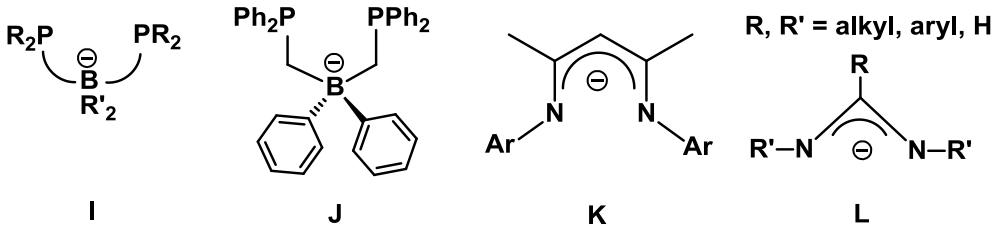

Figure 1-7. General bis(phosphino)borate (BP_2^-) ligand motif (**I**), a phenyl substituted example (**J**), general nacnac motif (**K**), and a general amidinate motif (**L**).

1.4.1 Bis(phosphino)borate Ligation

Peters and co-workers initially targeted the synthesis of low coordinate Pt(II) alkyl complexes supported by $[Ph_2B(CH_2PPh_2)_2]^-$ ligation with the hope of accessing

neutral alkyl complexes that could mediate facile C-H bond activation processes.[27] Indeed, the charge-neutral complex {$Ph_2B(CH_2PPh_2)_2$}Pt(Me)(THF) was shown to react with benzene C-H bonds at 50 °C to generate the corresponding phenyl complex, {$Ph_2B(CH_2PPh_2)_2$}Pt(Ph)(THF) (Scheme 1-5).

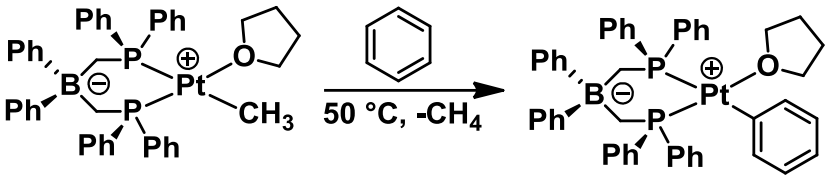

Scheme 1-5. Benzene C-H bond activation mediated by {$Ph_2B(CH_2PPh_2)_2$}Pt(Me)(THF).

Prior to this work, examples of intermolecular C-H bond activation at Pt(II) centers supported by phosphine donor ligands were sparse and these phosphine-supported systems required high temperatures (125-150 °C) for such reactivity to occur. In a subsequent study, Peters and co-workers examined the kinetic and mechanistic profiles of structurally related neutral and cationic Pt(II) systems that each mediate benzene C-H bond activation with the goal of highlighting potential mechanistic distinctions between the systems (Scheme 1-6).[28] The propensity for such structurally related neutral and cationic Pt(II) systems to mediate intermolecular benzene C-H bond activation was found to be generally comparable. However, the mechanism by which each system mediates this chemistry proved to be distinct, with intramolecular ligand metalation processes (C-H bond activation of both B*Ph* and P*Ph*) playing a large role in the reactivity of complexes supported by $[Ph_2B(CH_2PPh_2)_2]^-$ ligation. This phenomenon was postulated to be derived from electronic differences between the neutral and cationic complexes, whereby in the more electron rich neutral complex some of the anionic borate charge can be delocalized onto the aryl groups of the $[Ph_2B(CH_2PPh_2)_2]^-$ ligand, which renders the

aryl groups better electron-pair donors than the aryl groups of the neutral bis(phosphino) ligands. Therefore, although benzene coordinates readily to the cationic platinum centers by outcompeting the ligand aryl donors, benzene coordination does not outcompete coordination of the aryl groups of the bis(phosphino)borate ligand, and intramolecular metalation processes become prevalent in this instance.

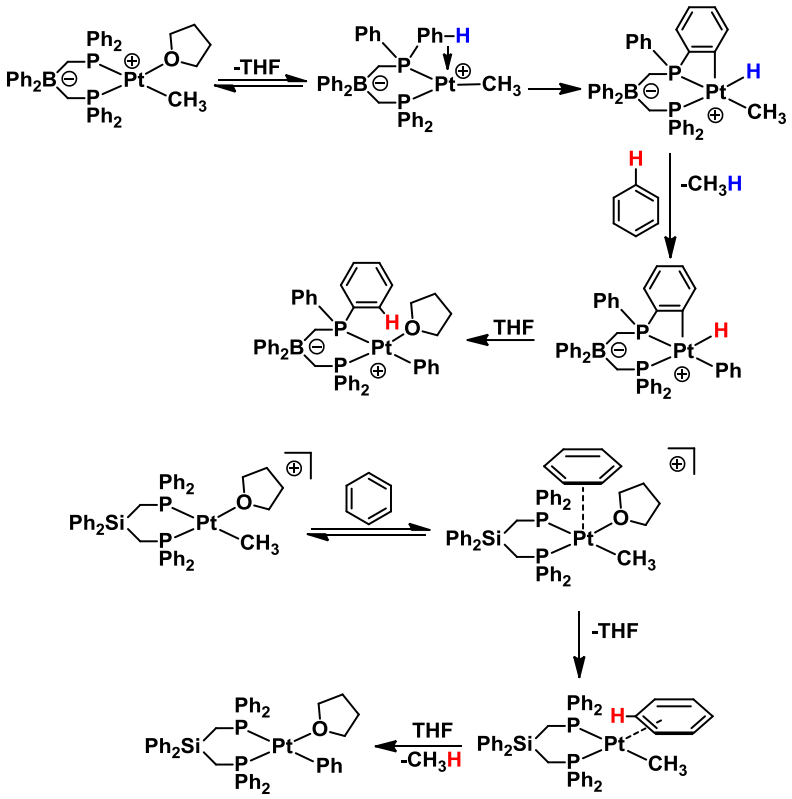

Scheme 1-6. Proposed mechanisms for benzene C-H activation by zwitterionic (bis)phosphino borate complexes (top, only one pathway shown) and a cationic SiP_2 complex (bottom).

Peters and co-workers also synthesized a series of (bis)phosphino borate ligands featuring different substitution at both boron and phosphorus, and studied the corresponding Pt(II) methyl carbonyl complexes to investigate how such different substitution motifs affected the overall electronic properties of the resulting complexes.[24] In this study, Peters further sought to address the issue of whether a zwitterionic

description is most appropriate for neutral complexes supported by such bis(phosphino) borate ligands. As an alternative to the zwitterionic, charge-separated structure, one can envision resonance structures that delocalize the borate negative charge onto the metal via a ylide resonance contributor (Figure 1-8). Upon studying the ν_{CO} of the resulting complexes, it became clear that altering substitution at the borate anion had little effect, whereas varying the substitution at the phosphorus donors had a more substantial effect on the CO stretching frequencies observed. Thus it can be concluded that the zwitterionic description of bis(phosphino)borate complexes is the most suitable.

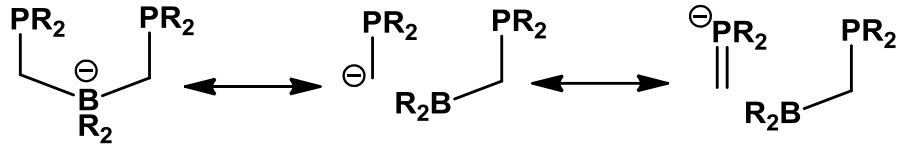

Figure 1-8. Resonance structures of the of (bis)phosphino borate ligands showing a potential ylide resonance contributor.

Following these initial reports by Peters, the chemistry of bis(phosphino) borate bearing complexes has mainly centered around the synthesis of low coordinate late metal complexes; a representative three-coordinate copper complex is shown in Figure 1-9.[29] With respect to catalytic applications, neutral bis(phosphino)borate palladium complexes were shown to be as active for the catalytic copolymerization of CO and ethylene as their cationic counterparts.[30] Recently, the copolymerization of CO and ethylene has also been successfully demonstrated by bis(phosphino)borate nickel complexes, however, the yield of this reaction is limited by poor stability of the catalyst under the required reaction conditions.[31] Peters has also shown that Rh(I) complexes supported by such ligands could successfully catalyze the intramolecular hydroacylation of 4-methyl-4-pentenal along with hydrogenation, hydrosilyation, and hydroboration of styrene.[32] To complement this,

Cramer and co-workers reported asymmetric C-C bond activation of cyclobutanones also mediated by a chiral Rh(I) bis(phosphino)borate complex (Scheme 1-7).[33]

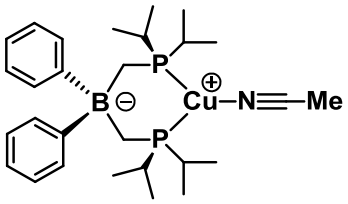

Figure 1-9. Three-coordinate copper(I) complex supported by a (bis)phosphino borate ligand.

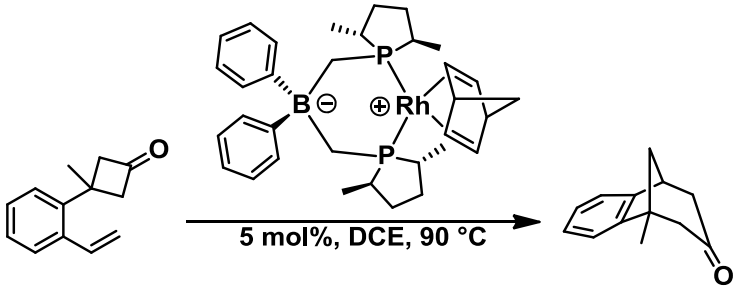

Scheme 1-7. Reaction scheme for Rh(I) mediated C-C bond activation of cyclobutanones.

1.4.2 Monoanionic N,N-donor Ligands

As a complement to monoanionic P,P-donor ligands, monoanionic N,N-ligands have also been investigated as ancillary ligands to support low-coordinate transition metal complexes. Moving from soft to hard donors, monoanionic N,N ligands typically function as LX-type ligands. Among these, diketiminates or "nacnac" ligands (**K**) represent a prominent example of this motif (Figure 1-10).[25a,34] A key characteristic of the nacnac ligand family is the modular design, whereby the N-aryl substituents can be readily tuned largely for steric purposes. As such, nacnac ligands featuring bulky N-aryl groups have displayed remarkable ability to support low coordinate complexes of both early and late transition metals (Figure 1-10).

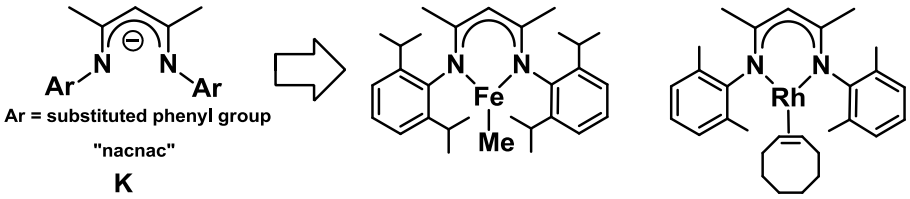

Figure 1-10. General depiction of nacnac ligands (**K**) and examples of low-coordinate Fe[35] and Rh[36] complexes supported by nacnac ligation.

With respect to catalytic potential, nacnac has been shown to act as a non-innocent ligand in bifunctional catalytic reactions including hydrogenation of alkenes and dehydrocoupling of amine boranes.[37] As an example, ruthenium cations of the type shown in Scheme 1-8 have been proposed to catalyze the hydrogenation of styrene and dehydrogenation of ammonia borane in a bifunctional fashion, whereby H_2 cleavage involves both the ruthenium center and the nacnac ligand. Nacnac-supported late metal complexes have demonstrated the ability to catalyze olefin hydrogenation,[37] polymerization,[38] transfer dehydrogenation,[39] selective alkene isomerization[40] and hydrosilyation[41] reactions. Reports of highly efficient catalysis using this ligand family are somewhat limited, most likely due to the rigidity and steric bulk typically associated with such complexes.

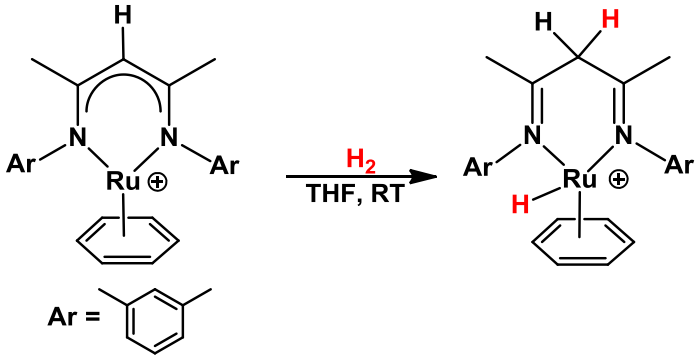

Scheme 1-8. Bifunctional activation of H_2 by a nacnac supported Ru complex.

Nacnac late metal complexes have also been shown to stoichiometrically activate a variety of E-H (E = main group element) bonds, including examples of C-H, B-H and

N-H bond cleavage processes. Goldberg and co-workers have demonstrated a remarkable example of C-H bond activation using a (nacnac)Pt^{IV} complex (Scheme 1-9).[42] In this reaction, (nacnac)$PtMe_3$ undergoes thermal ethane elimination to give a highly reactive, three-coordinate (nacnac)PtMe intermediate. Subsequent metalation of the nacnac ligand, followed by methane elimination generates a strained and highly reactive three-coordinate metalated species that can then undergo C-H bond activation of the alkane solvent. β-hydride elimination from the corresponding Pt(II) alkyl complex leads to the formation of an isolable olefin hydride complex. Olefin insertion into the Pt-H bond is reversible, which leads to the formation of an open coordination site that could allow for further alkane activation processes. Thus, a catalytic cycle for transfer dehydrogenation of alkanes can be envisioned, where olefin substitution in the Pt olefin hydride complex plays a key role (Scheme 1-10). Unfortunately, the olefin substitution process proved challenging, likely due to steric effects, and thus attempts to translate these stoichiometric C-H bond activation processes into a catalytic system were unsuccessful. It is important to note that this unusual chemistry is made possible by the ability of the nacnac ligand to support low-coordinate complexes.

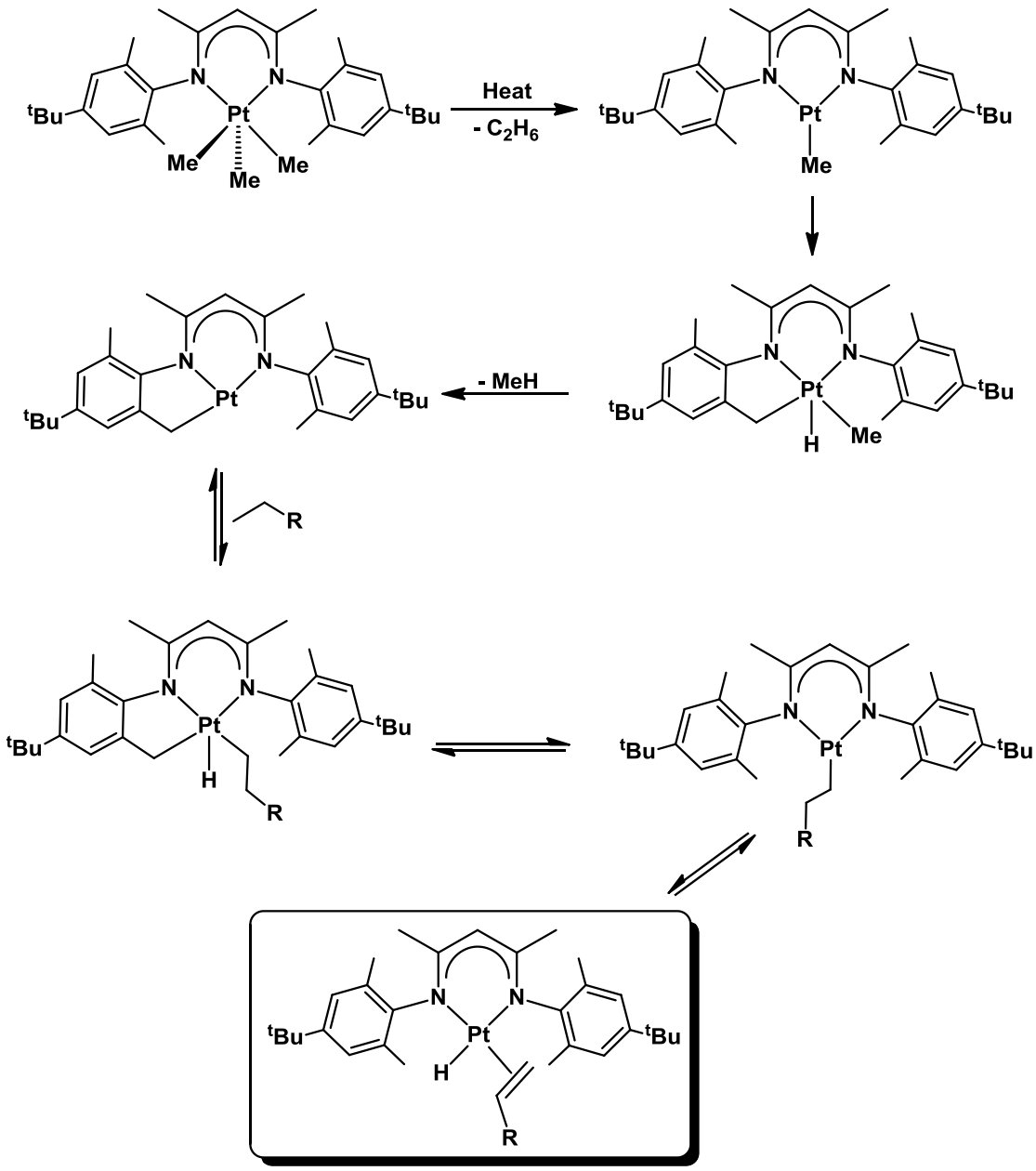

Scheme 1-9. C-H bond activation mediated by (nacnac)Pt complexes.

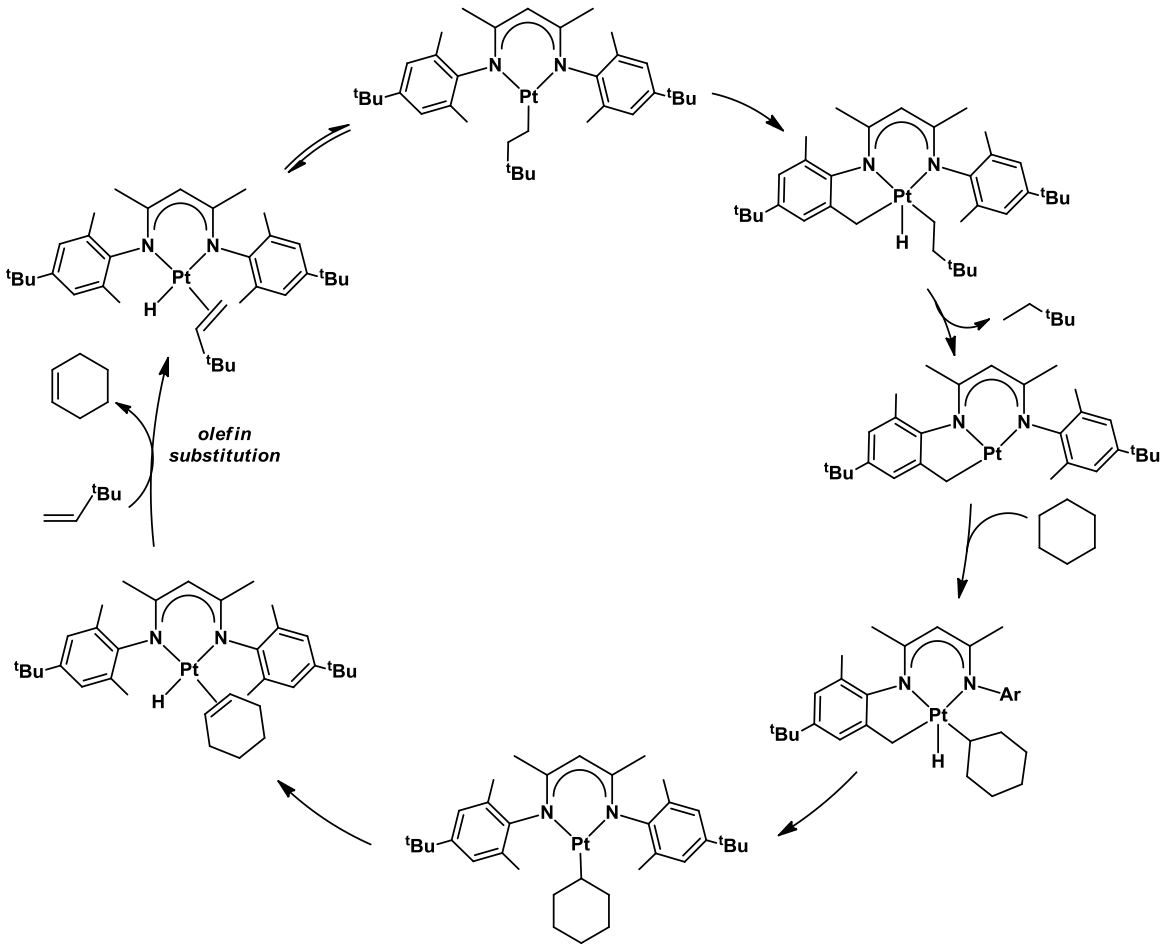

Scheme 1-10. Proposed catalytic cycle for an alkane transfer dehydrogenation process mediated by (nacnac)Pt.

Despite the limitations noted above, nacnac supported complexes remain an active area of research with novel reactivity being continually developed.[43]

Bearing many similarities to diketiminate N,N-donor ligands, amidinates (Figure 1-11, **L**) were developed by Sanger[44] and co-workers in the 1970s and have proven to be a versatile ligand class that has found utility in both transition metal and main group reactivity applications.[26] The substituents in amidinate ligands are readily modified, which allows for effective tuning of the steric and electronic features of their ensuing complexes. Amidinates typically behave as chelating LX-type ligands with small bite angles, similar to nacnac; however, they can also behave as monodentate or bridging

ligands (Figure 1-11). Transition metal amidinate complexes have shown diverse applications in catalysis and materials science.

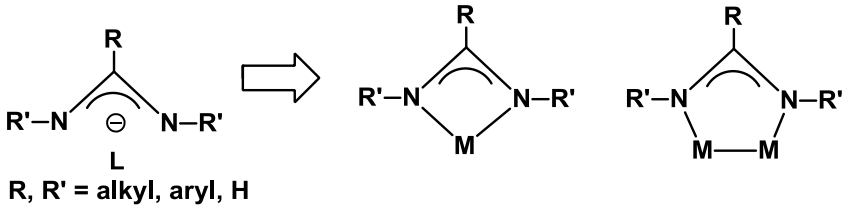

Figure 1-11. General motif of the amidinate ligand (**L**) family and some possible metal binding modes.

Amidinate complexes have been shown to readily activate various E-H bonds and have been especially useful as olefin polymerization catalysts.[45] Although recent studies have focused more on main group and lanthanide chemistry, a small number of catalytic reactions that make use of late transition metal amidinates have been reported. One interesting application involves the use of Ru(II) arene complexes to catalyze the redox isomerization of allylic alcohols into their corresponding saturated ketones (Scheme 1-11).[26] For the majority of ruthenium complexes that can facilitate this reaction, the addition of base is required to initiate the catalytic cycle.[46] In contrast to these examples, the ruthenium amidinate complex shown in Scheme 1-11 is able to operate under base-free conditions. Ruthenium amidinate complexes have also been shown to catalyze allylic substitution reactions (Scheme 1-12).[47] As shown in Scheme 1-12, the reaction begins with an oxidative addition of the allylic substrate to the metal center followed by CO_2 loss and nucleophilic attack on the resulting η^3-allyl intermediate, which results in the release of the organic product and regeneration of the active catalyst.

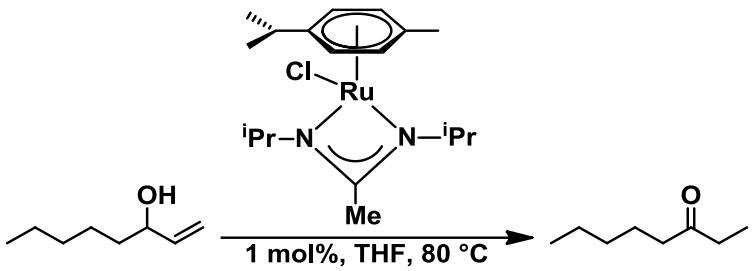

Scheme 1-11. Ruthenium amidinate-mediated redox isomerization of an allylic alcohol to the corresponding saturated ketone.[46]

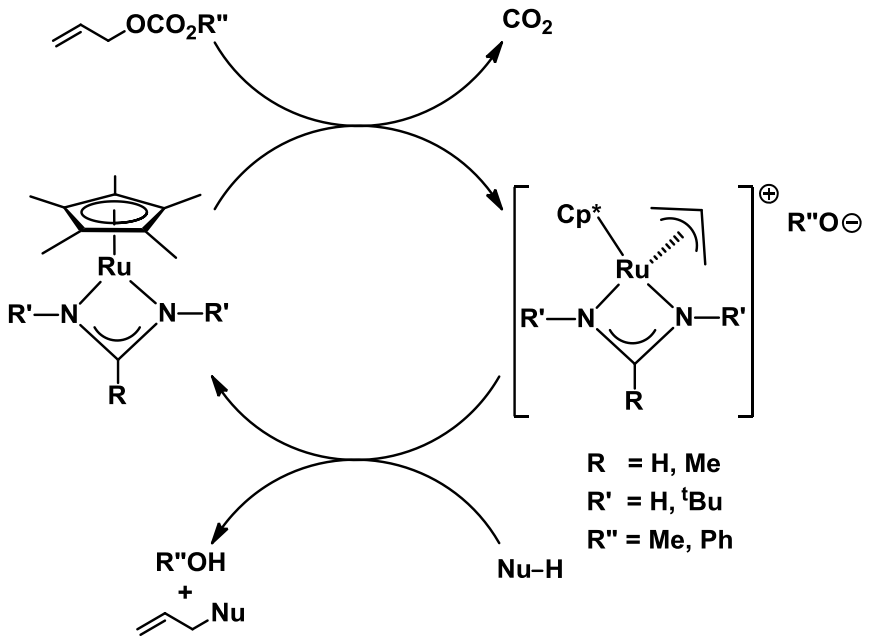

Scheme 1-12. Generalized mechanism for Ru-mediated allylic substitution redox catalysis.

In summary, P,P- and N,N-donor monoanionic ligands have displayed excellent ability to support reactive, low-coordinate complexes, an important prerequisite for the development of new catalytic processes. Whereas the catalytic activity of neutral late metal complexes supported by such ancillary ligands has not been explored nearly as extensively as that of analogous cationic complexes, examples of very challenging stoichiometric bond activation processes promoted by neutral low-coordinate late metal species have emerged.

1.4.3 Monoanionic P,N-donor Ligands

In comparison to monoanionic N,N- and P,P-donor ligands, the chemistry of monoanionic P,N-ligands is remarkably underexplored. Promising examples have been reported over the last two decades, but they are few and far between. Theoretically, anionic P,N-ligands are an interesting ligand motif to explore in late metal chemistry, as they offer a mix of hard and soft donors and the anionic charge should promote tight binding to facilitate the isolation of low-coordinate complexes.

Of the few reported examples of anionic P,N-ligation, Stradiotto and co-workers reported on an interesting system involving a proposed zwitterionic, P,N-supported, 16-electron ruthenium species that quickly decomposes by double geminal C-H activation of a RuN*Me*$_2$ group to form a carbene hydride complex (Scheme 1-13).[48,49] Treatment of the carbene hydride species with dichloromethane, followed by dehydrohalogenation of the resulting chloro carbene complex afforded a carbene complex where the indenyl ring has been further metalated; on the basis of EXSY NMR data, this latter complex was shown to provide access to the zwitterionic ruthenium carbene by way of a reversible Ru-C(sp^3) bond cleavage process (Scheme 1-13).[50] In this case, although the P,N-ligand itself proved highly reactive and susceptible to multiple metalation processes, the ensuing complexes exhibited some interesting stoichiometric bond activation reactivity.

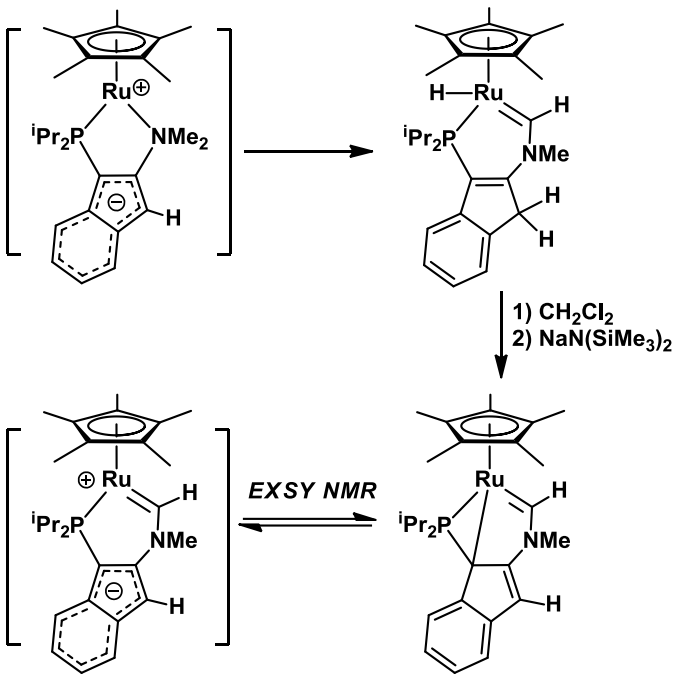

Scheme 1-13. Zwitterionic P,N-supported Ru species that quickly decomposes by double geminal C-H bond activation to produce a carbene hydride complex.

Anionic P,N-ligands have also recently attracted the interest of industrial researchers for their potential application in olefin polymerization catalysis.[51] Some motifs that bear significant structural similarities to the anionic ligands mentioned in Section 1.4 are shown in Figure 1-12. The coordination chemistry of these ligands has not been widely explored in the academic literature to date.

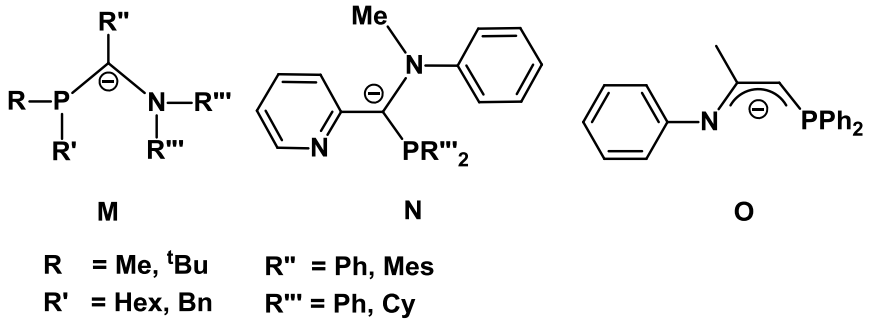

Figure 1-12. Examples of monoanionic P,N-ligands; **M** and **N** have been developed in part by Symyx Technologies[51] while **O** has been developed by Braunstein and co-workers.[52]

Some interest has also surrounded the synthesis of anionic PHOX-type ligands (Scheme 1-14); such ligands have shown considerable promise in the Ru-mediated catalytic transfer hydrogenation of ketones. A comparison of the catalytic activity of complexes supported by such anionic ligands versus complexes featuring their analogous neutral counterparts concluded that the anionic-PHOX-supported complexes made for more efficient catalysis.[53] Additionally, Kempe and Michlik recently reported on the alkylation of anilines by alcohols catalyzed by an anionic-P,N-ligated iridium complex (Scheme 1-15).[54] This study also compared the activity of complexes supported by anionic P,N-ligands to that of complexes featuring neutral versions of the ligands and concluded that the anionic motif leads to increased activity in this system.

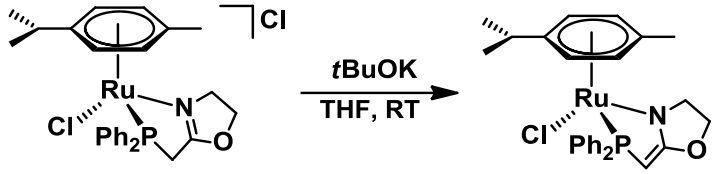

Scheme 1-14. Deprotonation of a PHOX ligated Ru complex to generate the anionic PHOX ligand in *situ.*

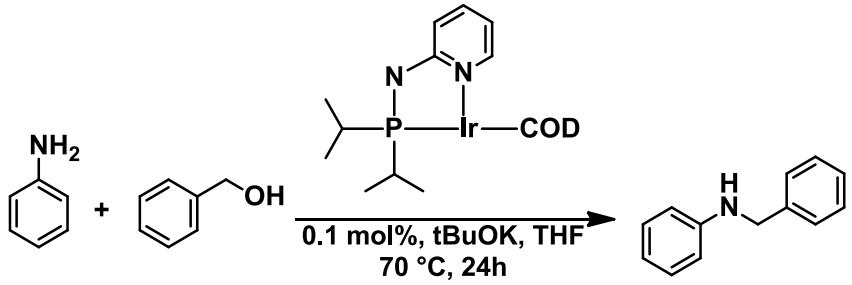

Scheme 1-15. Anionic-P,N-ligated Ir-catalyzed alkylation of anilines by alcohols.

1.5 Thesis Research Overview

In this context, this thesis details synthetic investigations into the late metal coordination chemistry of monoanionic, LX-type, P,N *N*-phosphinoamidinate ligands (Figure 1-13), including in some cases the application of such complexes in catalysis. The work described herein is part of an on-going collaborative effort between the Turculet and Stradiotto research groups at Dalhousie University and Chevron Phillips Chemical Company (herein, CPChem). Patented by CPChem,[4] this new class of ligand is highly modular, with potential variation arising from modifying the substituents on either the ligand backbone or the P or N terminus. Prior to our collaboration, CPChem had focused their investigations exclusively on the neutral *N*-phosphinoamidine motif (Figure 1-13), and showed that such neutral P,N-donor ligands have applications in olefin oligomerization catalysis (Scheme 1-16).[4] The coordination chemistry of anionic *N*-phosphinoamidinates had not been actively explored and represents the primary focus of my thesis studies.

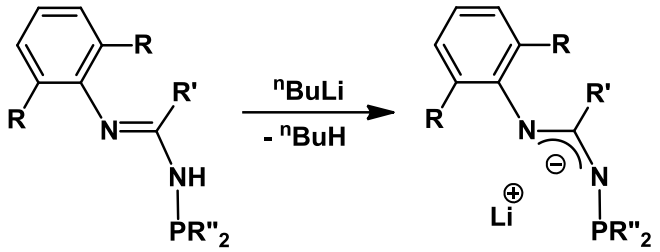

Figure 1-13. A neutral *N*-phosphinoamidine (left) and its deprotonation to give the lithium salt of an anionic N-phosphinoamidinate (right).

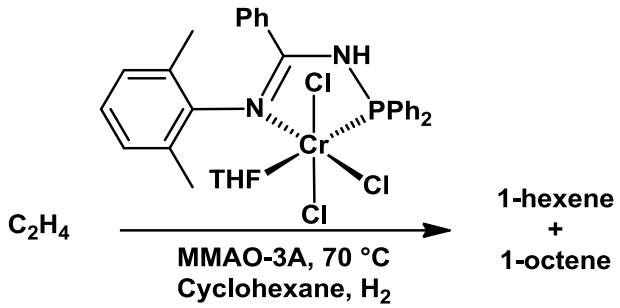

Scheme 1-16. General reaction scheme for the (*N*-phosphinoamidine)Cr catalyzed oligomerization of ethylene to selectively form 1-hexene and 1-octene.

The Dalhousie/CPChem research team has since demonstrated the remarkable ability of the monoanionic *N*-phosphinoamidinates in supporting unusual low-coordinate late metal complexes, and have since developed applications in bond activation and catalysis. Over the past several years, within the field of organometallic chemistry, there has been a major focus on developing efficient and inexpensive, base metal catalysts to replace the current state of the art that typically relies on expensive precious metal catalysts. Inspired by this challenge, *N*-phosphinoamidinate complexes of iron and cobalt were investigated by the CPChem/Turculet/Stradiotto team (Figure 1-14).[55] These complexes, most notably the more sterically hindered iron species **1-2**, displayed impressive activity toward the catalytic hydrosilyation of carbonyls under mild conditions. Complex **1-2** has proven to be among the most proficient Fe catalysts for such hydrosilyations reported in the literature to date. The scope, with respect to carbonyl compounds, extends to ketones, aldehydes, and esters.

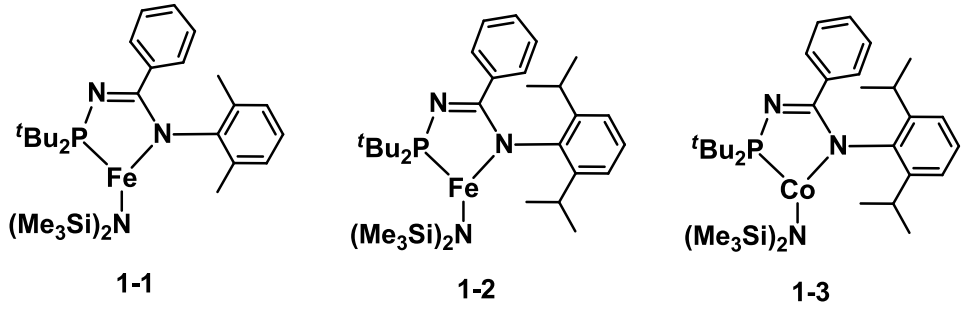

Figure 1-14. Recently reported Fe and Co pre-catalysts supported by *N*-phosphinoamidinates.[55]

Furthermore, these complexes were also tested toward the hydroboration of alkenes and ketones with HBpin.[56] Complex **1-3** proved particularly adept at mediating this reaction for a variety of substrates under mild conditions. Most notably, **1-3** was predisposed to isomerize internal alkenes prior to hydroboration to selectively yield the terminally borylated product (Scheme 1-17).

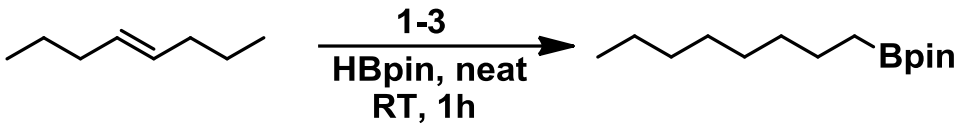

Scheme 1-17. Isomerization and subsequent terminal hydroboration of 4-octene.[56]

Encouraged by the remarkable reactivity of these first-row transition metal complexes, the initial goals of this thesis were to explore the synthesis and reactivity of low-coordinate second and third-row transition metal complexes. Chapter 2 will discuss the synthesis and reactivity of 16-electron Cp*Ru(II) (Cp* = η^5-C_5Me_5) complexes supported by *N*-phosphinoamidinates.[57] Coordinatively unsaturated Cp*RuL_n and related complexes have a well-established track record of exhibiting new and unusual metal-centered reactivity with diverse applications in organic synthesis.[47, 58] As such, considerable focus continues to be directed toward developing new and isolable classes of such complexes and exploring their stoichiometric reactivity.

Intrigued by the ability of related (nacnac)Pt species in supporting low-coordinate reactive complexes (Section 1.4.2), structurally and electronically unique low-coordinate Pt(II) complexes supported by *N*-phosphinoamidinate ligands were developed in pursuit of unusual bonding motifs and reactivity. Chapter 3 details the synthesis and reactivity of an isolable, three-coordinate, neutral, 14-electron Pt(II) species.[59] Chapter 4 will discuss the synthesis and reactivity of a Pt(II)-η^3-benzyl complex that undergoes an unprecedented benzylic borylation reaction.[60]

Within the spirit of moving toward the use of relatively abundant and inexpensive metals in catalysis, and building on previous advances in this area by the CPChem/Turculet/Stradiotto team, Chapter 5 examines the development of the manganese analog of **1-2** and **1-3.** The remarkable ability of this new (P,N)Mn(N(SiMe$_3$)$_2$) complex to reduce amides, ketones, aldehydes, and esters under mild conditions is described.

CHAPTER 2: Synthesis, Structural Characterization, and Reactivity of Cp*Ru(N-Phosphinoamidinate) Complexes

2.1 Introduction

As stated in Chapter 1, coordinatively unsaturated Cp^*RuL_n ($Cp^* = \eta^5$-C_5Me_5) and related half-sandwich type complexes have a well-established track record of exhibiting unusual metal-centered reactivity,[47, 58] with diverse applications in organic synthesis including but not restricted to redox isomerization/reductions, alkene-alkyne coupling, and cycloaddition chemistry.[61] As such, considerable focus continues to be directed toward developing new and isolable classes of such complexes and exploring their stoichiometric reactivity. Collectively, such studies serve to enhance our understanding of the substrate transformations that can occur within the coordination sphere of coordinatively unsaturated Cp^*RuL_n species, and can represent an initial step toward the establishment of new metal-catalyzed transformations.

One of the most notable early examples of ruthenium half-sandwich complexes exhibiting exceptional reactivity was reported by Noyori and co-workers.[62] Utilizing a 16-electron (η^6-*p*-cymene)Ru(κ^2-N~N) complex where both N donors are acting as X ligands, they were able to demonstrate the reversible asymmetric transfer hydrogenation between alcohols and ketones in a catalytic fashion (Scheme 2-1).

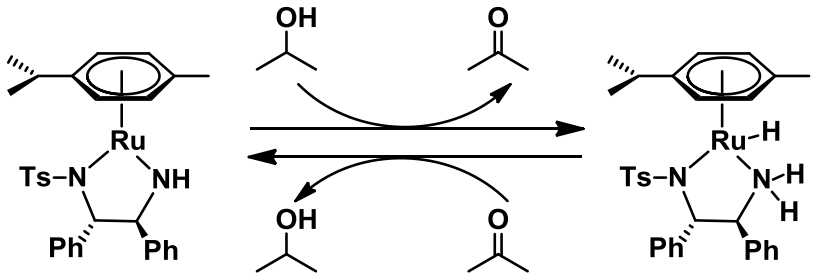

Scheme 2-1. Simplified transfer hydrogenation between alcohols and ketones with Noyori's (η^6-*p*-cymene) Ru(κ^2-N~N) catalyst.

This work was instrumental in establishing the potential of these coordinatively unsaturated ruthenium half-sandwich complexes as both catalysts and targets for developing novel reactivity. Of particular interest to the work herein, with respect to Scheme 2-1, was the bifunctional nature of the metal and ligand. In this regard, the unsaturated ligand, specifically the Ru-NH nitrogen, essentially acts as an additional reactive site and "H^+" acceptor as H_2 is abstracted from propanol and added across the metal-ligand linkage. Experiments designed to test the bifunctional nature of anionic *N*-phosphinoamidinate ligands in a similar manner would be informative in assessing their ability to participate in such reactions.

As alluded to above, our group was particularly interested in the Cp*Ru motif as Cp* is a bulky electron-rich ligand that acts as a strong donor, an important feature in developing reactive complexes. Although considerable attention has been paid to the study of both neutral Cp*RuL(X),[63] complexes and $[Cp^*RuL_2]^+X^-$ salts (**P**, Figure 2-1),[64] reports documenting the preparation of isolable, coordinatively unsaturated and formally 16-electron Cp*Ru(κ^2-L~X) chelate complexes supported by monoanionic, LX-type ligands are rare, and involve primarily synthetic investigations of κ^2-N,N amidinate (**Q**)[47, 58, 65] or β-diketiminate (**R**)[66] complexes with some niche applications in catalysis (refer to Schemes 1-11 and 1-12 for examples of Cp*Ru(amidinate)-mediated reactivity).

It is worthy of mention that analogous Cp*Ru(κ^2-P~N) species,[67] derived from 2-(diphenylphosphino)ethylamine and related ligands (**S**), have been implicated by Ikariya and co-workers as key intermediates in a diversity of synthetically useful metal-catalyzed transformations including the chemoselective hydrogenolysis of epoxides,[68] the isomerisation of allylic alcohols (Scheme 2-2),[69] the oxidative lactonization of 1,4-

diols,[70] and the hydrogenation of imides.[71] Control experiments featured in these reports confirm the importance of tethered phosphino and primary/secondary amine moieties as a means of achieving optimal catalytic performance via Ru/NH bifunctional catalysis; such complexes typically outperformed related Cp*Ru(κ^2-N~N) species.[72] However, despite recent research efforts,[48, 73] neither [Cp*Ru(κ^2-P~N)]$^+$X$^-$, nor related neutral Cp*Ru(κ^2-P~N) species of the type invoked by Ikariya and co-workers featuring a tethered amido-phosphine ancillary ligand (Scheme 2-2), have proven isolable prior to the work reported herein.

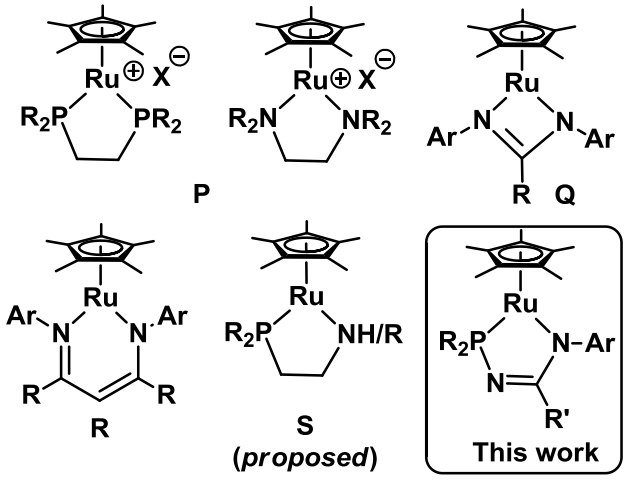

Figure 2-1. Previously studied [Cp*RuL$_2$]$^+$X$^-$ and Cp*Ru(κ^2-*L*~*X*) complexes, and the new Cp*Ru(*N*-phosphinoamidinate) complexes featured herein (Ar = substituted aryl).

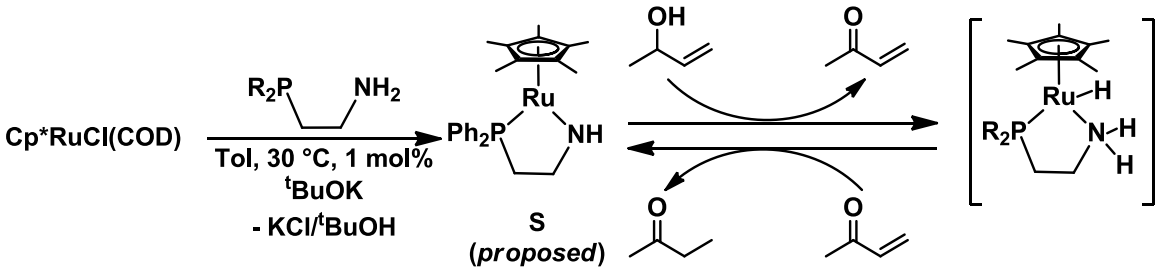

Scheme 2-2. *In situ* formation of a Cp*Ru(κ^2-P~N) invoked by Ikariya for the isomerisation of allylic alcohols.

Inspired by the challenge of preparing the first examples of formally 16-electron Cp*Ru(κ^2-*P~N*) species, the aforementioned Dalhousie/CPChem research team focused our attention on the application of *N*-phosphinoamidinate ligands in this regard. As mentioned in Section 1.5, this new P,N-ligand class was developed recently with an aim toward supporting highly active chromium-based ethylene tri-/tetramerization catalysts;[4] we have since shown that three-coordinate (*N*-phosphinoamidinate)metal(amido) have a variety of applications in catalysis.[55,56] My work in developing the synthesis and spectroscopic/crystallographic characterization of the first isolable, formally 16-electron Cp*Ru(κ^2-*P~N*) species, along with a brief stoichiometric reactivity survey involving these new complexes is detailed in this chapter.

2.2 Results and Discussion

*2.2.1 Synthesis and characterization of Cp*Ru(κ^2-P~N) species*

Having previously reported on the synthesis of the phosphinoamidine ligands **2-1a** and **2-1b**,[55] one could envision that the reaction of such species with $[Cp^*RuCl]_4$ in the presence of a suitable base could provide access to 16-electron Cp*Ru(*N*-phosphinoamidinate) complexes (Scheme 2-3). Treatment of **2-1a** or **2-1b** with 0.25 equiv of $[Cp^*RuCl]_4$ in the presence of excess Cs_2CO_3 afforded the corresponding 16-electron Ru complex **2-2a** or **2-2b** as a blue or dark green solid, respectively (quantitative on the basis of ^{31}P NMR spectroscopy). Alternatively, treatment of **2-1b** with ^{n}BuLi followed by reaction of the ensuing lithium salt with $[Cp^*RuCl]_4$ cleanly afforded **2-2b**; in contrast, the use of ^{n}BuLi in place of Cs_2CO_3 in the preparation of **2-2a** afforded multiple phosphorus-containing products, on the basis of ^{31}P NMR data. Both complexes **2-2a** (67%) and **2-2b** (using ^{n}BuLi, 82%) were readily isolated and appear to be stable at

room temperature under a nitrogen atmosphere both in solution and in the solid state. The highly colored nature of **2-2a** (dark blue) and **2-2b** (dark green) is consistent with previously reported 16-electron Cp*Ru complexes, including Cp*RuL(X),[58,63] Cp*Ru(amidinate),[58,65] and Cp*Ru(diketiminate),[66] which are typically blue or purple in color. The solution NMR (^{1}H, ^{13}C, ^{31}P) spectra of **2-2a** (Figure 2-4) and **2-2b** (Figure 2-5) are consistent with their formulation as C_s-symmetric, diamagnetic, *N*-phosphinoamidinate complexes. The ^{31}P NMR spectra of **2-2a** and **2-2b** feature resonances at 128.2 and 124.9 ppm, which are significantly downfield relative to **2-1a** (61.9 ppm) and **2-1b** (61.4 ppm). The ^{1}H NMR spectra (benzene-d_6) of **2-2a** and **2-2b** feature a resonance attributed to the Cp* ligand at 1.21 and 1.19 ppm, respectively, as well as a resonance at 1.45 and 1.46 ppm, respectively, corresponding to the magnetically equivalent P*t*Bu$_2$ substituents. The 2,6-dimethyl substituted N-aryl group in **2-2a** gives rise to a single C(aryl)Me ^{1}H NMR resonance at 2.27 ppm. In the case of **2-2b**, the 2,6-diisopropyl substituted N-aryl group gives rise to a single set of C(aryl)*i*Pr$_2$ resonances, where the methyl groups on these substituents are diastereotopic, as indicated by their appearance as two doublets that integrate to six protons each at 1.37 and 0.80 ppm. The spectroscopic signature of these formally 16-electron, C_s-symmetric species **2-2a** and **2-2b** differ significantly from their C_1-symmetric 18-electron adducts (*vide infra*).

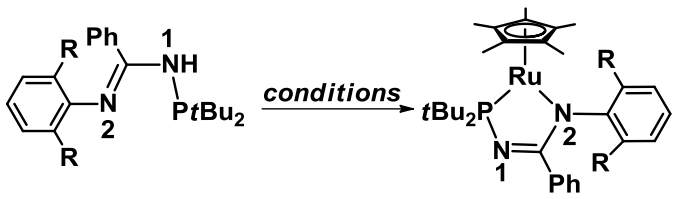

2-1a, R = Me
2-1b, R = *i*Pr

2-2a, R = Me, 67%
2-2b, R = *i*Pr, 82%

Scheme 2-3. Synthesis of Cp*Ru(*N*-phosphinoamidinate) complexes, **2-2a** and **2-2b**. *Conditions:* **2-1a**, 0.25 $[Cp^*RuCl]_4$, excess Cs_2CO_3 (for **2-2a**); **2-1b**, ^{n}BuLi (one equiv., -35 ºC), then 0.25 $[Cp^*RuCl]_4$ (for **2-2b**).

The solid state structures of both **2-2a** and **2-2b** were determined by using single crystal X-ray diffraction techniques (Figure 2-2, Tables 2-1 and 2-2; the latter are located at the end of the chapter). In both cases the complexes adopt a monomeric two-legged piano stool structure that is analogous to that previously observed for related crystallographically characterized Cp*RuL(X) complexes,[58, 63] as well as complexes of the type Cp*Ru(amidinate),[58, 65] and Cp*Ru(diketiminate).[66] The Ru-P distances of 2.3679(5) and 2.3599(5) Å for **2-2a** and **2-2b**, respectively, are slightly shorter than that of 2.395(2) Å reported for Cp*Ru(P*i*Pr$_3$)Cl,[63a] possibly due to the rigid chelating structure of the *N*-phosphinoamidinate complexes. The Ru-N(2) distance of 2.0734(16) Å in **2-2b** is somewhat elongated relative to that of 2.0458(13) Å in **2-2a**, which can most likely be ascribed to the greater steric demands of the isopropyl-functionalized ligand in **2-2b**. Nonetheless, these Ru-N distances fall within the range observed for crystallographically characterized Cp*Ru(amidinate) (2.073(3) Å)[65] and Cp*Ru(diketiminate) (2.025(6)-2.071(2) Å)[66] complexes. The solid state structures of **2-2a** and **2-2b** are consistent with the C_s-symmetric species observed in solution, as indicated by the perpendicular orientation of the P-Ru-N(2) plane relative to the plane of the Cp* ligand.

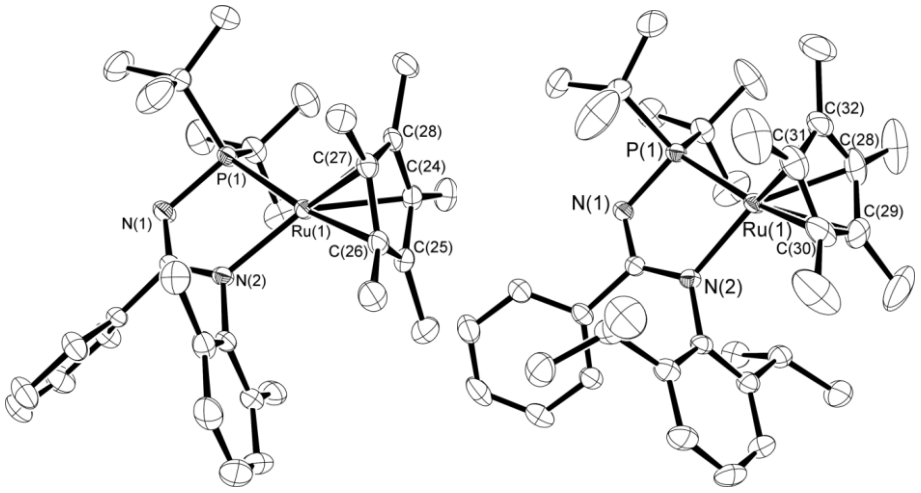

Figure 2-2. Crystallographically determined structures of **2-2a** (left) and **2-2b** (right) employing 50% ellipsoids and with hydrogen atoms omitted for clarity.

2.2.2 *Probing the Reactivity of 2-2a and 2-2b*

Despite the apparent stability of the coordinatively unsaturated species **2-2a** and **2-2b**, these complexes proved highly reactive towards two electron donor ligands, leading to the formation of 18-electron adducts (Scheme 2-4). Thus **2-2b** was found to react readily with an atmosphere of CO to form the corresponding adduct **2-3**, while **2-2a** reacted with one equiv. of 2,6-xylylisocyanide to form **2-4**. In the case of **2-3**, the identity of this product as being a CO adduct of **2-2b** was confirmed initially on the basis of NMR data, whereby a diagnostic ^{13}C NMR resonance for the CO group was detected (212.4 ppm), along with the observation of distinct resonances attributable to magnetically non-equivalent *t*Bu and isopropyl groups in both the ^{1}H and ^{13}C NMR spectra. Similarly for **2-4**, unique resonances in keeping with diastereotopic pairs of aryl-Me and *t*Bu groups were observed in both the ^{1}H and ^{13}C NMR spectra. The proposed connectivity in **2-3** and **2-4** was confirmed in the solid state on the basis of single-crystal X-ray diffraction data (Figure 2-3, Tables 2-1 and 2-2). While for both **2-3** and **2-4**, the Ru-P bond distances (2.3652(6) Å and 2.3578(7) Å) and the P-Ru-N(2) bite angles (76.20(6)º and 77.32(5)º)

do not differ significantly from those observed in the precursor 16-electron complexes, other more notable variations in interatomic distances are observed upon adduct formation. A significant lengthening of the Ru-N(2) distance occurs on going from **2-2a**/**2-2b** to **2-4**/**2-3**, possibly owing to a combination of increased congestion on forming a three-legged piano-stool structure, as well as a reduction in Ru-N π-bonding in the 18-electron adducts in keeping with concepts described by Caulton and co-workers.[63c] Furthermore, the observed P-N(1) and N(2)-C(9) distances are shorter, while the N(1)-C(9) distances are modestly longer in the adducts relative to **2-2a** and **2-2b**, thereby suggesting that adduct formation induces changes in the electronic structure of the coordinated *N*-phosphinoamidinate ligands. The Ru-CO (1.844(3) Å) distance in **2-3** is statistically equivalent to the related distances found in Cp*Ru(CO)(amidinate) (1.828(7) Å)[65] and Cp*Ru(CO)(diketiminate) (1.837(2) Å)[66a] complexes. Furthermore, the carbonyl stretch in **2-3** (1902 cm^{-1}) is intermediate between those reported for Cp*Ru(CO)(amidinate) (1888 cm^{-1})[65] and Cp*Ru(CO)(diketiminate) (1910 cm^{-1})[66a] species.

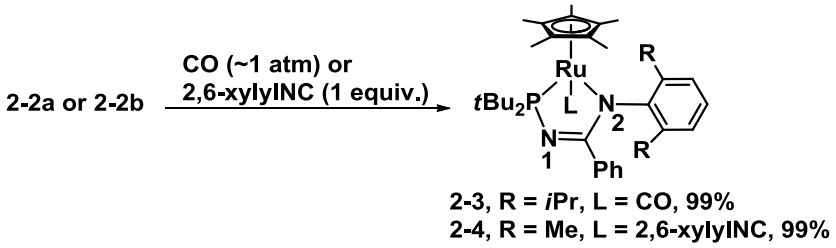

Scheme 2-4. Reactivity of Cp*Ru(*N*-phosphinoamidinate) complexes, **2-2a** and **2-2b** with two-electron (L) donors.

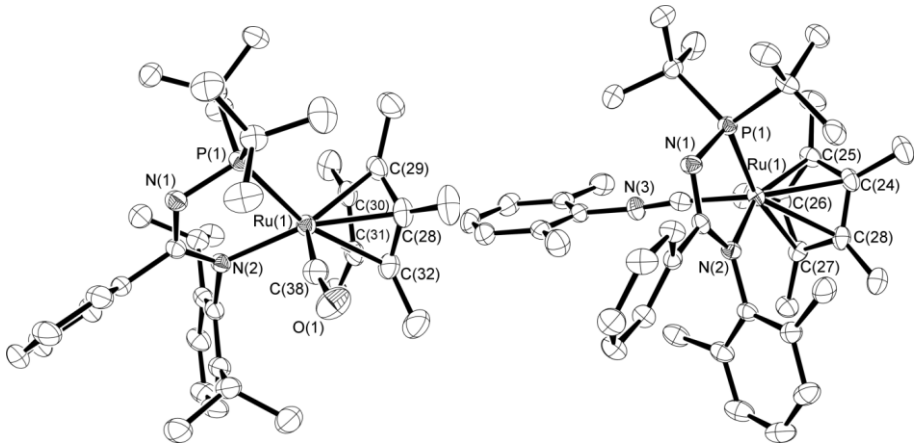

Figure 2-3. Crystallographically determined structures of **2-3** (left) and **2-4** (right) employing 50% ellipsoids and with hydrogen atoms omitted for clarity.

Encouraged by the ability of **2-2a** and **2-2b** to bind two-electron L-type donor ligands, attention was shifted toward exploring the reactivity of these complexes with E-H bonds (E = main group element). Initial efforts in this regard focused on exploring the reactivity of **2-2a** and **2-2b** with ammonia borane (AB) at room temperature, given current interest in the use of AB as a material from which hydrogen may be generated under mild conditions.[74,75] No reaction was observed upon combination of five equiv. of AB with **2-2b** in THF (ca. 3 mL) over the course of 24h on the basis of ^{31}P NMR data obtained from the reaction mixtures, possibly inhibited by the more bulky *i*Pr groups limiting facile access to the metal center. Under similar conditions using **2-2a**, the consumption of **2-2a** and formation of a new organometallic product (**2-5**) was observed over the course of four hours by use of ^{31}P NMR methods, accompanied by a change in colour of the solution from blue to dark red. Upon workup, **2-5** was obtained in 93% isolated yield. The structure of **2-5** depicted in Scheme 2.3 was elucidated on the basis of NMR spectroscopic data. Notably, ^{1}H NMR resonances (benzene-d_6) at 5.38 ppm and -12.16 ppm suggest the presence of NH and RuH groups, respectively, and the location of the NH group was confirmed on the basis of nOe interactions observed between the NH

and the P*t*Bu$_2$ group. Moreover, both the ^{1}H and ^{13}C NMR spectra of **2-5** feature diastereotopic pairs of aryl-Me and *t*Bu groups, in keeping with the proposed structural formulation. Efforts to monitor the progress of the reaction by use of NMR methods failed to detect any intermediates *en route* to **2-5**; as such it remains unclear if **2-5** represents the first-formed product of the reaction. Nonetheless, it is feasible that the initial site of protonation is at the Ru-N(aryl) nitrogen, followed by a net 1,3-proton shift to afford the observed product **2-5**. Interestingly, this represents the first example of the *N*-phosphinoamidinate ligands participating in a bifunctional fashion where H_2 is added across the metal-ligand framework in a similar manner to what is observed in Scheme 2-1 and 2-2.

While the formation of **2-5** from **2-2a** corresponds to the net dehydrogenation of AB as desired, continued monitoring of the reaction by use of ^{1}H and ^{11}B NMR methods over the course of 24h confirmed the modest consumption of AB along with the formation of small amounts of cyclotriborazane (and/or cross-linked oligomers) and borazine as observed by ^{11}B NMR,[76] with minimal hydrogen evolution detected. In an effort to assess the ability of **2-5** to release hydrogen and regenerate **2-2a**, benzene-d_6 solutions of **2-5** were heated at 75 °C and were monitored by use of ^{31}P NMR methods. Over the course of five days, the clean conversion of **2-5** to **2-2a** was observed. The rate of this conversion could be accelerated through the addition of norbornene (1-2 equiv.), whereby the clean conversion to **2-2a** was observed after only 4h at 75 °C (Scheme 2-5).

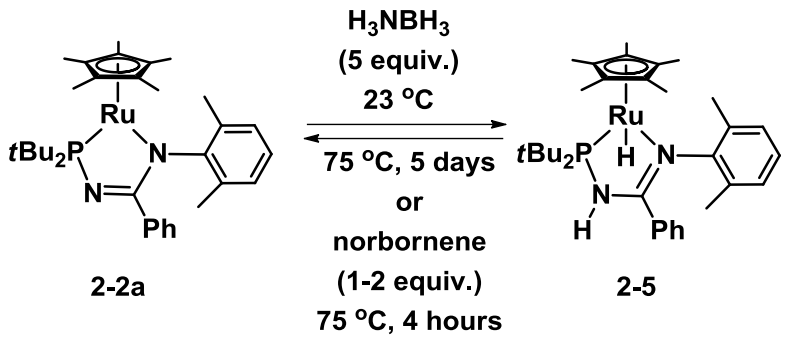

Scheme 2-5. Reactivity of the Cp*Ru(*N*-phosphinoamidinate) complex **2-2a** with ammonia borane and loss of dihydrogen from the resulting product **2-5**.

It is also important to note that a variety of other reactions were attempted with complexes **2-2a** and **2-2b**. Reactions with primary silanes and substituted amine boranes were slow, required heating over prolonged periods of time, and led to the formation of multiple phosphorus-containing products; attempts to isolate individual species were unsuccessful. Complexes **2-2a** and **2-2b** also proved to be remarkably stable toward a number of reagents such as aryl halides, anilines, pinacol borane, phenols, isopropanol, and phenyl acetylene. Examples of these attempted reactions are presented in Scheme 2-6. After deeming these reactions unsuccessful, efforts were refocused toward developing the platinum chemistry (Chapter 3 and 4) of the *N*-phosphinoamidinates, in hopes of synthesizing more reactive complexes.

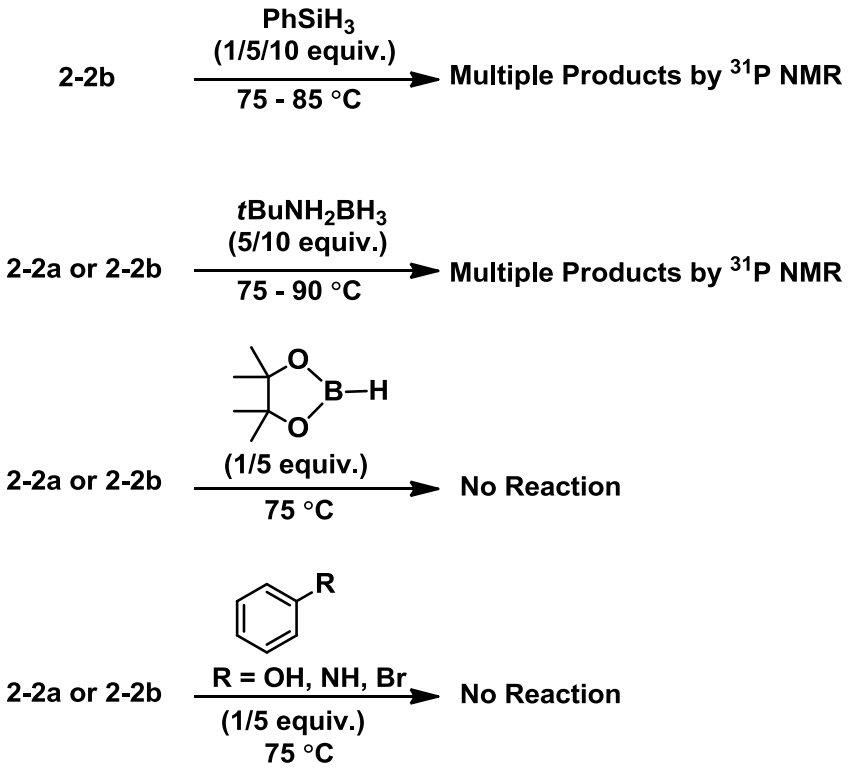

Scheme 2-6. Examples of unsuccessful reaction attempts with **2-2a** and **2-2b**.

2.3 Conclusions

In summary, within this chapter the synthesis and characterization of the first isolable, formally 16-electron Cp*Ru(κ^2-*P*~*N*) species (**2-2a** and **2-2b**), which are supported by *N*-phosphinoamidinate ligands has been described. These diamagnetic complexes exhibit a C_s-symmetric structure in both solution and the solid state, as determined on the basis of NMR spectroscopic and X-ray crystallographic data. Despite the stability of such complexes, they have been shown to readily coordinate two-electron (L) donors including carbon monoxide and 2,6-xylylisocyanide, affording crystallographically characterized C_1-symmetric 18-electron Cp*Ru(L)(κ^2-*P*~*N*) adducts (**2-3** and **2-4**). Preliminary reactivity studies confirmed that such complexes are capable of extruding hydrogen from ammonia borane in a bifunctional manner. Whereas no

reaction was observed upon combination of ammonia borane and **2-2b** at room temperature, under similar conditions the less sterically hindered Cp*Ru(*N*-phosphinoamidinate) complex **2-2a** was cleanly transformed into **2-5** – a process that corresponds to the net transfer of hydrogen from ammonia borane to **2-2a**.

2.4 Statement of Contributions

Several researchers helped to bring this project to publication in the *Canadian Journal of Chemistry* and they are recognized herein. Dr. Adam Ruddy worked to refine the synthesis of the *N*-phosphinoamidinate ligands used in this work and the crystal data was solved by Dr. Craig Wheaton.

2.5 Experimental Details

General Considerations. All experiments were conducted under nitrogen in an MBraun glovebox or using standard Schlenk techniques. Dry, oxygen-free solvents were used unless otherwise indicated. Benzene, toluene and pentane were deoxygenated and dried by sparging with nitrogen and subsequent passage through a double-column solvent purification system purchased from MBraun Inc. Tetrahydrofuran and diethyl ether were purified by distillation from Na/benzophenone. All purified solvents were stored over 4 Å molecular sieves. Benzene-d_6 was degassed via three freeze-pump-thaw cycles and stored over 4 Å molecular sieves. The ligands **2-1a** and **2-1b**,[55] and $[Cp^*RuCl]_4$[77] were prepared according to literature procedures. Ammonia borane was purchased from Aldrich and sublimed prior to use. All other reagents were used without further purification. ^1H, ^{13}C, and ^{31}P NMR characterization data were collected at 300K on a Bruker AV-500 spectrometer operating at 500.1, 125.7, and 202.5 MHz (respectively) with chemical shifts reported in parts per million downfield of $SiMe_4$ for ^1H and ^{13}C, and 85% H_3PO_4 in

D_2O for ^{31}P. ^{1}H and ^{13}C NMR chemical shift assignments are based on data obtained from ^{13}C-DEPTQ135, ^{1}H-^{1}H COSY, ^{1}H-^{13}C HSQC, and ^{1}H-^{13}C HMBC NMR experiments. In some cases, fewer than expected unique ^{13}C NMR resonances were observed, despite prolonged acquisition times. X-Ray data collection was carried out by Dr. Robert MacDonald and Dr. Michael J. Ferguson at the University of Alberta X-ray Crystallography Laboratory, Edmonton, Alberta. Structural solution and refinement was conducted by Dr .Craig Wheaton (Dalhousie). Infrared spectra were recorded as thin films between NaCl plates using a Bruker Tensor 27 FT-IR spectrometer at a resolution of 4 cm^{-1}.

Synthesis of 2-2a. A solution of **2-1a** (0.20 g, 0.54 mmol) in ca. 5 mL of THF was added by pipette to a solution of $[Cp^*RuCl]_4$ (0.15 g, 0.14 mmol) in ca. 5 mL of THF. An excess of Cs_2CO_3 (0.91 g, 2.79 mmol) was added to the resulting solution and the mixture was stirred for 5 hours at 45 °C. A gradual color change from brown to blue was observed. The solvent was removed under vacuum and the resulting blue solid was dissolved in ca. 10 mL of benzene. The benzene solution was subsequently filtered through Celite to remove any residual salts. The solvent was again removed under vacuum and the solid was triturated with pentane (1 mL x 3) to yield **2-2a** as a blue solid (0.22 g, 67%). ^{1}H NMR (500 MHz, benzene-d_6): δ 7.42 (d, 2 H, J = 7 Hz, H_{arom}), 7.03 (m, 2 H, H_{arom}), 6.95 - 6.82 (overlapping resonances, 4 H, H_{arom}), 2.27 (s, 6 H, *Me*), 1.45 (d, 18 H, P*tBu*$_2$, $^{3}J_{PH}$ = 13 Hz), 1.21 (s, 15 H, *Cp**). $^{13}C\{^{1}H\}$ NMR (125.7 MHz, benzene-d_6): δ 182.1 (N*C*N), 155.3 (C_{arom}), 139.8 (C_{arom}), 133.4 (C_{arom}), 128.8 (CH_{arom}), 128.6 (CH_{arom}), 128.0 (CH_{arom}), 127.0 (CH_{arom}), 123.7 (CH_{arom}), 75.5 (*Cp**), 35.9 (d, P*C*Me$_3$, $^{1}J_{PC}$ = 20 Hz), 29.4 (P*tBu*), 21.0 (C*Me*), 11.3 (*Cp**). $^{31}P\{^{1}H\}$ NMR (202.5 MHz,

benzene-d_6): δ 128.2. Anal. Calcd for $C_{33}H_{47}N_2PRu$: C, 65.64; H, 7.85; N, 4.64. Found: C, 65.29; H, 7.91; N, 4.34. Crystals of **2-2a** suitable for X-ray diffraction analysis were grown from Et_2O at -35° C.

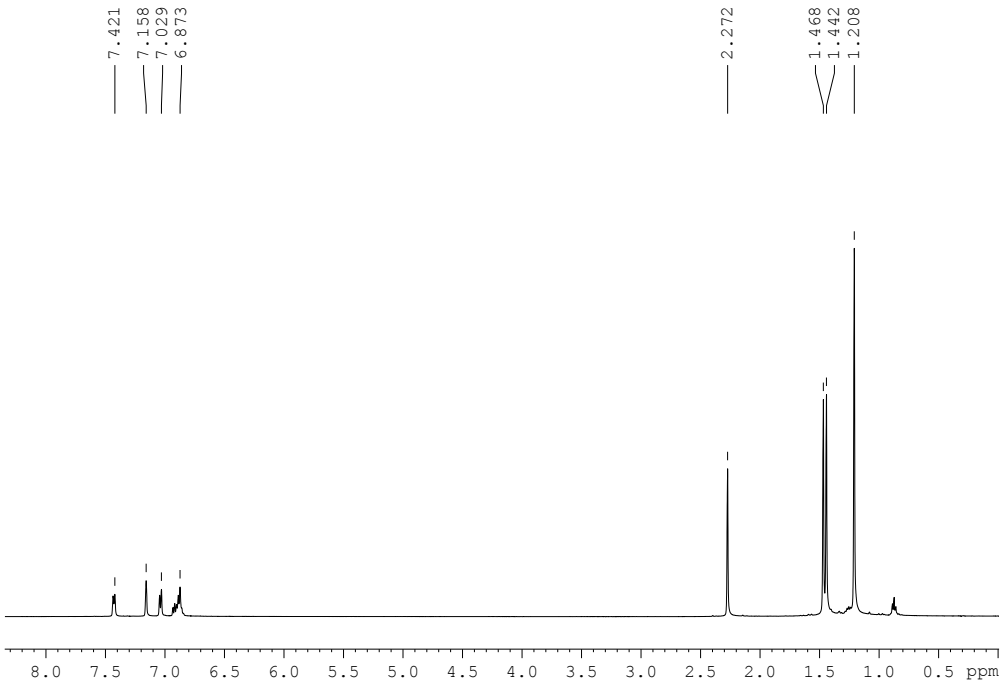

Figure 2-4. ^{1}H NMR spectrum of **2-2a.**

Synthesis of 2-2b. A solution of **2-1b** (0.36 g, 0.85 mmol) in ca. 20 mL of pentane was cooled to -35 °C and a slight excess of 2.5 M ^{n}BuLi (375 µl, 0.94 mmol) was added slowly by syringe. The reaction mixture was then allowed to warm to room temperature over the course of 15 minutes, during which time a white precipitate was observed. The supernatant was then carefully decanted and the remaining residue was dried under vacuum to yield the lithium salt of **2-1b** (0.35 g; ^{31}P NMR, 202.5 MHz, THF-d_8: δ 74.8, br), which was used subsequently without further purification. A solution of the so-formed lithium salt of **2-1b** (0.31 g, 0.72 mmol) in ca. 5 mL of THF was added by pipette to a solution of $[Cp^*RuCl]_4$ (0.20 g, 0.18 mmol) in ca. 5 mL of THF. An immediate color change from brown to dark green was observed. After approximately 20 minutes, the

solvent was removed under vacuum and the remaining green solid was taken up in ca. 10 mL of benzene. The benzene solution was filtered through Celite and the filtrate was collected. The filtrate solution was evaporated under vacuum and the solid was triturated with pentane (1 ml x 3) to yield **2-2b** as a dark green solid (0.39 g, 82%). ^{1}H NMR (500 MHz, benzene-d_6): δ 7.62 (broad apparent doublet, 2 H, H_{arom}), 7.29 - 7.27 (overlapping resonances, 3 H, H_{arom}), 6.91 - 6.85 (overlapping resonances, 3 H, H_{arom}), 3.46 (sept, 2 H, $^{3}J_{HH}$ = 7 Hz, *CH*Me$_2$), 1.46 (d, 18 H, P*tBu*$_2$, $^{3}J_{PH}$ = 13 Hz), 1.37 (d, 6 H, $^{3}J_{HH}$ = 7 Hz, CH*Me*$_2$), 1.19 (s, 15 H, *Cp**), 0.80 (d, 6 H, $^{3}J_{HH}$ = 7 Hz, CH*Me*$_2$). ^{13}C{^{1}H} NMR (125.7 MHz, benzene-d_6): δ 181.7 (d, J_{CP} = 9 Hz, N*C*N), 154.7 (C_{arom}), 142.8 (C_{arom}), 138.6 (d, J_{CP} = 18 Hz, C_{arom}), 133.1 (*C*H$_{arom}$), 129.3 (*C*H$_{arom}$), 127.4 (*C*H$_{arom}$), 124.9 (*C*H$_{arom}$), 124.7 (*C*H$_{arom}$), 76.1 (*Cp**), 36.8 (d, $^{1}J_{CP}$ = 20 Hz, P*C*Me$_3$), 29.8 (P*tBu*), 29.5 (*C*HMe$_2$), 25.3 (CH*Me*$_2$), 25.0 (CH*Me*$_2$), 12.3 (*Cp**). ^{31}P{^{1}H} NMR (202.5 MHz, benzene-d_6): δ 124.9. Anal. Calcd for $C_{37}H_{55}N_2PRu$: C, 67.34; H, 8.40; N, 4.25. Found: C, 67.55; H, 8.32; N, 4.41. Crystals of **2-2b** suitable for X-ray diffraction analysis were grown from pentane at -35 °C.

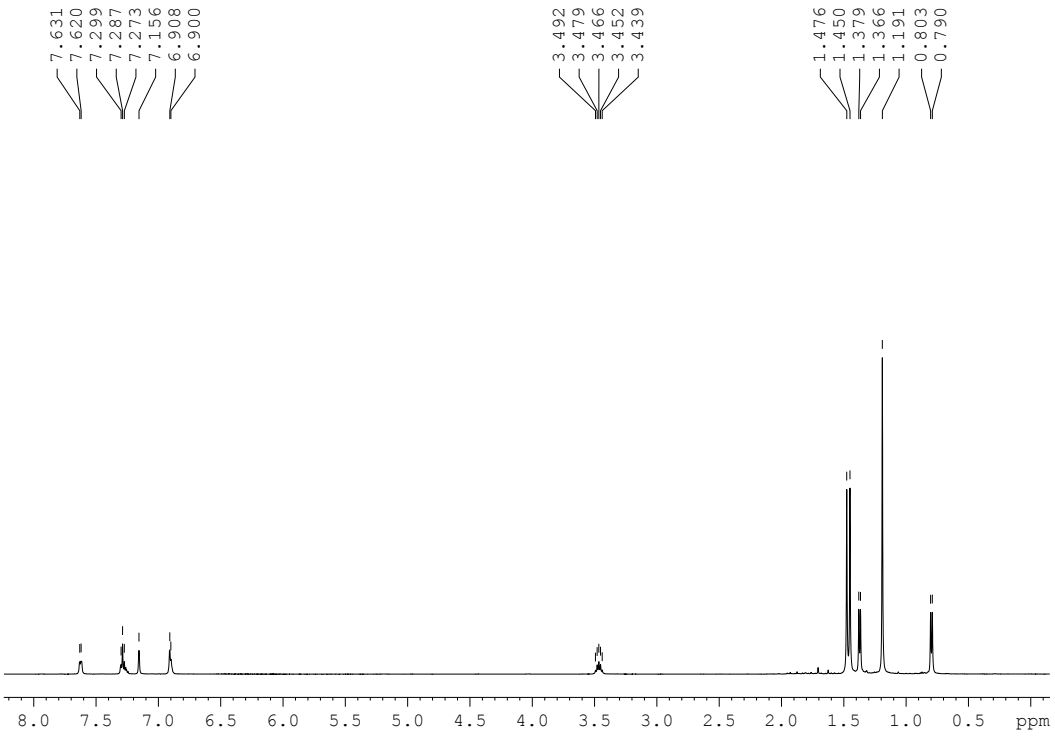

Figure 2-5. ^{1}H NMR spectrum of **2-2b.**

Synthesis of 2-3. A solution of **2-2b** (0.025 g, 0.038 mmol) in ca. 1 mL of benzene was transferred to a J. Young NMR tube. The solution was degassed via three freeze-pump-thaw cycles and the tube was subsequently exposed to ca. 1 atm of CO. A color change from dark green to amber brown was observed within five minutes after vigorous shaking. After approximately 20 minutes, the solvent was removed under vacuum to yield **2-3** as a pale yellow solid (0.026 g, 99 %). ^{1}H NMR (500 MHz, benzene-d_6): δ 7.58 (d, 2 H, J = 8 Hz, H_{arom}), 7.12 - 7.07 (overlapping resonances, 3 H, H_{arom}), 6.94 - 6.87 (overlapping resonances, 3 H, H_{arom}), 3.52 (sept, 1 H, $^{3}J_{HH}$ = 7 Hz, *CH*Me$_2$), 3.08 (sept, 1 H, $^{3}J_{HH}$ = 7 Hz, *CH*Me$_2$), 1.56 (d, 9 H, $^{3}J_{PH}$ = 13 Hz, P*tBu*), 1.40 - 1.29 (overlapping resonances, 27 H, *Cp**, P*tBu*, CH*Me*$_2$), 1.29 (d, 3 H, $^{3}J_{HH}$ = 7 Hz, CH*Me*$_2$), 1.07 (d, 3 H, $^{3}J_{HH}$ = 7 Hz, CH*Me*$_2$), 0.55 (d, 3 H, $^{3}J_{HH}$ = 7 Hz, CH*Me*$_2$). ^{13}C{^{1}H} NMR (125.7 MHz, benzene-d_6): δ 212.4 (d, $^{2}J_{CP}$ = 20 Hz, *C*O), 175.1 (N*C*N), 149.9 (C_{arom}), 144.8 (d, J_{CP} =

15 Hz, C_{arom}), 138.3 (d, J_{CP} = 19 Hz, C_{arom}), 132.7 (CH_{arom}), 127.1 (CH_{arom}), 125.8 (CH_{arom}), 125.4 (CH_{arom}), 123.3 (CH_{arom}), 96.0 (*Cp**), 40.4 - 39.9 (overlapping resonances, P*C*Me$_3$), 30.8 (P*tBu*), 29.6 (P*tBu*), 28.4 (*C*HMe$_2$), 28.3 (*C*HMe$_2$), 26.7 (CH*Me*$_2$), 25.9 (CH*Me*$_2$), 24.9 (CH*Me*$_2$), 23.8 (CH*Me*$_2$), 10.9 (*Cp**). $^{31}P\{^1H\}$ NMR (202.5 MHz, benzene-d_6): δ 139.9. IR (cm^{-1}): 1902 (ν_{CO}). Anal. Calcd for $C_{38}H_{55}N_2OPRu$: C, 66.35; H, 8.06; N, 4.07. Found: C, 66.24 H, 8.21; N, 4.36. Crystals of **2-3** suitable for X-ray diffraction analysis were grown from Et_2O at -35 °C.

Synthesis of 2-4. A solution of 2,6-xylylisocyanide (0.012 g, 0.094 mmol) in ca. 1 mL of Et_2O was added by pipette to a solution of **2-2a** (0.057 g, 0.094 mmol) in ca. 1 mL of Et_2O. An immediate color change from blue to orange-yellow was observed. After approximately 20 minutes, the solvent was removed under vacuum to yield **2-4** as a bright yellow solid (0.027 g, 99 %). ^1H NMR (500 MHz, benzene-d_6): δ 7.68 (d, 2 H, *J* = 7 Hz, H_{arom}), 6.99 - 6.88 (overlapping resonances, 4 H, H_{arom}), 6.85 - 6.77 (overlapping resonances, 4 H, H_{arom}), 6.66 (m, 1 H, H_{arom}), 2.67 (s, 3 H, *Me*), 2.42 (s, 6 H, *xylyl*NC), 1.98 (s, 3 H, *Me*), 1.58 (d, 9 H, P*tBu*, $^3J_{PH}$ = 13 Hz), 1.43 - 1.39 (overlapping resonances, 24 H, *Cp** + P*tBu*). $^{13}C\{^1H\}$ NMR (125.8 MHz, benzene-d_6): δ 182.5 (d, J_{CP} = 20 Hz, xylylN*C*), 176.5 (N*C*N), 153.2 (C_{arom}), 141.1 (d, *J* = 19 Hz, C_{arom}), 135.9 (C_{arom}), 135.4 (C_{arom}), 134.2 (C_{arom}), 133.1 (C_{arom}), 130.6 (CH_{arom}), 129.6 (CH_{arom}), 129.5 (CH_{arom}), 129.1 (CH_{arom}), 128.0 (CH_{arom}), 127.3 (CH_{arom}), 125.7 (CH_{arom}), 123.8 (CH_{arom}), 93.6 (*Cp**), 40.9 (d, P*C*Me$_3$, $^1J_{CP}$ = 14 Hz), 39.2 (d, $^1J_{CP}$ = 31 Hz, P*C*Me$_3$), 31.8 (P*tBu*), 30.5 (P*tBu*), 23.4 (C*Me*), 22.8 (C*Me*), 21.1 (*xylyl*NC), 11.4 (*Cp**). $^{31}P\{^1H\}$ NMR (500 MHz, benzene-d_6): δ 149.1. Anal. Calcd for $C_{42}H_{56}N_3PRu$: C, 68.64; H, 7.68; N, 5.72. Found:

C, 68.59; H, 7.54; N, 5.66. Crystals of **2-4** suitable for X-ray diffraction analysis were grown from Et_2O at -35 °C.

Synthesis of 2-5. A solution of ammonia borane (0.15 g, 4.9 mmol) in ca. 2 mL of THF was added by pipette to a solution of **2-2a** (0.057 g, 0.094 mmol) in ca. 1 mL of THF. A slow colour change from blue to dark red was observed over a period of 4 hours. The solvent was removed under vacuum, and the remaining red residue was redissolved in ca. 5 mL of pentane and filtered through Celite. The filtrate solution was collected and was evaporated to dryness and the solid was triturated with pentane (1 ml x 3) to yield **5** as a dark red solid (0.053 g, 93 %). ^{1}H NMR (500 MHz, benzene-d_6): δ 7.02 (m, 2 H, H_{arom}), 6.92 (d, 1 H, J = 7 Hz, H_{arom}), 6.78 - 6.73 (overlapping resonances, 4 H, H_{arom}), 6.69 (d, 1 H, J= 8 Hz, H_{arom}), 5.38 (br d, 1 H, J = 5 Hz, N*H*), 2.68 (s, 3 H, C*Me*), 1.94 (s, 3 H, C*Me*), 1.75 (s, 15 H, *Cp**), 1.36 (d, 9 H, P*tBu*, $^3J_{PH}$ = 13 Hz), 1.30 (d, 9 H, P*tBu*, $^3J_{PH}$ = 13 Hz), -12.16 (d, 1 H, $^2J_{HP}$ = 42 Hz, Ru*H*). ^{13}C{^{1}H} NMR (125.7 MHz, benzene-d_6): δ 158.3 (d, N*C*N, J = 14 Hz), 149.4 (C_{arom}), 134.7 (C_{arom}), 133.1 (C_{arom}), 131.0 (C_{arom}), 129.0 (CH_{arom}), 128.9 (CH_{arom}), 127.4 (CH_{arom}), 124.5 (CH_{arom}), 87.9 (*Cp**), 40.2 (P*C*Me$_3$), 39.0 (d, P*C*Me$_3$, $^1J_{PC}$ = 26 Hz), 30.4 (d, P*tBu*, $^3J_{CP}$ = 5 Hz), 29.5 (d, P*tBu*, $^3J_{CP}$ = 8 Hz), 19.5 (C*Me*), 19.4 (C*Me*), 12.4 (*Cp**). ^{31}P{^{1}H} NMR (202.5 MHz, benzene-d_6): δ 160.8. IR (cm^{-1}): 3404 (w, ν_{NH}), 1981 (m, ν_{RuH}). Anal. Calcd for $C_{33}H_{49}N_2PRu$: C, 65.43; H, 8.15; N, 4.62. Found C, 65.51; H, 8.27; N, 4.48.

Details of Crystallographic Studies. Crystallographic data were obtained at 173(2) K on a Bruker PLATFORM/SMART 1000 CCD diffractometer or a Bruker D8/APEX II CCD diffractometer using graphite-monochromated Mo Kα (λ = 0.71073 Å) radiation for **2-2a**, **2-2b**, and **2-4**, or CuKα (λ = 1.54178 Å) for **2-3**. Unit cell parameters were determined

and refined on all reflections. Data reduction and correction for Lorentz polarization were performed using Saint-plus, and scaling and absorption correction were performed using the SADABS software package. Structure solution by direct methods and least-squares refinement on F^2 were performed using the SHELXTL software suite. Except where noted, non-hydrogen atoms were refined with anisotropic displacement parameters, while hydrogen atoms were placed in calculated positions and refined with a riding model. Structural figures were generated with ORTEP-3. During the refinement of **2-3**, the asymmetric unit was found to contain half an equivalent of diethyl ether, which was found to exhibit positional disorder that was treated satisfactorily. Due to this disorder within this solvate, hydrogen atoms on the solvate were omitted in the solution and refinement process.

Table 2-1. Crystallographic Solution and Refinement Data for **2-2a**, **2-2b**, **2-3** and **2-4**.

	2-2a	**2-2b**	**2-3**
Empirical formula	$C_{33}H_{47}N_2PRu$	$C_{37}H_{55}N_2PRu$	$C_{40}H_{55}N_2O_{1.5}PRu$
Wavelength (Å)	0.71073	0.71073	1.54178
Temperature (K)	173(2)	173(2)	173(2)
Formula weight	603.77	659.87	719.90
Crystal dimensions	0.40 x 0.29 x 0.17	0.34 x 0.07 x 0.04	0.25 x 0.23 x 0.14
Crystal system	Triclinic	monoclinic	monoclinic
Space group	*P*(-1)	$P2_1/n$	$P2_1/n$
a (Å)	9.5189(5)	14.4690(5)	12.1772(5)
b (Å)	10.5877(5)	16.2674(5)	15.7345(7)
c (Å)	15.5381(8)	14.9573(5)	19.4462(8)
α (deg)	101.607(1)	90	90
β (deg)	98.993(1)	102.87(1)	94.405(2)
γ (deg)	92.575(1)	90	90
V (Å^3)	1510.37(13)	3432.0(2)	3714.9(3)
Z	2	4	4
ρcalcd (Mg/m^3)	1.328	1.277	1.287
μ (mm^{-1})	0.596	0.530	4.072
Range of trans.	0.9076-0.7949	0.979-0.8416	0.5917-0.4353
θ limit (deg)	27.59	27.52	71.32
	$-12 \le h \le 12$	$-18 \le h \le 18$	$-14 \le h \le 14$
	$-13 \le k \le 13$	$-21 \le k \le 21$	$-19 \le k \le 19$
	$-20 \le l \le 20$	$-19 \le l \le 19$	$-23 \le l \le 23$
Total data collected	28597	30526	24246
Independent reflections	6961	7893	7204
R_{int}	0.0289	0.0414	0.0439
Data/restraints/parameters	6961 / 0 / 347	7893 / 0 / 385	7204 / 0 / 439
Goodness-of-fit	1.055	1.038	1.059
$R1$ [$F_o^2 \ge 2\sigma(F_o^2)$][a]	0.0242	0.0303	0.0418
$wR2$ [$F_o^2 \ge -3\sigma(F_o^2)$][a]	0.0558	0.0699	0.1110
Largest peak, hole (eÅ^{-3})	0.350, -0.394	0.442, -0.377	2.747, -0.560

[a] $R_1 = \Sigma| |F_o| - |F_c| |/\Sigma|F_o|$. $wR_2 = [\Sigma [w(F_o^2 - F_c^2)^2]/ \Sigma [w(F_o^2)^2]]^{1/2}$. $w = 1/[\sigma^2(F_o^2) + (mP)^2 + nP]$, where $P = (F_o^2 + 2F_c^2)/3$.

Table 2-1 Continued

	2-4
Empirical formula	$C_{42}H_{56}N_3PRu$
Wavelength (Å)	0.71073
Temperature (K)	173(2)
Formula weight	734.94
Crystal dimensions	0.44 x 0.31 x 0.07
Crystal system	triclinic
Space group	*P*(-1)
a (Å)	9.6910(6)
b (Å)	10.7791(7)
c (Å)	18.5223(12)
α (deg)	82.126(1)
β (deg)	89.982(1)
γ (deg)	73.472(1)
V (Å^3)	1835.9(2)
Z	2
ρcalcd (Mg/m^3)	1.329
μ (mm^{-1})	0.504
Range of trans.	0.9656-0.8083
θ limit (deg)	27.54
	$-12 \le h \le 12$
	$-13 \le k \le 14$
	$-23 \le l \le 24$
Total data collected	24290
Independent reflections	8369
R_{int}	0.0453
Data/restraints/parameters	8369 / 0 / 439
Goodness-of-fit	1.031
$R1$ [$F_o^2 \ge 2\sigma(F_o^2)$][a]	0.0383
$wR2$ [$F_o^2 \ge -3\sigma(F_o^2)$][a]	0.0757
Largest peak, hole (eÅ^{-3})	0.731, -0.644

[a]$R_1 = \Sigma| |F_o| - |F_c| |/\Sigma|F_o|$. w$R_2 = [\Sigma [w(F_o^2 - F_c^2)^2]/ \Sigma [w(F_o^2)^2]]^{1/2}$. $w = 1/[\sigma^2(F_o^2) + (mP)^2 + nP]$, where $P = (F_o^2 + 2F_c^2)/3$.

Table 2-2. Selected Interatomic Distances (Å) and Angles (º) for **2-2a**, **2-2b**, **2-3** and **2-4**.

	2-2a	**2-2b**	**2-3**[a]	**2-4**[b]
Ru-P	2.3679(5)	2.3599(5)	2.3652(6)	2.3578(7)
Ru-N(2)	2.0458(13)	2.0734(16)	2.199(2)	2.1823(19)
P-N(1)	1.7059(15)	1.6964(17)	1.668(2)	1.668(2)
N(1)-C(9)	1.305(2)	1.308(2)	1.322(3)	1.318(3)
(aryl)N(2)-C(9)	1.369(2)	1.374(3)	1.349(3)	1.348(3)
P-Ru-N(2)	77.00(4)	77.76(5)	76.20(6)	77.32(5)

[a]Ru-CO 1.844(3); RuC-O 1.147(4). [b]Ru-CN(xylyl) 1.878(3); [b]RuC-N(xylyl) 1.182(3).

CHAPTER 3: Synthesis and Reactivity of a Neutral, Three-Coordinate Platinum(II) Complex Featuring Terminal Amido Ligation

3.1 Introduction

Encouraged by the ability of *N*-phosphinoamidinate ligands to support low-coordinate Cp*Ru complexes (Chapter 2), attention was turned to the preparation of alternative classes of low-coordinate complexes that might exhibit new and possibly useful reactivity with substrate molecules. As part of this effort, the synthesis and study of platinum derivatives was pursued, based in part on the intriguing behavior of related (nacnac)Pt species (Section 1.4.2).

Low-coordinate platinum-group metal complexes are commonly invoked as key reactive intermediates in a range of prominent organometallic transformations.[78] Focusing on three-coordinate intermediates, these transformations include β-hydrogen elimination, C-H activation, thermal decomposition of dialkyls, insertion of olefins into Pt-H bonds, and electrophilic attack at Pt-C bonds, among others.[79] The (nacnac)Pt chemistry of Goldberg and co-workers described in Section 1.4.2 features both C-H activation and β-hydrogen elimination initiated by proposed three-coordinate Pt(II) intermediates.[42] The coordinatively unsaturated nature of these species leads to highly reactive intermediates, making their isolation a significant challenge (refer to Scheme 1-9 and 1-10 for examples of C-H activation and β-hydrogen elimination initiated by transient three-coordinate (nacnac)Pt complexes). Furthermore, the propensity of the monoanionic nacnac ligands to support such low-coordinate, reactive platinum species is encouraging, considering their structural and electronic similarities with the *N*-phosphinoamidinate ligands.

As alluded to above, there is considerable interest in preparing isolable examples of such otherwise transient species, so as to gain a more thorough appreciation of their structural and reactivity properties. While the conversion of stable four-coordinate (square planar), 16-electron complexes into highly reactive three-coordinate,[80] 14-electron species is a commonly invoked mechanistic paradigm in platinum chemistry,[81] isolable three-coordinate Pt(II) complexes have until recently proven elusive.[82] Indeed, the coordination chemistry of d^8 species of Pt(II) is almost exclusively dominated by square planar species. Notwithstanding the utility of "operationally" or "masked" three-coordinate Pt(II) compounds, such as those featuring a weak agostic interaction occupying the fourth coordination site where a C-H bond interacts with the metal center to form a three-center two electron bond (Figure 3-1),[83] the structural characterization of *bona fide* three-coordinate Pt(II) species is limited to reports by the groups of Braunschweig[84] and Conejero/Lledós[85] (**T** and **U**, Figure 3-2). In each of these systems, the three-coordinate Pt(II) motif is achieved *via* anion abstraction, resulting in (di)cationic complexes.

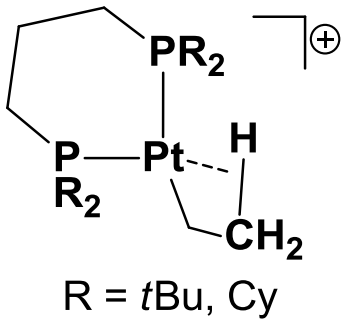

Figure 3-1. Early example of a "masked" three-coordinate Pt(II) complex featuring a weak agostic interaction occupying the fourth coordination site reported by Spencer and co-workers.[83d]

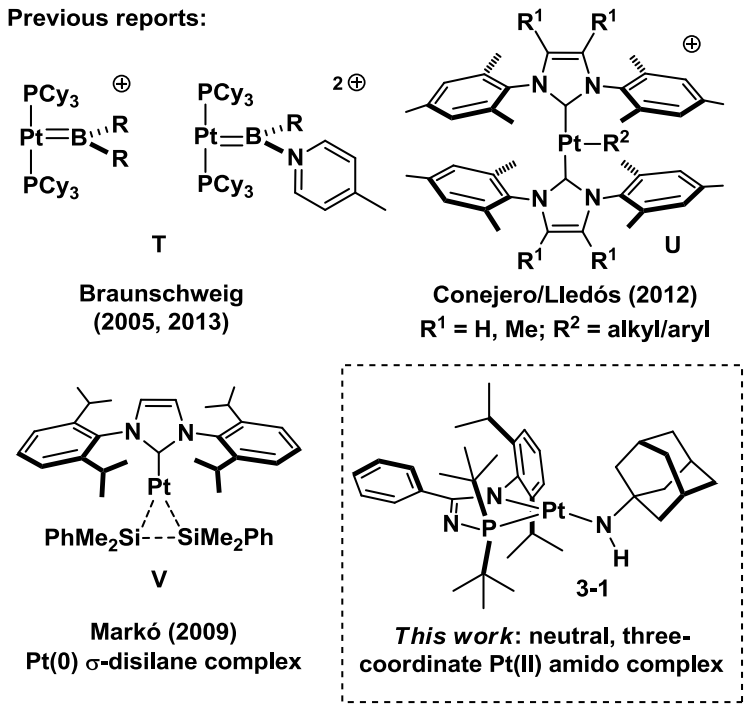

Figure 3-2. Previously reported low-coordinate platinum complexes (**T**–**V**), and the three-coordinate, formally 14-electron Pt(II) amido complex **3-1** featured here.

Both **T** and **U** adopt T-shaped geometries, in keeping with calculations that predict the electronic stabilization of a T-shaped structure for low-spin Pt(II).[82] The favored T-shaped molecular orbital diagram can be qualitatively derived by envisioning the removal of a ligand from the preferred square planar geometry for four-coordinate Pt(II) species resulting in minimal changes to the orbital energies. While the apparently Y-shaped neutral Pt(II) complex [(*i*Pr)Pt($SiMe_2Ph$)$_2$] **V** has been described in the literature,[86] subsequent analysis suggests that this complex is more appropriately viewed as a Pt(0) σ-disilane species (Figure 3-2).[87] By comparison, isolable three-coordinate, formally 14-electron Pt(II) complexes featuring terminal amido ligation have yet to be reported in the literature, owing in part to the considerable synthetic challenges associated with preparing monomeric (non-bridging) species of this type. Notably, such compounds are anticipated to be chemically distinct from **T** and **U**, due to the potential

for repulsive interactions between the amido lone pair and the Pt(II) d^8 metal center.[88] Reactivity and computational investigations of such under-explored Pt(II) amido compounds are of particular significance, in that they would serve to advance our fundamental understanding of the chemical behavior of such low-coordinate, non-dative Pt-N species, as well as to provide the basis for developing new catalytic substrate transformations of nitrogen compounds to complement existing methodologies (e.g., hydroamination, Buchwald-Hartwig amination). In the context of hydroamination, one could envision the development of a protocol involving a three-coordinate Pt(II) amido species that could insert an alkene into the Pt-N bond, followed by oxidative addition of the desired amine, and subsequent reductive elimination of the hydroaminated product (Scheme 3-1); alternative processes involving protection of the alkyl could also be envisioned. Additionally, Gunnoe and co-workers have previously reported reactivity with four-coordinate Pt(II) diamido complexes that can readily cleave H_2 across the Pt-N bond and have proposed that 1,2 C-H addition across this bond could also be feasible with a three-coordinate Pt amido.[88e, 89]

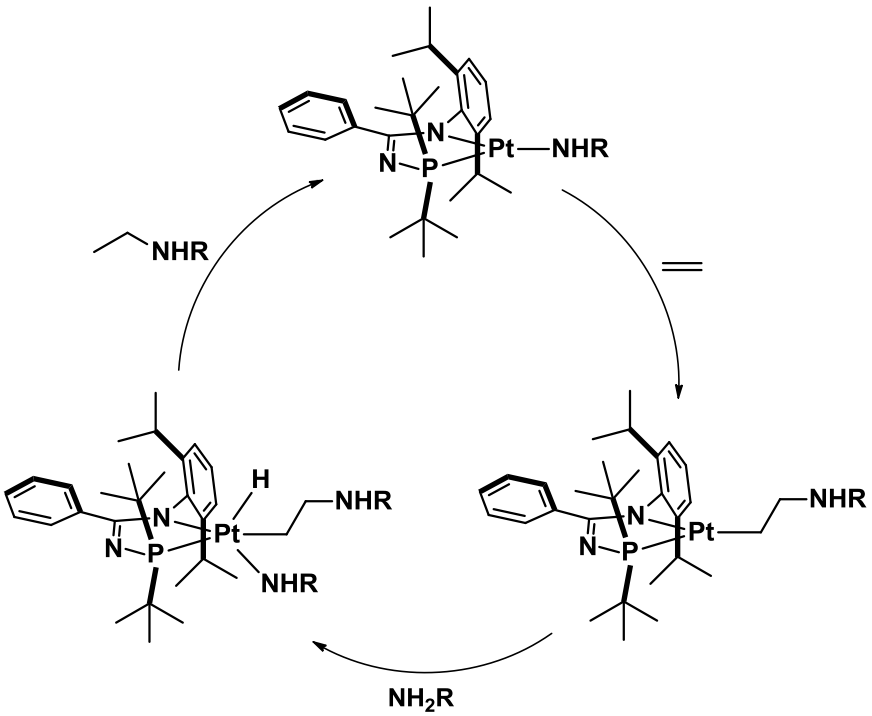

Scheme 3-1. Potential hydroamination mechanism utilizing a three-coordinate Pt amido species supported by the *N*-phosphinoamidinate ligand, **2-1b**.

In this regard, Hartwig and Wolfe have only recently reported the first examples of alkene insertion into Pd-N bonds.[90,91] Notably, the mechanism proposed by Hartwig and co-workers shown in Scheme 3-2 begins with dissociation of THF to form a three-coordinate Pd amide species. This three-coordinate intermediate binds ethylene affording an olefin amido species that undergoes migratory insertion of the alkene into the Pd-N bond followed by β-hydrogen elimination to release the enamine and form a Pd-H species that rapidly decomposes.

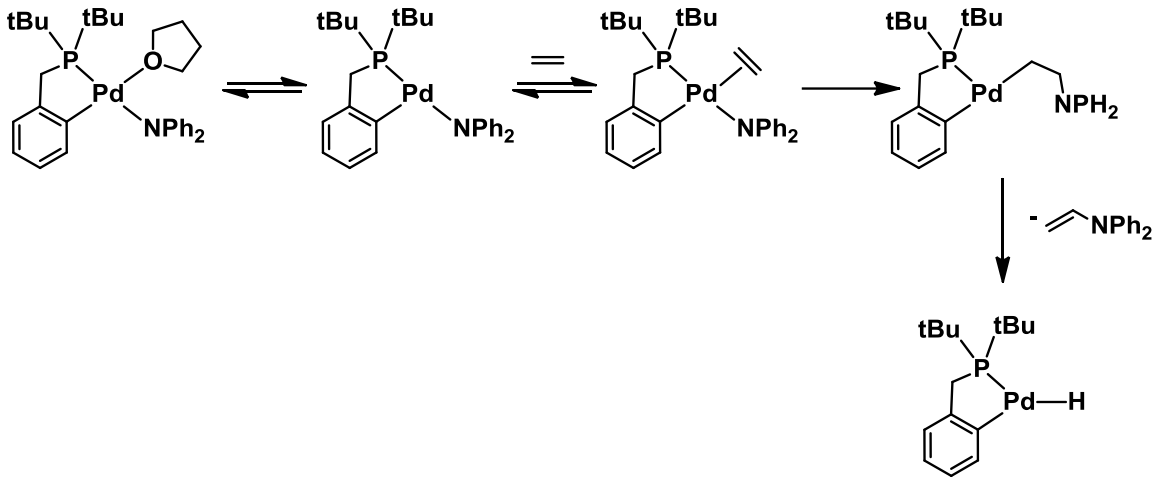

Scheme 3-2. Proposed mechanism for the intermolecular migratory insertion of ethylene into a Pd-N bond.

In this chapter the first isolable and crystallographically characterized three-coordinate Pt(II) complex featuring terminal amido ligation (**3-1**) is presented, which is achieved by use of a sterically demanding *N*-phosphinoamidinate ancillary co-ligand. Density functional theory (DFT) calculations suggest relatively weak amide lone pair-to-Pt π-donation and support a 14-electron assignment for **3-1**. Stoichiometric reactivity studies confirm the viability of net O-H and C-H additions across, as well as isonitrile insertion into, the Pt-NH(1-Ad) linkage of the formally 14-electron complex **3-1**. DFT calculations also provide insight into the reactivity and mechanisms of such O-H and C-H addition reactions.

3.2 Results and Discussion

3.2.1 Synthesis and Characterization of Platinum Amido Species

Initial synthetic investigations explored ligating the protonated *N*-phosphinoamidine ligand **2-1b** to platinum to generate useful precursors to a three-coordinate Pt(II) complex beginning with the synthesis of a dichloride dimer **3-2**.

Treatment of (COD)$PtCl_2$ with **2-1b**, followed by *in situ* HCl removal with Cs_2CO_3 afforded the desired dimer **3-2** in 60% isolated yield (Scheme 3-3). The structure of **3-2** was established on the basis of NMR data and confirmed by X-ray crystallography (Figure 3-3).

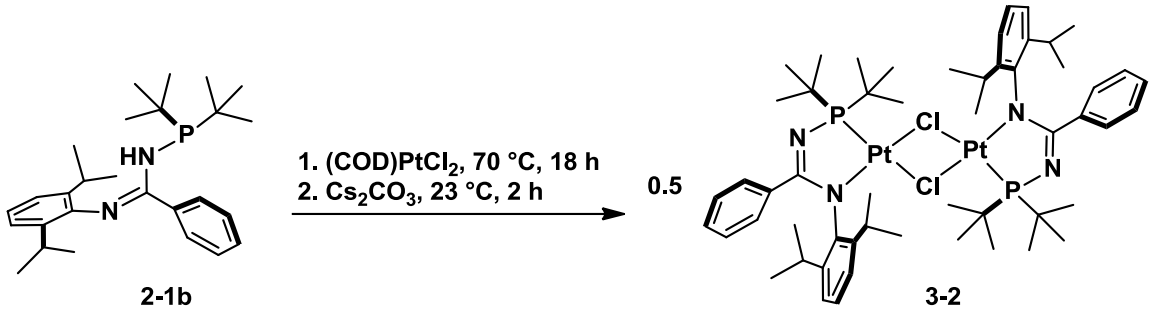

Scheme 3-3. Synthesis of the dichloride dimer **3-2**.

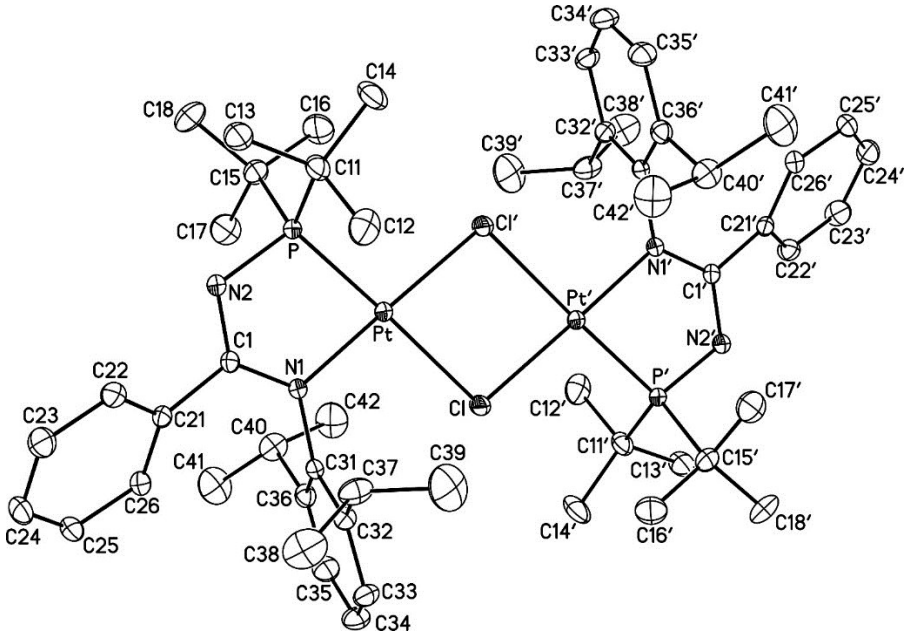

Figure 3-3. Crystallographically determined structures of **3-2.** Non-hydrogen atoms are represented by 30% Gaussian ellipsoids. Hydrogen atoms omitted for clarity.

One could envision that reactions designed to cleave **3-2** by selectively abstracting the halide atoms could offer a useful entry point toward synthesizing various low-coordinate platinum complexes. In particular, by using bulky lithium amides, the

dimer could be cleaved via halide abstraction to yield neutral three-coordinate Pt(II) amido complexes, anticipating that steric bulk from the amido, in harmony with the strongly donating and sterically demanding monoanionic P,N ligand **2-1b**, could provide sufficient electron density and steric protection to stabilize a three-coordinate Pt(II) complex. Upon reacting **3-2** with 2,6-dimethyl anilide, the immediate formation of a new product **3-3** was detected on the basis of ^{31}P NMR (δ 85.0, $^{1}J_{PtP}$ = 3533 Hz); this first formed product slowly and cleanly converted to a new phosphorus-containing species **3-4** (^{31}P = δ 92.5, $^{1}J_{PtP}$ = 3995 Hz). Attempts to crystallize **3-4** resulted in crystals that were twinned and could not be fully characterized. However, the connectivity information that could be obtained (Figure 3-4) suggests that upon ligation of the amide to give putative **3-3**, the complex underwent C-H activation of one of the peripheral methyl groups to afford what the X-ray data suggests is **3-4** (Scheme 3-4). A similar result was also observed on the basis of ^{31}P NMR when **3-2** was exposed to the bulkier 2,6 diisopropyl anilide, however, no crystals suitable for refraction could be obtained of this material.

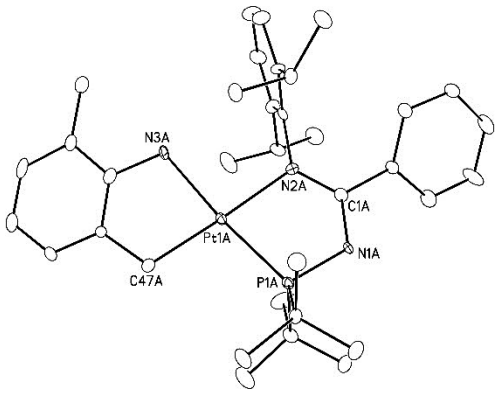

Figure 3-4. Proposed final product **3-4** from the reaction of **3-2** with 2 equivalents of 2,6 dimethyl anilide as determined by X-ray crystallography.

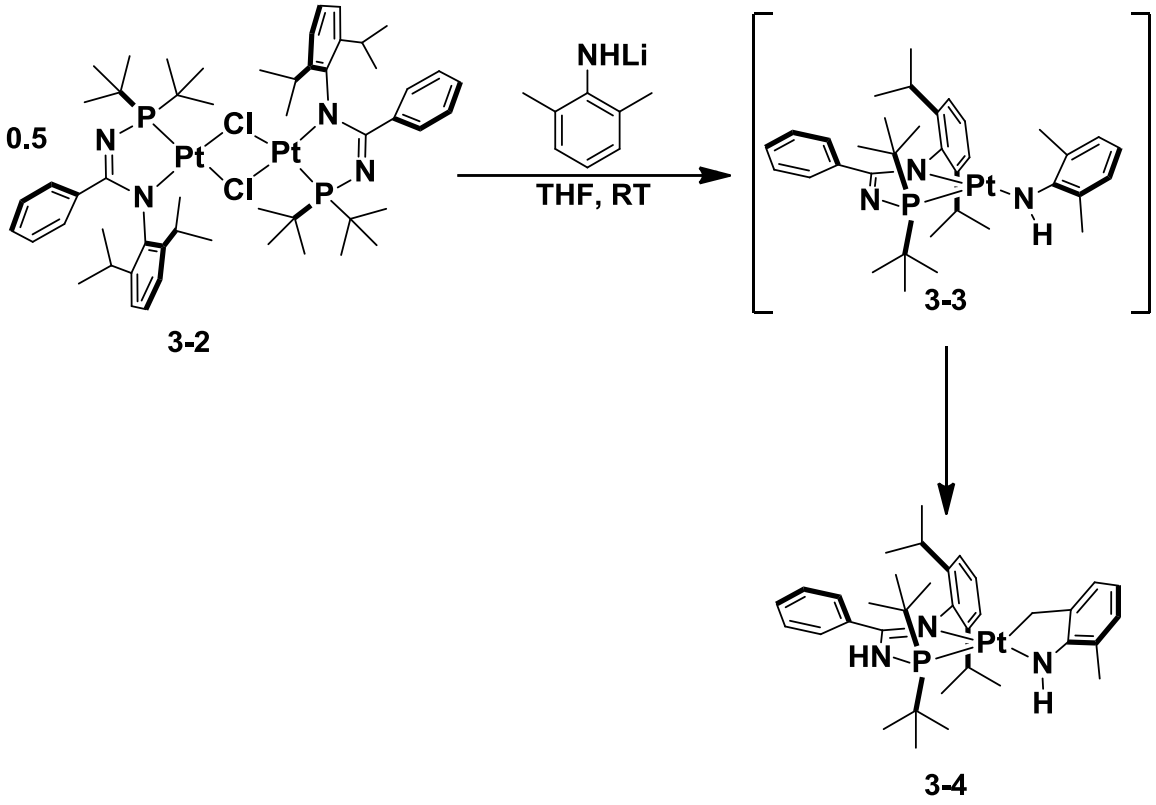

Scheme 3-4. Proposed scheme for the reaction of **3-2** with 2 equivalents of 2,6 dimethyl anilide, involving conversion of **3-3** to **3-4**.

Although the apparent formation of **3-4** was both encouraging and interesting, it did not satisfy the search for an isolable three-coordinate platinum complex. In order to prevent metallation, the bulkier adamantyl amide was selected as it did not have any easily accessibly C-H bonds relative to 2,6-dimethyl or diisopropyl anilide. The synthetic route to the targeted three-coordinate Pt(II) amido complex **3-1** is presented in Scheme 3-5.

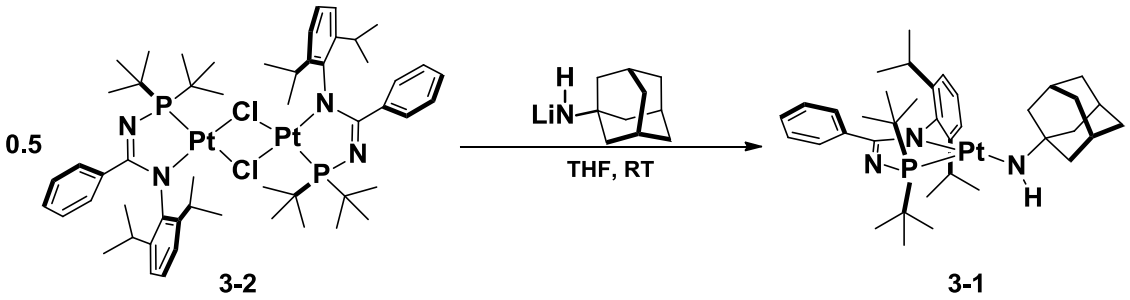

Scheme 3-5. Synthesis of the neutral, three-coordinate, 14-electron Pt(II) amido species **3-1.**

Treatment of 0.5 equiv of **3-2** with LiNH(1-adamantyl) afforded **3-1** as an orange solid in 75% isolated yield. Both NMR and elemental analysis data support the view of **3-1** as being a species of empirical formula [(P,N)Pt(NH(1-Ad))], lacking additional co-ligands. Subsequent crystallographic characterization established the identity of **3-1** as being a three-coordinate Pt(II) complex featuring terminal (1-adamantyl)amido ligation (Figure 3-5).

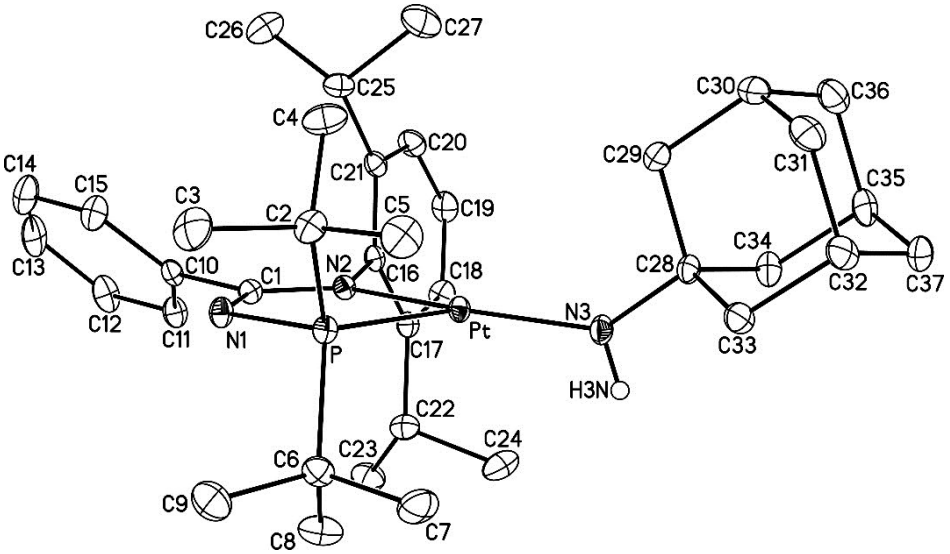

Figure 3-5. Crystallographically determined structures of **3-1.** Non-hydrogen atoms are represented by 30% Gaussian ellipsoids. Hydrogen atoms with the exception of the amido N*H* are omitted for clarity.

The coordination geometry at platinum in **3-1** deviates significantly from the T-shaped configuration observed for **T** and **U**, owing in part to the steric demands of the

chelating *N*-phosphinoamidinate ligand (P-Pt-N2 bite angle of 77.88(5)º). Furthermore, the inequivalent P-Pt-N3(Ad) (129.82(7)º) and N2(aryl)-Pt-N3(Ad) (151.77(9)º) angles ($\Sigma_{L\text{-}Pt\text{-}L}$ 359.5º) indicate that the geometry about platinum in **3-1** also cannot simply be described as being trigonal or Y-shaped. No other crystallographically characterized Pt(II)-NH(alkyl) complex (three- or four-coordinate) has been reported previously. Hartwig and co-workers have detailed a series of T-shaped three-coordinate LPd(aryl)(NAr_2) complexes supported by a bulky phosphine ligand (Figure 3-6).[92] L-Pd-N (166.00(9)-170.66(7) °) and C-Pd-N (88.75(11)-93.60(14) °) angles showed much closer agreement to a T-shaped assignment than **3-1** even with the bulky nature of the supporting phosphine ligand further suggesting that geometry of **3-1** was being strongly influenced by the bidentate *N*-phosphinoamidinate ligand.

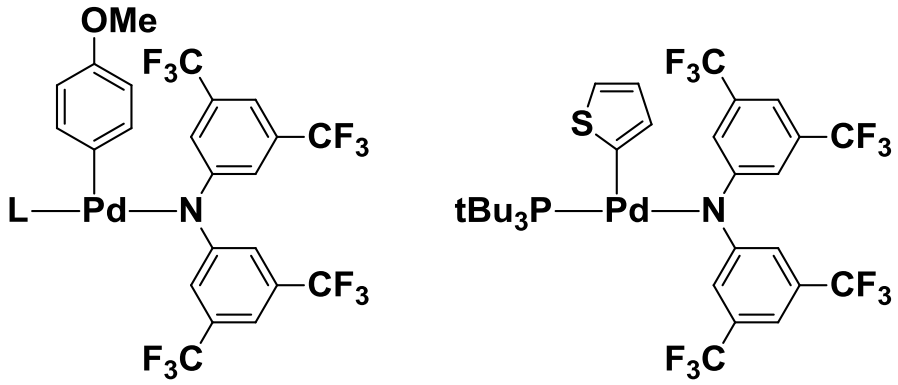

L = P*t*Bu$_3$, Ph$_5$FcP*t*Bu$_2$, FcP*t*Bu$_2$

Figure 3-6. T-shaped three-coordinate LPd(aryl)(amido) species.

A survey of crystallographically characterized four-coordinate Pt(II)-NH(aryl) complexes revealed Pt-N_{amido} distances (1.984(5)-2.125(5) Å)[89, 93] that are statistically longer than the Pt-NH(1-Ad) distance found in **3-1** (1.914(2) Å). Although **3-1** proved to be unstable in air, no decomposition was observed upon heating THF solutions of **3-1** at 75 ºC over the course of 72 h on the basis of ^{31}P NMR analysis.

In an effort to evaluate possible $Pt_{d\pi}$-$N(1\text{-}Ad)_{\pi}$ interactions in **3-1**, a variable-temperature solution ^1H NMR (300 MHz) study was conducted. At room temperature, **3-1** exhibits sharp C-H resonances and effective C_S symmetry that renders the isopropyl methine protons equivalent on the NMR timescale, in keeping with rapid rotation about the Pt-NH(1-Ad) bond. Upon cooling, decoalescence of the methine signal occurs (T_C = -65 ºC), with two somewhat broad methine proton signals observed at -80 ºC (Figure 3-7). Analysis of these NMR lineshape changes using the Gutowsky-Holm approximation[94] yields an estimated $\Delta G^{\ddagger}$ value of 9.8 kcal/mol. This value is intermediate between those reported by Gunnoe and co-workers for hindered Ru-N bond rotation in TpRu(L)(L')(NHPh) complexes (< 9 kcal/mol for L = L' = $P(OMe)_3$; 12 kcal/mol for L = CO, L' = PPh_3), which is remarkable given the three-coordinate nature of the alkylamido complex **3-1** relative to these octahedral, 18-electron complexes, and in light of competing RuN-Ph π-bonding, which serves to further disrupt potential $Ru_{d\pi}$-NPh_{π} bonding interactions.[95] These observations, along with the DFT results (*vide infra*), suggest the barrier to bond rotation of Pt-N is considerably small and supports the absence of a strong Pt-NH(1-Ad) multiple bond in **3-1**.

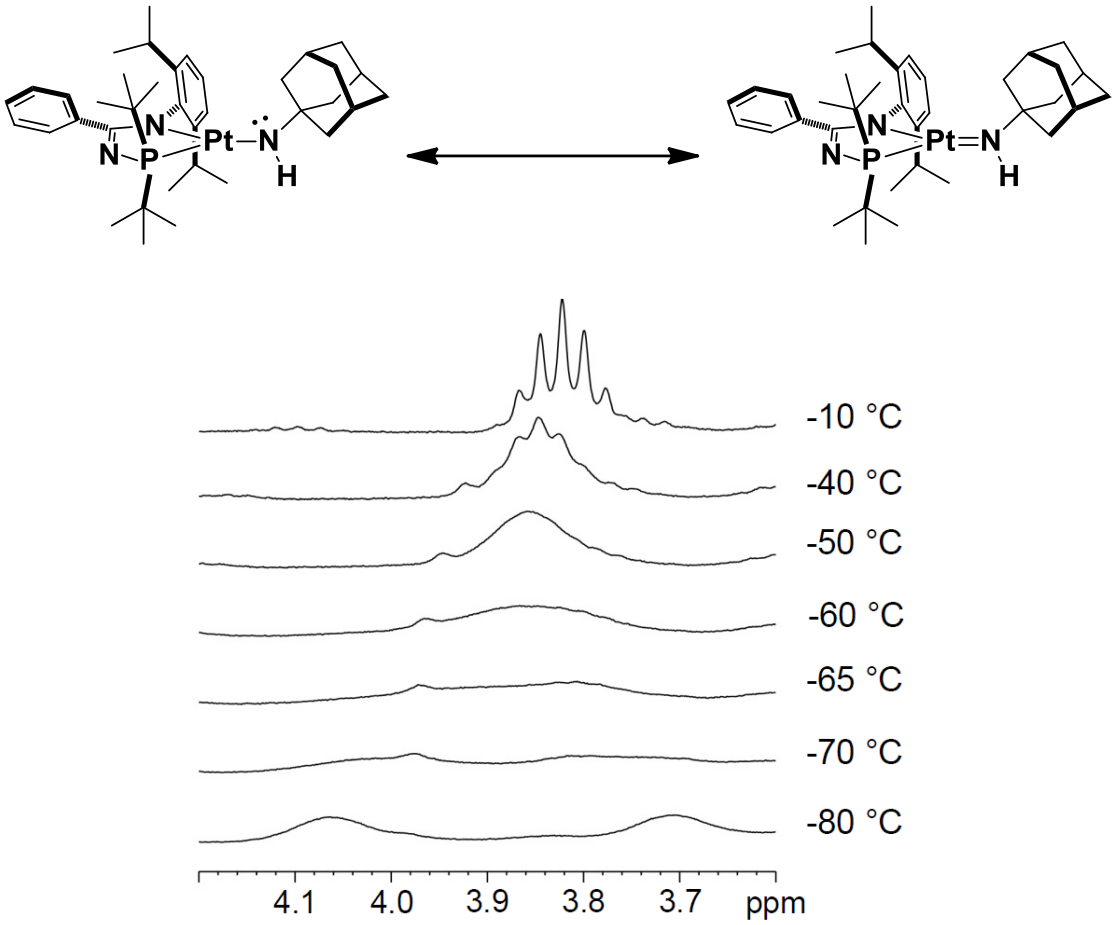

Figure 3-7. Variable-temperature ^{1}H NMR data for **3-1** (300 MHz, toluene-d_8) investigating the possible $Pt_{d\pi}$-N(1-Ad)$_{\pi}$ interactions shown above.

*3.2.2 Probing the Reactivity of **3-1***

The migratory insertion of unsaturated substrates (e.g. alkenes, alkynes, isonitriles) into late metal-amido linkages represents a potentially useful elementary step in the functionalization of organonitrogen compounds and is uncommon in Pt-amido chemistry (see Section 3.1; Scheme 3-2 for recent developments in Pd-amido migratory insertion of alkenes).[88d, 96] In a preliminary effort to ascertain if such insertion chemistry was feasible in the present system, **3-1** was treated with 2,6-xylyl isocyanide (2 equiv). Gratifyingly, the resulting platinum-functionalized amidine **3-5** was isolated as an analytically pure yellow solid (Scheme 3-6). The connectivity within **3-5**, as observed in

the crystal structure (Figure 3-8), can be viewed as arising from desired 1,1-insertion of isonitrile into the Pt-NH(1-Ad) linkage of **3-1**, followed by tautomerization and coordination of a second equivalent of isonitrile. It should be noted that performing this reaction with 1 equiv. of 2,6-xylyl isocyanide led to a mixture of products, suggesting that the coordination of a second equivalent of isonitrile was required to ensure stability of the resultant complex and/or that the kinetics of binding the second equivalent is fast. Attempts to extend this chemistry to unsaturated C-C bonds utilizing activated reagents such as diphenylacetylene were unsuccessful.

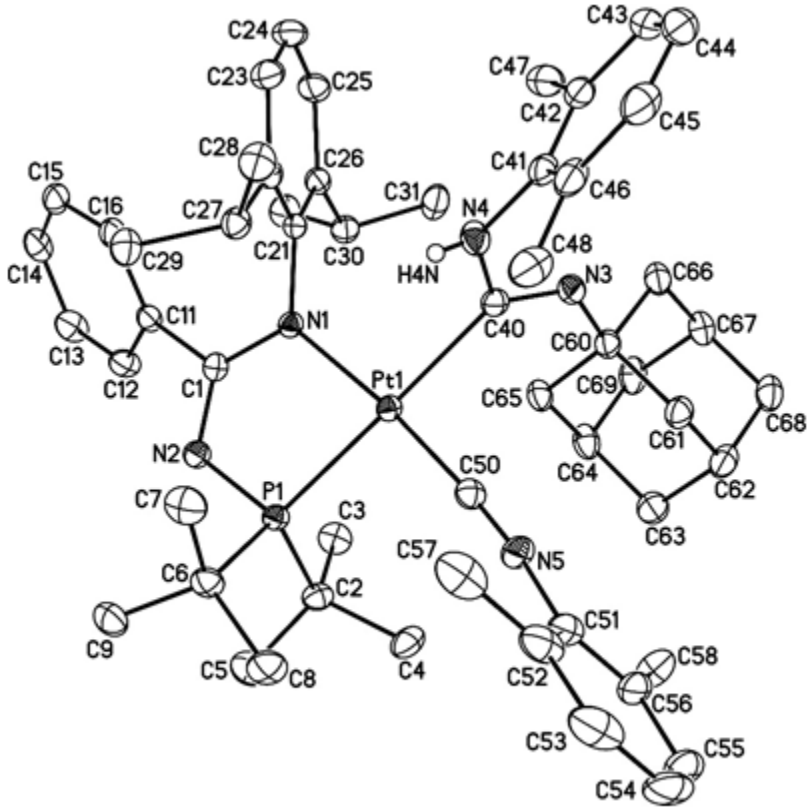

3-5

Figure 3-8. Crystallographically determined structures of **3-5**. Non-hydrogen atoms are represented by 30% Gaussian ellipsoids. Hydrogen atoms with the exception of the H4N hydrogens are omitted for clarity.

There is considerable interest in exploiting 1,2-E-H bond additions (E = main group element) across late metal-amido fragments in the development of new substrate transformations.[88] In this regard, the basic and nucleophilic character of terminal amido groups within four-coordinate formally 16-electron Pt(II) amido complexes, which arises due to disruption of nitrogen-to-platinum π-bonding, has been established.[89a] However, given the view of three-coordinate **3-1** as being a formally 14-electron species on the basis of NMR and DFT data (*vide infra*), it is feasible to envision that analogous E-H bond additions would be inhibited by the expected propensity of **3-1** to simply bind two-electron donors. In an initial test of this hypothesis, **3-1** was treated with 2,6-xylenol (Scheme 3-6); from this reaction mixture analytically pure [(P,N)Pt(O-2,6-xylyl)(NH_2(1-Ad))] **3-6**, arising from net O-H bond addition across the Pt-NH(1-Ad) linkage of **3-1**, was obtained as a pale yellow solid. The crystal structure of the formally 16-electron Pt(II) complex **3-6** (Figure 3-9) features a Pt-NH_2(1-Ad) distance of 2.108(2) Å, which is notably longer (~0.2 Å) than the Pt-NH(1-Ad) distance found in **3-1** suggesting a weaker Pt-N bond. This could be potentially explained by increased steric crowding around the metal center or the reduced donating ability of NH_2(1-Ad). The Pt-O(2,6-xylyl) distance in **3-6** (2.0760(17) Å) falls within the range observed in some other four-coordinate, formally 16-electron Pt(II) aryloxy complexes.[89a, 93a, 97]

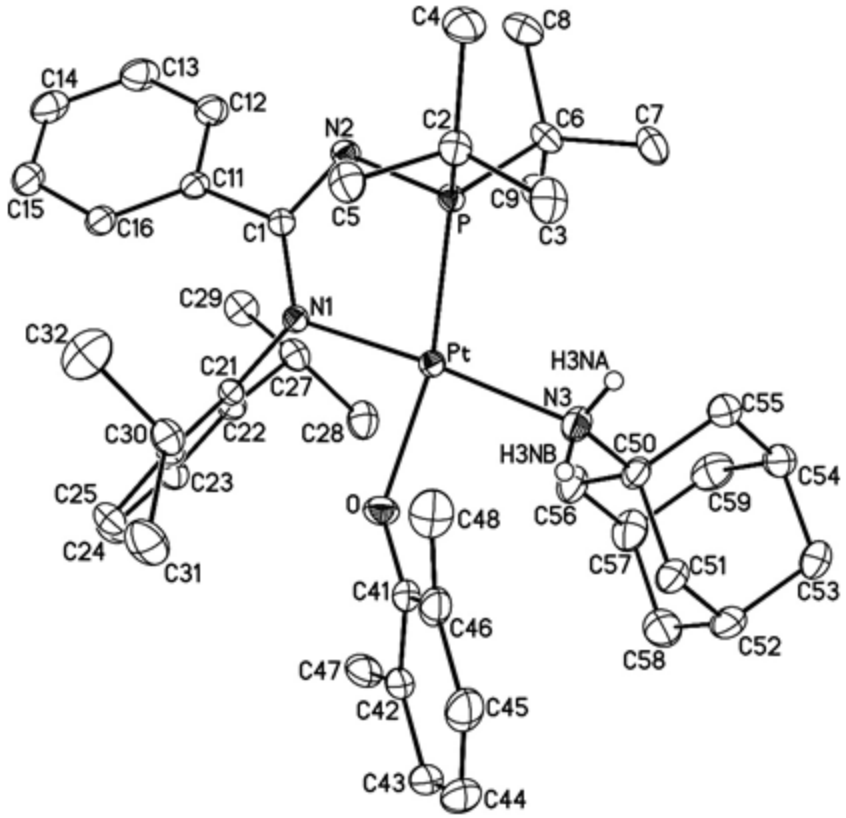

3-6

Figure 3-9. Crystallographically determined structures of **3-6**. Non-hydrogen atoms are represented by 30% Gaussian ellipsoids. Hydrogen atoms with the exception of the H3NA/H3NB are omitted for clarity.

Encouraged by the observed net O-H bond addition across the Pt-NH(1-Ad) linkage of **3-1**, attention was turned to exploring the reactivity of **3-1** with cyclohexylallene, given the dual propensity of allenes to participate in migratory insertion reactions, as well as to undergo deprotonation by Brønsted bases.[98] Exposure of **3-1** to cyclohexylallene enabled the isolation of analytically pure pale yellow **3-7** (Scheme 3-6); single-crystal X-ray data (Figure 3-10) and solution NMR data support the identification of **3-7** as the depicted alkynyl methyl species (Figure 3-11).

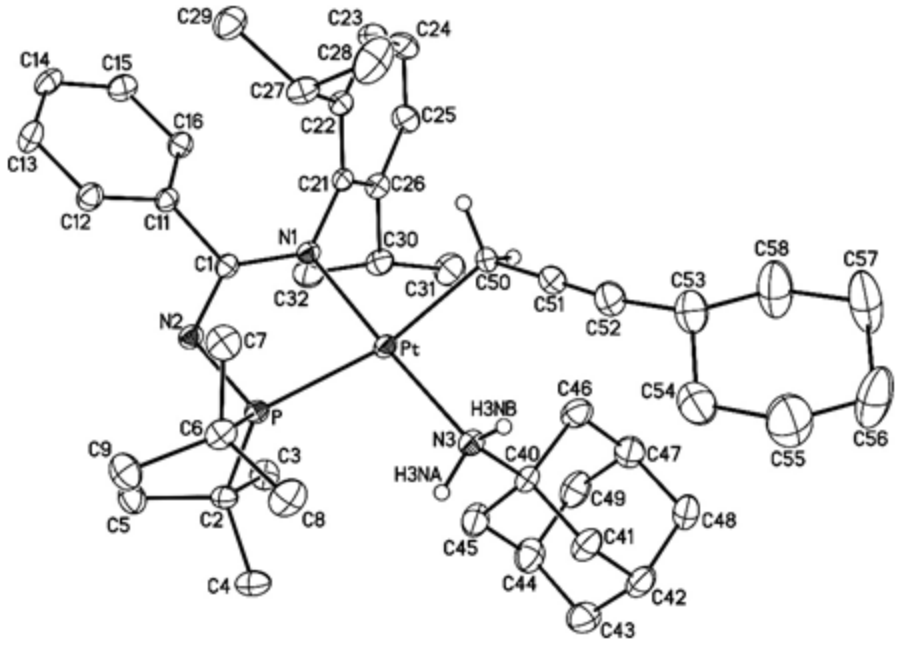

3-7

Figure 3-10. Crystallographically determined structures of **3-7**. Non-hydrogen atoms are represented by 30% Gaussian ellipsoids. Most hydrogen atoms are omitted for clarity.

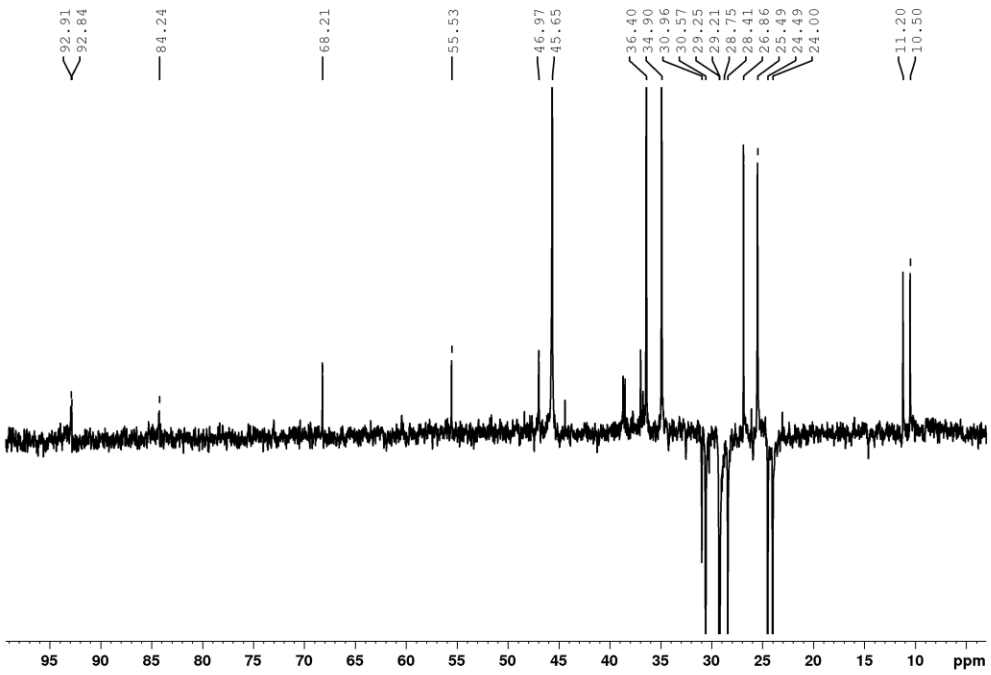

Figure 3-11. ^{13}C DeptQ 135 NMR spectrum of **3-7**, aryl region is omitted for clarity. Diagnostic signals: 92.9 (d, $CH_2C{\equiv}CCy$, $^3J_{CP}$ = 9 Hz), 84.2 ($CH_2C{\equiv}CCy$), 10.9 (d, $PtCH_2$, $^2J_{CP}$ = 88 Hz).

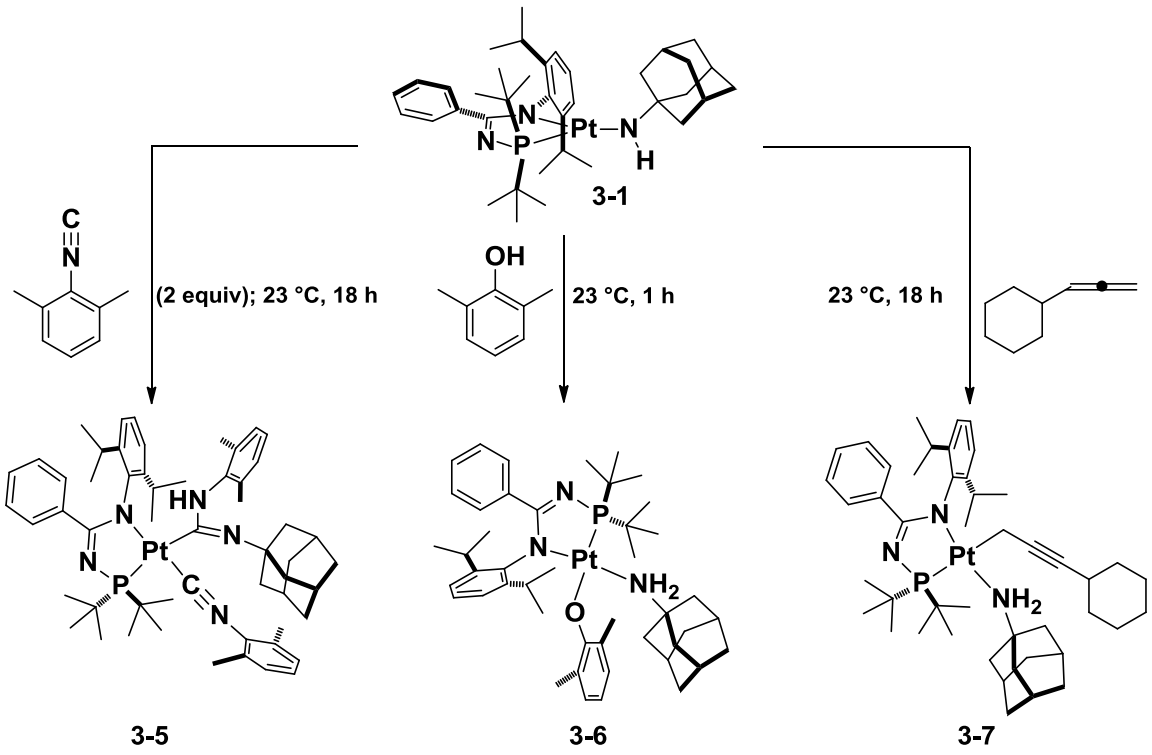

Scheme 3-6. Synthesis of **3-5**, **3-6**, and **3-7** from **3-1**

3.2.3 Computational Investigations

To examine the unique bonding of **3-1** and the mechanisms/activation barriers for phenol O-H and allene C-H bond additions across the Pt-NH(1-Ad) group DFT calculations were carried out in Gaussian 09. The free energies (and enthalpies in parenthesis) reported refer to M06/6-311+G(2d,p)[LANL2TZ(f)]//M06//6-31G(d,p)[LANL2DZ] (see the experimental details at the end of this chapter). This methodology provides geometries very close to the crystal structures of **3-1**, **3-5**, **3-6**, and **3-7**. For example, calculated Pt-C, Pt-N, Pt-O, and Pt-P distances deviate by an average of only 0.05 Å and the P-Pt-N2 and P-Pt-N3(Ad) angles in **3-1** differ by ~4°. For all reaction pathways examined solvation was incorporated using the implicit SMD model of n-pentane.

While **3-1** is formally a 14-electron Pt(II) complex there is the possibility that the NH(1-Ad) amido group can donate an electron pair to the platinum center, which corresponds to Pt-NHR ↔ Pt=NHR resonance and an increase in electron count around platinum (Figure 3-7). Variable temperature NMR analysis of **3-1** suggested that such bonding interactions were negligible (Section 3.2.1; Figure 3-7). Inspection of the M06 molecular orbitals (Figure 3-12) indeed shows overlap of the NH(1-Ad) amido electron pair with the platinum metal center in the highest occupied molecular orbital (HOMO), but the wavefunction has a significant degree of localization on the amido nitrogen. This suggests that **3-1** is best described as a 14-electron complex. There is also the possibility that the nitrogen from the P,N-ligand results in π donation to Pt; however, there is overall a N_{π}-$Pt_{d\pi}$ antibonding interaction.

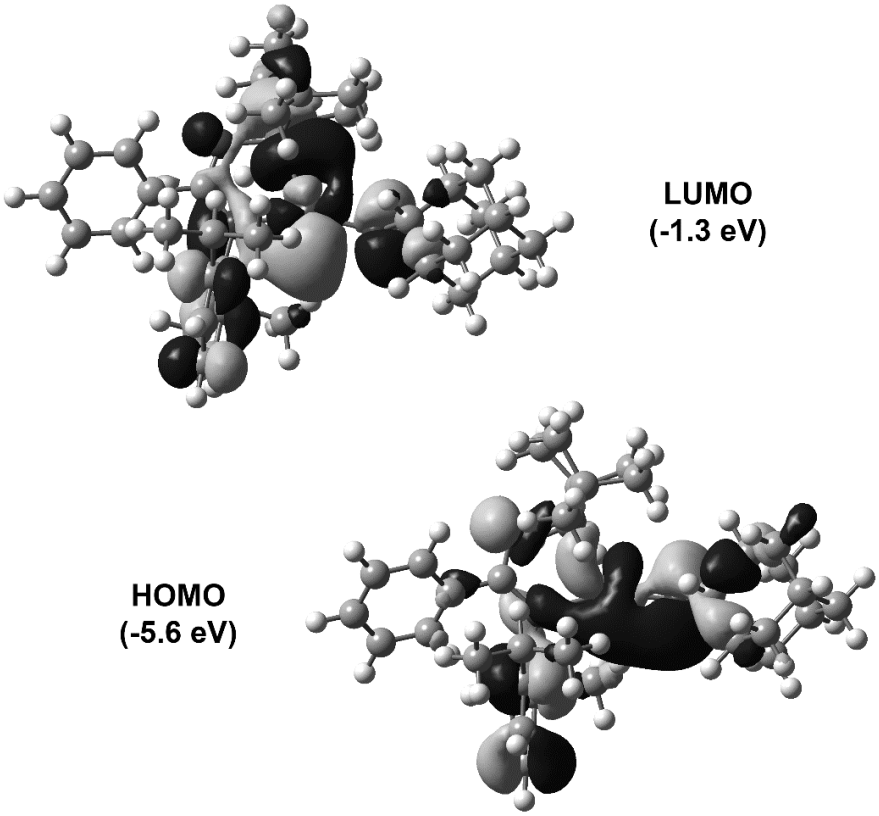

Figure 3-12. HOMO and LUMO orbitals for **3-1**.

The reaction of 2,6-xylenol with **3-1** leads to the Pt(II) aryloxy complex **3-6** by net O-H bond addition across the Pt-N bond (Scheme 3-5). Despite significant searching a stable π-coordination between 2,6-xylenol and 3-1 could not be located. Instead, there is an O-coordination complex that precedes O-H bond addition and leads to ***TS1*** (Figure 3-13) with $\Delta G^{\ddagger}$ = 12.5 kcal/mol relative to separated reactants. ***TS1*** is similar to other 1,2-addition reactions to metal-amido complexes and involves simultaneous phenol deprotonation and formation of the Pt-OAr bond. The polar nature of the breaking O-H bond and forming N-H suggests that this transition state is probably best described as an intramolecular proton transfer followed by an ion-pair collapse to form the Pt-O bond. Intrinsic reaction coordinate (IRC) calculations indicate that ***TS1*** directly connects **3-4** with the O-coordination complex and no intervening species. Intermolecular proton transfer and an oxidative addition/reductive elimination sequence was also examined. Both of these pathways were found to be higher in energy versus the pathway involving ***TS1***.

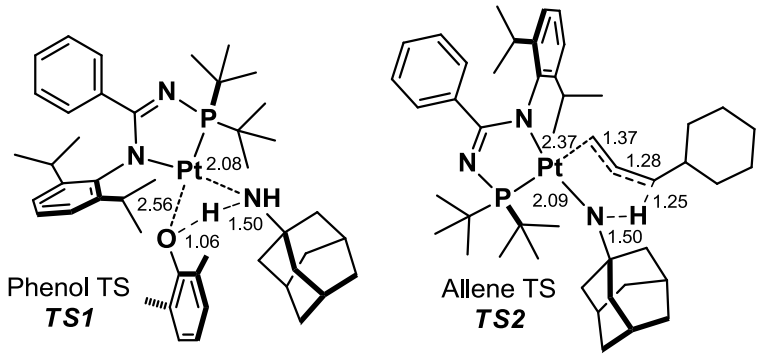

Figure 3-13. Transition-state structures for **3-6** and **3-7** with bond lengths in Å.

Cyclohexylallene C-H addition to **3-1** leads to the Pt(II) alkynyl complex **3-7** (Scheme 3-5). Similar to the reaction with 2,6-xylenol, the reaction pathways for intermolecular proton transfer and oxidative addition/reductive elimination between

cyclohexylallene and **3-1** are not energetically viable. The lowest energy reaction pathway identified that leads to **3-7** occurs by ***TS2*** (Figure 3-13) with $\Delta G^{\ddagger}$ = 22.3 ($\Delta H^{\ddagger}$ 4.5) kcal/mol relative to reactants. This transition state involves concomitant C-H deprotonation by the terminal NH(1-Ad) fragment, allene to alkyne π electron rearrangement, and nucleophilic attack of the allene CH_2 terminus to the platinum metal center.

3.3 Conclusions

In summary, an unprecedented three-coordinate Pt(II) complex (**3-1**) featuring terminal amido ligation was prepared and characterized by use of NMR spectroscopic, X-ray crystallographic, and DFT methods. No evidence for strong stabilizing agostic interactions was found and both NMR spectroscopic and DFT analysis supports a 14-electron formulation with minimal Pt-N π bonding. Net O-H and C-H additions across, as well as isonitrile insertion into, the terminal Pt-amido linkage of **3-1** were observed. The coordinative/electronic unsaturation of the platinum amido species **3-1** described herein makes it an attractive precursor for investigations of intermolecular substrate activation and functionalization. Additional comments with respect to future work utilizing **3-1** and complexes of this nature will be detailed in Chapter 6.

3.4 Statement of Contributions

Several researchers helped to bring this project to publication in *Angewandte Chemie* and they are recognized herein. Doo-Hyun Kwan and Daniel H. Ess of Brigham Young University were responsible for all computational work featured in this chapter. Michael J. Ferguson of the University of Alberta was responsible for X-ray crystallography data collection and structure elucidation.

3.5 Experimental Details

General Considerations. All experiments were conducted under nitrogen in an MBraun® glovebox or using standard Schlenk techniques. Dry, oxygen-free solvents were used unless otherwise indicated. Benzene, toluene and pentane were deoxygenated and dried by sparging with nitrogen and subsequent passage through a double-column solvent purification system purchased from MBraun® Inc. Tetrahydrofuran and diethyl ether were purified by distillation from Na/benzophenone. All purified solvents were stored over 4 Å molecular sieves. Benzene-d_6 was degassed via three freeze-pump-thaw cycles and stored over 4 Å molecular sieves. All reagents were purchased from commercial suppliers and used without further purification. Throughout, Ad is used as an abbreviation for 1-adamantyl. ^{1}H, ^{13}C, and ^{31}P NMR characterization data were collected at 300K on a Bruker® AV-500 spectrometer operating at 500.1, 125.7, and 202.5 MHz (respectively) with chemical shifts reported in parts per million downfield of $SiMe_4$ for ^{1}H and ^{13}C, and 85% H_3PO_4 in D_2O for ^{31}P. ^{1}H and ^{13}C NMR chemical shift assignments are based on data obtained from ^{13}C-DEPTQ135, ^{1}H-^{1}H COSY, ^{1}H-^{13}C HSQC, and ^{1}H-^{13}C HMBC NMR experiments. In some cases, fewer than expected unique ^{13}C NMR resonances were observed, despite prolonged acquisition times. In the syntheses of **3-5**, **3-6**, and **3-7** the reported yields correspond to isolated analytically pure material; ^{31}P{^{1}H} NMR analysis of the corresponding reactions in progress revealed ≥80% conversion to the desired products.

Synthesis of 3-1. A room temperature solution of **3-2** (0.21 g, 0.16 mmol) in ca. 5 mL of THF was treated with a solution of LiNHAd (0.051 g, 0.32 mmol) in ca. 1 mL of THF. A color change from yellow to orange was noted immediately upon addition. The reaction

mixture was allowed to stand at room temperature for 1 hour. The volatile components of the reaction mixture were then removed *in vacuo* to afford an orange solid. The solid residue was triturated with pentane (3 × 1 mL) and then redissolved in ca. 5 mL of benzene. The benzene solution was filtered through Celite® and evaporated to dryness. The remaining solid residue was once again triturated with pentane (3 × 1 mL) and dried under vacuum to afford **3-1** as an orange solid (0.19 g, 75%). ^{1}H NMR (500 MHz, benzene-d_6): δ 7.62 (d, 2 H, J_{HH} = 7 Hz, H_{arom}), 7.04 - 6.98 (overlapping resonances, 3 H, H_{arom}), 6.93 - 6.87 (overlapping resonances, 3 H, H_{arom}), 4.94 (br d, 1 H, $^{3}J_{HP}$ = 8 Hz, NH), 3.85 (sept, 2 H, $^{3}J_{HH}$ = 7 Hz, C*H*Me$_2$), 1.95 (br s, 3 H, H_{Ad}), 1.60 - 1.55 (overlapping resonances, 12 H, H_{Ad} + CH*Me*$_2$), 1.54 - 1.47 (overlapping resonances, 24 H, H_{Ad} + P*tBu*), 1.04 (d, 6 H, $^{3}J_{HH}$ = 7 Hz, CH*Me*$_2$). ^{13}C{^{1}H} NMR (125.7 MHz, benzene-d_6): δ 177.39 (C_{arom}), 146.0 (C_{arom}), 145.6 (C_{arom}), 131.2 (CH_{arom}), 129.6 (CH_{arom}), 127.8 (CH_{arom}), 127.2 (CH_{arom}), 124.5 (CH_{arom}), 57.4 (NC_{Ad}), 48.8 (CH_{2Ad}), 39.4 (d, P*C*Me$_3$, $^{1}J_{CP}$ = 41 Hz), 37.3 (CH_{2Ad}), 31.1 (CH_{Ad}), 29.4 (PC*tBu*), 28.7 (*C*HMe$_2$), 25.7 (CH*Me*$_2$), 23.5 (CH*Me*$_2$). ^{31}P{^{1}H} NMR (202.5 MHz, benzene-d_6): δ 122.7 (s with Pt satellites,$^{1}J_{PPt}$ = 3226 Hz). Anal. Calcd for $C_{37}H_{56}N_3PPt$: C, 57.80; H, 7.34; N, 5.46. Found: C, 57.44; H, 7.12; N, 5.57. Crystals of **3-1** suitable for X-ray diffraction analysis were grown from a concentrated pentane solution at -35 °C.

Synthesis of 3-2. A thick-walled glass reaction vessel containing a magnetic stir bar and adapted with a PTFE stopcock was charged with (COD)PtCl$_2$ (0.30 g, 0.80 mmol). A solution of **2-1b** (0.34 g, 0.80 mmol) in ca. 20 mL of THF was added, resulting in a tan-colored suspension. The reaction mixture was stirred and heated at 70 °C for 18 h, giving rise to a clear yellow solution. The solution was allowed to cool to room temperature and

a suspension of Cs_2CO_3 (0.52 g, 1.60 mmol) in a minimal amount of THF was added. The reaction mixture was then stirred for 2 h at room temperature. The resulting bright yellow suspension was filtered through Celite® and the volatile components were subsequently removed in vacuo. The remaining yellow solid was then redissolved in ca. 10 mL of toluene and filtered through a Celite® plug to remove any residual salts. The solution was then concentrated to ca. 1 mL volume and refrigerated at -35 °C to precipitate yellow crystalline **3-2** (0.30 g, 60% yield). ^{1}H NMR (500 MHz, benzene-d_6): δ 7.53 (m, 2 H, H_{arom}), 7.09 (m, 1 H, H_{arom}), 7.02-7.00 (overlapping resonances, 2 H, H_{arom}), 6.84 (m, 3 H, H_{arom}), 3.70 (sept, 2 H, $^3J_{HH}$ = 7 Hz, C*H*Me$_2$), 1.64 (d, 6 H, $^3J_{HH}$ = 7 Hz, CH*Me*$_2$), 1.40 (d, 18 H, P*tBu*, $^3J_{PH}$ = 15 Hz), 0.99 (d, 6 H, $^3J_{HH}$ = 7 Hz, CH*Me*$_2$). ^{13}C{^{1}H} NMR (125.7 MHz, benzene-d_6): δ 179.01 (C$_{arom}$), 145.9 (*C*$_{arom}$), 144.8 (*C*$_{arom}$), 134.5 (d, N*C*N, $^2J_{CP}$ = 24 Hz), 131.4 (*C*H$_{arom}$), 129.5 (*C*H$_{arom}$), 127.7 (*C*H$_{arom}$), 127.5 (*C*H$_{arom}$), 124.2 (*C*H$_{arom}$), 39.9 (d, P*C*Me$_3$, $^1J_{CP}$ = 40 Hz), 28.9 (*C*HMe$_2$), 28.6 (PC*Me$_3$*), 25.2 (CH*Me$_2$*), 23.9 (CH*Me$_2$*). ^{31}P{^{1}H} NMR (202.5 MHz, benzene-d_6): δ 97.6 (s with Pt satellites, $^1J_{PPt}$ = 3900 Hz). Anal. Calcd for $C_{54}H_{80}Cl_2N_4P_2Pt_2$: C, 49.58; H, 6.16; N, 4.28. Found: C, 49.32; H, 6.36; N, 4.09. Crystals of **3-2** suitable for X-ray diffraction analysis were grown from a concentrated toluene solution at room temperature.

Synthesis of 3-5. A solution of **3-1** (0.10 g, 0.13 mmol) in ca. 3 mL of pentane was treated with a solution of 2,6-xylyl isocyanide (0.035 g, 0.27 mmol) in ca. 1.5 mL of 2:1 pentane:THF. The reaction mixture was allowed to stand at room temperature for 18 h. The solution was then concentrated *in vacuo* to ca. 1 mL volume and was refrigerated at -35 °C for 18 h to afford **3-5** (0.048 g, 35%) as a yellow crystalline solid. ^{1}H NMR (500 MHz, benzene-d_6): δ 7.54 (d, 2 H, J_{HH} = 7 Hz, H_{arom}), 7.07 (d, 2 H, J_{HH} = 7 Hz, H_{arom}),

7.03 (d, 2 H, J_{HH} = 7 Hz, H_{arom}), 7.00 - 6.84 (overlapping resonances, 8 H, H_{arom}), 6.28 (s, 1 H, N*H*), 3.89 (sept, 2 H, $^3J_{HH}$ = 7 Hz, C*H*Me$_2$), 2.54 (s, 6 H, *Me$_2$*C$_6$H$_3$), 2.48 (s, 6 H, *Me$_2$*C$_6$H$_3$), 1.57 - 1.54 (overlapping resonances, 21 H, H_{Ad} + P*tBu*), 1.38 (d, 6 H, $^3J_{HH}$ = 7 Hz, CH*Me$_2$*), 1.35 (br s, 6 H, H_{Ad}), 1.17 (m, 6 H, H_{Ad}), 1.04 (d, 6 H, $^3J_{HH}$ = 7 Hz, CH*Me$_2$*). ^{13}C{^{1}H} NMR (125.7 MHz, benzene-d_6): δ 178.3 (C_{arom}), 151.3 (C_{arom}), 149.9 (C_{arom}), 144.2 (C_{arom}), 142.2 (C_{arom}), 136.9 (d, PN*C*N, $^2J_{CP}$ = 19 Hz), 133.6 (C_{arom}), 131.2 (CH_{arom}), 129.5 (C_{arom}), 129.0 (CH_{arom}), 128.9 (CH_{arom}), 128.6 (CH_{arom}), 127.3 (CH_{arom}), 125.6 (CH_{arom}), 124.4 (CH_{arom}), 123.8 (2C, CH_{arom}), 121.0 (CH_{arom}), 57.2 (NC_{Ad}), 42.0 (CH_{2Ad}), 38.7 (d, P*C*Me$_3$, $^1J_{CP}$ = 35 Hz), 35.5 (CH_{2Ad}), 29.2 (d, PC*Me$_3$*, $^2J_{CP}$ = 4 Hz), 29.1 (CH_{Ad}), 28.5 (*C*HMe$_2$), 25.1 (CH*Me$_2$*), 23.8 (CH*Me$_2$*), 21.8 (*Me$_2$*C$_6$H$_3$), 21.7 (*Me$_2$*C$_6$H$_3$). ^{31}P{^{1}H} NMR (202.5 MHz, benzene-d_6): δ 100.1 (s with Pt satellites, $^1J_{PPt}$ = 3314 Hz). Anal. Calcd for $C_{55}H_{74}N_5PPt$: C, 64.06; H, 7.23; N, 6.79. Found: C, 64.23; H, 7.41; N, 6.55. Crystals of **3-5** suitable for X-ray diffraction analysis were grown from a concentrated pentane/THF solution at -35 °C.

Synthesis of 3-6. A room temperature solution of 2,6-xylenol (0.035 g, 0.19 mmol) in ca. 1 mL of pentane was added to a suspension of **3-1** (0.15 g, 0.19 mmol) in ca. 5 mL of pentane. The resulting pale yellow solution was allowed to stand at room temperature for 1 h, over the course of which yellow crystals precipitated from solution. The reaction mixture was refrigerated at -35 °C to facilitate further precipitation of crystalline material. The supernatant solution was discarded and the remaining yellow crystalline solid was dried in *vacuo* to afford **3-6** as a pale yellow solid (0.080 g, 46% yield). ^{1}H NMR (500 MHz, benzene-d_6): δ 7.61 - 7.58 (overlapping resonances, 2 H, H_{arom}), 7.27 (t, 1 H, J_{HH} = 8 Hz, H_{arom}), 7.10 - 7.03 (overlapping resonances, 4 H, H_{arom}), 6.93 - 6.88

(overlapping resonances, 3 H, H_{arom}), 6.62 (t, 1 H, J_{HH} = 7 Hz, H_{arom}), 3.95 (sept, 2 H, $^3J_{HH}$ = 7 Hz, C*H*Me$_2$), 3.12 (br s, 2 H, PtN*H*$_2$), 2.38 (s, 6 H, O-2,6-*Me*$_2$C$_6$H$_3$), 1.77 (br s, 3 H, H_{Ad}), 1.45 - 1.43 (overlapping resonances, 24 H, H_{Ad} + P*tBu*), 1.37 (d, 6 H, $^3J_{HH}$ = 7 Hz, CH*Me*$_2$), 1.32 (br s, 6 H, H$_{Ad}$), 0.96 (d, 6 H, $^3J_{HH}$ = 7 Hz, CH*Me*$_2$). ^{13}C{^{1}H} NMR (125.7 MHz, benzene-d_6): δ 179.8 (C_{arom}), 164.6 (C_{arom}), 146.7 (C_{arom}), 144.3 (C_{arom}), 135.7 (d, PN*C*N, $^2J_{CP}$ = 23 Hz), 132.4 (*C*H$_{arom}$), 130.4 (*C*H$_{arom}$), 129.3 (*C*H$_{arom}$), 127.7 (*C*H$_{arom}$), 126.9 (*C*H$_{arom}$), 123.9 (*C*H$_{arom}$), 114.9 (*C*H$_{arom}$), 55.8 (N*C*$_{Ad}$), 44.6 (*C*H$_{2Ad}$), 38.3 (d, P*C*Me$_3$, $^1J_{CP}$ = 40 Hz), 36.2 (*C*H$_{2Ad}$), 30.8 (*C*H$_{Ad}$), 29.0 - 29.1 (overlapping resonances, PC*Me*$_3$ + *C*HMe$_2$), 25.0 (CH*Me*$_2$), 24.5 (CH*Me*$_2$), 19.7 (OCC*Me*). ^{31}P{^{1}H} NMR (202.5 MHz, benzene-d_6): δ 86.1 (s with Pt satellites, $^1J_{PPt}$ = 3770 Hz). Anal. Calcd for C$_{45}$H$_{66}$N$_3$OPPt: C, 60.66; H, 7.47; N, 4.72. Found: C, 60.77; H, 7.83; N, 4.39. Crystals of **3-6** suitable for X-ray diffraction analysis were grown from a concentrated pentane solution at -35 °C.

Synthesis of 3-7. A solution of **3-1** (0.11 g, 0.14 mmol) in ca. 3 mL of 5:1 pentane:THF was treated with cyclohexylallene (21 μL, 0.14 mmol). The reaction mixture was allowed to stand at room temperature for 18 h, over the course of which a subtle color change from orange to light orange-yellow was observed. Concentration of the solution to ca. 1 mL volume resulted in the formation of small pale yellow crystals. The crystals were washed with ca. 2 mL of cold (-30 °C) pentane and dried in vacuo to afford analytically pure **3-7** (0.036 g, 28%). ^{1}H NMR (500 MHz, benzene-d_6): δ 7.60 (d, 2 H, J_{HH} = 7 Hz, H_{arom}), 7.13 - 7.07 (overlapping resonances, 3 H, H_{arom}), 6.95 - 6.86 (overlapping resonances, 3 H, H_{arom}), 4.52 (br s with Pt satellites, 2 H, $^2J_{HPt}$ = 65 Hz, N*H*$_2$), 3.92 (br s, 2 H, C*H*Me$_2$), 2.36 (br s, 1 H, H_{Cy}), 1.97 (s, 6 H, H_{Ad}), 1.90 (s, 3 H, H_{Ad}), 1.77 (m, 2 H,

H_{Cy}), 1.69 (m, 2 H, H_{Cy}) 1.51 - 1.43 (overlapping resonances, 32 H, H_{Ad} + P*tBu* + CH*Me*$_2$ + H_{Cy}), 1.38 (br d, 2 H, $^3J_{PH}$ = 8 Hz, PtCH_2), 1.31 - 1.18 (overlapping resonances, 4 H, H_{Cy}), 0.99 (br d, 6 H, $^3J_{HH}$ = 7 Hz, CH*Me*$_2$). $^{13}C\{^1H\}$ NMR (125.7 MHz, benzene-d_6): δ 180.5 (C_{arom}), 147.2 (C_{arom}), 145.1 (C_{arom}), 137.8 (d, PN*C*N, $^2J_{CP}$ = 21 Hz), 131.5(CH_{arom}), 127.2 (CH_{arom}), 126.3 (CH_{arom}), 123.9 (CH_{arom}). 92.9 (d, $CH_2C{\equiv}CCy$, $^2J_{CP}$ = 9 Hz), 84.2 ($CH_2C{\equiv}CCy$), 55.5 (NC_{Ad}), 45.7 (CH_{2Ad}), 38.6 (d, P*C*Me$_3$, $^1J_{CP}$ = 25 Hz), 36.4 (CH_{2Ad}), 34.9 (CH_{2Cy}), 31.0 (CH_{Cy}), 30.6 (CH_{Ad}), 29.2 (d, PC*Me*$_3$, $^2J_{CP}$ = 5 Hz), 28.5 ($CHMe_2$), 26.9 (CH_{2Cy}), 25.5 (CH_{2Cy}), 24.5 (CH*Me*$_2$), 24.0 (CH*Me*$_2$), 10.9 (d, Pt*C*H$_2$, $^2J_{CP}$ = 88 Hz). $^{31}P\{^1H\}$ NMR (202.5 MHz, benzene-d_6): δ 102.0 (s with Pt satellites, $^1J_{PPt}$ = 2235 Hz). Anal. Calcd for $C_{46}H_{70}N_3PPt$: C, 62.00; H, 7.29; N, 4.71. Found: C, 61.88; H, 7.63, N, 4.82. Crystals of **3-7** suitable for X-ray diffraction analysis were grown from a concentrated THF/pentane solution at room temperature.

Crystallographic Solution and Refinement Details. Crystallographic data for each of **3-2**, **3-5**, and **3-7** were obtained at 173(±2) K on a Bruker® D8/APEX II CCD diffractometer using graphite-monochromated Cu Kα (λ = 1.54178 Å) radiation, employing a sample that was mounted in inert oil and transferred to a cold gas stream on the diffractometer. Crystallographic data for **3-1** were obtained at 173(±2) K and for **3-6** at 193(±2) K on a Bruker® D8/APEX II CCD diffractometer using graphite-monochromated Mo Kα (λ = 0.71073 Å) radiation, employing a sample that was mounted in inert oil and transferred to a cold gas stream on the diffractometer. Programs for diffractometer operation, data collection, and data reduction (including SAINT) were supplied by Bruker®. Gaussian integration (face-indexed) was employed as the absorption correction method throughout. All structures were solved by use of intrinsic

phasing methods and were refined by use of full-matrix least-squares procedures (on F^2) with R_1 based on $F_o^2 \geq 2\sigma$ (F_o^2) and wR_2 based on $F_o^2 \geq -3\sigma$ (F_o^2). Anisotropic displacement parameters were employed for all the non-hydrogen atoms of **3-1**, **3-2** and **3-7**. During the structure solution process for **3-5**, two crystallographically-independent molecules of (P,N)$^{i\text{Pr}}$Pt[C(NH-2,6-$Me_2C_6H_3$)(=NAd)](C≡N-2,6-$Me_2C_6H_3$) (A and B) along with 0.75 equivalents of pentane and 0.25 equivalents of THF were located in the asymmetric unit; for convenience, only molecule A is discussed in the text. Anisotropic displacement parameters were employed for all non-hydrogen atoms of molecules A and B. The non-hydrogen atoms of the THF solvate were modeled anisotropically with an occupancy of 0.5. The disordered pentane solvate was comprised of three pentane molecules (C5-C19). The carbon atoms in two of the pentane molecules (C10-C14 and C15-C19) were refined anisotropically with an occupancy of 0.5. The carbon atoms in the remaining pentane molecule (C5-C9) were refined isotropically with an occupancy of 0.5. The C–C and the C…C distances within the solvent pentane molecules were restrained to be 1.53(1) and 2.50(1) Å, respectively. During the structure solution process for **5** an equivalent of pentane was located in the asymmetric unit. The carbon atoms in this disordered pentane molecule (C1S-C5S) were modeled in a satisfactory manner over two positions with occupancies of 0.6667 and 0.3333, respectively. The carbon atoms (C1SA-C5SA) in the major component of the disordered solvent pentane molecule were refined anisotropically, while the atoms in the minor component (C1SB-C5SB) were refined with a common isotropic displacement parameter. The C–C distances of the minor component of the disordered solvent pentane molecule were restrained to be 1.53(1) Å. Anisotropic displacement parameters were employed for all remaining non-

hydrogen atoms in **5**. The N-*H* atoms in **3-1**, **3-5**, **3-6,** and **3-7** were each located in the difference map and refined isotropically. Otherwise, all hydrogen atoms were added at calculated positions and refined by use of a riding model employing isotropic displacement parameters based on the isotropic displacement parameter of the attached atom. In all cases non-hydrogen atoms are represented by Gaussian ellipsoids at the 30% probability level. Additional crystallographic information is provided in Appendix A.

Computational Details. All geometry optimizations were converged to stationary points and evaluated by a full Hessian calculation and vibrational analysis to confirm each structure as a minimum or first-order saddle point (transition state). All energy calculations were performed with an ultrafine integration grid. The LANL2TZ(f) pseudopotential/basis set for Pt was obtained from the EMSL Basis Set Exchange website (https://bse.pnl.gov/bse/portal).

M06/6-311+G(2d,p)[LANL2TZ(f)](large)//M06//6-31G(d,p)[LANL2DZ](small) free energies and enthalpies (at 298 K and 1 atm) are the sum of: $\Delta E_{(large)} + \Delta G_{solv(small)} + \Delta E_{ZPE(small)} + \Delta H_{(small)} + nRT - T\Delta S$. NBO analysis was carried with the default version connect with Gaussian® 09.

CHAPTER 4: Dehydrogenative B-H/C(sp^3)-H Benzylic Borylation Within the Coordination Sphere of Platinum(II)

4.1 Introduction

In working toward the goals of this thesis related to the pursuit of low-coordinate and reactive late metal species, (κ^2-P,N)M(η^3-benzyl) complexes of the group 10 metals were identified as attractive targets for inquiry.[99] $L_nM(\eta^3$-benzyl) compounds are well-known for both palladium and nickel, with palladium η^3-benzyl species being the most extensively studied of such complexes to date. These complexes have been employed as pre-catalysts and invoked as intermediates in a number of cross-coupling,[100] benzylic alkylation,[101] arene functionalization,[102] and cycloaddition[103] reactions among others. Nickel species of this type have a smaller reaction scope than their palladium counterparts. However, they are competent catalysts in olefin polymerizations[104] and are often invoked as intermediates in a variety of cross-coupling,[105] hydrovinylation,[106] and hydrocyanation[107] reactions. Surprisingly, studies on platinum η^3-benzyl complexes are comparatively limited.[99] Spencer and co-workers studied a series of platinum η^3-benzyl complexes featuring bisphosphine ligands with a focus on establishing the structural and electronic properties of these complexes; this work did not feature any substantial reactivity surveys.[108] Previous work within the Stradiotto group explored some stoichiometric reactivity of a zwitterionic (κ^2-P,S)Pt(η^3-benzyl) complex supported by a P,S indene co-ligand; however, reactivity studies for such (η^3-benzyl)platinum complexes can still be considered in their infancy.[109]

In developing reactivity of (η^3-benzyl)metal complexes, one could envision that the reaction of the target 16-electron (κ^2-P,N)M(η^3-benzyl) species with R_nE-H bonds (E

= main group element) could, upon loss of toluene, afford new and potentially unusual low-coordinate (κ^2-P,N)M(ER_n) compounds similar to **3-1** (Scheme 4-1).[110]

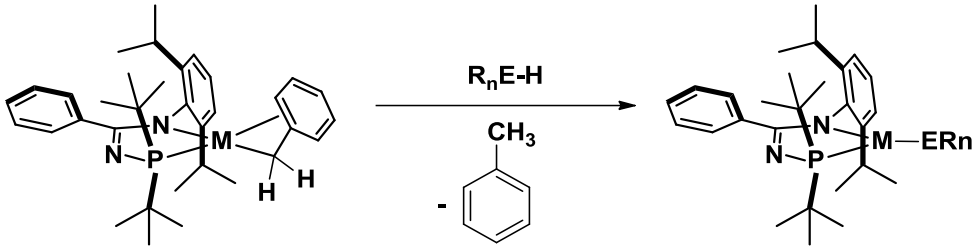

Scheme 4-1. Theoretical activation of an E-H bond to give (κ^2-P,N)M(ER_n) upon loss of toluene.

Alternatively, *in situ* dissociation of the aryl moiety of the benzyl ligand, which restores aromaticity and thus should be considered energetically favorable, would expose an additional reactive site. In this context, such species could be described as "masked" three-coordinate complexes (Scheme 4-2).

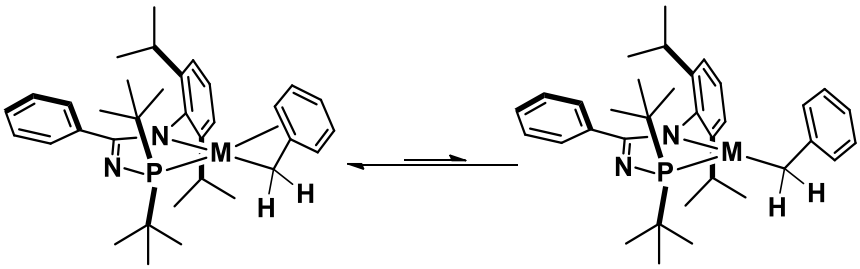

Scheme 4-2. Theoretical *in situ* dissociation to form (κ^2-P,N)M(η^1-benzyl).

Of particular interest to the Dalhousie/CPChem research team is the application of such complexes toward C-H borylation reactions following the success of **1-3** in mediating hydroboration reactions. The direct borylation of C-H bonds has emerged as an effective strategy for the functionalization of hydrocarbons,[111] whereby the derived organoboranes can be exploited as synthons in a diversity of transformations,[112] including Suzuki-Miyaura[113] cross-couplings. Although a number of metal catalysts have been identified that are capable of promoting C(sp^2)-H borylation reactions, selective benzylic

borylation of methylarenes has proven challenging, in keeping with the established favorability of C(sp^2)-H versus C(sp^3)-H bond activation.[114] The first efficient catalytic benzylic borylations were disclosed by Marder and co-workers,[115] whereby toluene, *p*-xylene and mesitylene were each preferentially borylated at benzylic positions by use of pinacolborane (HBPin) in the presence of catalytic amounts of $RhCl(P\textit{i}Pr_3)_2(N_2)$; alternative catalyst systems capable of selective benzylic (poly)borylation have been identified,[116] in some cases making use of B_2Pin_2 or $Et_3SiBPin$ as borylating agents. A notable trend that is observed in this chemistry is the activating effect of a BPin group with regard to subsequent C(sp^3)-H benzylic borylation reactions, in some cases resulting in di- or triborylation of the methylarene substrate thus making the monoborylated product a challenging target (Scheme 4-3). Additionally, such systems often require elevated temperatures, which are typically in excess of 100 °C.

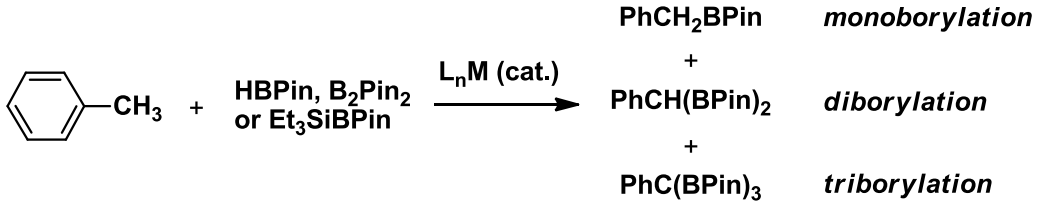

Scheme 4-3. Prototypical metal-catalyzed benzylic (poly)borylation of toluene.

One plausible mechanism for the benzylic borylation of toluene with HBPin proposed by Marder and co-workers,[115] and later supported on the basis of computational analysis,[117] is outlined in Scheme 4-4.

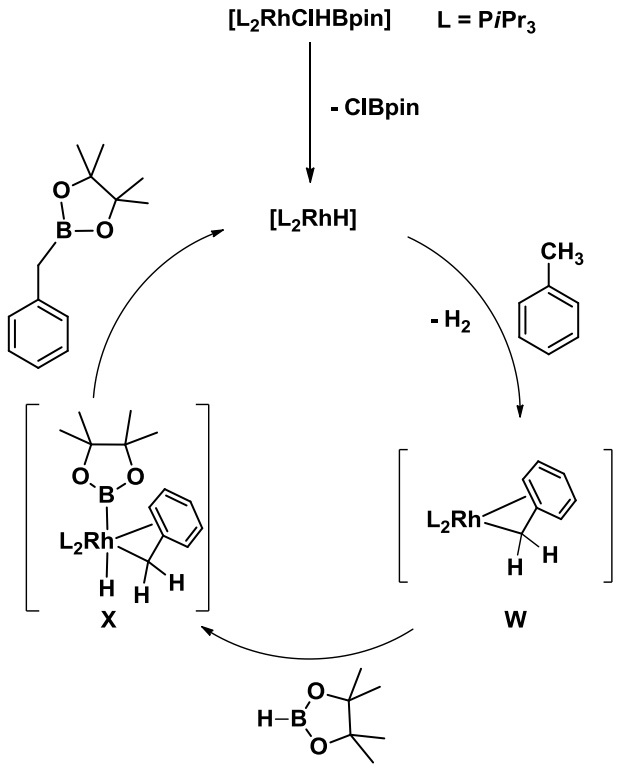

Scheme 4-4. Mechanism for the benzylic borylation of toluene with HBPin proposed by Marder and co-workers.

This reactivity involves formation of an $L_2Rh(\eta^3$-benzyl) complex (**W**) via toluene C(sp^3)-H bond activation, followed by borane B-H oxidative addition to give intermediate **X**, and C-B reductive elimination to give L_2RhH and the benzylic monoborylation product $PhCH_2BPin$; related pathways involving σ-bond metathesis could also be envisioned. Subsequent benzylic C(sp^3)-H bond activation of $PhCH_2BPin$ by L_2RhH with loss of H_2 to give **Y** represents a potentially important stoichiometric step *en route* to what for some catalysts is the favored diborylation product $PhCH(BPin)_2$ (Scheme 4-5).

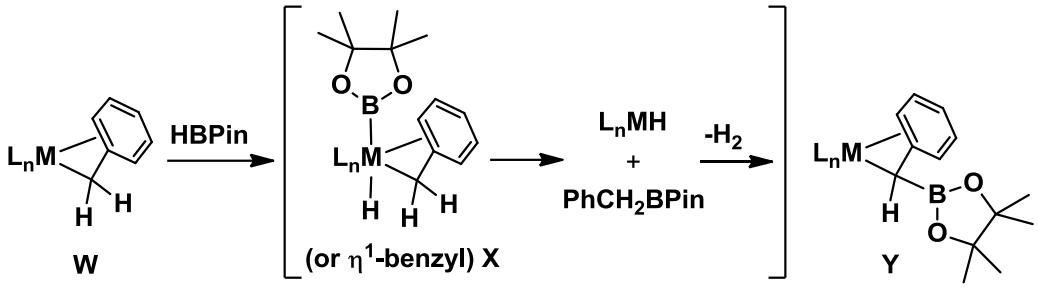

Scheme 4-5. Generalized benzylic borylation of toluene derived from Scheme 4-4 with the proposed precursor to diborylation **Y**.

Despite the significant recent progress with regard to the development of metal catalysts for benzylic (poly)borylation (*vide supra*), no experimental support for key stoichiometric steps that may underpin such important C-H functionalization reactions (e.g., **W** → **X** → **Y**, Scheme 4-5), has been reported. This chapter will detail the first transformations of the type **W** → **Y**, in which a pre-formed (η^3-benzyl)platinum complex (**4-1**) undergoes net stoichiometric dehydrogenative B-H/C(sp^3)-H benzylic borylation under mild conditions. Density functional theory (DFT) calculations provide insight regarding the mechanism of these transformations.

4.2 Results and Discussion

4.2.1 Synthesis and Characterization of (κ^2-P,N)M(η^3-benzyl) Complexes

As stated above, the initial goal of this project was the synthesis of late metal η^3-benzyl complexes to pursue potentially novel and unusual reactivity. In this regard, work began in isolating a series of (κ^2-P,N)M(η^3-benzyl) species (M = Ni, Pd, Pt).

Beginning with the synthesis of the (κ^2-P,N)Pt(η^3-benzyl) complex **4-1,** treatment of the platinum chloride dimer **3-2** with BnMgCl was envisioned as the most direct route to the desired complex. However, this approach afforded a mixture of products, as evidenced by the complexity of the ^{31}P NMR spectrum acquired of the crude reaction mixture. In this regard, an alternative synthetic strategy had to be developed. Treatment

of the *N*-phosphinoamidine **2-1b** with (COD)PtCl(η^1-benzyl), followed by exposure to base afforded the *N*-phosphinoamidinate complex **4-1** in 73% isolated yield (Scheme 4-6).

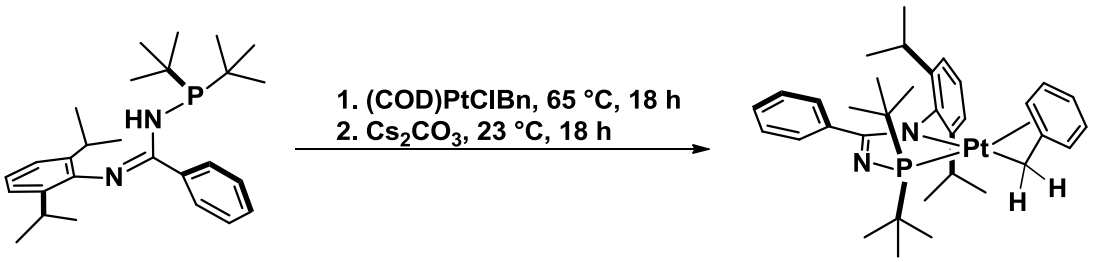

2-1b **4-1**

Scheme 4-6. Synthesis of the (κ^2-P,N)Pt(η^3-benzyl) complex **4-1**.

Synthesis of the related (κ^2-P,N)M(η^3-benzyl) (M= Ni, Pd) species was approached in a stepwise fashion by first synthesizing the precursor [(κ^2-P,N)MCl]$_2$ dimers. Treatment of the *N*-phosphinoamidine **2-1b** with $NiCl_2$(dme), followed by exposure to base afforded [(κ^2-P,N)NiCl]$_2$ (**4-2**) in 84% isolated yield (Scheme 4-7). [(κ^2-P,N)PdCl]$_2$ (**4-3**) was synthesized using an analogous protocol beginning with $(CH_3CN)_2PdCl_2$, and was isolated in 64% yield (Scheme 4-7). The structures of **4-2** and **4-3** were confirmed on the basis of both NMR spectroscopic and X-ray crystallography analysis (Figure 4-1). In contrast to what was observed with **3-2**, treatment of **4-2** and **4-3** with BnMgCl resulted in the desired (κ^2-P,N)M(η^3-benzyl) complexes (M = Ni, **4-4**, yield = 93%; M = Pd, **4-5**, yield = 72%) (Scheme 4-7).

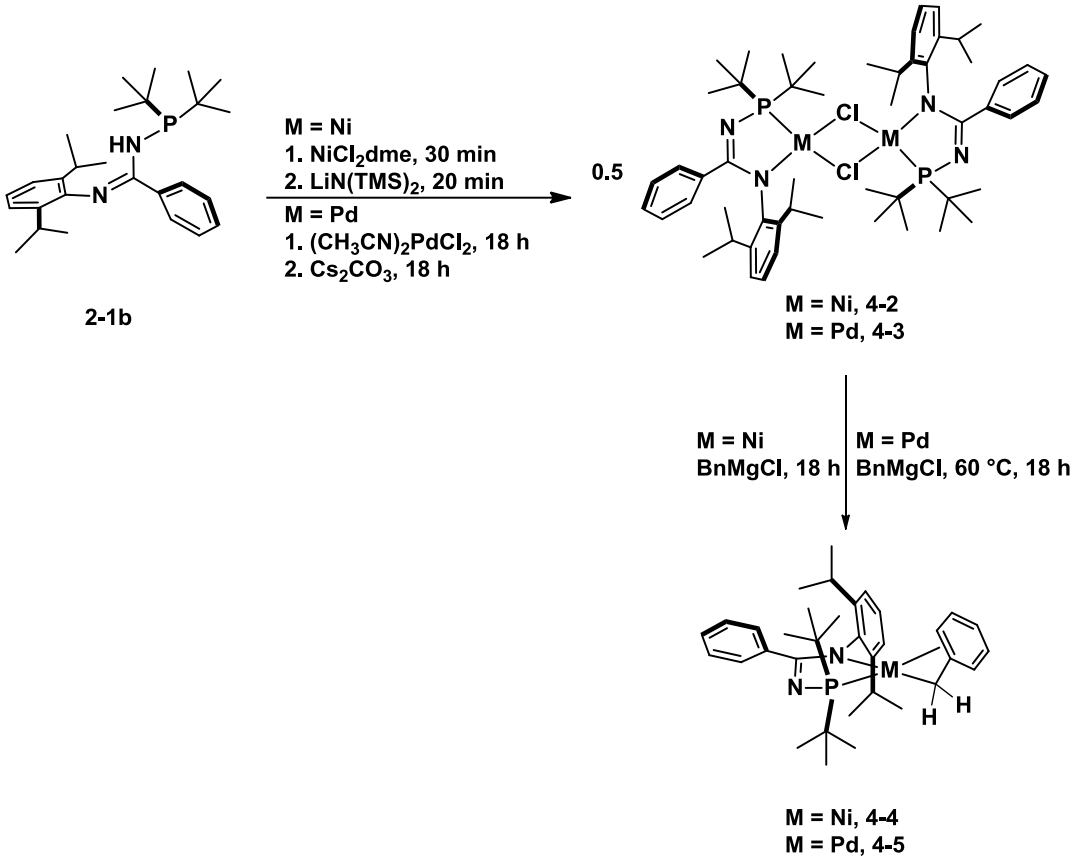

Scheme 4-7. Synthetic protocol for the isolation of chloride dimers **4-2** and **4-3** followed by treatment with BnMgCl to yield (η^3-benzyl)metal complexes **4-4** and **4-5**.

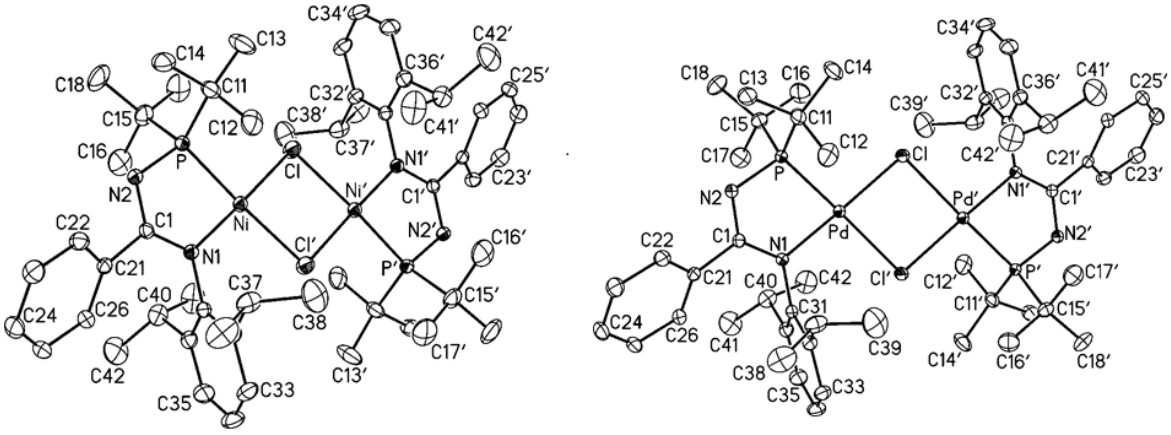

Figure 4-1. Crystallographically determined structures of **4-2** and **4-3.** Non-hydrogen atoms are represented by 30% Gaussian ellipsoids. Hydrogen atoms omitted for clarity.

The connectivity within each of **4-1**, **4-4**, and **4-5** was confirmed on the basis of NMR spectroscopic and X-ray crystallographic data (Figure 4-2). In keeping with the relatively few crystallographically characterized (η^3-benzyl)metal complexes reported thus far in the literature,[108a, 109] each of the two crystallographically independent molecules of **4-1** exhibit progressively longer Pt-C distances on going from Pt-CH_2 (~2.06-2.07 Å) to Pt-C_{ipso} (~2.31-2.32 Å) to Pt-C_{ortho} (~2.42-2.44 Å) (Figure 4-2); similar trends were observed for the related complexes **4-4** (Ni-C: 1.9584(15), 2.0765(13), and 2.2205(15) Å; Figure 4-3) and **4-5** (Pd-C: 2.082(4), 2.233(4), and 2.372(5) Å; Figure 4-4). A summary of relevant bond lengths is presented in Table 4-1.

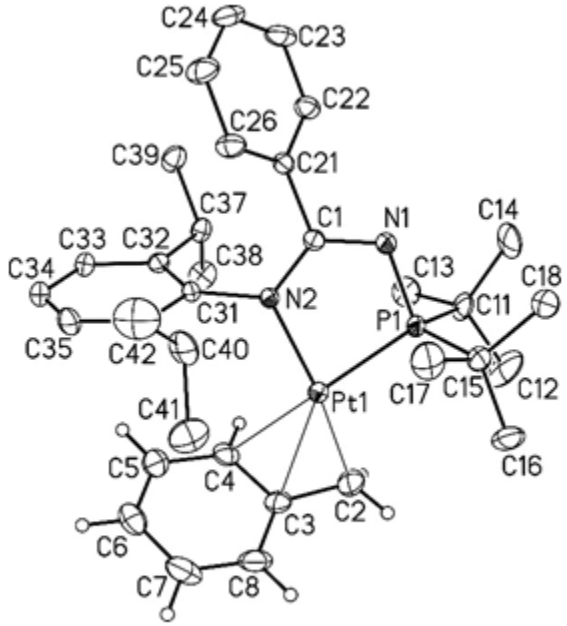

4-1

Figure 4-2. Crystallographically determined structure of **4-1** showing one of the two crystallographically independent molecules. Non-hydrogen atoms are represented by 30% Gaussian ellipsoids. Most hydrogen atoms omitted for clarity.

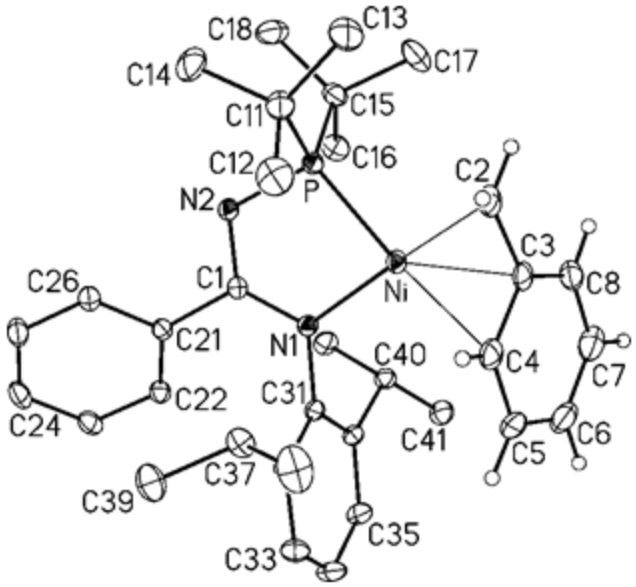

4-4

Figure 4-3. Crystallographically determined structure of **4-4.** Non-hydrogen atoms are represented by 30% Gaussian ellipsoids. Most hydrogen atoms omitted for clarity.

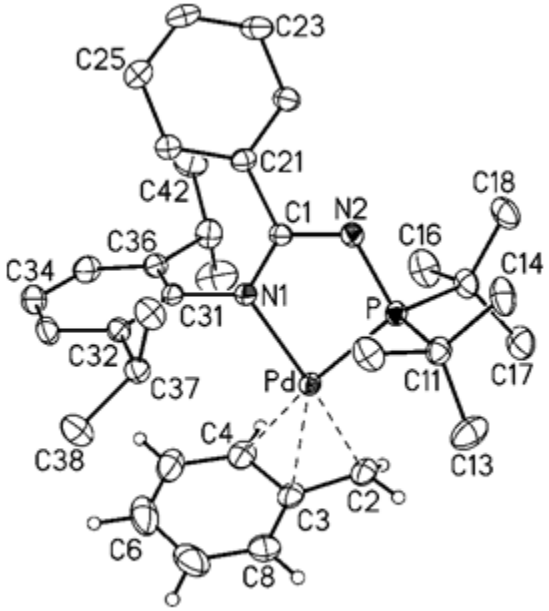

4-5

Figure 4-4. Crystallographically determined structure of **4-5.** Non-hydrogen atoms are represented by 30% Gaussian ellipsoids. Most hydrogen atoms omitted for clarity.

4.2.2 Probing the Reactivity of (κ^2-P,N)M(η^3-benzyl) Complexes

Initially the reactivity between **4-1** and R_2NHBH_3 (R_2N = H_2N, *t*BuHN or Me_2N, 5 equiv) at 23 ˚C in THF was examined. In all cases relatively clean conversion to a single product **4-6** was detected after 18 h on the basis of ^{31}P NMR data. The same transformation was observed under similar conditions when using only 1 equiv *t*$BuNH_2BH_3$, from which **4-6** was isolated in 92% yield (Scheme 4-8). While under analogous conditions (5 equiv NH_3BH_3, 23 ˚C, THF) no reaction was observed when using **4-4** in place of **4-1**, vigorous bubbling was observed in reactions with **4-5**. However, unlike the clean formation of **4-6**, ^{31}P NMR analysis of the reaction mixture after 18 h revealed less than 50% consumption of **4-5**, along with the formation of multiple unidentified phosphorus-containing products.

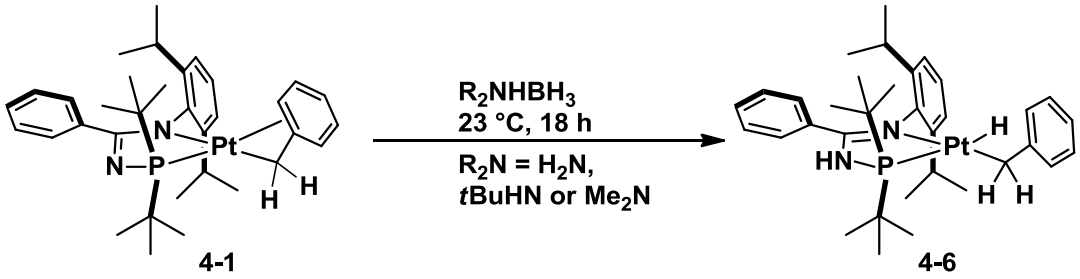

Scheme 4-8. Synthesis of **4-6** displaying the net H_2 transfer from R_2NHBH_3 across the metal-ligand framework.

The identification of **4-6** as (κ^2-P,N-[H])PtH(η^1-benzyl) (Scheme 4-8) was made initially on the basis of ^1H NMR data, with diagnostic resonances observed for Pt-H (-1.85 ppm; $^2J_{PH}$ = 237 Hz, $^1J_{PtH}$ = 1413 Hz), Pt-CH_2 (4.02 ppm; $^3J_{PH}$ = 8 Hz, $^2J_{PtH}$ = 119 Hz), and N-H (5.18 ppm) groups. X-Ray diffraction analysis confirmed this structural assignment (Figure 4-5), with the observed (aryl)N-CN and PN-CN distances in **4-6** (1.289(6) and 1.364(6) Å, respectively), relative to those in **4-1** (1.344(4), 1.350(3); 1.315(4), 1.318(3) Å, respectively), supporting the view of *N*-phosphinoamidine ligation

in **4-6**.[118] Negligible conversion to **4-6** was observed upon exposure of **4-1** to H_2 (~ 1 atm, 23 ˚C, THF or C_6D_6), and upon heating (C_6D_6, 90 ˚C, 72 h) slow loss of H_2 from **4-6** to regenerate **4-1** was observed as the dominant transformation (^{31}P NMR), rather than toluene elimination. Notably, this reactivity parallels that described in Chapter 2 concerning the reaction of **2-2a** with NH_3BH_3 (Scheme 2-5), and provides additional evidence for the ability of complexes supported by *N*-phosphinoamidinates to behave in a bifunctional manner. Additionally, this reaction suggests that *in situ* dissociation of the aryl moiety of the benzyl ligand within (η^3-benzyl)metal complexes to open up an additional reactive site is feasible; such complexes can be envisioned as "masked" three-coordinate species (Scheme 4-2).

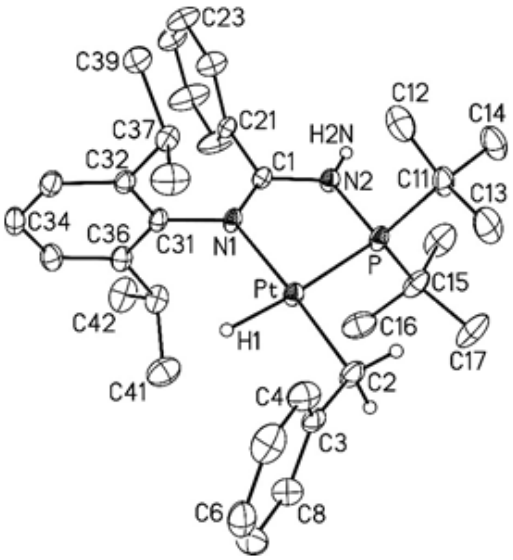

4-6

Figure 4-5. Crystallographically determined structure of **4-6.** Non-hydrogen atoms are represented by 30% Gaussian ellipsoids. Most Hydrogen atoms omitted for clarity.

With the knowledge that (κ^2-P,N)Pt-NH(1-Ad) **3-1** is a stable three-coordinate species, **4-1** was treated with adamantyl amine in an attempt to synthesize **3-1** by N-H activation of the amine followed by loss of toluene as proposed in Scheme 4-1. However,

no conversion to **3-1** was detected by use of NMR spectroscopy even after prolonged heating at elevated temperatures. X-Ray crystallography data indicated that crystals isolated from the mother liquor were simply the (κ^2-P,N)Pt(NH_2(1-Ad))(η^1-benzyl) adduct (Figure 4-6). This reaction was not pursued further.

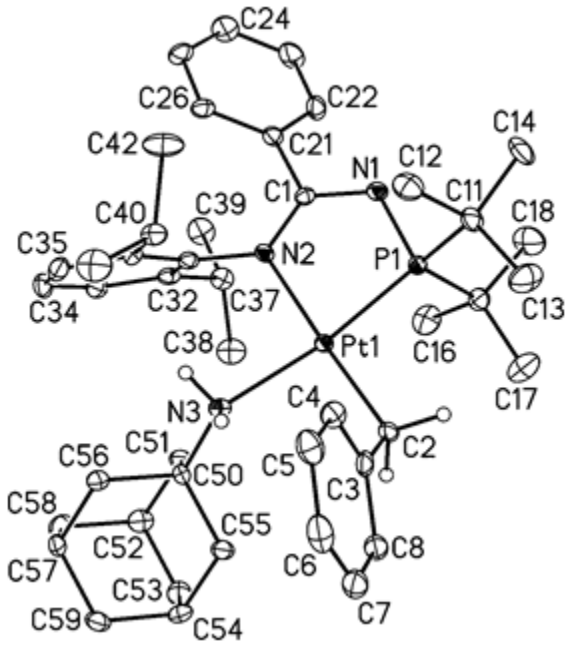

Figure 4-6. Crystallographically determined structure of (κ^2-P,N)Pt(NH_2(1-Ad))(η^1-benzyl). Non-hydrogen atoms are represented by 30% Gaussian ellipsoids. Most hydrogen atoms omitted for clarity.

Intrigued by the reactivity properties of **4-1** with amine boranes, attention was turned to reactions involving HBPin and catecholborane (HBCat, Scheme 4-9). Preliminary experiments involved treatment of **4-1** with equimolar HBPin in C_6D_6 at 45 ˚C, whereby slow but complete conversion of **4-1** to (κ^2-P,N)Pt(η^3-PhCH(BPin)) (**4-7**) in the absence of intermediates was observed over 5 days (^{1}H and ^{31}P NMR). Unlike **4-6**, neither Pt-H nor N-H resonances were present in the ^{1}H NMR spectrum of **4-7**; rather, signals attributable to a coordinated PhCH(BPin) ligand were apparent within a C_1-symmetric structure. When excess HBPin is employed, the conversion of **4-1** into **4-7** is

quantitative at 23 ˚C (5 equiv, 36 h; 10 equiv, 12 h), thereby highlighting the remarkably mild nature of this selective benzylic C(sp^3)-H borylation chemistry in contrast to the elevated temperatures typically requiered to promote such reactions. Treatment of **4-1** with HBCat either at 23 ˚C (5 equiv, 18 h) or 65 ˚C (1 equiv, 18 h) similarly resulted in the clean formation of the structurally analogous C(sp^3)-H borylation product **4-8** (Scheme 4-9); the more reactive nature of HBCat relative to HBPin is in keeping with established trends.[111-112]

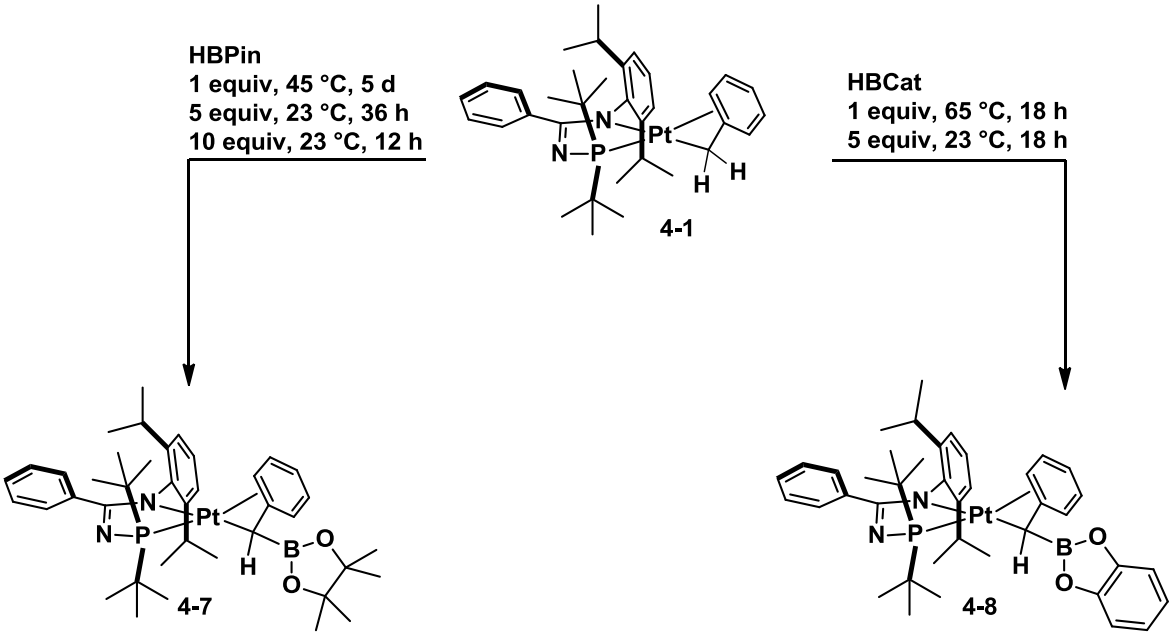

Scheme 4-9. Synthesis of **4-7** and **4-8** derived from benzylic borylation of the benzyl ligand.

The metrical parameters within the X-ray structures of **4-7** and **4-8** (Figure 4-7) mirror those found in **4-1**, including progressively longer Pt-CHB (**4-7**, 2.119(3) Å; **4-8**, 2.1351(19) Å), Pt-C_{ipso} (**4-7**, 2.260(3) Å; **4-8**, 2.2682(19) Å), and Pt-C_{ortho} (**4-7**, 2.394(3) Å; **4-8**, 2.3860(19) Å) distances (Table 4-8).

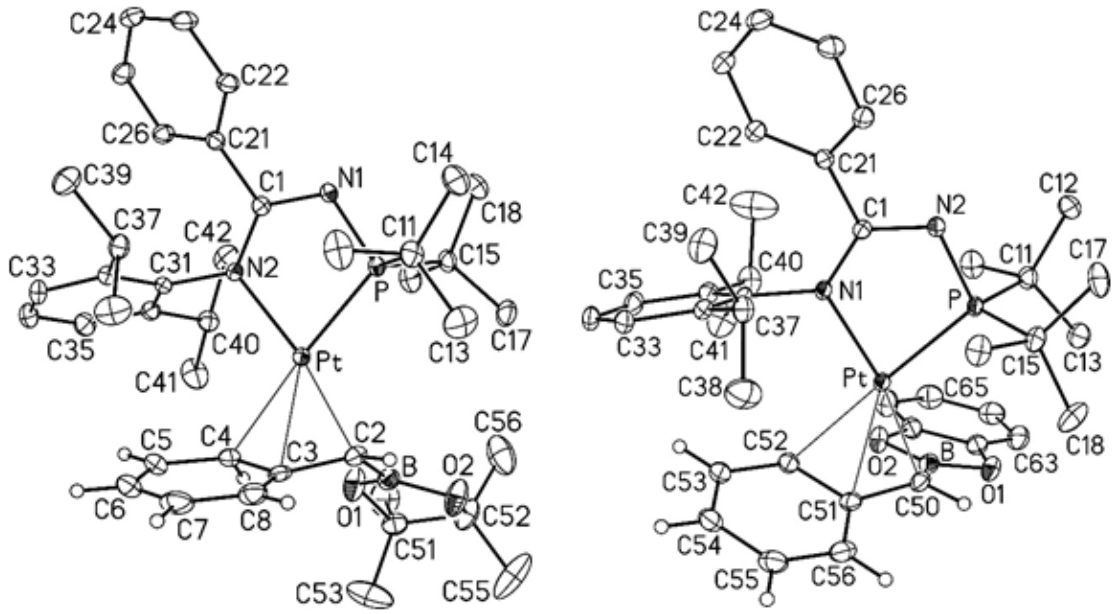

4-7 **4-8**

Figure 4-7. Crystallographically determined structures of **4-7** and **4-8.** Non-hydrogen atoms are represented by 30% Gaussian ellipsoids. Most hydrogen atoms omitted for clarity.

	4-1	**4-4**	**4-5**	**4-7**	**4-8**
M-P	2.2073(8); 2.2037(7)	2.1248(4)	2.2278(11)	2.2177(7)	2.2253(5)
M-N	2.091(2); 2.081(2)	1.9293(11)	2.089(3)	2.078(2)	2.0766(15)
M-CH_2	2.072(3); 2.063(3)	1.9584(15)	2.082(4)	2.119(3)	2.1351(19)
M-C_{ipso}	2.308(3); 2.321(3)	2.0765(13)	2.233(4)	2.260(3)	2.2682(19)
M-C_{ortho}	2.416(3); 2.439(3)	2.2205(15)	2.372(5)	2.394(3)	2.3860(19)

Table 4-1. Selected interatomic distances (Å) for **4-1**, **4-4**, **4-5, 4-7,** and **4-8**. Independent molecules of **4-1** are separated by a semicolon.

Notably, the transformation of **4-1** into **4-7** or **4-8** represents the first reported stoichiometric dehydrogenative B-H/C(sp^3)-H benzylic borylation reactions (*cf* **W** → **Y**, Scheme 4-5). The distinct ability of **4-1** to engage in this chemistry was apparent in

reactivity studies employing the nickel and palladium species **4-4** and **4-5** in combination with excess borane (5 equiv, C_6D_6, 23 ˚C); negligible conversion was observed with HBPin, whereas partial consumption of **4-4** and **4-5**, along with the formation of multiple phosphorus-containing products, was observed when using HBCat (^{31}P NMR).

Platinum-catalyzed C-H borylation chemistry is limited to two recent reports involving C(sp^2)-H borylation with HBPin or B_2Pin_2.[119] In an effort to observe a catalytic turnover corresponding to the dehydrogenative C(sp^3)-H benzylic borylation of toluene with HBPin, toluene solutions of **4-7** were heated either conventionally (105 ˚C, 24 h) or by use of microwave methods (200 ˚C, 1 h). Under both conditions **4-7** proved to be remarkably inert, with no evidence of decomposition or conversion to **4-1** observed (^{31}P NMR). In keeping with **4-1**, no reaction between **4-7** and H_2 (~ 1 atm, C_6D_6, 23 ˚C, 72 h) was detected on the basis of ^{1}H and ^{31}P NMR data. Furthermore, in monitoring the reaction of **4-1** with excess HBPin at 23 ˚C in toluene-d_8 solution, no evidence for deuterium incorporation into the product **4-7** was observed (^{1}H and ^{2}H NMR).

4.2.3 Computational Mechanistic Studies

To directly examine mechanistic details of the unusual stoichiometric benzylic borylation reaction between **4-1** and HBPin, we performed DFT calculations. In all calculations, the complete κ^2-P,N (**2-1b)** ligand was modeled along with comprehensive conformational searching. Gaussian 09[120] was used to calculate all structures and energies using M06/def2-TZVP//M06/LANL2DZ[6-31G**] theory[121] with the SMD[122] continuum solvent model for toluene. As a structural comparison, M06 accurately replicated the crystallographically determined unsymmetrical η^3-benzyl interaction in **4-1**, with the more weakly donating Ph moiety coordinated *trans* to phosphorus. However, the ground-

state conformation of **4-1** can be fluxional. Isomerization of the η^3-benzyl ligand where the Ph group is *trans* to the amido donor requires a free energy change of only ~6 kcal/mol, which is important for accessible reaction pathways.

Scheme 4-10 shows a few of the most important reaction mechanisms that were considered for benzylic borylation. Pathway A initiates possible open-shell mechanisms through Pt-benzyl bond homolysis to give Pt and benzyl radicals, which in turn could react with HBPin. Despite benzylic radical stabilization, the Pt-C bond homolysis requires a moderately large ΔG of 48 kcal/mol, and therefore is not favorable. Pathway B begins with benzylic α-hydrogen migration, affording a Pt(H)=CHPh intermediate that could then undergo 1,2-addition with HBPin. The kinetics and thermodynamics of pathway B are potentially viable with $\Delta G^{\ddagger}$ of 35 kcal/mol and ΔG = 34 kcal/mol; however, these energetics are larger than pathway C, which involves σ-HBPin coordination to give **4-1(HBPin)** followed by B-H bond activation.

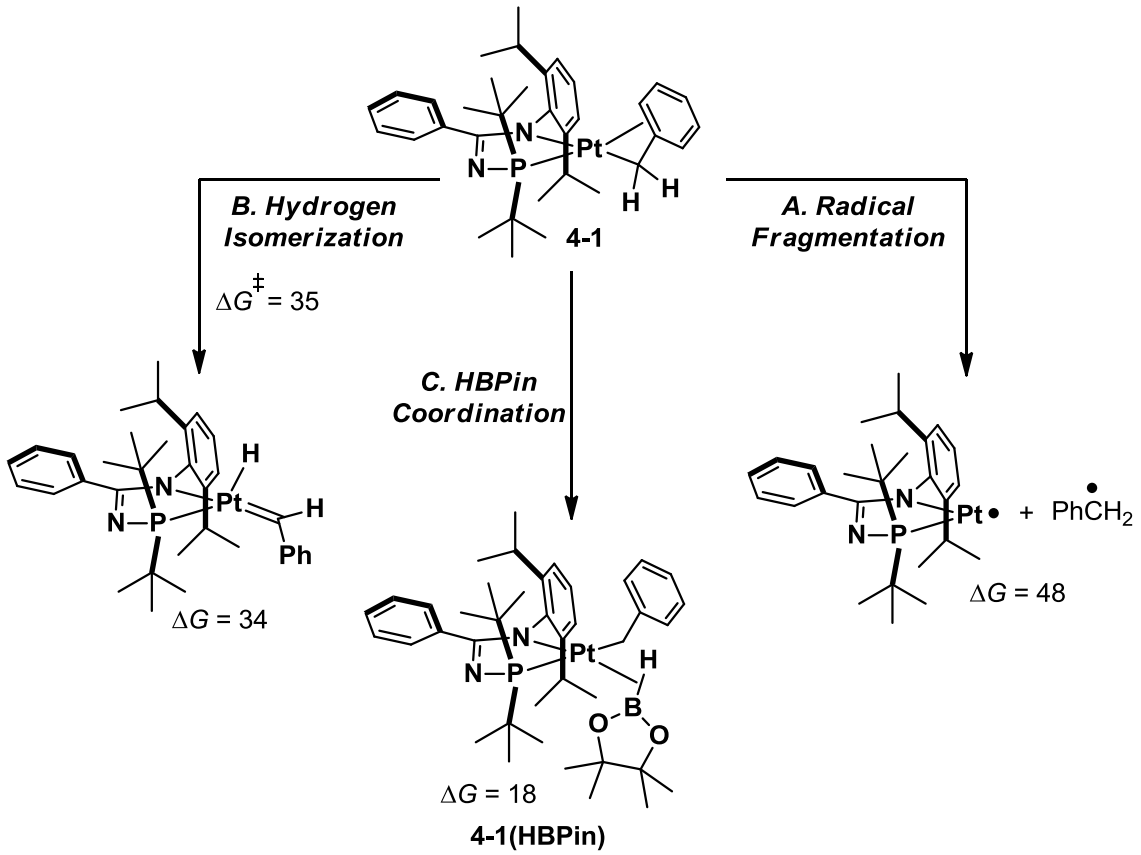

Scheme 4-10. Plausible mechanisms considered by use of DFT calculations for B-H/C(sp^3)-H benzylic borylation. Thermodynamic and kinetic free energies in kcal/mol relative to separated **4-1** + HBPin.

The most favorable σ-HBPin coordination intermediate, **4-1(HBPin)** (Figure 4-8) features an elongated B-H bond (1.40 Å) *trans* to the amido group, in keeping with reports of σ-B-H bonding to Ru.[123] Relatively short Pt-B (2.14 Å) and Pt-H (1.66 Å) distances are observed, along with pyramidalization at boron.

After coordination of HBPin to **4-1** to give **4-1(HBPin)**, there are several possible B-H activation transition states. The lowest free energy transition-state structure identified, **TS1**, is shown in Figure 4-8. In this σ-bond metathesis transition state[124] the major changes from **4-1(HBPin)** involve rupture of the Pt-benzyl bond and formation of the B-benzyl bond. The B-H and Pt-H bond lengths are only slightly perturbed. **TS1**

directly borylates the benzylic carbon and forms a Pt-H intermediate with $\Delta G^{\ddagger}$ = 19.4 kcal/mol. The alternative σ-bond metathesis transition state where toluene is formed along with a Pt-BPin intermediate is ~10 kcal/mol higher in free energy than **TS1**, in keeping with our qualitative experimental observations (*vide supra*). **TS1** is geometrically similar to a transition state proposed by Hartwig and co-workers,[116e] in which an Ir-benzyl fragment undergoes σ-bond metathesis with coordinated HBPin.

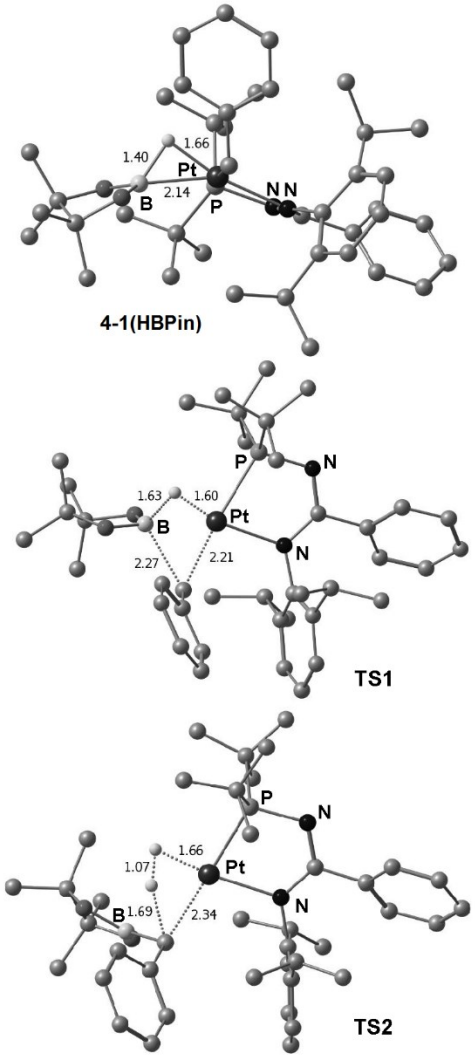

Figure 4-8. DFT structures for **4-1(HBPin)**, B-H activation **TS1**, and C-H activation **TS2.** Most hydrogen atoms omitted for clarity. Distances reported in Å.

Conformational rearrangement of the (κ^2-P,N)Pt(H)-coordinated $PhCH_2BPin$ provides an orientation for benzylic C-H activation by way of a second σ-bond metathesis transition state, **TS2** (Figure 4-8). Coordination of $PhCH_2BPin$ in this context is a few kcal/mol more favorable than toluene due to the more electron rich benzylic C-H groups in the former; it is possible that $PhCH_2BPin$ remains coordinated between **TS1** and **TS2**.

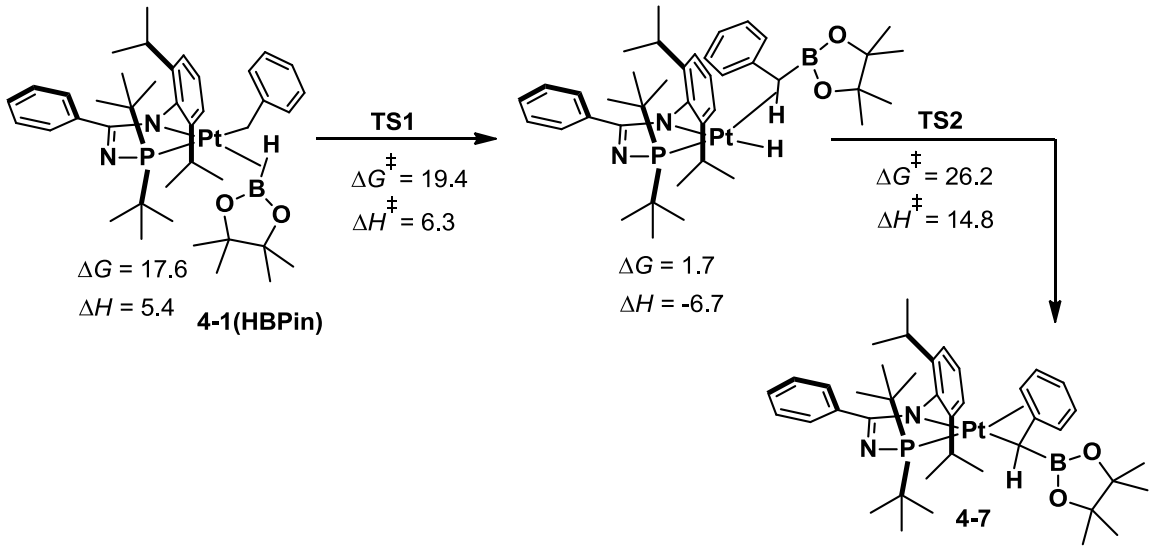

Scheme 4-11. Outline of proposed B-H activation and C-H activation *en route* to dihydrogen and **4-7**. All energies in kcal/mol.

In traversing **TS2**, dihydrogen and **4-7** are formed in a process that is ~4 kcal/mol lower in free energy than an oxidative addition/reductive elimination sequence; however, this relatively small energy difference indicates that these two pathways may be competitive. The $\Delta G^{\ddagger}$ for **TS2** is 26.2 kcal/mol and $\Delta H^{\ddagger}$ = 14.8 kcal/mol. The magnitude of this activation enthalpy calculated at 298 K is consistent with this transition state governing the reaction rate and the experimentally measured Eyring activation parameters $\Delta H^{\ddagger}$ = 18(1) kcal/mol and $\Delta S^{\ddagger}$ = 6(3) eu at 300 K. Our proposal of rate limiting C-H activation in this double σ-bond metathesis pathway (Scheme 4-11)

complements the computationally based proposal by Marder and co-workers,[117] whereby Rh-C*H*$_2$Ph borylation occurs by an oxidative addition/reductive elimination sequence featuring rate limiting C-H activation. After **TS2** there is a weakly coordinated Pt-H_2 complex (H-H distance = 0.87 Å), and subsequent liberation of dihydrogen from the Pt coordination sphere followed by η^3-benzyl coordination results in **4-7** and a reaction free energy that is exothermic by ~5 kcal/mol.

4.3 Conclusion

In summary, this chapter outlines the first stoichiometric dehydrogenative B-H/C(sp^3)-H benzylic borylation reactions, which arise from the reactivity of the pre-formed (η^3-benzyl)metal complex **4-1** with pinacolborane or catecholborane at room temperature. Exploration of the mechanism by use of density-functional calculations indicates that such reactions proceed via consecutive σ-bond metathesis steps. Given the considerable relevance of such reactivity to catalytic methylarene C-H functionalization processes, significant interest remains in exploring the generality of such transformations. Additionally, **4-6** represents a rare example of a platinum alkyl hydride species generated by the bifunctional abstraction of H_2 from amine boranes. As stated in Section 4.1, the (η^3-benzyl)platinum motif remains remarkably underexplored and the reactivity studies detailed herein demonstrate the potential of such complexes to participate in novel and unusual reactivty.

4.4 Statement of Contributions

Several researchers helped to bring this project to publication in *Angewandte Chemie* and they are recognized herein. Jack T. Fuller and Daniel H. Ess of Brigham Young University were responsible for all computational work featured in this chapter.

Michael J. Ferguson and Robert McDonald of the University of Alberta were responsible for X-ray crystallography data collection and structure elucidation. Casper Macaulay was responsible for the synthesis and reactivity studies of **4-2** and **4-4**.

4.5 Experimental Details

General experimental considerations. Unless stated all experiments were conducted at 23 °C under nitrogen in an MBraun glovebox or using standard Schlenk techniques. Dry, oxygen-free solvents were used unless otherwise indicated. Benzene, toluene, and pentane were deoxygenated and dried by sparging with nitrogen and subsequent passage through a double-column solvent purification system purchased from MBraun Inc. packed with alumina and copper-Q5 reactant. Tetrahydrofuran and diethyl ether were purified by distillation under nitrogen from Na/benzophenone. All purified solvents were stored over 4 Å molecular sieves. Benzene-d_6 and toluene-d_8 were degassed via three freeze-pump-thaw cycles and stored over 4 Å molecular sieves. All other reagents were purchased from commercial suppliers and used without further purification. ^{1}H, ^{13}C, and ^{31}P NMR characterization data were collected at 300 K on a Bruker AV-500 spectrometer operating at 500.1, 125.7, and 202.5 MHz (respectively) with chemical shifts reported in parts per million downfield of $SiMe_4$ for ^{1}H and ^{13}C, and 85% H_3PO_4 in D_2O for ^{31}P. ^{1}H and ^{13}C NMR chemical shift assignments are based on data obtained from ^{13}C-DEPTQ135, ^{1}H-^{1}H COSY, ^{1}H-^{13}C HSQC, and ^{1}H-^{13}C HMBC NMR experiments. In some cases, fewer than expected unique ^{13}C NMR resonances were observed, despite prolonged acquisition times.

Synthesis of 4-1. To a glass flask fitted with a re-sealable PTFE stopper was added a magnetic stir bar and a solution of **2-1b** (0.36 g, 0.84 mmol) in THF (20 mL), followed by the addition of CODPtBnCl (0.36 g, 0.84 mmol) resulting in a dark yellow solution. After sealing the flask with a PTFE stopper, the reaction flask was partially submerged in an oil bath that was set to 65 °C and magnetic stirring was initiated. After 18 h, the reaction mixture was cooled to room temperature, the flask was opened, and then a suspension of Cs_2CO_3 (0.55 g, 1.7 mmol) in a minimal amount of THF was added to the reaction flask. The reaction flask was then re-sealed and magnetic stirring at room temperature was initiated; after 18 h a bright yellow opaque reaction mixture resulted. This solution was filtered through Celite, the eluent was collected, and the solvent was removed *in vacuo*. The resulting yellow powder was then redissolved in benzene (10 mL) and filtered through a Celite plug to remove any residual salts. The benzene was then removed *in vacuo* from the collected eluent and the resulting yellow solid was triturated with pentane (3 x 1 mL) and dried *in vacuo* yielding analytically pure **4-1** (0.44 g, 73%). ^{1}H NMR (500 MHz, benzene-d_6): δ 7.70 (m, 2H, H_{arom}), 7.07-7.05 (m, 2H, H_{arom}), 7.00 (m, 1H, H_{arom}), 6.90 (m, 3H, H_{arom}), 6.49 (m, 5H, H_{arom}), 3.37 (apparent septet, 2H, $^3J_{HH}$ = 7 Hz, Me*CH*Me), 2.47 (s with Pt satellites, 2H, $^2J_{PtH}$ = 34 Hz, Pt*CH*$_2$Ph), 1.40 (d, 18H, $^3J_{PH}$ = 15 Hz, P*tBu*$_2$), 1.05 (d, 6H, $^3J_{HH}$ = 7 Hz, *MeC*HMe), 0.90 (d, 6H, $^3J_{HH}$ = 7 Hz, MeCH*Me*). ^{13}C{^{1}H} NMR (125.7 MHz, benzene-d_6): δ 176.1 (C_{arom}), 149.6 (C_{arom}), 142.7 (C_{arom}), 136.1 (d, $^2J_{PC}$ = 20 Hz, PN*C*N), 133.5 (C_{arom}), 131.2 (*C*H$_{arom}$), 128.6 (*C*H$_{arom}$), 127.1 (*C*H$_{arom}$), 126.9 (*C*H$_{arom}$), 124.9 (*C*H$_{arom}$), 123.2 (*C*H$_{arom}$), 120.3 (C_{arom}), 115.0 (d, $^2J_{PC}$ = 7 Hz, *C*H$_{arom}$), 38.6 (d, $^1J_{PC}$ = 41 Hz, P*C*Me$_3$), 28.5 (d with Pt satellites, $^2J_{PC}$ = 4 Hz, $^3J_{PtC}$ = 25 Hz, PC*Me*$_3$), 28.2 (Me*C*HMe), 24.3 (*Me*CHMe), 23.7 (MeCH*Me*),

18.1 (s with Pt satellites, $^{1}J_{PtC}$ = 343 Hz, Pt*C*H_2Ph). $^{31}P\{^{1}H\}$ NMR (202.5 MHz, benzene-d_6): δ 109.6 (s with Pt satellites, $^{1}J_{PtP}$ = 5075 Hz). Anal. Calcd for $C_{34}H_{47}N_2PPt$: C, 57.53; H, 6.67; N, 3.95. Found: C, 57.87; H, 6.93; N, 3.96. Crystals suitable for X-ray diffraction analysis were grown from pentane at -35 °C.

Synthesis of 4-2. A glass vial containing a magnetic stir bar was charged with **2-1b** (0.40 g, 0.95 mmol), $NiCl_2$(dme) (0.21 g, 0.95 mmol), and subsequently THF (8 mL), resulting in the formation of a bright purple solution. Magnetic stirring was initiated. After 30 min, a solution of $LiN(SiMe_3)_2$ (0.16 g, 0.95 mmol) dissolved in THF (4 mL) was added to the stirring solution, which turned orange-red. After 20 min, the volatile components were removed *in vacuo*. The remaining residue was triturated with pentane (3 × 3 mL), taken up in benzene (10 mL), and the mixture was filtered through Celite. The eluent was collected and the volatile components were removed *in vacuo.* The resulting red residue was triturated with pentane (3 × 3 mL) and dried *in vacuo* to afford analytically pure **4-2** (0.41 g, 84% yield) as a dark red solid. ^{1}H NMR (500 MHz, benzene-d_6): δ 7.31 (m, 4H, H_{arom}), 7.03 (m, 2H, H_{arom}), 6.91-6.89 (overlapping resonances, 4H, H_{arom}), 6.84-6.75 (overlapping resonances, 6H, H_{arom}), 4.03 (apparent septet, 4H, $^{3}J_{HH}$ = 7 Hz, Me*CH*Me), 1.94 (d, 12 H, $^{3}J_{HH}$ = 7 Hz, *Me*CHMe), 1.55 (d, 36 H, $^{3}J_{PH}$ = 14 Hz, P*tBu*$_2$), 0.98 (d, 12 H, $^{3}J_{HH}$ = 7 Hz, MeCH*Me*). $^{13}C\{^{1}H\}$ NMR (125.7 MHz, benzene-d_6): δ 177.4 (C_{arom}, from HMBC), 145.2 (C_{arom}), 135.2 (d, $^{2}J_{PC}$ = 22 Hz, PN*C*N), 130.8 (CH$_{arom}$), 128.8 (CH$_{arom}$), 127.1 (CH$_{arom}$), 126.0 (CH$_{arom}$), 123.4 (CH$_{arom}$), 39.3 (d, $^{1}J_{PC}$ = 25 Hz, P*C*Me$_3$), 29.1 (Me*C*HMe), 28.4 (PC*Me*$_3$), 24.7 (*Me*CHMe), 23.5 (MeCH*Me*). $^{31}P\{^{1}H\}$ NMR (202.5 MHz, benzene-d_6): δ 118.5. Anal. Calcd for $C_{54}H_{80}C_{l2}N_4Ni_2P_2$: C, 62.64; H, 7.79; N, 5.41. Found: C, 62.53; H, 7.90; N, 5.43.

Synthesis of 4-3. To a glass vial containing a magnetic stir bar and $(CH_3CN)_2PdCl_2$ (0.15 g, 0.44 mmol) was added a solution of **2-1b** (0.19 g, 0.44 mmol) in THF (15 mL). Magnetic stirring was initiated, and after 18 h the reaction mixture (containing the presumptive intermediate (κ^2-P,N-**[H]**)$PdCl_2$) was comprised of an orange solution and a yellow precipitate. The reaction mixture was then treated with Cs_2CO_3 (0.29 g, 0.89 mmol), followed by magnetic stirring for 18 h. Afterwards, the reaction mixture was filtered through Celite, and the solvent was removed from the collected eluent *in vacuo*. The resulting yellow powder was then redissolved in toluene (10 mL) and filtered through a Celite plug. The solvent was then removed from the collected eluent *in vacuo*, and the yellow solid residue was triturated with pentane (3 x 1 mL). The residue was then dried *in vacuo* yielding analytically pure **4-3** (0.16 g, 64%). ^{1}H NMR (500 MHz, benzene-d_6): δ 7.48 (m, 4H, H_{arom}), 7.10 (m, 2H, H_{arom}), 7.02-7.00 (m, 4H, H_{arom}), 6.85 (m, 6H, H_{arom}), 3.77 (apparent septet, 4H, $^3J_{HH}$ = 7 Hz, MeC*H*Me), 1.69 (d, 12H, $^3J_{HH}$ = 7 Hz, *Me*CHMe), 1.43 (d, 36H, $^3J_{PH}$ = 15 Hz, P*tBu*$_2$), 1.01 (d, 12H, $^3J_{HH}$ = 7 Hz, Me*C*H*Me*). ^{13}C{^{1}H} NMR (125.7 MHz, benzene-d_6): δ 176.8 (C_{arom}), 145.5 (C_{arom}), 145.0 (C_{arom}), 134.6 (d, $^2J_{PC}$ = 26 Hz, PN*C*N), 131.0 (*C*H$_{arom}$), 129.0 (*C*H$_{arom}$), 127.2 (*C*H$_{arom}$), 126.6 (*C*H$_{arom}$), 123.6 (*C*H$_{arom}$), 40.6 (d, $^1J_{PC}$ = 30 Hz, P*C*Me$_3$), 28.8 (Me*C*HMe), 28.3 (m, PC*Me*$_3$), 24.7 (*Me*CHMe), 23.4 (MeCH*Me*). ^{31}P{^{1}H} NMR (202.5 MHz, benzene-d_6): δ 142.8. Anal. Calcd for $C_{54}H_{80}Cl_2N_4P_2Pd_2$: C, 57.35; H, 7.13; N, 4.95. Found: C, 57.21; H, 7.14; N, 4.60. Crystals suitable for X-ray diffraction analysis were grown from toluene at room temperature.

Synthesis of 4-4. A glass vial containing a magnetic stir bar was charged with [(κ^2-P,N-**1**)NiCl]$_2$ (0.078 g, 0.075 mmol) and Et_2O (4 mL), and magnetic stirring was initiated. Into

a separate vial BnMgCl (1.0M in Et_2O, 150 μL, 0.150 mmol) was delivered via microsyringe, followed by the addition of Et_2O (2 mL); this mixture was then added to the solution of **4-2** as prepared above, resulting in a color change from red-orange to orange. After 18 h, the volatile components were removed *in vacuo*, leaving an orange, amorphous solid residue. This residue was triturated with pentane (2 × 3 mL) and was then extracted into benzene (10 mL), followed by filtration through Celite. From the collected eluent the benzene was removed *in vacuo*. The resulting orange residue was triturated with pentane (3 × 3 mL) and dried *in vacuo* to afford analytically pure **4-4** (0.080 g, 93%). ^{1}H NMR (300 MHz, benzene-d_6): δ 7.59 (m, 2H, H_{arom}), 7.11 – 7.01 (overlapping resonances, 3H, H_{arom}), 6.91 – 6.87 (overlapping resonances, 3H, H_{arom}), δ 6.66 (m, 1H, H_{arom}), 6.47 (m, 2H, H_{arom}), 6.20 (m, 2H, H_{arom}), 3.37 (apparent septet, 2H, $^3J_{HH}$ = 7 Hz, Me*CH*Me), 1.59 (d, 2H, $^3J_{PH}$ = 3 Hz, Ni*CH*$_2$Ph), 1.43 (d, 18H, $^3J_{PH}$ = 14 Hz, P*tBu*$_2$), 1.11 (d, 6H, $^3J_{HH}$ = 7 Hz, *Me*CHMe), 0.85 (d, 6H, $^3J_{HH}$ = 7 Hz, MeCH*Me*). ^{13}C{^{1}H} NMR (75.4 MHz, benzene-d_6): δ 176.1 (C_{arom}, from HMBC), 150.4 (C_{arom}, from HMBC), 142.5 (C_{arom}), 137.3 (d, $^2J_{PC}$ = 20 Hz, PN*C*N), 133.7 (d, $^3J_{PC}$ = 2 Hz, *C*H$_{arom}$), 131.4 (*C*H$_{arom}$), 128.3 (*C*H$_{arom}$, from HMBC), 126.9 (*C*H$_{arom}$), 126.2 (d, $^4J_{PC}$ = 2 Hz, *C*H$_{arom}$), 124.4 (*C*H$_{arom}$), 123.4 (*C*H$_{arom}$), 117.2 (apparent singlet, *C*$_{arom}$), 112.4 (d, $^2J_{PC}$ = 5 Hz, *C*H$_{arom}$), 38.1 (d, $^1J_{PC}$ = 28 Hz, P*C*Me$_3$), 28.8-28.7 (overlapping resonances, Me*C*HMe and PC*Me*$_3$), 24.1 (*Me*CHMe), 23.9 (MeCH*Me*), 19.5 (d, $^2J_{PC}$ = 11 Hz, Ni*C*H$_2$Ph). ^{31}P{^{1}H} NMR (121.5 MHz, benzene-d_6): δ 118.9. Anal. Calcd. for $C_{34}H_{47}N_2NiP$: C, 71.22; H, 8.26; N, 4.89. Found: C, 71.26; H, 8.31; N, 4.95. Crystals suitable for X-ray diffraction analysis were grown from a concentrated pentane/Et_2O solution at room temperature.

Synthesis of 4-5. To a glass flask fitted with a re-sealable PTFE stopper was added a magnetic stir bar, a solution of **4-3** (0.22 g, 0.192 mmol) in benzene (20 mL), and BnMgCl (1.0 M, 384 μL, 0.384 mmol), the latter via microsyringe. After sealing the flask with a PTFE stopper, the reaction flask was partially submerged in an oil bath that was set to 60 °C and magnetic stirring was initiated. Over the course of 18 h, the initially orange reaction mixture transitioned to dark brown coloration. After cooling to room temperature, the reaction mixture was filtered through Celite and the solvent was removed from the collected eluent *in vacuo*. The resulting brown powder residue was redissolved in a minimal amount of toluene, and was set to crystallize at -35 °C. Brown crystals of **4-5** that formed were isolated via removal of the supernatant, and drying of the crystals *in vacuo* (0.17 g, 72%). ^{1}H NMR (500 MHz, benzene-d_6): δ 7.68 (m, 2H, H_{arom}), 7.03 (s, 3H, H_{arom}), 6.91 (m, 3H, H_{arom}), 6.59 (m, 3H, H_{arom}), 6.43 (m, 2H, H_{arom}), 3.35 (apparent septet, 2H, $^{3}J_{HH}$ = 7 Hz, Me*CH*Me), 2.48 (s, 2H, Pd*CH*$_2$Bn), 1.38 (d, 18H, $^{3}J_{PH}$ = 15 Hz, P*t*Bu$_2$), 1.04 (d, 6H, $^{3}J_{HH}$ = 7 Hz, *Me*CHMe), 0.93 (d, 6H, $^{3}J_{HH}$ = 7 Hz, MeCH*Me*). ^{13}C{^{1}H} NMR (125.7 MHz, benzene-d_6): δ 174.1 (C_{arom}), 149.6 (C_{arom}), 142.0 (C_{arom}), 137.1 (d, $^{2}J_{PC}$ = 20 Hz, PN*C*N), 132.3 (d, $^{3}J_{PC}$ = 3 Hz, *C*H$_{arom}$), 131.0 (*C*H$_{arom}$), 128.5 (*C*H$_{arom}$), 127.1 (*C*H$_{arom}$), 127.0 (d, $^{4}J_{PC}$ = 4 Hz, *C*H$_{arom}$), 124.3 (C_{arom}), 124.1 (*C*H$_{arom}$), 123.2 (*C*H$_{arom}$), 117.0 (d, $^{2}J_{PC}$ = 8 Hz, *C*H$_{arom}$), 38.5 (d, $^{1}J_{PC}$ = 29 Hz, P*C*Me$_3$), 28.6 (d, $^{2}J_{PC}$ = 4 Hz, PC*Me*$_3$), 28.5 (Me*C*HMe), 26.0 ($^{2}J_{PC}$ = 8 Hz, Pd*C*H$_2$Ph), 24.2 (*Me*CHMe), 23.5 (MeCH*Me*). ^{31}P{^{1}H} NMR (202.5 MHz, benzene-d_6): δ 130.3. Anal. Calcd for $C_{34}H_{47}N_2PPd$: C, 65.74; H, 7.63; N, 4.51. Found: C, 65.49; H, 7.71; N, 4.24. Crystals suitable for X-ray diffraction analysis were grown from mixture of pentane and toluene at -35 °C.

Synthesis of 4-6. To a solution of **4-1** (0.10 g, 0.14 mmol) in THF (10 mL) in a glass vial containing a magnetic stir bar was added a solution of *t*-butylamine borane (0.012, 0.14 mmol) that had been dissolved in a minimal amount of THF. Magnetic stirring was initiated and the reaction solution changed from a pale yellow to brown within 0.5 h. After 18 h the solvent was removed *in vacuo* and the resultant yellow-brown solid was re-dissolved in toluene (5 mL). This solution was then filtered through a Celite plug. The eluent was collected and then concentrated *in vacuo* to about 1 mL, followed by storage at -35 °C to induce crystallization. The dark supernatant solution was then removed via pipette and the resulting yellow crystals were dried *in vacuo*, yielding analytically pure **4-6** (0.092, 92%). ^{1}H NMR (500 MHz, benzene-d_6): δ 7.70 (m, 2H, H_{arom}), 7.24 (m, 2H, H_{arom}), 7.11 (m, 2H, H_{arom}), 7.00 (m, 1H, H_{arom}), 6.91 (s, 3H, H_{arom}) 6.80-6.75 (m, 3H, H_{arom}), 5.18 (br s, 1H, N*H*), 4.02 (d with Pt satellites, 2H, $^{3}J_{PH}$ = 8 Hz, $^{2}J_{PtH}$ = 119 Hz, Pt*CH*$_2$Ph), 3.44 (apparent septet, 2H, $^{3}J_{HH}$ = 7 Hz, Me*CH*Me), 1.54 (d, 6H, $^{3}J_{HH}$ = 7 Hz, *Me*CHMe), 1.18 (d, 18H, $^{3}J_{PH}$ = 14 Hz, P*tBu*$_2$), 1.04 (d, 6H, $^{3}J_{HH}$ = 7 Hz, MeCH*Me*), -1.85 (d with Pt satellites, 1H, $^{2}J_{PH}$ = 237 Hz, $^{1}J_{PtH}$ = 1413 Hz, Pt*H*). ^{13}C{^{1}H} NMR (125.7 MHz, benzene-d_6): δ 165.2 (C_{arom}), 165.1 (C_{arom}), 155.7 (C_{arom}), 148.3 (C_{arom}), 140.5 (C_{arom}), 132.7 (d, $^{2}J_{PC}$ = 5 Hz, PN*C*N), 130.2 (*C*H$_{arom}$), 129.7 (*C*H$_{arom}$), 128.4 (*C*H$_{arom}$), 127.6 (*C*H$_{arom}$), 127.4 (*C*H$_{arom}$), 126.3 (C_{arom}), 123.3 (*C*H$_{arom}$), 121.9 (*C*H$_{arom}$), 38.0 (d, $^{1}J_{PC}$ = 9 Hz, P*C*Me$_3$), 28.4 (Me*C*HMe), 28.1 (d, $^{2}J_{PC}$ = 8 Hz, PC*Me*$_3$), 24.2 (*Me*CHMe), 22.9 (MeCH*Me*), -2.05 (s with Pt satellites, $^{1}J_{PtC}$ = 667 Hz, Pt*C*H$_2$Ph). ^{31}P{^{1}H} NMR (202.5 MHz, benzene-d_6): 107.6 (s with Pt satellites, $^{1}J_{PtP}$ = 1762 Hz). Anal. Calcd for $C_{34}H_{49}N_2PPt$: C, 57.35; H, 6.94; N, 3.94. Found: C, 57.14; H, 6.82, N, 4.17. Crystals suitable for X-ray diffraction analysis were grown from toluene at -35 °C.

Synthesis of 4-7. To a solution of **4-1** (0.15 g, 0.20 mmol) in toluene (10 mL) in a glass vial containing a magnetic stir bar was added pinacolborane (148 μL, 1.0 mmol) via microsyringe; magnetic stirring was then initiated. After 36 h, ^{31}P NMR analysis of the reaction mixture revealed the clean formation of **4-7**. At this point, the reaction mixture was concentrated *in vacuo* to about 1 mL followed by storage at -35 °C to induce crystallization, which afforded **4-7** as a yellow crystalline solid. The supernatant was removed via pipette. The yellow crystals were then washed with a minimal amount of cold (-35 °C) pentane and dried *in vacuo* yielding analytically pure **4-7** (0.077, 45%). ^{1}H NMR (500 MHz, benzene-d_6): δ 7.70 (m, 2H, H_{arom}), 7.26 (d, 1H, $^{3}J_{HH}$ = 7 Hz, H_{arom}), 7.06 (t, 1H, $^{3}J_{HH}$ = 8 Hz, H_{arom}), 6.90-6.70 (m, 7H, H_{arom}), 6.50 (br t, 1H, $^{3}J_{HH}$ = 7 Hz, H_{arom}), 6.07 (br s, 1H, H_{arom}), 4.77 (apparent septet, 1H, $^{3}J_{HH}$ = 7 Hz, Me*CH*Me), 3.20 (s, 1H, C*H*BPin), 2.54 (apparent septet, 1H, $^{3}J_{HH}$ = 7 Hz, Me*CH*Me), 1.69 (d, 3H, $^{3}J_{HH}$ = 7 Hz, *Me*CHMe), 1.61 (d, 9H, $^{3}J_{PH}$ = 15 Hz, P*tBu*$_2$), 1.39 (d, 3H, $^{3}J_{HH}$ = 7 Hz, *Me*CHMe), 1.31 (d, 9H, $^{3}J_{PH}$ = 15 Hz, P*tBu*$_2$), 1.13 (s, 6H, OC*Me*$_2$), 1.05 (s, 6H, OC*Me*$_2$), 0.55 (d, 3H, $^{3}J_{HH}$ = 7 Hz, MeCH*Me*), 0.48 (d, 3H, $^{3}J_{HH}$ = 7 Hz, MeCH*Me*). ^{13}C{^{1}H} NMR (125.7 MHz, benzene-d_6): δ 176.2 (C_{arom}), 150.1 (C_{arom}), 143.4 (C_{arom}), 143.1 (C_{arom}), 135.8 (d, $^{2}J_{PC}$ = 20 Hz, PN*C*N), 131.4 (C_{arom}), 128.5 (CH$_{arom}$), 128.3 (CH$_{arom}$), 127.1 (CH$_{arom}$), 126.1 (CH$_{arom}$), 125.2 (CH$_{arom}$), 124.1 (C_{arom}), 123.4 (CH$_{arom}$), 123.2 (CH$_{arom}$), 100.4 (CH$_{arom}$, from HSQC/HMBC), 82.5 (O*C*Me$_2$), 39.2-38.3 (m, 2 P*C*Me$_3$), 29.2 (Me*C*HMe), 29.0 (d, $^{2}J_{PC}$ = 4 Hz, PC*Me*$_3$), 28.5 (d, $^{2}J_{PC}$ = 3 Hz, PC*Me*$_3$), 27.6 (Me*C*HMe), 25.8 (OC*Me*$_2$), 25.2 (OC*Me*$_2$), 25.1 (*Me*CHMe), 24.8 (*Me*CHMe), 23.8 (MeCH*Me*), 22.4 (MeCH*Me*), 18.0 (*C*HBPin, from HSQC). ^{31}P{^{1}H} NMR (202.5 MHz, benzene-d_6): δ 111.9 (s with Pt satellites, $^{1}J_{PtP}$ = 5285 Hz). ^{11}B NMR (96.3 MHz, benzene-d_6): δ 32.6

(broad s, $\Delta\nu_{1/2}$ = 860 Hz). Anal. Calcd for $C_{40}H_{58}N_2O_2BPPt$: C, 57.48; H, 6.99; N, 3.38. Found: 57.19; H, 6.81; N, 3.17. Crystals suitable for X-ray diffraction analysis were grown from toluene at -35 °C.

Synthesis of 4-8. A method directly analogous to the preparation of **4-7** was employed, using **4-1** (0.15, 0.21 mmol), and catecholborane (113 μL, 1.05 mmol) in place of pinacolborane, with a reaction time of 18 h. The target product **4-8** was obtained as an analytically pure, yellow crystalline solid (0.12 g, 64 %). ^{1}H NMR (500 MHz, benzene-d_6): δ 7.62 (m, 2H, H_{arom}), 7.25 (d, 1H, $^3J_{HH}$ = 8 Hz, H_{arom}), 7.07 (m, 4H, H_{arom}), 6.95 (d, 1H, $^3J_{HH}$ = 8 Hz, H_{arom}), 6.88-6.83 (m, 6H, H_{arom}), 6.79 (m, 1H, H_{arom}) 6.71 (m, 1H, H_{arom}) 6.57 (br t, 1H, $^3J_{HH}$ = 7 Hz, H_{arom}), 4.55 (apparent septet, 1H, $^3J_{HH}$ = 7 Hz, Me*CH*Me), 3.37 (s, 1H, C*H*BCat), 2.60 (apparent septet, 1H, $^3J_{HH}$ = 7 Hz, Me*CH*Me), 1.69 (d, 3H, $^3J_{HH}$ = 7 Hz, *Me*CHMe), 1.32 (d, 9H, $^3J_{PH}$ = 15 Hz, P*tBu*$_2$), 1.31 (d, 9H, $^3J_{PH}$ = 15 Hz, P*tBu*$_2$), 1.21 (d, 3H, $^3J_{HH}$ = 7 Hz, *Me*CHMe), 0.59 (d, 3H, $^3J_{HH}$ = 7 Hz, MeCH*Me*), 0.53 (d, 3H, $^3J_{HH}$ = 7 Hz, MeCH*Me*). ^{13}C{^{1}H} NMR (125.7 MHz, benzene-d_6): δ 176.2 (C_{arom}), 149.8 (C_{arom}), 148.9 (C_{arom}), 143.7 (C_{arom}), 143.1 (C_{arom}), 135.2 (d, $^2J_{PC}$ = 23 Hz, PN*C*N), 131.3 (CH$_{arom}$), 128.7 (CH$_{arom}$), 127.2 (CH$_{arom}$), 127.1 (CH$_{arom}$), 125.6 (CH$_{arom}$), 123.4 (CH$_{arom}$), 122.5 (CH$_{arom}$), 118.0 (CH$_{arom}$), 112.0 (CH$_{arom}$), 108.9 (CH$_{arom}$), 39.3-38.1 (m, 2 P*C*Me$_3$), 29.1 (Me*C*HMe), 28.4 (d, $^2J_{PC}$ = 3 Hz, PC*Me*$_3$), 28.2 (d, $^2J_{PC}$ = 4 Hz, PC*Me*$_3$), 27.7 (Me*C*HMe), 25.0 (*Me*CHMe), 24.7 (*Me*CHMe), 23.6 (MeCH*Me*), 22.5 (MeCH*Me*), 18.0 (*C*HBCat, from HSQC). ^{31}P{^{1}H} NMR (202.5 MHz, benzene-d_6): δ 111.0 (s with Pt satellites, $^1J_{PtP}$ = 4799 Hz). ^{11}B NMR (96.3 MHz, benzene-d_6): δ 34.6 (broad s, $\Delta\nu_{1/2}$ = 700 Hz). Anal. Calcd for $C_{40}H_{50}BN_2O_2PPt$: C, 58.04; H, 6.09; N, 3.38.

Found: C, 58.19; H, 6.32, N, 3.27. Crystals suitable for X-ray diffraction analysis were grown from toluene at -35 °C.

Protocol for kinetic experiments. The reaction of **4-1** with HBPin leading to **4-7** was chosen for kinetic analysis, as it was found to proceed slower than the reaction with HBcat, thereby enabling more data to be collected. To obtain the rate constant k at 300 K, **4-1** was treated with five different concentrations of HBPin (10, 15, 20, 25, 30 equiv) and in each case the formation of **4-7** was plotted against time to establish k_{obs} for each reaction as seen below. The k_{obs} data were then plotted against concentration of HBPin, from which the second order rate constant was extracted (Figure 4-15). In the case of room temperature kinetic experiments, **4-1** was weighed out into a small shell vial (0.010 g, 0.0141 mmol). Ferrocene was weighed out into a separate shell vial (0.005, 0.0282 mmol). A calibrated microsyringe was used to transfer 0.5 mL of toluene-d_8 to **4-1**. A pipette was then used to transfer the solution to the vial containing ferrocene and then to an NMR tube. HBPin was added via microsyringe in varying concentrations (10, 15, 20, 25, 30 equiv with respect to **4-1**) and the time of addition was noted. The NMR tube was then inserted to a 300 MHz Bruker NMR spectrometer and the function multizg3.ml was used to standardize sampling time. Acquisition parameters were adjusted to 16 scans and a relaxation delay of 6 seconds to ensure proper integration values. The resulting spectra were integrated against the ferrocene standard to determine the concentration of **4-7** in the sample. Experiments conducted at 310, 315, 320, and 325 K, from which an Eyring plot was derived, were performed in a similar manner, with the exception that 20 equiv HBPin was employed throughout. The NMR spectrometer was heated to the selected temperature prior to addition of HBPin and the temperature was confirmed by using an

80% ethylene glycol sample in DMSO-d_6.[125] Once the sample was inserted it was given 10 minutes to equilibrate before sampling began to ensure the rate measured aligned with the desired temperature. In all cases the graphing software Kaleidagraph was used to plot and analyze the data.

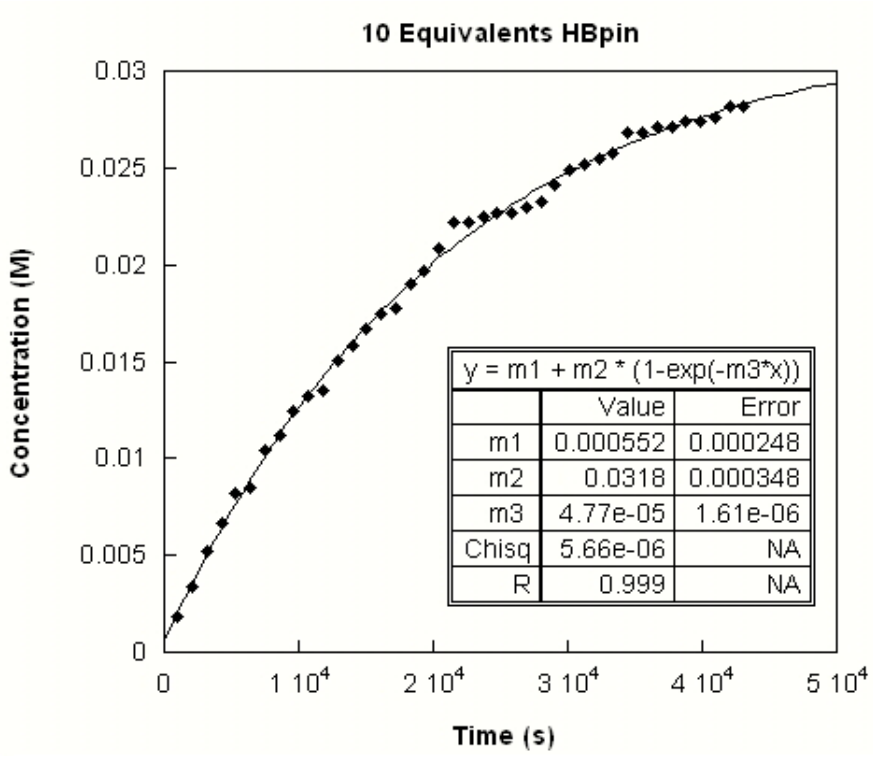

Figure 4-9. Concentration of **4-7** vs. time in the reaction of **4-1** with HBPin (10 equiv) at 300 K.

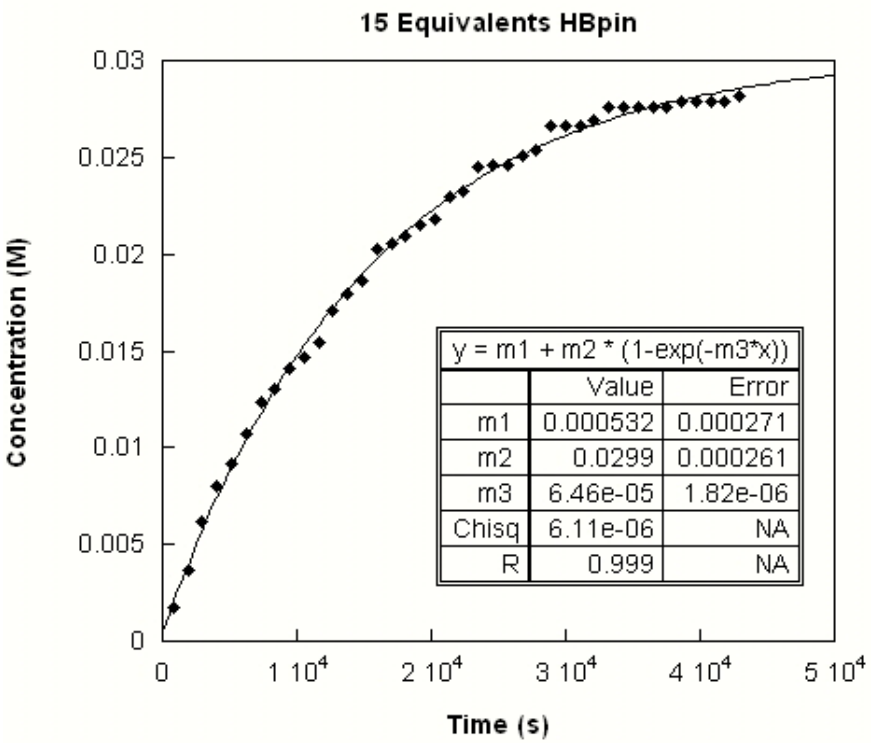

Figure 4-10. Concentration of **4-7** vs. time in the reaction of **4-1** with HBPin (15 equiv) at 300 K.

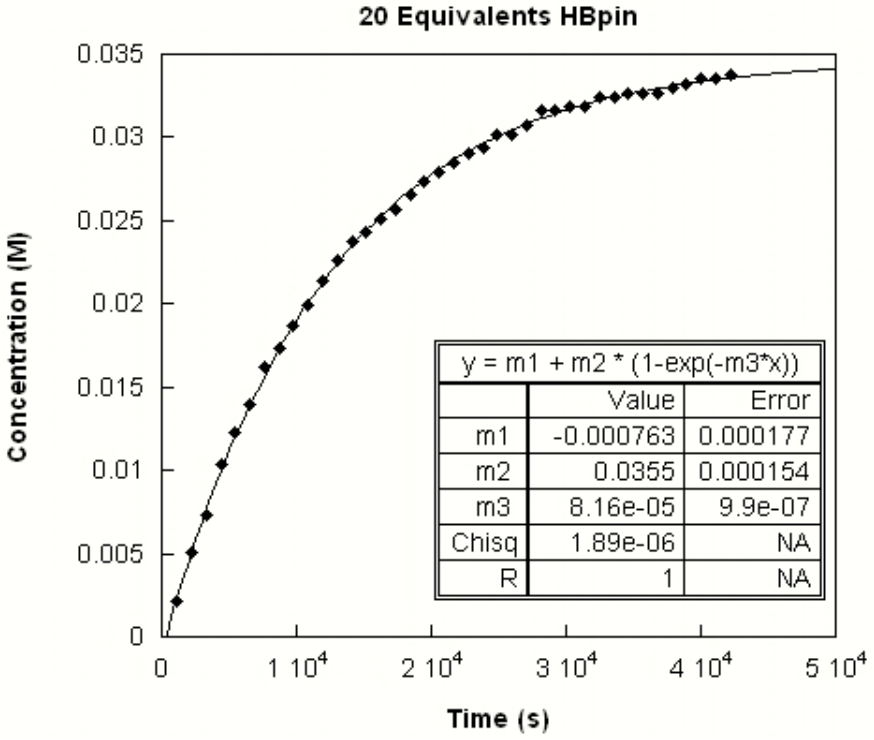

Figure 4-11. Concentration of **4-7** vs. time in the reaction of **4-1** with HBPin (20 equiv) at 300 K.

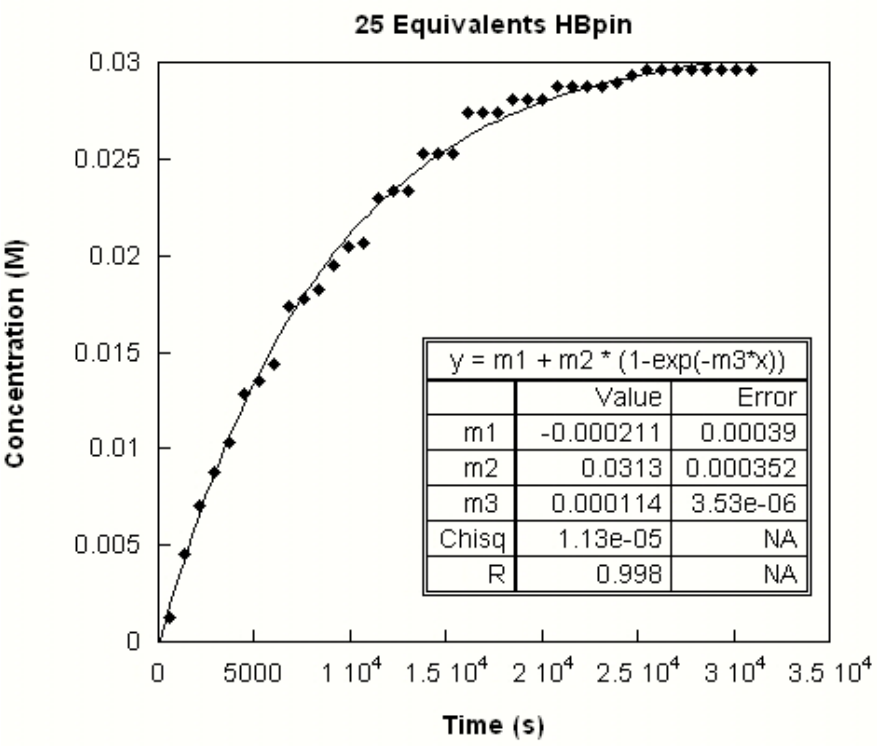

Figure 4-12. Concentration of **4-7** vs. time in the reaction of **4-1** with HBPin (25 equiv) at 300 K.

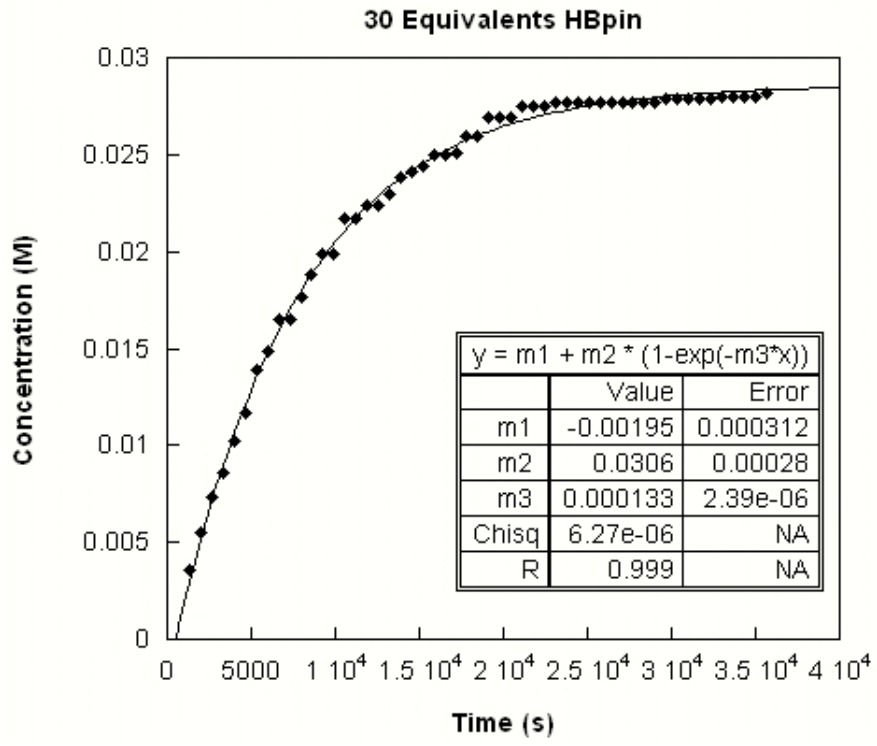

Figure 4-13. Concentration of **4-7** vs. time in the reaction of **4-1** with HBPin (30 equiv) at 300 K.

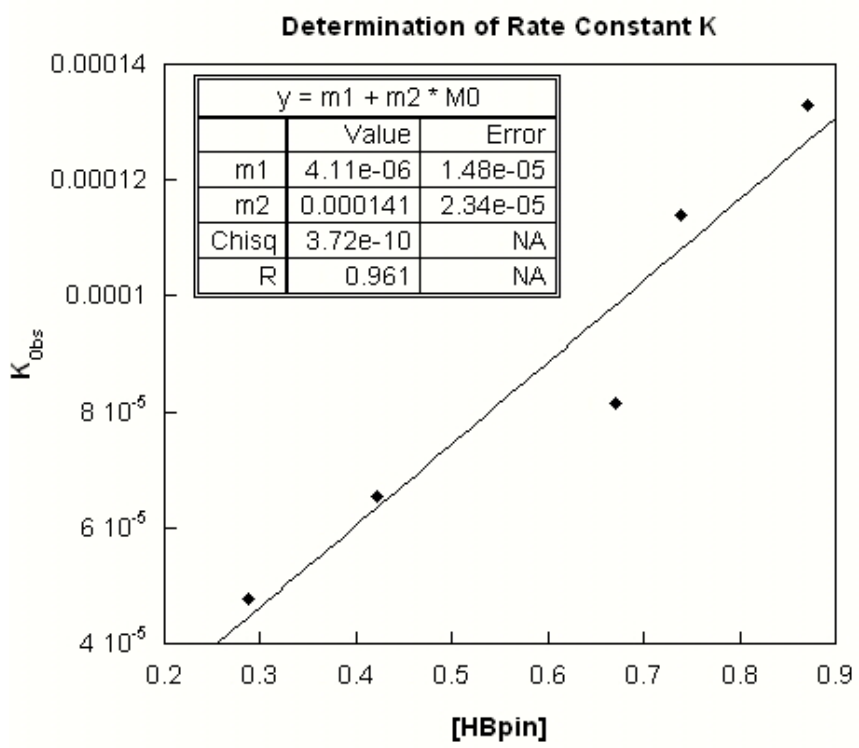

Figure 4-14. Determination of the second order rate constant (m2 in $M^{-1}s^{-1}$) for the reaction of **4-1** with HBPin at 300 K.

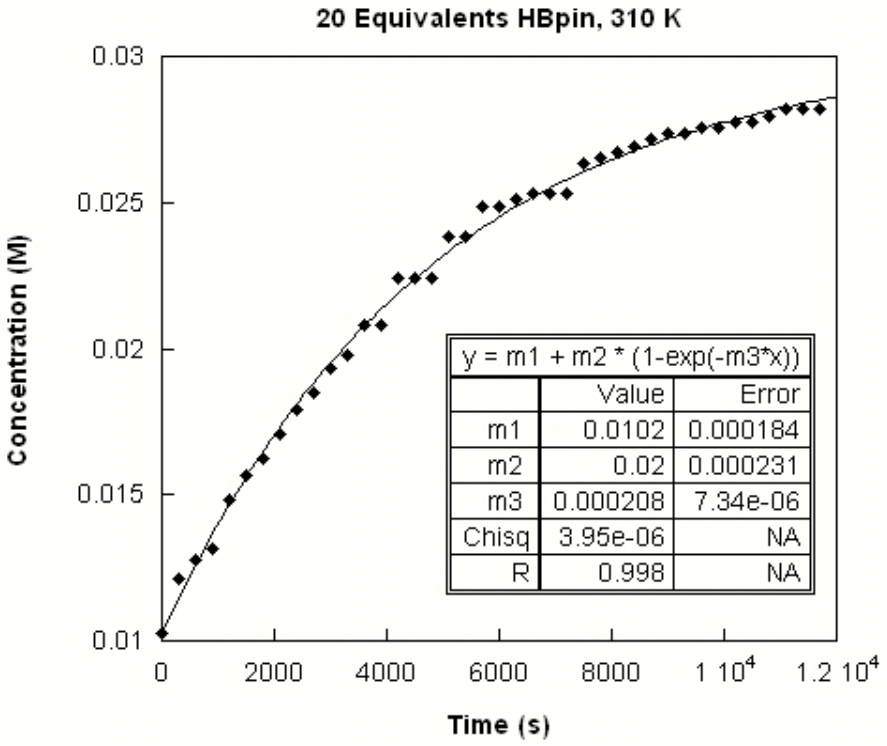

Figure 4-15. Concentration of **4-7** vs. time in the reaction of **4-1** with HBPin (20 equiv) at 310 K.

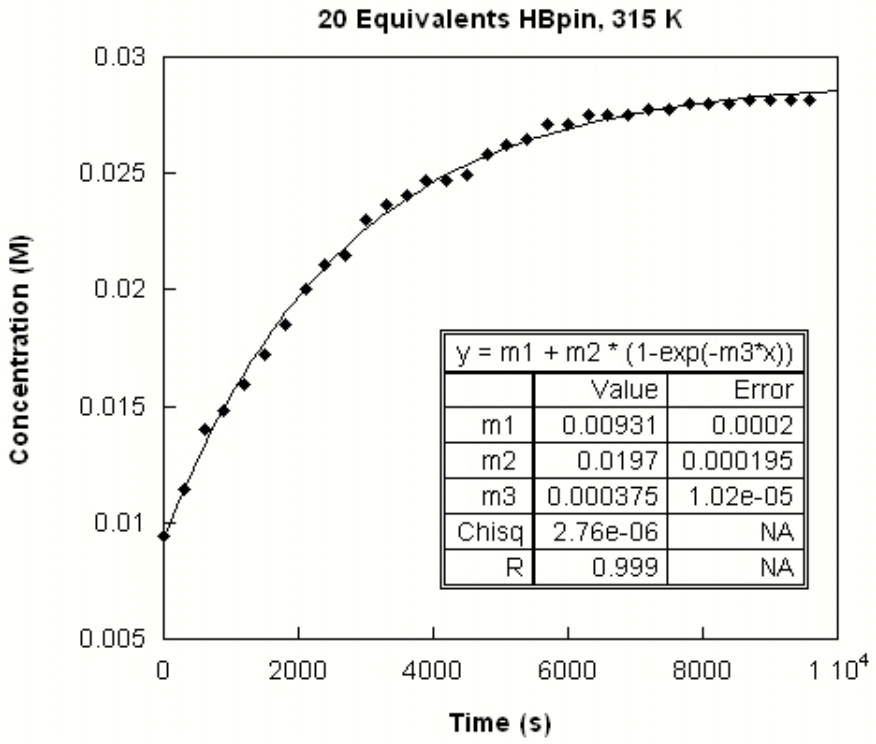

Figure 4-16. Concentration of **4-7** vs. time in the reaction of **4-1** with HBPin (20 equiv) at 315 K.

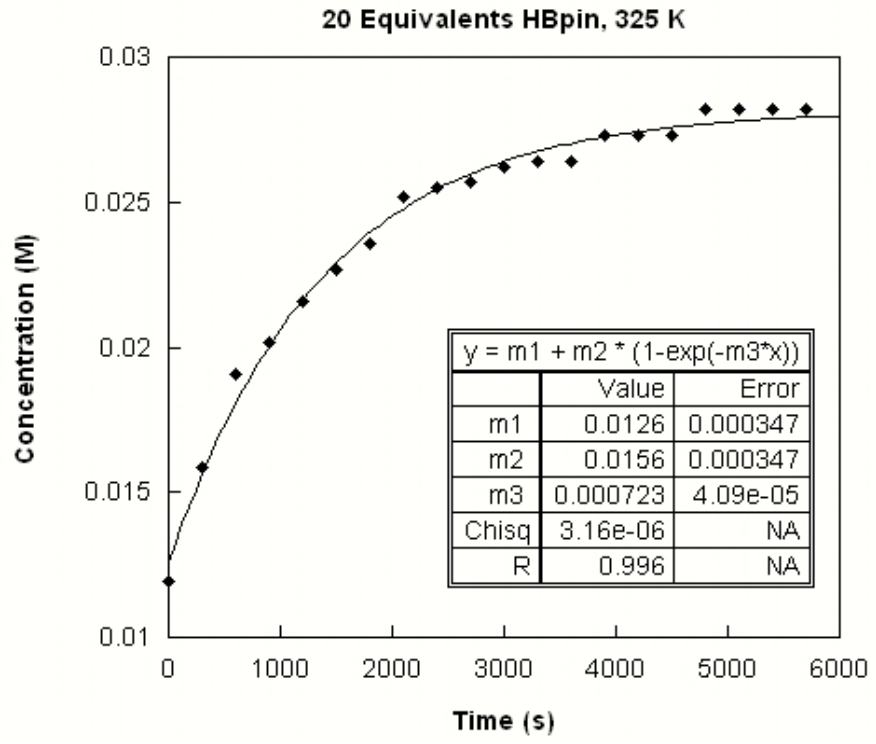

Figure 4-17. Concentration of **4-7** vs. time in the reaction of **4-1** with HBPin (20 equiv) at 325 K.

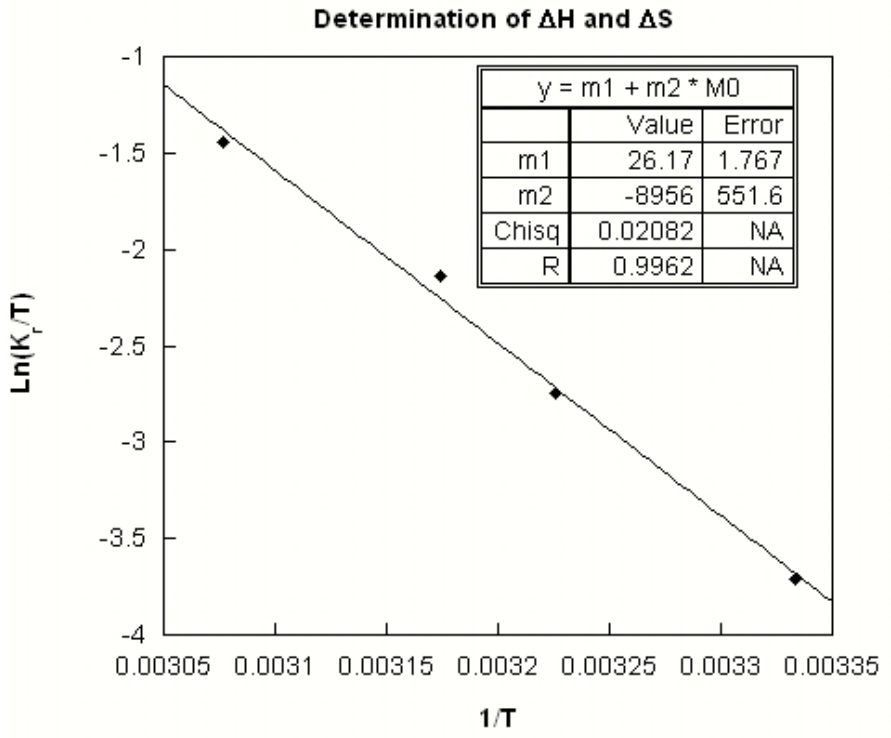

Figure 4-18. Eyring analysis based on the temperature dependence of the reaction of **4-1** with HBPin to give **4-7** (20 equiv HBPin; 300-325 K) yielding $\Delta H^{\ddagger}$ = 18(1) kcal/mol and $\Delta S^{\ddagger}$ = 6(3) eu at 300 K.

Crystallographic solution and refinement details. In each case crystallographic data were obtained at or below 193(±2) K on a Bruker D8/APEX II CCD diffractometer using either graphite-monochromated Mo Kα (λ = 0.71073 Å) or Cu Kα (λ = 1.54178 Å) radiation, employing a sample that was mounted in inert oil and transferred to a cold gas stream on the diffractometer. Programs for diffractometer operation, data collection, and data reduction (including SAINT) were supplied by Bruker. Gaussian integration (face-indexed) was employed as the absorption correction method throughout. All structures were refined by use of full-matrix least-squares procedures (on F^2) with R_1 based on $F_o^2 \geq 2\sigma(F_o^2)$ and wR_2 based on $F_o^2 \geq -3\sigma(F_o^2)$. Anisotropic displacement parameters were employed for all the non-hydrogen atoms of each complex. During the structure solution

process for **4-1**, two crystallographically independent molecules (A and B) were located in the asymmetric unit and were refined in a satisfactory manner. During the structure solution processes for **4-3** and **4-8** half an equivalent of toluene was located in the asymmetric unit and was refined in a satisfactory manner whereby all atoms were refined with an occupancy of 0.5 and a common isotropic displacement parameter. Distances involving the methyl carbon of the disordered solvent toluene molecule were constrained during refinement: d(C1S–C7S) = 1.52(1) Å, d(C2S...C7S) = d(C6S...C7S) = 2.52(1) Å. The carbon-atom positions for the toluene phenyl ring were refined as an idealized regular hexagon with a C–C bond distance of 1.390 Å. During the structure solution process for **4-2** half an equivalent of Et_2O was located in the asymmetric unit and was refined in a satisfactory manner whereby all atoms in the solvent molecule were refined with an occupancy factor of 0.5. In the case of **4-7**, the near-zero final refined value of the Flack parameter (0.020(2)) suggests that the correct configuration was chosen. The crystal structure of $[(\kappa^2\text{-P,N})PdCl]_2$ features half a molecule in the asymmetric unit, with the other half of the molecule (primed atoms) generated via the crystallographic inversion center (0.5, 0, 0.5) at the center of the Pd_2Cl_2 ring. Otherwise, all hydrogen atoms were added at calculated positions and refined by use of a riding model employing isotropic displacement parameters based on the isotropic displacement parameter of the attached atom. In all cases non-hydrogen atoms are represented by Gaussian ellipsoids at the 30% probability level. Additional crystallographic information is provided in the Appendix A.

CHAPTER 5: A Manganese Pre-Catalyst for the Mild Reduction of Amides, Ketones, Aldehydes, and Esters

5.1 Introduction

As stated in Chapter 1, over the past several years there has been a major focus on developing efficient and cheap base metal catalysts to replace the current state-of-the-art that typically relies on expensive precious metal catalysts. The recent development of (κ^2-P,N)M(N(SiMe$_3$)$_2$ (M = Fe **1-2**; Co **1-3**) species by the Dalhousie/CPChem research team has led to impressive applications in base metal catalysis. Notably, complex **1-2** has proven to be among the most proficient iron catalysts for hydrosilyation of carbonyl compounds reported in the literature to date.[55] In moving beyond iron and cobalt, and inspired by the recent renaissance of manganese catalysis in organic synthesis,[126] the Dalhousie/CPchem team focused on synthesizing a manganese analog of **1-2**/**1-3** to pursue potentially novel and improved reactivity**.**

A variety of factors contribute to making manganese an attractive metal for catalysis. As it is the third most abundant transition metal in the earth's crust behind iron and titanium, it can be cheaply obtained. Furthermore, manganese is relatively non-toxic and biocompatible, which makes it particularly attractive to the pharmaceutical industry. Of particular interest to the Dalhousie/CPChem research team are the impressive recent examples of manganese-mediated carbonyl reductions based on transfer hydrogenation,[127] hydrogenation,[128] hydroboration,[129] and hydrosilylation.[130]

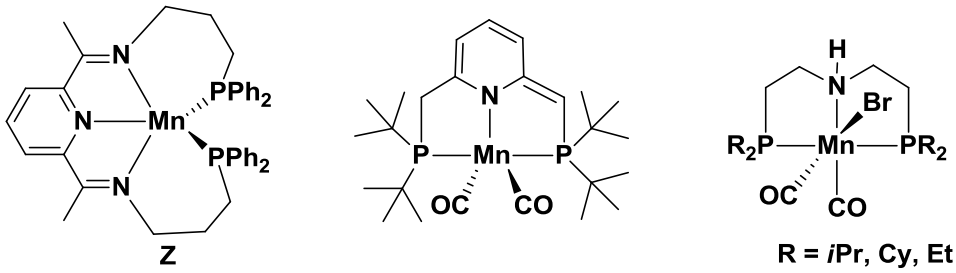

Figure 5-1. Recently reported manganese homogeneous catalysts**:** (PDI)Mn hydrosilylation catalyst (**Z**);[130a] (PNP)Mn pincer catalyst for imine synthesis from alcohols and amines (middle);[131] (PNP)Mn pincer catalyst for the hydrogenation of esters to alcohols (right)[132].

The reduction of carbonyl compounds is an important class of transformations that is employed widely in synthetic chemistry.[133] In moving beyond the use of harsh alkali metal hydrides (e.g., $LiAlH_4$) and related reductants, transition metal catalysis offers an effective alternative for such transformations. While platinum-group metal catalysts were examined early on, the high cost and low abundance of such metals has created motivation for the development of competitive late 3d transition metal catalysts,[134] most notably featuring iron, cobalt, and nickel. As such, a diversity of effective base metal-catalyzed carbonyl reduction protocols have emerged, including atom-economical transformations using hydrogen as the reductant. Complementary transformations such as hydrosilylation[135] are also of interest, in that in some cases they are successful when direct hydrogenation fails, and can be carried out conveniently without the need for pressurized reaction vessels.

Whereas useful base metal catalysts for the hydrosilative reduction of ketones, aldehydes, and/or esters have been developed,[134, 135b] selective reductions of amides to amines have proven to be significantly more challenging.[136] The first reports of such transformations were disclosed simultaneously by the groups of Beller[137] and Nagashima,[138] whereby tertiary amides were reduced by use of PMHS (PMHS =

polymethylhydrosiloxane) in the presence of $Fe(CO)_5$ or $Fe_3(CO)_{12}$ (6-30 mol% Fe), either under thermal (100 ˚C, 24 h) or photochemical activation (25 ˚C, 9 h). Subsequent reports by the groups of Sortais and Darcel,[139] Buitrago and Adolfsson,[140] and Driess[141] document the use of *N*-heterocyclic carbene-ligated Fe species for such transformations, which in some cases operate under mild reaction conditions. The Co-catalyzed hydrosilative reduction of amides is limited to a report by the group of Darcel and Sortais,[142] whereby $Co_2(CO)_8$ (1 mol% Co) was used primarily in combination with PMHS (100 ˚C, 3-16 h); in selected challenging transformations $PhSiH_3$ proved to be more effective, and photochemically activated reductions were also described. Amide reductions employing Ni catalysis are also rather uncommon. Following a report by Mamillapalli and Sekar,[143] whereby complete reduction of both keto and amide groups in α-keto amides was achieved by use of Ni-catalyzed hydrosilylation with Ph_2SiH_2 (5 mol% $Ni(OAc)_2$, 10 mol% TMEDA, 10 mol% KO*t*Bu, 25 ˚C), Garg and co-workers[144] disclosed the use of $PhSiH_3$ in amide reductions by use of $NiCl_2$(dme) (10 mol% Ni, 115 ˚C, 24 h). Remarkably, Beller and co-workers have recently reported on the relatively mild reduction of tertiary and secondary amides using $Zn(OAc)_2$ (tertiary amides: 10 mol%, 25-65 °C, 20-30 h; secondary amides: 20 mol%, 100 °C, 72 h); however, these typically required long reaction times and an excess of the silane reductant.[145] This was followed by a report by Adolfsson and co-workers using $ZnEt_2$ to reduce tertiary amides in the presence of LiCl and PMHS (5 mol% Zn, 10 mol% LiCl, 25-40 °C, 24 h), again requiring long reaction times and an excess of the silane reductant.[146] This progress notwithstanding, the base metal-catalyzed reduction of amides remains a significant

challenge. Moreover, no single catalyst system (base metal or other) that is capable of effecting the hydrosilative reduction of amides, ketones, aldehydes, and esters is known.

Conversely, prior to the work presented in this chapter, the Mn-catalyzed reduction of amides to amines was limited to two entries (dimethylformamide or diethylformamide)[147] employing a tertiary silane reductant and $CpMn(CO)_3$ (5 mol%), either under thermal (120 ˚C, 24 h) or photochemical activation (25 ˚C, 12-18 h).[148]

In this context, as part of the Dalhousie/CPChem research team's goals of targeting highly effective base metal catalysts supported by *N*-phosphinoamidinate ligation,[55] attention was turned to the preparation and application of manganese pre-catalysts of this type. This chapter will detail the preparation of the new (κ^2-P,N)Mn($N(SiMe_3)_2$) complex **5-1,** which is capable of effecting the hydrosilative reduction of tertiary amides to tertiary amines in a manner that is competitive with the most effective catalysts known for such transformations. Pre-catalyst **5-1** is also shown to accommodate a breadth of carbonyl substrates in such reductions (amides, ketones, aldehydes, and esters) that is unrivaled by any previously reported catalyst, in most cases at room temperature.

5.2 Results and Discussion

*5.2.1 Synthesis and Characterization of (κ^2-P,N)Mn($N(SiMe_3)_2$) (**5-1**)*

The targeted (κ^2-P,N)Mn($N(SiMe_3)_2$) pre-catalyst **5-1** was selected as an entry point for exploration of the Mn-catalyzed reduction of amides and other carbonyl compounds, on the basis of the outstanding performance of the analogous iron complex (**1-2**) in the reduction of ketones, aldehydes, and esters.[56] Treatment of the appropriate *N*-phosphinoamidine pro-ligand (**2-1b**) with $Mn(N(SiMe_3)_2)_2$ afforded **5-1**, which was

isolated as an analytically pure yellow solid in 73% yield (Scheme 5-1). The measured magnetic moment (Evans' method, 300 K, μ_{eff} = 5.9 μ_B) is consistent with a high-spin Mn(II) (S_{Mn} = 5/2) center, and crystallographic data (Figure 5-2) confirm the three-coordinate, distorted trigonal planar nature of **5-1** ($\Sigma_{anglesMn}$ = 360˚).

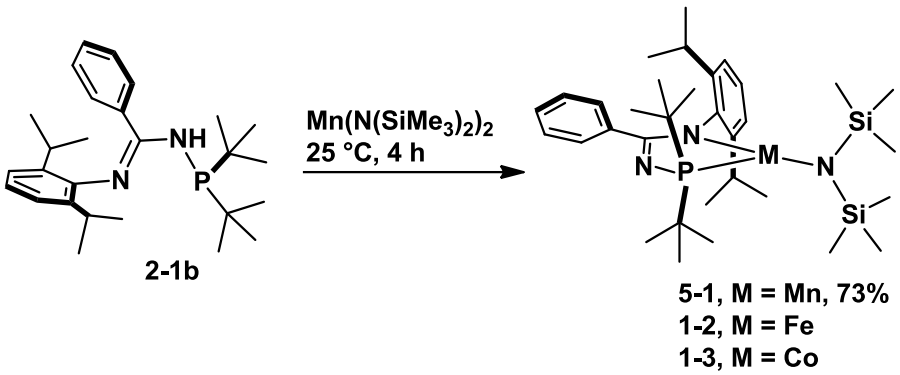

Scheme 5-1. Synthesis of (κ^2-P,N)Mn(N(SiMe$_3$)$_2$), the manganese analog of **1-2**/**1-3**.

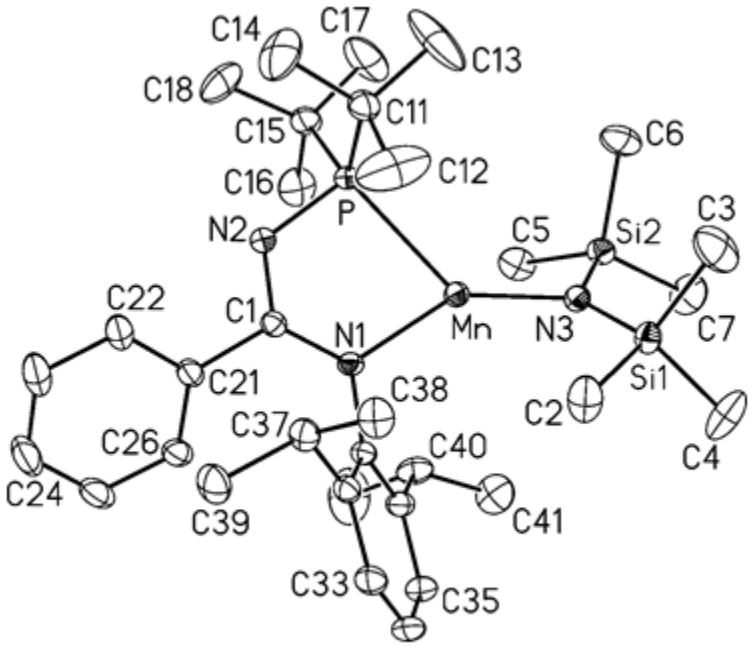

5-1

Figure 5-2. Crystallographically determined structure of **5-1**. Selected interatomic distances (Å) and angles (˚) within the two crystallographically independent molecules of **5-1**: Mn-P 2.5319(4) and 2.5045(4), Mn-N(1) 2.0722(12) and 2.0946(11), Mn-N(3)

1.9742(12) and 1.9696(12), P-Mn-N(1) 78.93(3) and 78.25(3), P-Mn-N(3) 135.20(4) and 141.28(4), N(1)-Mn-N(3) 145.54(5) and 140.11(5).

*5.2.2 Catalytic Reduction of Tertiary Amides Employing **5-1***

Having prepared **5-1**, the ability of this pre-catalyst to effect the reduction of tertiary amides under conditions of modest heating and relatively short reaction times was evaluated (5 mol% **5-1**, 75 ˚C, 1 h; Figure 5-3). The choice of $PhSiH_3$ as the reductant was made in light of the utility of this reductant in other base metal-catalyzed hydrosilative reduction of amides (*vide supra*), and on the basis of our previous examination of acetophenone reduction employing **1-2**, whereby the use of alternative silanes including PMHS afforded poor results. Under these conditions, pre-catalyst **5-1** proved effective in enabling the high-yielding and selective reduction of various tertiary amides to the corresponding tertiary amines. By use of this protocol, *N*-benzyl piperidines featuring substitution on both the piperidine and aryl rings were successfully generated, including the hindered variant **5-2e**; *N*-benzylmorpholine (**5-2f**) was obtained similarly in high isolated yield (85%). In examining the reduction of tertiary dibenzylamide variants, derived tertiary dibenzylamines featuring (hetero)benzyl, substituted benzyl, and aliphatic substituents (**5-(2g-2k)**) were prepared efficiently. The reduction of tertiary amides leading to dialkyl or aryl/alkyl benzylamine products (**5-2l** and **5-2m**) also proved feasible.

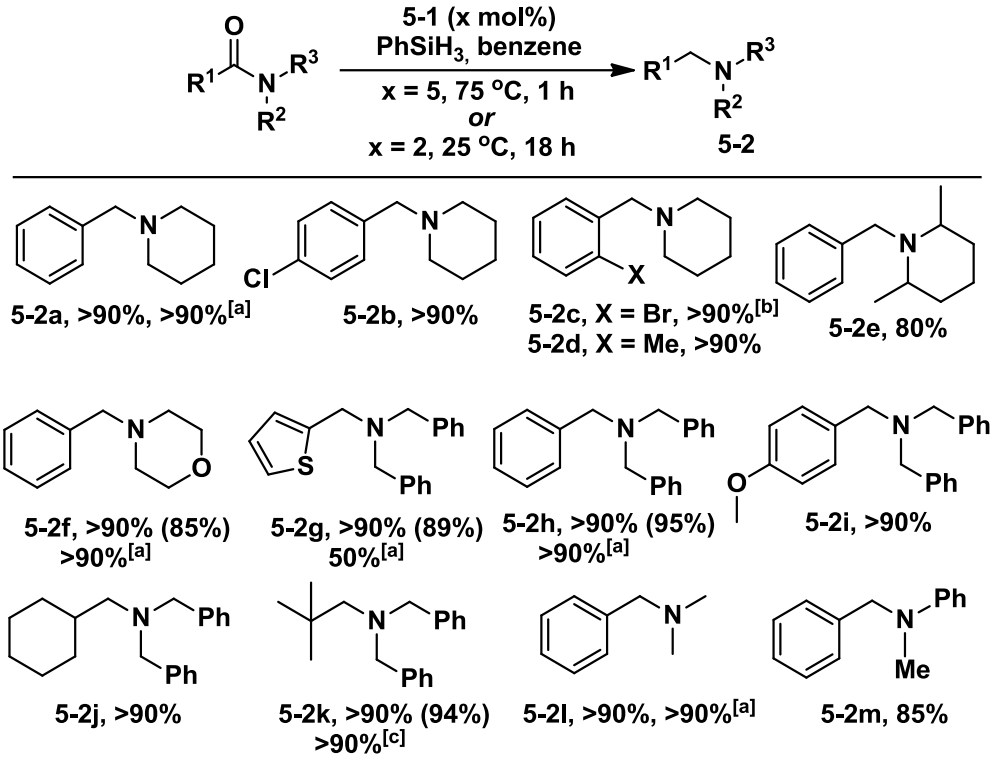

Figure 5-3. Catalytic reduction of tertiary amides to tertiary amines employing **5-1**. Reaction conditions: Unless stated otherwise, amide (0.4 mmol), $PhSiH_3$ (0.4 mmol), benzene (500 μL), **5-1** (5 mol%), 75 ˚C, 1 h. Target product identity confirmed on the basis of NMR analysis, and conversion to **5-2** determined by use of calibrated GC methods. Isolated yields in parentheses. [a] **5-1** (2 mol%), 25 ˚C, 18 h. [b] 3 h. [c] 2 mol% 1, 25 ˚C, 48 h.

Comparative experiments confirmed the superiority of **5-1** relative to both **1-2** and $Mn(N(SiMe_3)_2)_2$. In the case of amide reductions leading to **5-2k** (5 mol% pre-catalyst, 75 ˚C, 1 h) 70% conversion was achieved by use of $Mn(N(SiMe_3)_2)_2$ (*cf.* >90% with **5-1**), whereas a complex mixture of products including unreacted tertiary amide and **5-2k** (~1:1 ratio) was formed when using **1-2**. Similarly, <50% conversion to **5-2l** was achieved when using either $Mn(N(SiMe_3)_2)_2$ or **1-2** under conditions where >90% conversion to **5-2l** was attained by use of **5-1** (5 mol% pre-catalyst, 75 ˚C, 1 h). In keeping with our preliminary conjecture (*vide supra*), the use of PMHS (1 or 2 equiv, in a manner analogous to that described by Beller and co-workers[137]) with **5-1** in several test

reactions afforded low conversion of the tertiary amide, under conditions where complete conversion to the target tertiary amine was achieved when using $PhSiH_3$ (Figure 5-3). The ability to conduct such reductions on a proportionally larger scale (3.55 mmol amide) was demonstrated in the successful synthesis of **5-2k** (0.930 g, 98% isolated yield; 5 mol%, **5-1**, 75 ˚C, 4 h).

It is worthy of mention that in the absence of photochemical activation, the reduction of simple tertiary amides at room temperature by use of a 3d transition metal catalyst is unknown.[146, 149] In this context, the ability of **5-1** to effect such unprecedented transformations (2 mol% **5-1**, 25 ˚C, 18 h; Figure 5-3) was examined. Several of the tertiary amide substrates under investigation herein displayed high conversion to the desired tertiary amine under room temperature conditions, including the formation of *N*-benzylpiperidine (**5-2a**), *N*-benzylmorpholine (**5-2f**), tribenzylamine (**5-2h**), and *N*,*N*-dimethylbenzylamine (**5-2l**). However, limitations to this chemistry were encountered. Despite the high isolated yield of **5-2g** (89%) that was achieved by use of **5-1** at elevated temperature, poor conversion of the thiophene-derived amide substrate was observed at room temperature. In this regard, room temperature experiments for each amide substrate were not conducted as it became evident that elevated temperatures were required for full conversion in select cases. In stating this, 75 °C was chosen to accommodate the broad range of substrates shown in Figure 5-3, whilst keeping reaction times short. Furthermore, efforts to extend the use of **5-1** to the reduction of secondary amides have thus far proven unsuccessful.

*5.2.3 Catalytic Reduction of Ketones and Aldehydes Employing **5-1***

Given the success of **5-1** in the room temperature reduction of tertiary amides, the ability of this pre-catalyst to effect the reduction of alternative carbonyl substrates under mild conditions was explored further (1 mol% **5-1**, 25 ˚C, 4 h). Acetophenone and derivatives featuring electron-donating, electron-withdrawing, and extended aromatic substituents were each reduced successfully (**5-3a** to **5-3d)**, as was benzophenone leading to **5-3e** (Figure 5-4). Related acetophenone variants featuring sterically demanding alkyl or heteroaryl functionality, as well as 4-heptanone, were also well accommodated, leading to **5-3f** to **5-3h** in high yield. Aldehyde reduction was also achieved under mild conditions by use of **5-1**, leading to benzyl alcohol variants featuring electron-donating, electron-withdrawing, *ortho*-, and heteroaryl functionality (**5-3i** to **5-3m**). The observation of unreacted $PhSiH_3$ (each featuring three reducing equivalents) in these reactions suggests that that sub-stoichiometric amounts of the reductant may, in principle, be employed.

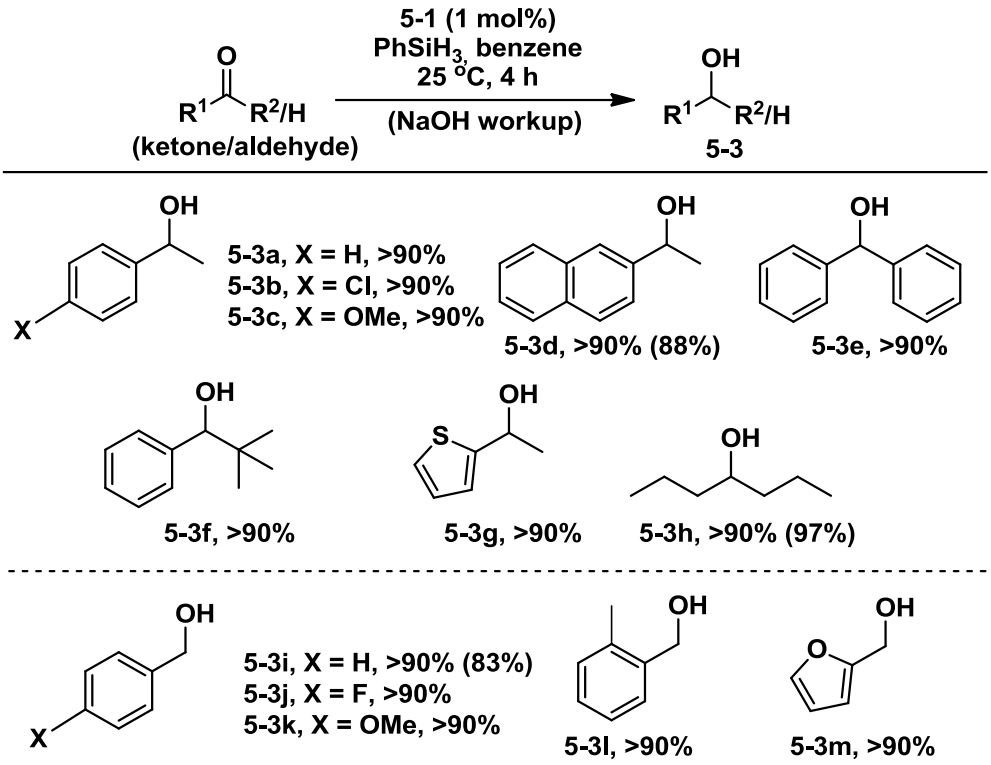

Figure 5-4. Catalytic reduction of ketones and aldehydes employing **5-1**. Reaction conditions: Ketone/aldehyde (0.8 mmol), $PhSiH_3$ (0.8 mmol), benzene (500 μL), **5-1** (1 mol%), 25 ˚C, 4 h. Conversion to **5-3** determined by use of calibrated GC methods. Isolated yields in parentheses.

To place this work in context, Trovitch's manganese pre-catalysts featuring phosphine-tethered bis(imino)pyridine ligation[130a, 130b, 130d] can function effectively at <1 mol% loading, and represent the most active catalysts known for the hydrosilylation of aldehydes and ketones. While lower loadings or shorter reaction times were not explored exhaustively, it is evident that **5-1** is less active than the Trovitch catalysts (Figure 5-1, **Z**). However, 4-heptanone proved to be an unusually reactive substrate in our study using **5-1**, with vigorous bubbling and a distinct exotherm noted upon mixing under our standard conditions (Figure 5-4). Further examination revealed that at the 0.25 mol% **5-1** loading level the reduction of 4-heptanone is complete within 2 minutes; high conversion is also achieved for this ketone at lower loadings (0.1 mol% **5-1**, 25 ˚C, 4 h).

*5.2.4 Catalytic Reduction of Esters Employing **5-1***

In exploring further the scope of carbonyl reductions that can be achieved by use of **5-1**, the selective reduction of methyl esters to alcohols under mild conditions was briefly examined (1 mol% **5-1**, 25 ˚C, 4 h; Figure 5-5); the first examples of such room temperature transformations were achieved by use of **1-2**.[55] A series of methyl benzoate derivatives featuring electron-donating or electron-withdrawing groups were efficiently reduced under these conditions, as was methyl heptanoate. Tracking the reaction progress revealed that high (but incomplete) conversions were achieved throughout after only 1-2 h. In this regard, pre-catalyst **5-1** is apparently more effective for the hydrosilative reduction of methyl esters, in comparison to Trovitch's phosphine-tethered bis(imino)pyridine manganese pre-catalyst system (**Z**) under similar conditions,[130a] and is competitive with the most effective catalysts known for the hydrosilative reduction of esters to alcohols at room temperature.[55 ,150]

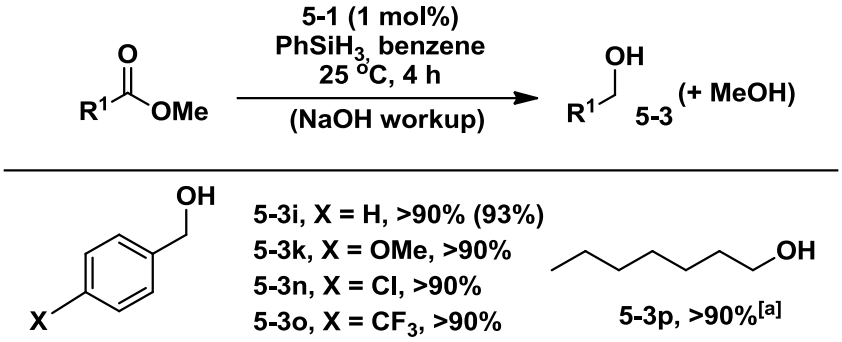

Figure 5-5. Catalytic reduction of esters employing **5-1**. Reaction conditions: Ester (0.8 mmol), $PhSiH_3$ (0.8 mmol), benzene (500 μL), **5-1** (1 mol%), 25 ˚C, 4 h. Conversion to **5-3** determined by use of calibrated GC methods. Isolated yields in parentheses. [a]Conversion based on silyl ether formation.

5.3 Conclusions

In summary, the newly developed Mn pre-catalyst **5-1** is shown to be broadly useful for the hydrosilative reduction of carbonyl compounds, including at room

temperature, with the established scope (amides, ketones, aldehydes, and esters) exceeding that demonstrated previously by any other catalyst system under such mild conditions. In particular, the normally challenging reduction of tertiary amides to tertiary amines that is achieved with broad scope by use of **5-1** proceeds under conditions that are competitive with the most effective 3d transition metal catalysts known for such transformations, thereby establishing a new class of synthetically useful Mn-catalyzed transformations. These results complement the already established utility of the *N*-phoshphinoamidinates in supporting low-coordinate, highly reactive, base metal catalysts.

5.4 Statement of Contributions

This work is published in *Angewandte Chemie*. Robert McDonald of the University of Alberta was responsible for X-ray crystallography data collection and structure elucidation of **5-1.**

5.5 Experimental Details

General experimental considerations. Unless stated all experiments were conducted under nitrogen in an inert-atmosphere glovebox or by using standard Schlenk techniques. Dry, oxygen-free solvents were used unless otherwise indicated. Benzene and pentane were deoxygenated and dried by sparging with nitrogen and subsequent passage through a double-column solvent purification system packed with alumina and copper-Q5 reactant. All purified solvents were stored under nitrogen over 4 Å molecular sieves. Benzene-d_6 was degassed via three freeze-pump-thaw cycles and stored under nitrogen over 4 Å molecular sieves. Benchtop dichloromethane used in the synthesis of amide substrates was stored over 4 Å molecular sieves. All liquid ketones, aldehydes, esters,

and phenylsilane were degassed via three repeated freeze−pump−thaw cycles and stored over 4 Å molecular sieves. The *N*-phosphinoamidine **2-1b** and $[Mn(N(SiMe_3)_2)_2]$[151] were prepared using literature procedures. All other solvents and reagents were purchased from commercial suppliers and were used without further purification. ^1H and ^{13}C NMR characterization data were collected at 300 K on a Bruker AV-300 spectrometer operating at 300.1 and 75.5 MHz (respectively) with chemical shifts reported in parts per million downfield of $SiMe_4$. Flash chromatography was carried out on silica gel using Silicycle SiliaFlash 60 silica (particle size 40–63 μm; 230–400 mesh), or using neutral alumina (150 mesh; Brockmann-III; activated).

Synthesis of 5-1. A solution of the *N*-phosphinoamidine **2-1b** (0.295 g, 0.692 mmol) in pentane (10 mL) was added by pipette to a vial containing $[Mn(N(SiMe_3)_2)_2]$ (0.260 g, 0.692 mmol), resulting in a beige slurry that quickly changed to a clear yellow solution. This mixture was allowed to react for 4 h, and was subsequently filtered through a short Celite plug. The reaction solution was then concentrated under vacuum to ca. 1 mL, followed by storage at -35 °C to induce crystallization. Following crystallization, the yellow-brown supernatant was then removed via pipette, and the remaining bright yellow crystals were crushed and dried under vacuum, affording analytically pure **5-1** as a bright yellow powder (0.324 g, 73%). Magnetic susceptibility (Evans' method, 300 K) $\mu_{eff} = 5.9$ μ_B. ^1H NMR (300 MHz, benzene-d_6): δ 9.49 (broad singlet), 2.28 (broad singlet), 1.40-0.88 (overlapping resonances), 0.10 (singlet). $C_{33}H_{58}MnN_3PSi_2$, Calculated: C, 62.03; H, 9.15; N, 6.58. Found: C, 62.44; H, 8.97; N, 6.51. Crystals suitable for X-ray diffraction analysis were grown from pentane at -35 °C.

Synthesis of amide substrates. With the exception of reactions involving cyclohexanecarbonyl chloride, 2-thiophenylcarbonyl chloride, and trimethylacetyl chloride, which were conducted under nitrogen, amide substrates were prepared in air following modified literature procedures.[152] The acyl chloride (10 mmol) was added slowly to a magnetically stirred solution of the amine (11 mmol), Et_3N (12.5 mmol), and dichloromethane (30 mL) at room temperature. The exothermic reactions typically boiled for a short time following complete addition of the acyl chloride. The reaction mixture was stirred magnetically for 1 h at room temperature and then was diluted with dichloromethane (20 mL). The solution was transferred to a separation funnel and was washed with 1M HCl (50 mL). The organic layer was filtered on a short silica gel column, and was washed with ethyl acetate/hexane (1:1). The solvent was removed under reduced pressure. The substrate was then transferred to an inert-atmosphere glovebox and redissolved in a minimal amount of benzene. The solution was filtered through a short Celite plug to remove any residual solids, and the benzene was removed under reduced pressure. Purity of the amide was confirmed by ^1H and ^{13}C NMR. Note that commercially available "2,6-dimethylpiperidine (mostly *cis*)" was used in the synthesis of the amide that in turn was reduced to form **5-2e**.

General procedure for determining conversions of amide substrates (GP1). In an inert-atmosphere glovebox, **5-1** (5 mol%, 13 mg) was weighed into an oven-dried vial to which benzene-d_6 (500 μL) was added. The amide substrate (0.4 mmol) and phenylsilane (49 μL, 0.4 mmol) were then added to the vial and the reaction mixture was transferred to an oven-dried NMR tube and the tube was sealed. The NMR tube containing the reaction mixture was then placed into an oil bath at 75 °C and allowed to react for 1 h (unless

indicated). Full conversion to the desired amine product was verified on the basis of ^{1}H and ^{13}C NMR spectroscopic analysis of the crude reaction mixture. The reaction mixture was then diluted with Et_2O (1 mL) and filtered through a short Celite plug. The mixture thus obtained was then analyzed by use of GC methods against a dodecane internal standard, to determine the conversion of the amide substrate to the corresponding amine.

General procedure for determining conversions of carbonyl substrates other than amides (GP2). In an inert-atmosphere glovebox, **5-1** (1 mol%, 5 mg) was weighed into an oven-dried vial to which benzene-*d*$_6$ (500 μL) was added. The carbonyl substrate (0.8 mmol) and phenylsilane (98 μL, 0.8 mmol) were added to the vial and the reaction mixture was transferred to an oven-dried NMR tube and the tube was sealed. The reaction was monitored by use of ^{1}H NMR spectroscopic methods to ensure full conversion of the carbonyl substrate to a mixture of silyl ether products. After 4 h (full consumption of the carbonyl substrate was often observed earlier), the reaction mixture was hydrolyzed via treatment with 20% NaOH (2 mL) and stirred for 3 h; ester substrates were allowed to stir for 18 hours in 3 mL of 20% NaOH to ensure full hydrolysis to the corresponding alcohol. The organic layer was extracted with Et_2O (3 × 3 mL), dried over $MgSO_4$, filtered through a short Celite plug, and concentrated under reduced pressure. The crude residue was then analyzed by use of GC methods against a dodecane internal standard, to determine the conversion of the substrate to the corresponding alcohol.

Characterization of isolated catalytic products.

NMR Spectra for isolated products provided in Appendix B

1-Benzylmorpholine, 5-2f

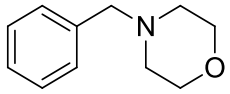

The title compound was prepared following **GP1**. The reaction mixture was purified through filtration on a neutral alumina column followed by a short silica gel column, both washed with ethyl acetate. 85% yield. ^{1}H NMR (300.1 MHz, $CDCl_3$) δ 2.44 (m, 4H), 3.50 (s, 2H), 3.71 (m, 4H), 7.22-7.32 (m, 5H). $^{13}C\{^{1}H\}$ NMR (75.5 MHz, $CDCl_3$) δ 53.7, 63.6, 67.1, 127.3, 128.4, 129.3, 137.8. Spectral data are in close agreement with previously reported ^{1}H and $^{13}C\{^{1}H\}$ NMR characterization data for the title compound.[152b]

***N*,*N*-Dibenzyl-1-(thiophen-2-yl)methanamine, 5-2g**

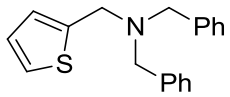

The title compound was prepared following **GP1**. The reaction mixture was purified through filtration on a neutral alumina column, washing with ethyl acetate and hexane (1:10). The resultant white solid was washed with a minimal amount of ice cold pentane. 89% yield. ^{1}H NMR (300.1 MHz, $CDCl_3$) δ 3.53 (s, 4H), 3.69 (s, 2H), 6.82-6.86 (m, 2H), 7.12-7.17 (m, 3H), 7.22-7.26 (m, 4H), 7.34-7.37 (m, 4H). $^{13}C\{^{1}H\}$ NMR (75.5 MHz, $CDCl_3$) δ 52.3, 57.7, 124.8, 125.6, 126.5, 127.1, 128.4, 128.8, 139.5, 143.4. Spectral data are in close agreement with previously reported ^{1}H and $^{13}C\{^{1}H\}$ NMR characterization data for the title compound.[152b]

Tribenzylamine, 5-2h

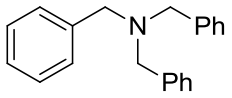

The title compound was prepared following **GP1**. The reaction mixture was purified through filtration on a neutral alumina column, washing with ethyl acetate and hexane (1:10). 95% yield. ^{1}H NMR (300.1 MHz, $CDCl_3$) δ 3.48 (s, 6H), 7.12-7.17 (m, 3H), 7.21-7.26 (m, 6H), 7.32-7.35 (m, 6H). $^{13}C\{^{1}H\}$ NMR (75.5 MHz, $CDCl_3$) δ 58.0, 127.0, 128.4, 128.9, 139.8. Spectral data are in close agreement with previously reported ^{1}H and $^{13}C\{^{1}H\}$ NMR characterization data for the title compound.[152b]

***N*,*N*-Dibenzyl-2,2-dimethylpropan-1-amine, 5-2k**

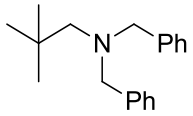

The title compound was prepared following **GP1**. The reaction mixture was purified through filtration on a short silica gel column, washing with ethyl acetate and hexane (1:10). 94% yield. ^{1}H NMR (300.1 MHz, $CDCl_3$) δ 0.68 (s, 9H), 2.21 (s, 2H), 3.48 (s, 4H), 7.08-7.28 (m, 10H). $^{13}C\{^{1}H\}$ NMR (75.5 MHz, $CDCl_3$) δ 28.6, 33.2, 60.9, 65.9, 126.9, 128.2, 129.3, 140.4. Spectral data are in close agreement with previously reported ^{1}H and $^{13}C\{^{1}H\}$ NMR characterization data for the title compound.[152b]

1-Naphthyl ethanol, 5-3d

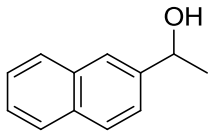

The title compound was prepared following **GP2**. The reaction mixture was purified through filtration on a short silica gel column, washing with diethyl ether. The resultant white solid was washed with a minimal amount of ice cold pentane. 88% yield. ^{1}H NMR (300.1 MHz, $CDCl_3$) δ 1.60 (d, J = 6.3 Hz, 3H), 2.02 (br s, 1H), 5.08 (q, J = 6.3 Hz, 1H), 7.48-7.54 (m, 3H), 7.82-7.87 (m, 4H). ^{13}C{^{1}H} NMR (75.5 MHz, $CDCl_3$) δ 25.3, 70.6, 123.9. 125.9, 126.3, 127.8, 128.1, 128.4, 133.0, 133.4, 143.3. Spectral data are in close agreement with previously reported ^{1}H and ^{13}C{^{1}H} NMR characterization data for the title compound.[153]

4-Heptanol, 5-3h

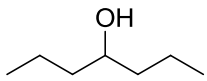

The title compound was prepared following **GP2**. The reaction mixture was purified through filtration on a short silica gel column, washing with diethyl ether. 97% yield. ^{1}H NMR (300.1 MHz, $CDCl_3$) δ 0.91 (t, J = 6.9 Hz, 6H). 1.35-1.45 (m, 8H), 1.76 (br s, 1H), 3.59 (m, 1H). ^{13}C{^{1}H} NMR (75.5 MHz, $CDCl_3$) δ 14.2, 18.9, 39.7, 71.5. Spectral data are in close agreement with previously reported ^{1}H and ^{13}C{^{1}H} NMR characterization data for the title compound.[154]

Benzyl alcohol, 5-3i

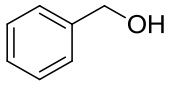

The title compound was prepared following **GP2**. The reaction mixture was purified through filtration on a short silica gel column, washing with diethyl ether. 83% yield (benzaldehyde), 93% yield (methyl benzoate). ^{1}H NMR (300.1 MHz, $CDCl_3$) δ 2.52 (br s, 1H), 4.66 (s, 2H), 7.28-7.40 (m, 5H). $^{13}C\{^{1}H\}$ NMR (75.5 MHz, $CDCl_3$) δ 65.2, 127.1, 127.7, 128.6, 140.9. Spectral data are in close agreement with previously reported ^{1}H and $^{13}C\{^{1}H\}$ NMR characterization data for the title compound.[55]

CHAPTER 6: Conclusion

As stated in Chapter 1 (Section 1.5), the overarching theme of this thesis was to investigate the ability of the *N*-phosphinoamidinate ligand class in supporting low-coordinate, reactive complexes. In this regard, this work has demonstrated the successful application of this relatively new class of ligands in supporting such complexes, including species that display unusual bonding motifs, unprecedented reactivity, and exceptional catalytic activity.

Chapter 2 detailed the synthesis and characterization of the first isolable, formally 16-electron Cp*Ru(κ^2-*P*~*N*) species (**2-2a** and **2-2b**) supported by *N*-phosphinoamidinate ligands. Species of this nature have been commonly invoked as key intermediates in a variety of catalytic transformations. Despite the stability of these complexes, they have been shown to readily coordinate two-electron (L) donors including carbon monoxide and 2,6-xylylisocyanide, affording crystallographically characterized C_1-symmetric 18-electron Cp*Ru(L)(κ^2-*P*~*N*) adducts (**2-3** and **2-4**). Perhaps the most notable result was the extrusion of hydrogen from ammonia borane in a bifunctional manner by **2-2a** displaying the ability of the *N*-phosphinoamidinate ligand to play an active role in reactions via protonation of the ligand backbone. Encouragingly, this process was also found to be cleanly reversible which is of particular importance when considering applications of similar species in reactions such as transfer hydrogenation. Additional reactivity studies on **2-2a**/**2-2b** showed that they were relatively inert toward a variety of reagents, or the reactivity was uncontrolled leading to multiple new complexes that could

not be easily separated and isolated. Potential avenues for future work regarding these complexes could include experimenting with different substitution patterns on the *N*-phosphinoamidinate or varying the co-ligand (Cp*) to fine tune the electronic and steric properties of these complexes.

Chapter 3 detailed the synthesis and characterization of an unprecedented three-coordinate 14-electron Pt(II) complex (**3-1**) featuring terminal amido ligation, which is the first of this type. The coordinative and electronic unsaturation of the **3-1** makes it an attractive precursor for future investigations of intermolecular substrate activation and functionalization. In this regard, **3-1** readily added E-H bonds across the Pt-amido linkage. Furthermore, it displayed a propensity for isonitrile insertion into the Pt-N bond. This is particularly interesting considering the notable reports of alkene insertion into Pd-N bonds discussed in Section 3.1. Although preliminary studies toward alkene/alkyne insertion into the Pt-N bond of **3-1** were unsuccessful they can still be considered in their infancy. As mentioned above, very little variation of the *N*-phosphinoamidinate ligand motif has been fully explored in a systematic manner (ligand variant → transition metal complex → reactivity studies) and perhaps advances in this area could help to guide future synthetic design of such three-coordinate Pt(II) complexes. Again, another logical route to pursue in fine tuning these complexes for the desired reactivity is the variation of the amide co-ligand. It became evident that exposure to amides with easily accesible C-H bonds will result in metalation to form a four-coordinate species (Scheme 3-4, **3-4**); however, the proposed three-coordinate Pt-N(aryl) precursor to the metalation product was observable by use of ^{31}P NMR, suggesting that a species of this type could be isolable if substitution on the aryl ring was moved from the ortho to the meta or para

position to distance it from the metal center. Furthermore, considering the stability of **3-1** even under prolonged periods of heating, the exploration of the three-coordinate Pt(II) motif should not be limited to platinum amido species. The work reported herein focused on platinum amido species as it was speculated donation from the nitrogen lone pair could be crucial in the stabilization of such species; perhaps the strongly donating, monoanionic *N*-phosphinoamidinate provides enough electron density to the metal center to stabilize other classes of three-coordinate Pt(II) complexes. In this regard, it could be envisoned that a new series of complexes based on **3-1** could be synthesized and systematically studied.

Chapter 4 describes the first stoichiometric dehydrogenative B-H/C(sp^3)-H benzylic borylation reactions, which arise from the reactivity of the pre-formed (η^3-benzyl)metal complex **4-1** with pinacolborane or catecholborane at room temperature. Notably, this reaction was not catalytic even when heated in toluene and an excess of the desired borane. In this regard, study of these key stoichiometric steps could help guide catalyst design to address the current challenges in borylation chemistry (mono vs polyborylation). Additionally, **4-6** represents a rare example of a platinum alkyl hydride species generated by the bifunctional abstraction of H_2 from amine boranes and remains an interesting target for further studies considering the ability of these complexes to release H_2 and reform **4-1**. With the view that (η^3-benzyl)metal complexes can be seen as "masked" three-coordinate complexes, one could envision multiple reaction pathways for substrate binding and activation (see Scheme 4-1 and 4-2 for examples) and as stated in Section 4.1, the (η^3-benzyl)platinum motif remains remarkably underexplored. Further reactivity studies are required to ascertain the full utility of such species .

Chapter 5 details the synthesis of the newly developed manganese pre-catalyst **5-1** and the applications of this species in hydrosilative reduction of carbonyl compounds, including at room temperature, with the established scope (amides, ketones, aldehydes, and esters) exceeding that demonstrated previously by any other catalyst system under such mild conditions. Most notably, the reduction of tertiary amides to tertiary amines proceeds under conditions that are competitive with the most effective 3d transition metal catalysts known for such transformations, thereby establishing a new class of synthetically useful Mn-catalyzed transformations. However, the mechanism of action of **5-1** in these hydrosilative reductions is unknown. Studies intended to evaluate the mechanism of such reactions could aid in directing the design of future pre-catalysts. One could envision multiple possible pathways that include but are not limited to: *in situ* formation of a (κ^2-P,N)MnH species followed by CO insertion into the Mn-H bond, alternatively, an *in situ* manganese species behaves as a Lewis acid interacting with CO and thus making the carbon susceptible to hydride attack.

In conclusion, the *N*-phosphinoamidinates have thus far proven to be highly modular ligands capable of supporting low-coordinate, electron rich, reactive complexes. This ligand motif has allowed access to stable complexes of ruthenium, platinum, palladium, nickel, manganese, iron, and cobalt. Many of the complexes presented have unique characteristics, unusual bonding motifs, and/or mediate unprecedented reactivity and in some cases represent a new class of complexes entirely. In this regard, these novel species can be viewed as templates for future innovation and continued exhaustive and thorough reactivity studies will continue to expand upon the utility of the complexes and chemistry detailed herein

References

1. Knowles, W. S., *Angew. Chem. Int. Ed.* **2002,** *41*, 1998-2007.

2. (a) Chauvin, Y., *Angew. Chem. Int. Ed.* **2006,** *45*, 3740-3747; (b) Grubbs, R. H., *Angew. Chem. Int. Ed.* **2006,** *45*, 3760-3765; (c) Schrock, R. R., *Angew. Chem. Int. Ed.* **2006,** *45*, 3748-3759.

3. Wu, X.-F.; Anbarasan, P.; Neumann, H.; Beller, M., *Angew. Chem. Int. Ed.* **2010,** *49*, 9047-9050.

4. Sydora, O. L.; Jones, T. C.; Small, B. L.; Nett, A. J.; Fischer, A. A.; Carney, M. J., *ACS Catal.* **2012,** *2*, 2452-2455.

5. Tolman, C. A., *Chem. Rev.* **1977,** *77*, 313-348.

6. Osborn, J. A.; Jardine, F. H.; Young, J. F.; Wilkinson, G., *J. Chem. Soc. A* **1966**, 1711-1732.

7. Nguyen, S. T.; Johnson, L. K.; Grubbs, R. H.; Ziller, J. W., *J. Am. Chem. Soc.* **1992,** *114*, 3974-3975.

8. Miyaura, N.; Suzuki, A., *Chem. Rev.* **1995,** *95*, 2457-2483.

9. Blaser, H.-U.; Brieden, W.; Pugin, B.; Spindler, F.; Studer, M.; Togni, A., *Topics in Catalysis* **2002,** *19*, 3-16.

10. Burk, M. J., *J. Am. Chem. Soc.* **1991,** *113*, 8518-8519.

11. Clark, T.; Landis, C., *Tetrahedron* **2004,** *15*, 2123-2137.

12. Michelet, B.; Lebœuf, D.; Bour, C.; Škoch, K.; Horký, F.; Štěpnička, P.; Gandon, V., *ChemPlusChem* **2017,** *82*, 442-448.

13. Chen, S.-J.; Li, Y.-Q.; Wang, Y.-Y.; Zhao, X.-L.; Liu, Y., *J. Mol. Catal. A: Chem.* **2015,** *396*, 68-76.

14. Carroll, M. P.; Guiry, P. J., *Chem. Soc. Rev.* **2014,** *43*, 819-833.

15. Helmchen, G.; Pfaltz, A., *Acc. Chem. Res.* **2000,** *33*, 336-345.

16. Lundgren, R. J.; Hesp, K. D.; Stradiotto, M., *Synlett* **2011,** *2011*, 2443-2458.

17. Koch, G.; Lloyd-Jones, G. C.; Loiseleur, O.; Pfaltz, A.; Prétôt, R.; Schaffner, S.; Schnider, P.; von Matt, P., *Recl. Trav. Chim. Pays-Bas* **1995,** *114*, 206-210.

18. Lundgren, R. J.; Peters, B. D.; Alsabeh, P. G.; Stradiotto, M., *Angew. Chem. Int. Ed.* **2010,** *49*, 4071-4074.

19. Lundgren, R. J.; Stradiotto, M., *Angew. Chem. Int. Ed.* **2010,** *49*, 8686-8690.

20. Hesp, K. D.; Lundgren, R. J.; Stradiotto, M., *J. Am. Chem. Soc.* **2011,** *133*, 5194-5197.

21. Hesp, K. D.; Stradiotto, M., *J. Am. Chem. Soc.* **2010,** *132*, 18026-18029.

22. (a) Ji, K.; Nelson, J.; Zhang, L., *Beilstein J. Org. Chem.* **2013,** *9*, 1925-1930; (b) Wu, G.; Zheng, R.; Nelson, J.; Zhang, L., *Adv. Synth. Catal.* **2014,** *356*, 1229-1234; (c) Wang, Y.; Zheng, Z.; Zhang, L., *J. Am. Chem. Soc.* **2015,** *137*, 5316-5319.

23. Lavoie, C. M.; MacQueen, P. M.; Rotta-Loria, N. L.; Sawatzky, R. S.; Borzenko, A.; Chisholm, A. J.; Hargreaves, B. K. V.; McDonald, R.; Ferguson, M. J.; Stradiotto, M., *Nat Commun* **2016,** *7*.

24. Thomas, J. C.; Peters, J. C., *Inorg. Chem.* **2003,** *42*, 5055-5073.

25. (a) Bourget-Merle, L.; Lappert, M. F.; Severn, J. R., *Chem. Rev.* **2002,** *102*, 3031-3066; (b) McGeachin, S. G., *Can. J. Chem.* **1968,** *46*, 1903-1912; (c) Parks, J. E.; Holm, R. H., *Inorg. Chem.* **1968,** *7*, 1408-1416.

26. Edelmann, F. T., *Adv. Organomet. Chem.* **2013,** *Volume 61*, 55-374.

27. Thomas, J. C.; Peters, J. C., *J. Am. Chem. Soc.* **2001,** *123*, 5100-5101.

28. Thomas, J. C.; Peters, J. C., *J. Am. Chem. Soc.* **2003,** *125*, 8870-8888.

29. Thomas, J.; Peters, J. C., *Polyhedron* **2004,** *23*, 2901-2913.

30. Lu, C. C.; Peters, J. C., *J. Am. Chem. Soc.* **2002,** *124*, 5272-5273.

31. Schmidt, B. M.; Engle, J. T.; Zhang, M.; Babahan, I.; Ziegler, C. J.; Jia, L., *J. Organomet. Chem.* **2016,** *805*, 94-99.

32. Betley, T. A.; Peters, J. C., *Angew. Chem. Int. Ed.* **2003,** *42*, 2385-2389.

33. Parker, E.; Cramer, N., *Organometallics* **2014,** *33*, 780-787.

34. Zhu, D.; Budzelaar, P. H. M., *Dalton Trans.* **2013,** *42*, 11343-11354.

35. Holland, P. L.; Cundari, T. R.; Perez, L. L.; Eckert, N. A.; Lachicotte, R. J., *J. Am. Chem. Soc.* **2002,** *124*, 14416-14424.

36. Budzelaar, P. H. M.; de Gelder, R.; Gal, A. W., *Organometallics* **1998,** *17*, 4121-4123.

37. Schreiber, D. F.; O'Connor, C.; Grave, C.; Müller-Bunz, H.; Scopelliti, R.; Dyson, P. J.; Phillips, A. D., *Organometallics* **2013,** *32*, 7345-7356.

38. Hitchcock, P. B.; Lappert, M. F.; Liu, D.-S., *Chem. Commun.* **1994**, 2637-2638.

39. Bernskoetter, W. H.; Lobkovsky, E.; Chirik, P. J., *Organometallics* **2005,** *24*, 6250-6259.

40. Chen, C.; Dugan, T. R.; Brennessel, W. W.; Weix, D. J.; Holland, P. L., *J. Am. Chem. Soc.* **2014,** *136*, 945-955.

41. Geier, S. J.; Stephan, D. W., *Chem. Commun.* **2008**, 99-101.

42. (a) Fekl, U.; Kaminsky, W.; Goldberg, K. I., *J. Am. Chem. Soc.* **2001,** *123*, 6423-6424; (b) Fekl, U.; Goldberg, K. I., *J. Am. Chem. Soc.* **2002,** *124*, 6804-6805; (c) Fekl, U.; Kaminsky, W.; Goldberg, K. I., *J. Am. Chem. Soc.* **2003,** *125*, 15286-15287.

43. Webster, R. L., *Dalton Trans* **2017,** *46*, 4483-4498.

44. Sanger, A., *Inorg. Nucl. Chem. Letters* **1973,** *9*, 351-354.

45. Collins, S., *Coord. Chem. Rev.* **2011,** *255*, 118-138.

46. García-Álvarez, R.; Suárez, F. J.; Díez, J.; Crochet, P.; Cadierno, V.; Antiñolo, A.; Fernández-Galán, R.; Carrillo-Hermosilla, F., *Organometallics* **2012,** *31*, 8301-8311.

47. Nagashima, H.; Kondo, H.; Hayashida, T.; Yamaguchi, Y.; Gondo, M.; Masuda, S.; Miyazaki, K.; Matsubara, K.; Kirchner, K., *Coord. Chem. Rev.* **2003,** *245*, 177-190.

48. Rankin, M. A.; McDonald, R.; Ferguson, M. J.; Stradiotto, M., *Angew. Chem. Int. Ed.* **2005,** *44*, 3603-3606.

49. Stradiotto, M.; Hesp, K. D.; Lundgren, R. J., *Angew. Chem. Int. Ed.* **2010,** *49*, 494-512.

50. Rankin, M. A.; Schatte, G.; McDonald, R.; Stradiotto, M., *J. Am. Chem. Soc.* **2007,** *129*, 6390-6391.

51. Speiser, F.; Braunstein, P.; Saussine, L., *Acc. Chem. Res.* **2005,** *38*, 784-793.

52. Braunstein, P.; Pietsch, J.; Chauvin, Y.; Mercier, S.; Saussine, L.; DeCian, A.; Fischer, J., *Dalton Trans.* **1996**, 3571-3574.

53. Braunstein, P.; Naud, F.; Rettig, S. J., *New J. Chem.* **2001,** *25*, 32-39.

54. Michlik, S.; Kempe, R., *Chem. Eur. J.* **2010,** *16*, 13193-13198.

55. Ruddy, A. J.; Kelly, C. M.; Crawford, S. M.; Wheaton, C. A.; Sydora, O. L.; Small, B. L.; Stradiotto, M.; Turculet, L., *Organometallics* **2013,** *32*, 5581-5588.

56. Ruddy, A. J.; Sydora, O. L.; Small, B. L.; Stradiotto, M.; Turculet, L., *Chem. Eur. J.* **2014,** *20*, 13918-13922.

57. Kelly, C. M.; Ruddy, A. J.; Wheaton, C. A.; Sydora, O. L.; Small, B. L.; Stradiotto, M.; Turculet, L., *Can. J. Chem.* **2014,** *92*, 194-200.

58. Jimenez-Tenorio, M.; Puerta, M. C.; Valerga, P., *Eur. J. Inorg. Chem.* **2004**, 17-32.

59. Kelly, C. M.; Kwon, D.-H.; Ferguson, M. J.; Bischof, S. M.; Sydora, O. L.; Ess, D. H.; Stradiotto, M.; Turculet, L., *Angew. Chem. Int. Ed.* **2015,** *54*, 14498-14502.

60. Kelly, C. M.; Fuller, J. T.; Macaulay, C. M.; McDonald, R.; Ferguson, M. J.; Bischof, S. M.; Sydora, O. L.; Ess, D. H.; Stradiotto, M.; Turculet, L., *Angew. Chem. Int. Ed.* **2017,** *56*, 6312-6316.

61. (a) Bruneau, C.; Renaud, J. L.; Demerseman, B., *Chem. Eur. J.* **2006,** *12*, 5178-5187; (b) Trost, B. M.; Frederiksen, M. U.; Rudd, M. T., *Angew. Chem., Int. Ed.* **2005,** *44*, 6630-6666; (c) Davies, S. G.; McNally, J. P.; Smallridge, A. J., *Adv. Organomet. Chem.* **1990,** *30*, 1-76.

62. Haack, K.-J.; Hashiguchi, S.; Fujii, A.; Ikariya, T.; Noyori, R., *Angew. Chem. Int. Ed.* **1997,** *36*, 285-288.

63. (a) Campion, B. K.; Heyn, R. H.; Tilley, T. D., *Chem. Commun.* **1988**, 278-80; (b) Loren, S. D.; Campion, B. K.; Heyn, R. H.; Tilley, T. D.; Bursten, B. E.; Luth, K. W., *J. Am. Chem. Soc.* **1989,** *111*, 4712-18; (c) Johnson, T. J.; Folting, K.; Streib, W. E.; Martin, J. D.; Huffman, J. C.; Jackson, S. A.; Eisenstein, O.; Caulton, K. G., *Inorg. Chem.* **1995,** *34*, 488-499.

64. (a) Gemel, C.; Mereiter, K.; Schmid, R.; Kirchner, K., *Organometallics* **1997,** *16*, 5601-5603; (b) Gemel, C.; Sapunov, V. N.; Mereiter, K.; Ferencic, M.; Schmid, R.; Kirchner, K., *Inorg. Chim. Acta* **1999,** *286*, 114-120; (c) Jimenez, T. M.; Mereiter, K.; Puerta, M. C.; Valerga, P., *J. Am. Chem. Soc.* **2000,** *122*, 11230-11231; (d) Palacios, M. D.; Puerta, M. C.; Valerga, P.; Lledos, A.; Veilly, E., *Inorg. Chem.* **2007,** *46*, 6958-6967.

65. Yamaguchi, Y.; Nagashima, H., *Organometallics* **2000,** *19*, 725-727.

66. (a) Huang, H.; Hughes, R. P.; Rheingold, A. L., *Polyhedron* **2008,** *27*, 734-738; (b) Phillips, A. D.; Thommes, K.; Scopelliti, R.; Gandolfi, C.; Albrecht, M.; Severin, K.; Schreiber, D. F.; Dyson, P. J., *Organometallics* **2011,** *30*, 6119-6132.

67. Ito, M.; Osaku, A.; Kobayashi, C.; Shiibashi, A.; Ikariya, T., *Organometallics* **2009,** *28*, 390-393.

68. Ito, M.; Hirakawa, M.; Osaku, A.; Ikariya, T., *Organometallics* **2003,** *22*, 4190-4192.

69. Ito, M.; Kitahara, S.; Ikariya, T., *J. Am. Chem. Soc.* **2005,** *127*, 6172-6173.

70. Ito, M.; Osaku, A.; Shiibashi, A.; Ikariya, T., *Org. Lett.* **2007,** *9*, 1821-1824.

71. (a) Ito, M.; Sakaguchi, A.; Kobayashi, C.; Ikariya, T., *J. Am. Chem. Soc.* **2007,** *129*, 290-291; (b) Ito, M.; Kobayashi, C.; Himizu, A.; Ikariya, T., *J. Am. Chem. Soc.* **2010,** *132*, 11414-11415.

72. (a) Ikariya, T.; Murata, K.; Noyori, R., *Org. Biomol. Chem.* **2006,** *4*, 393-406; (b) Noyori, R.; Yamakawa, M.; Hashiguchi, S., *J. Org. Chem.* **2001,** *66*, 7931-7944.

73. Mauthner, K.; Slugovc, C.; Mereiter, K.; Schmid, R.; Kirchner, K., *Organometallics* **1997,** *16*, 1956-1961.

74. (a) Sanyal, U.; Demirci, U. B.; Jagirdar, B. R.; Miele, P., *ChemSusChem* **2011,** *4*, 1731-1739; (b) Staubitz, A.; Robertson, A. P. M.; Manners, I., *Chem. Rev.* **2010,** *110*, 4079-4124.

75. (a) Hamilton, C. W.; Baker, R. T.; Staubitz, A.; Manners, I., *Chem. Soc. Rev.* **2009,** *38*, 279-293; (b) Stephens, F. H.; Pons, V.; Tom Baker, R., *Dalton Trans* **2007**, 2613-2626.

76. Keaton, R. J.; Blacquiere, J. M.; Baker, R. T., *J. Am. Chem. Soc.* **2007,** *129*, 1844-1845.

77. Fagan, P. J.; Ward, M. D.; Calabrese, J. C., *J. Am. Chem. Soc.* **1989,** *111*, 1698-1719.

78. Hartwig, J. F., *Organotransition Metal Chemistry: From Bonding to Catalysis*. University Science Books: Sausalito, CA, 2010.

79. Romeo, R.; D'Amico, G.; Sicilia, E.; Russo, N.; Rizzato, S., *J. Am. Chem. Soc.* **2007,** *129*, 5744-5755.

80. Alvarez, S., *Coord. Chem. Rev.* **1999,** *193-5*, 13-41.

81. Romeo, R., *Comments Inorg. Chem.* **1990,** *11*, 21-57.

82. Ortuno, M. A.; Conejero, S.; Lledos, A., *Beilstein J. Org. Chem.* **2013,** *9*, 1352-1382.

83. (a) Baratta, W.; Stoccoro, S.; Doppiu, A.; Herdtweck, E.; Zucca, A.; Rigo, P., *Angew. Chem. Int. Ed.* **2003,** *42*, 105-109; (b) Crosby, S. H.; Clarkson, G. J.; Rourke, J. P., *J. Am. Chem. Soc.* **2009,** *131*, 14142-14143; (c) Ingleson, M. J.; Mahon, M. F.; Weller, A. S., *Chem Commun* **2004**, 2398-2399; (d) Mole, L.; Spencer, J. L.; Carr, N.; Orpen, A. G., *Organometallics* **1991,** *10*, 49-52; (e) Rivada-Wheelaghan, O.; Donnadieu, B.; Maya, C.; Conejero, S., *Chem. Eur. J.* **2010,** *16*, 10323-10326.

84. (a) Braunschweig, H.; Brenner, P.; Dewhurst, R. D.; Jimenez-Halla, J. O. C.; Kupfer, T.; Rais, D.; Uttinger, K., *Angew. Chem. Int. Ed.* **2013,** *52*, 2981-2984; (b) Braunschweig, H.; Radacki, K.; Rais, D.; Scheschkewitz, D., *Angew. Chem. Int. Ed.* **2005,** *44*, 5651-5654; (c) Braunschweig, H.; Radacki, K.; Uttinger, K., *Chem. Eur. J.* **2008,** *14*, 7858-7866.

85. Rivada-Wheelaghan, O.; Ortuno, M. A.; Diez, J.; Lledos, A.; Conejero, S., *Angew. Chem. Int. Ed.* **2012,** *51*, 3936-3939.

86. Berthon-Gelloz, G.; de Bruin, B.; Tinant, B.; Marko, I. E., *Angew. Chem. Int. Ed.* **2009,** *48*, 3161-3164.

87. Takagi, N.; Sakaki, S., *J. Am. Chem. Soc.* **2012,** *134*, 11749-11759.

88. (a) Fulton, J. R.; Holland, A. W.; Fox, D. J.; Bergman, R. G., *Acc. Chem. Res.* **2002,** *35*, 44-56; (b) Glueck, D. S., *Dalton Trans.* **2008**, 5276-5286; (c) Gunnoe, T. B., *Eur. J. Inorg. Chem.* **2007**, 1185-1203; (d) Hartwig, J. F., *Nature* **2008,** *455*, 314-322; (e) Webb, J. R.; Burgess, S. A.; Cundari, T. R.; Gunnoe, T. B., *Dalton Trans.* **2013,** *42*, 16646-16665.

89. (a) Webb, J. R.; Munro-Leighton, C.; Pierpont, A. W.; Gurkin, J. T.; Gunnoe, T. B.; Cundari, T. R.; Sabat, M.; Petersen, J. L.; Boyle, P. D., *Inorg. Chem.* **2011,** *50*, 4195-4211; (b) Webb, J. R.; Pierpont, A. W.; Munro-Leighton, C.; Gunnoe, T. B.; Cundari, T. R.; Boyle, P. D., *J. Am. Chem. Soc.* **2010,** *132*, 4520-4521.

90. (a) Hanley, P. S.; Hartwig, J. F., *J. Am. Chem. Soc.* **2011,** *133*, 15661-15673; (b) Hanley, P. S.; Marković, D.; Hartwig, J. F., *J. Am. Chem. Soc.* **2010,** *132*, 6302-6303.

91. (a) Neukom, J. D.; Perch, N. S.; Wolfe, J. P., *Organometallics* **2011,** *30*, 1269-1277; (b) Neukom, J. D.; Perch, N. S.; Wolfe, J. P., *J. Am. Chem. Soc.* **2010,** *132*, 6276-6277.

92. Yamashita, M.; Hartwig, J. F., *J. Am. Chem. Soc.* **2004,** *126*, 5344-5345.

93. (a) Cowan, R. L.; Trogler, W. C., *J. Am. Chem. Soc.* **1989,** *111*, 4750-4761; (b) Albeniz, A. C.; Calle, V.; Espinet, P.; Gomez, S., *Inorg. Chem.* **2001,** *40*, 4211-4216.

94. Gutowsky, H. S.; Holm, C. H., *J Chem Phys* **1956,** *25*, 1228-1234.

95. Conner, D.; Jayaprakash, K. N.; Gunnoe, T. B.; Boyle, P. D., *Inorg. Chem.* **2002,** *41*, 3042-3049.

96. (a) Hartwig, J. F., *Acc. Chem. Res.* **1998,** *31*, 852-860; (b) Seul, J. M.; Park, S., *Dalton Trans.* **2002**, 1153-1158; (c) Hanley, P. S.; Hartwig, J. F., *Angew. Chem. Int. Ed.* **2013,** *52*, 8510-8525; (d) Vlaar, T.; Ruijter, E.; Maes, B. U. W.; Orru, R. V. A., *Angew. Chem. Int. Ed.* **2013,** *52*, 7084-7097; (e) Qiu, G.; Ding, Q.; Wu, J., *Chem. Soc. Rev.* **2013,** *42*, 5257-69; (f) Nishina, N.; Yamamoto, Y., *Top. Organomet. Chem.* **2013,** *43*, 115-144.

97. Osakada, K.; Kim, Y. J.; Yamamoto, A., *J. Organomet. Chem.* **1990,** *382*, 303-317.

98. Allen, A. D.; Tidwell, T. T., *Chem. Rev.* **2013,** *113*, 7287-7342.

99. Trost, B. M.; Czabaniuk, L. C., *Angew. Chem. Int. Ed.* **2014**, n/a-n/a.

100. (a) Heck, R. F.; Nolley, J. P., *J Org Chem* **1972,** *37*, 2320-2322; (b) Wu, G. Z.; Lamaty, F.; Negishi, E., *J Org Chem* **1989,** *54*, 2507-2508.

101. (a) Legros, J.-Y.; Toffano, M.; Fiaud, J.-C., *Tetrahedron* **1995,** *51*, 3235-3246; (b) Kuwano, R.; Kondo, Y.; Matsuyama, Y., *J. Am. Chem. Soc.* **2003,** *125*, 12104-12105.

102. (a) Bao, M.; Nakamura, H.; Yamamoto, Y., *J. Am. Chem. Soc.* **2001,** *123*, 759-760; (b) Ueno, S.; Komiya, S.; Tanaka, T.; Kuwano, R., *Org. Lett.* **2012,** *14*, 338-341.

103. (a) Liégault, B.; Renaud, J.-L.; Bruneau, C., *Adv. Synth. Catal.* **2007,** *349*, 841-845; (b) Kuwano, R.; Shige, T., *J. Am. Chem. Soc.* **2007,** *129*, 3802-3803.

104. (a) Komon, Z. J. A.; Bu, X.; Bazan, G. C., *J. Am. Chem. Soc.* **2000,** *122*, 12379-12380; (b) Zhou, X.; Bontemps, S.; Jordan, R. F., *Organometallics* **2008,** *27*, 4821-4824; (c) Sujith, S.; Noh, E. K.; Lee, B. Y.; Han, J. W., *J Org Chem* **2008,** *693*, 2171-2176.

105. (a) Lipshutz, B. H.; Bulow, G.; Fernandez-Lazaro, F.; Kim, S.-K.; Lowe, R.; Mollard, P.; Stevens, K. L., *J. Am. Chem. Soc.* **1999,** *121*, 11664-11673; (b) Matsubara, R.; Gutierrez, A. C.; Jamison, T. F., *J. Am. Chem. Soc.* **2011,** *133*, 19020-19023.

106. RajanBabu, T. V., *Synlett* **2009,** *2009*, 853-885.

107. Casalnuovo, A. L.; RajanBabu, T. V.; Ayers, T. A.; Warren, T. H., *J. Am. Chem. Soc.* **1994,** *116*, 9869-9882.

108. (a) Crascall, L. e.; Litster, S. A.; Redhouse, A. D.; Spencer, J. L., *J. Organomet. Chem.* **1990,** *394*, c35-c38; (b) Crascall, L. E.; Spencer, J. L., *Dalton Trans.* **1992**, 3445-3452; (c) Crascall, L. E.; Spencer, J. L., *Dalton Trans.* **1995**, 2391-2396.

109. Hesp, K. D.; McDonald, R.; Ferguson, M. J.; Schatte, G.; Stradiotto, M., *Chem. Commun.* **2008**, 5645-5647.

110. (a) Fryzuk, M. D.; McConville, D. H.; Rettig, S. J., *J. Organomet. Chem.* **1993,** *445*, 245-256; (b) Hesp, K. D.; Kannemann, F. O.; Rankin, M. A.; McDonald, R.; Ferguson, M. J.; Stradiotto, M., *Inorg. Chem.* **2011,** *50*, 2431-2444; (c) Stradiotto, M.; Fujdala, K. L.; Tilley, T. D., *Helv Chim Acta* **2001,** *84*, 2958-2970; (d) Waterman, R.; Hayes, P. G.; Tilley, T. D., *Acc. Chem. Res.* **2007,** *40*, 712-719.

111. (a) Ishiyama, T.; Miyaura, N., *Pure Appl Chem* **2006,** *78*, 1369-1375; (b) Mkhalid, I. A. I.; Barnard, J. H.; Marder, T. B.; Murphy, J. M.; Hartwig, J. F., *Chem. Rev.* **2010,** *110*, 890-931; (c) Hartwig, J. F., *Acc. Chem. Res.* **2012,** *45*, 864-873.

112. (a) Pelter, A., *Chem. Soc. Rev.* **1982,** *11*, 191-225; (b) Crudden, C. M.; Glasspoole, B. W.; Lata, C. J., *Chem. Commun.* **2009**, 6704-6716; (c) Leonori, D.; Aggarwal, V. K., *Acc. Chem. Res.* **2014,** *47*, 3174-3183.

113. Suzuki, A., *Angew. Chem. Int. Ed.* **2011,** *50*, 6722-6737.

114. Jones, W. D.; Feher, F. J., *Acc. Chem. Res.* **1989,** *22*, 91-100.

115. Shimada, S.; Batsanov, A. S.; Howard, J. A. K.; Marder, T. B., *Angew. Chem. Int. Ed.* **2001,** *40*, 2168-2171.

116. (a) Ishiyama, T.; Ishida, K.; Takagi, J.; Miyaura, N., *Chem. Lett.* **2001,** *30*, 1082-1083; (b) Mertins, K.; Zapf, A.; Beller, M., *J. Mol. Cat. A* **2004,** *207*, 21-25; (c) Cho, S. H.; Hartwig, J. F., *J. Am. Chem. Soc.* **2013,** *135*, 8157-8160; (d) Cho, S. H.; Hartwig, J. F., *Chem. Sci.* **2014,** *5*, 694-698; (e) Larsen, M. A.; Wilson, C. V.; Hartwig, J. F., *J. Am. Chem. Soc.* **2015,** *137*, 8633-8643; (f) Palmer, W. N.; Obligacion, J. V.; Pappas, I.; Chirik, P. J., *J. Am. Chem. Soc.* **2016,** *138*, 766-769.

117. Lam, W. H.; Lam, K. C.; Lin, Z. Y.; Shimada, S.; Perutz, R. N.; Marder, T. B., *Dalton Trans.* **2004**, 1556-1562.

118. Rossin, A.; Peruzzini, M., *Chem. Rev.* **2016,** *116*, 8848-72.

119. (a) Takaya, J.; Ito, S.; Nomoto, H.; Saito, N.; Kirai, N.; Iwasawa, N., *Chem. Commun.* **2015,** *51*, 17662-17665; (b) Furukawa, T.; Tobisu, M.; Chatani, N., *J. Am. Chem. Soc.* **2015,** *137*, 12211-12214.

120. M. J. Frisch et al., Gaussian 09 (Revision B.01), Gaussian, Inc., Wallingford, CT, 2009.

121. (a) Weigend, F.; Ahlrichs, R., *Phys Chem Chem Phys* **2005,** *7*, 3297-3305; (b) Weigend, F., *Phys Chem Chem Phys* **2006,** *8*, 1057-1065; (c) Zhao, Y.; Truhlar, D. G., *Theor Chem Acc* **2008,** *120*, 215-241.

122. Marenich, A. V.; Cramer, C. J.; Truhlar, D. G., *J Phys Chem B* **2009,** *113*, 6378-6396.

123. (a) Rudolf, G. C.; Hamilton, A.; Orpen, A. G.; Owen, G. R., *Chem. Commun.* **2009**, 553-555; (b) Benac-Lestrille, G.; Helmstedt, U.; Vendier, L.; Alcaraz, G.; Clot, E.; Sabo-Etienne, S., *Inorg. Chem.* **2011,** *50*, 11039-11045; (c) Gloaguen, Y.; Benac-Lestrille, G.; Vendier, L.; Helmstedt, U.; Clot, E.; Alcaraz, G.; Sabo-Etienne, S., *Organometallics* **2013,** *32*, 4868-4877.

124. Perutz, R. N.; Sabo-Etienne, S., *Angew. Chem. Int. Ed.* **2007,** *46*, 2578-2592.

125. Raiford, D. S.; Fisk, C. L.; Becker, E. D., *Analytical Chemistry* **1979,** *51*, 2050-2051.

126. (a) Valyaev, D. A.; Lavigne, G.; Lugan, N., *Coord. Chem. Rev.* **2016,** *308*, 191-235; (b) Carney, J. R.; Dillon, B. R.; Thomas, S. P., *Eur J Org Chem* **2016**, 3912-3929; (c) Garbe, M.; Junge, K.; Beller, M., *Eur J Org Chem* **2017**, 4344-4362.

127. (a) Zirakzadeh, A.; de Aguiar, S. R. M. M.; Stoger, B.; Widhalm, M.; Kirchner, K., *Chemcatchem* **2017,** *9*, 1744-1748; (b) Bruneau-Voisine, A.; Wang, D.; Dorcet, V.; Roisnel, T.; Darcel, C.; Sortais, J. B., *Org. Lett.* **2017,** *19*, 3656-3659.

128. (a) Bertini, F.; Glatz, M.; Gorgas, N.; Stoger, B.; Peruzzini, M.; Veiros, L. F.; Kirchner, K.; Gonsalvi, L., *Chem. Sci.* **2017,** *8*, 5024-5029; (b) Elangovan, S.; Topf, C.; Fischer, S.; Jiao, H. J.; Spannenberg, A.; Baumann, W.; Ludwig, R.; Junge, K.; Beller, M., *J. Am. Chem. Soc.* **2016,** *138*, 8809-8814; (c) Espinosa-Jalapa, N. A.; Nerush, A.; Shimon, L. J. W.; Leitus, G.; Avram, L.; Ben-David, Y.; Milstein, D., *Chem. Eur. J.* **2017,** *23*, 5934-5938; (d) Garbe, M.; Junge, K.; Walker, S.; Wei, Z.; Jiao, H.; Spanneberg, A.; Bachmann, S.; Scalone, M.; Beller, M., *Angew. Chem. Int. Ed.* **2017,** *56*, 11237-11241; (e) Kallmeier, F.; Irrgang, T.; Dietel, T.; Kempe, R., *Angew. Chem. Int. Ed.* **2016,** *55*, 11806-11809; (f) van Putten, R.; Uslamin, E. A.; Garbe, M.; Liu, C.; Gonzalez-de-Castro, A.; Lutz, M.; Junge, K.; Hensen, E. J. M.; Beller, M.; Lefort, L.; Pidko, E. A., *Angew. Chem. Int. Ed.* **2017,** *56*, 7531-7534; (g) Widegren, M. B.; Harkness, G. J.; Slawin, A. M. Z.; Cordes, D. B.; Clarke, M. L., *Angew. Chem. Int. Ed.* **2017,** *56*, 5825-5828.

129. (a) Zhang, G.; Zeng, H.; Wu, J.; Yin, Z.; Zheng, S.; Fettinger, J. C., *Angew. Chem. Int. Ed.* **2017,** *55*, 14369-14372; (b) Vasilenko, V.; Blasius, C. K.; Wadepohl, H.; Gade, L. H., *Angew. Chem. Int. Ed.* **2017,** *56*, 8393-8397.

130. (a) Mukhopadhyay, T. K.; Flores, M.; Groy, T. L.; Trovitch, R. J., *J. Am. Chem. Soc.* **2014,** *136*, 882-885; (b) Ghosh, C.; Mukhopadhyay, T. K.; Flores, M.; Groy, T. L.;

Trovitch, R. J., *Inorg. Chem.* **2015,** *54*, 10398-10406; (c) Valyaev, D. A.; Wei, D.; Elangovan, S.; Cavailles, M.; Dorcet, V.; Sortais, J. B.; Darcel, C.; Lugan, N., *Organometallics* **2016,** *35*, 4090-4098; (d) Mukhopadhyay, T. K.; Rock, C. L.; Hong, M.; Ashley, D. C.; Groy, T. L.; Baik, M. H.; Trovitch, R. J., *J. Am. Chem. Soc.* **2017,** *139*, 4901-4915.

131. Elangovan, S.; Neumann, J.; Sortais, J. B.; Junge, K.; Darcel, C.; Beller, M., *Nat Commun* **2016,** *7*.

132. Elangovan, S.; Garbe, M.; Jiao, H.; Spannenberg, A.; Junge, K.; Beller, M., *Angew. Chem. Int. Ed.* **2016,** *55*, 15364-15368.

133. (a) *Reductions in Organic Synthesis, Recent Advances and Practical Applications*. American Chemical Society: Washington D.C., 1996; Vol. 641; (b) Magano, J.; Dunetz, J. R., *Organic Process Research and Development* **2012,** *16*, 1156-1184.

134. Chakraborty, S.; Guan, H., *Dalton Trans.* **2010,** *39*, 7427-7436.

135. (a) Marciniec, B., *Hydrosilylation: A Comprehensive Review on Recent Advances*. Springer Science: 2009; (b) Trovitch, R. J., *Synlett* **2014,** *25*, 1638-1642.

136. (a) Addis, D.; Das, S.; Junge, K.; Beller, M., *Angew. Chem. Int. Ed.* **2011,** *50*, 6004-6011; (b) Volkov, A.; Tinnis, F.; Stagbrand, T.; Trillo, P.; Adolfsson, H., *Chem. Soc. Rev.* **2016,** *45*, 6685-6697; (c) Li, B.; Sortais, J. B.; Darcel, C., *Rsc Adv* **2016,** *6*, 57603-57625.

137. Zhou, S.; Junge, K.; Addis, D.; Das, S.; Beller, M., *Angew. Chem. Int. Ed.* **2009,** *48*, 9507-9510.

138. Sunada, Y.; Kawakami, H.; Imaoka, T.; Motoyama, Y.; Nagashima, H., *Angew. Chem. Int. Ed.* **2009,** *48*, 9511-9514.

139. Bezier, D.; Venkanna, G. T.; Sortais, J.-B.; Darcel, C., *Chemcatchem* **2011,** *3*, 1747-1750.

140. Volkov, A.; Buitrago, E.; Adolfsson, H., *Eur J Org Chem* **2013**, 2066-2070.

141. Blom, B.; Tan, G. W.; Enthaler, S.; Inoue, S.; Epping, J. D.; Driess, M., *J. Am. Chem. Soc.* **2013,** *135*, 18108-18120.

142. Dombray, T.; Helleu, C.; Darcel, C.; Sortais, J. B., *Adv. Synth. Catal.* **2013,** *355*, 3358-3362.

143. Mamillapalli, N. C.; Sekar, G., *Chem. Commun.* **2014,** *50*, 7881-7884.

144. Simmons, B. J.; Hoffmann, M.; Hwang, J.; Jackl, M. K.; Garg, N. K., *Org. Lett.* **2017,** *19*, 1910-1913.

145. (a) Das, S.; Addis, D.; Junge, K.; Beller, M., *Chem. Eur. J.* **2011,** *17*, 12186-12192; (b) Das, S.; Addis, D.; Zhou, S.; Junge, K.; Beller, M., *J. Am. Chem. Soc.* **2010,** *132*, 1770-1771.

146. Kovalenko, O. O.; Volkov, A.; Adolfsson, H., *Org. Lett.* **2015,** *17*, 446-449.

147. Arias-Ugarte, R.; Sharma, H. K.; Morris, A. L. C.; Pannell, K. H., *J. Am. Chem. Soc.* **2012,** *134*, 848-851.

148. Papa, V.; Cabrero-Antonino, J. R.; Alberico, E.; Spanneberg, A.; Junge, K.; Junge, H.; Beller, M., *Chem. Sci.* **2017,** *8*, 3576-3585.

149. Chardon, A.; El Dine, T. M.; Legay, R.; De Paolis, M.; Rouden, J.; Blanchet, J., *Chem. Eur. J.* **2017,** *23*, 2005-2009.

150. (a) Kovalenko, O. O.; Adolfsson, H., *Chem. Eur. J.* **2015,** *21*, 2785-2788; (b) Merel, D. S.; Do, M. L. T.; Gaillard, S.; Dupau, P.; Renaud, J. L., *Coord. Chem. Rev.* **2015,** *288*, 50-68.

151. (a) Andersen, R. A.; Faegri, K.; Green, J. C.; Haaland, A.; Lappert, M. F.; Leung, W. P.; Rypdal, K., *Inorg. Chem.* **1988,** *27*, 1782-1786; (b) Bürger, H.; Wannagat, U., *Monatsh. Chem.* **1964,** *95*, 1099-1102.

152. (a) Barbe, G.; Charette, A. B., *J. Am. Chem. Soc.* **2008,** *130*, 18-19; (b) Zhou, S.; Addis, D.; Das, S.; Junge, K.; Beller, M., *Chem. Commun.* **2009**, 4883-4885.

153. Dieskau, A. P.; Begouin, J. M.; Plietker, B., *Eur J Org Chem* **2011**, 5291-5296.

154. Kim, J. W.; Koike, T.; Kotani, M.; Yamaguchi, K.; Mizuno, N., *Chem. Eur. J.* **2008,** *14*, 4104-4109.

APPENDIX A: Crystallographic Experimental Details

(κ^2-P,N)Pt-NH(1-Ad) ***3-1***

A. Crystal Data

formula	$C_{37}H_{56}N_3PPt$
formula weight	768.90
crystal dimensions (mm)	0.27 × 0.19 × 0.18
crystal system	triclinic
space group	$P\bar{1}$ (No. 2)
unit cell parameters[a]	
a (Å)	9.7878 (4)
b (Å)	12.6667 (6)
c (Å)	14.4464 (7)
α (deg)	83.7643 (5)
β (deg)	86.5283 (6)
γ (deg)	83.8496 (6)
V (Å^3)	1768.04 (14)
Z	2
ρ_{calcd} (g cm^{-3})	1.444
μ (mm^{-1})	4.042

B. Data Collection and Refinement Conditions

diffractometer	Bruker D8/APEX II CCD[b]
radiation (λ [Å])	graphite-monochromated Mo Kα (0.71073)
temperature (°C)	–100

scan type	ω scans (0.3°) (20 s exposures)
data collection 2θ limit (deg)	54.98
total data collected	15799 (-12 ≤ h ≤ 12, -16 ≤ k ≤ 16, -18 ≤ l ≤ 18)
independent reflections	8065 (R_{int} = 0.0105)
number of observed reflections (*NO*)	7782 [$F_o^2 \geq 2\sigma(F_o^2)$]
structure solution method	intrinsic phasing (*SHELXT*[c])
refinement method	full-matrix least-squares on F^2 [c]
absorption correction method	Gaussian integration (face-indexed)
range of transmission factors	0.6719–0.4336
data/restraints/parameters	8065 / 0 / 393
goodness-of-fit (*S*)[d] [all data]	1.115
final *R* indices[e]	
R_1 [$F_o^2 \geq 2\sigma(F_o^2)$]	0.0179
wR_2 [all data]	0.0540
largest difference peak and hole	1.762 and –0.546 e Å^{-3}

[a]Obtained from least-squares refinement of 9787 reflections with 5.04° < 2θ < 54.96°.

[b]Programs for diffractometer operation, data collection, data reduction and absorption correction were those supplied by Bruker.

[c]Sheldrick, G. M. *Acta Crystallogr.* **2008**, *A64*, 112–122.

[d]$S = [\Sigma w(F_o^2 - F_c^2)^2/(n-p)]^{1/2}$ (n = number of data; p = number of parameters varied; w

$= [\sigma^2(F_o^2) + (0.0336P)^2 + 1.0260P]^{-1}$ where $P = [\text{Max}(F_o^2, 0) + 2F_c^2]/3)$.

${}^eR_1 = \Sigma||F_o| - |F_c||/\Sigma|F_o|$; $wR_2 = [\Sigma w(F_o^2 - F_c^2)^2/\Sigma w(F_o^4)]^{1/2}$.

[(κ²-P,N)PtCl]₂ ***3-2***

Crystal Data

formula	$C_{54}H_{80}Cl_2N_4P_2Pt_2$
formula weight	1308.24
crystal dimensions (mm)	0.26 × 0.21 × 0.18
crystal system	monoclinic
space group	$P2_1/n$ (an alternate setting of $P2_1/c$ [No. 14])
unit cell parameters[a]	
a (Å)	13.2827 (3)
b (Å)	14.2524 (4)
c (Å)	15.0859 (4)
β (deg)	91.2451 (7)
V (Å^3)	2855.24 (13)
Z	2
ρ_{calcd} (g cm^{-3})	1.522
μ (mm^{-1})	10.69

B. Data Collection and Refinement Conditions

diffractometer	Bruker D8/APEX II CCD[b]
radiation (λ [Å])	Cu Kα (1.54178) (microfocus source)
temperature (°C)	–100
scan type	ω and ϕ scans (1.0°) (5 s exposures)
data collection 2θ limit (deg)	145.80
total data collected	19460 (-16 ≤ *h* ≤ 16, -17 ≤ *k* ≤ 17, -18 ≤ *l* ≤ 18)

independent reflections	5681 (R_{int} = 0.0194)
number of observed reflections (*NO*)	5664 [$F_o^2 \geq 2\sigma(F_o^2)$]
structure solution method	intrinsic phasing (*SHELXT-2013*[c])
refinement method	full-matrix least-squares on F^2 [c]
absorption correction method	Gaussian integration (face-indexed)
range of transmission factors	0.3503–0.1667
data/restraints/parameters	5681 / 0 / 289
goodness-of-fit (*S*)[d] [all data]	1.199
final *R* indices[e]	
R_1 [$F_o^2 \geq 2\sigma(F_o^2)$]	0.0165
wR_2 [all data]	0.0407
largest difference peak and hole	0.334 and –1.001 e Å^{-3}

[a]Obtained from least-squares refinement of 9615 reflections with 6.66° < 2θ < 144.52°.

[b]Programs for diffractometer operation, data collection, data reduction and absorption correction were those supplied by Bruker.

[c]Sheldrick, G. M. *Acta Crystallogr.* **2008**, *A64*, 112–122.

[d]$S = [\Sigma w(F_o^2 - F_c^2)^2/(n-p)]^{1/2}$ (n = number of data; p = number of parameters varied; $w = [\sigma^2(F_o^2) + (0.0136P)^2 + 2.3882P]^{-1}$ where $P = [\text{Max}(F_o^2, 0) + 2F_c^2]/3$).

[e]$R_1 = \Sigma||F_o| - |F_c||/\Sigma|F_o|$; $wR_2 = [\Sigma w(F_o^2 - F_c^2)^2/\Sigma w(F_o^4)]^{1/2}$.

(κ^2-P,N)Pt{C(N-2,6-xylyl)(=NAd)}(CN-2,6-xylyl) ***3-5***

Crystal Data

formula	$C_{59.75}H_{85}N_5O_{0.25}PPt$
formula weight	1103.38
crystal dimensions (mm)	0.40 × 0.33 × 0.08
crystal system	monoclinic
space group	$P2_1/c$ (No. 14)
unit cell parameters[a]	
a (Å)	31.2970 (10)
b (Å)	13.4510 (4)
c (Å)	27.5873 (9)
β (deg)	94.2671 (14)
V (Å^3)	11581.4 (6)
Z	8
ρ_{calcd} (g cm^{-3})	1.266
μ (mm^{-1})	5.087

Data Collection and Refinement Conditions

diffractometer	Bruker D8/APEX II CCD[b]
radiation (λ [Å])	Cu Kα (1.54178) (microfocus source)
temperature (°C)	–100
scan type	ω and ϕ scans (1.0°) (5 s exposures)
data collection 2θ limit (deg)	139.42
total data collected	74907 (-38 ≤ *h* ≤ 37, -16 ≤ *k* ≤ 16, -33 ≤ *l* ≤ 33)

independent reflections	21770 (R_{int} = 0.0279)
number of observed reflections (*NO*)	19513 [$F_o^2 \geq 2\sigma(F_o^2)$]
structure solution method	intrinsic phasing (*SHELXT-2014*[c])
refinement method	full-matrix least-squares on F^2 [c]
absorption correction method	Gaussian integration (face-indexed)
range of transmission factors	0.7256–0.1431
data/restraints/parameters	21770 / 21[d] / 1312
goodness-of-fit (*S*)[e] [all data]	1.146
final *R* indices[f]	
R_1 [$F_o^2 \geq 2\sigma(F_o^2)$]	0.0344
wR_2 [all data]	0.1039
largest difference peak and hole	1.754 and –1.007 e Å^{-3}

[a]Obtained from least-squares refinement of 9452 reflections with 7.32° < 2θ < 138.06°.

[b]Programs for diffractometer operation, data collection, data reduction and absorption correction were those supplied by Bruker.

[c]Sheldrick, G. M. *Acta Crystallogr.* **2008**, *A64*, 112–122.

[d]The C–C and the C···C distances within the solvent pentane molecules were restrained to be 1.53(1) and 2.50(1) Å, respectively.

[e]$S = [\Sigma w(F_o^2 - F_c^2)^2/(n-p)]^{1/2}$ (n = number of data; p = number of parameters varied; $w = [\sigma^2(F_o^2) + (0.0407P)^2 + 30.9619P]^{-1}$ where $P = [\text{Max}(F_o^2, 0) + 2F_c^2]/3$).

[f]$R_1 = \Sigma||F_o| - |F_c||/\Sigma|F_o|$; $wR_2 = [\Sigma w(F_o^2 - F_c^2)^2/\Sigma w(F_o^4)]^{1/2}$.

(κ^2-P,N)Pt(O-2,6-xylyl)(NH_2(1-Ad)) ***3-6***

Crystal Data

formula	$C_{50}H_{78}N_3OPPt$
formula weight	963.21
crystal dimensions (mm)	0.34 × 0.27 × 0.21
crystal system	monoclinic
space group	$P2_1/n$ (an alternate setting of $P2_1/c$ [No. 14])
unit cell parameters[a]	
a (Å)	17.4203 (5)
b (Å)	14.5259 (5)
c (Å)	19.2195 (6)
β (deg)	102.4193 (4)
V (Å^3)	4749.6 (3)
Z	4
ρ_{calcd} (g cm^{-3})	1.347
μ (mm^{-1})	3.026

Data Collection and Refinement Conditions

diffractometer	Bruker PLATFORM/APEX II CCD[b]
radiation (λ [Å])	graphite-monochromated Mo Kα (0.71073)
temperature (°C)	–80
scan type	ω scans (0.3°) (20 s exposures)
data collection 2θ limit (deg)	56.66
total data collected	42538 (-22 ≤ h ≤ 22, -19 ≤ k ≤ 19, -24 ≤ l ≤ 25)

independent reflections	11659 (R_{int} = 0.0268)
number of observed reflections (*NO*)	9807 [$F_o^2 \geq 2\sigma(F_o^2)$]
structure solution method	intrinsic phasing (*SHELXT-2013*[c])
refinement method	full-matrix least-squares on F^2 [c]
absorption correction method	Gaussian integration (face-indexed)
range of transmission factors	0.5141–0.3429
data/restraints/parameters	11659 / 4[d] / 541
goodness-of-fit (*S*)[e] [all data]	1.065
final *R* indices[f]	
R_1 [$F_o^2 \geq 2\sigma(F_o^2)$]	0.0237
wR_2 [all data]	0.0575
largest difference peak and hole	2.331 and –0.910 e Å^{-3}

[a]Obtained from least-squares refinement of 9846 reflections with 4.34° < 2θ < 56.40°.

[b]Programs for diffractometer operation, data collection, data reduction and absorption correction were those supplied by Bruker.

[c]Sheldrick, G. M. *Acta Crystallogr.* **2008**, *A64*, 112–122.

[d]The C–C distances of the minor component of the disordered solvent pentane molecule were restrained to be 1.53(1) Å.

[e]$S = [\Sigma w(F_o^2 - F_c^2)^2/(n-p)]^{1/2}$ (n = number of data; p = number of parameters varied; $w = [\sigma^2(F_o^2) + (0.0282P)^2 + 2.0295P]^{-1}$ where $P = [\text{Max}(F_o^2, 0) + 2F_c^2]/3$).

[f]$R_1 = \Sigma||F_o| - |F_c||/\Sigma|F_o|$; $wR_2 = [\Sigma w(F_o^2 - F_c^2)^2/\Sigma w(F_o^4)]^{1/2}$.

(κ^2-P,N)Pt($CH_2C{\equiv}CCy$)(NH_2Ad) ***3-7***

Crystal Data

formula	$C_{46}H_{70}N_3PPt$
formula weight	891.11
crystal dimensions (mm)	0.24 × 0.19 × 0.02
crystal system	monoclinic
space group	$P2_1/c$ (No. 14)
unit cell parameters[a]	
a (Å)	16.0181 (3)
b (Å)	14.8697 (3)
c (Å)	18.6692 (3)
β (deg)	106.8808 (11)
V (Å^3)	4255.11 (14)
Z	4
ρ_{calcd} (g cm^{-3})	1.391
μ (mm^{-1})	6.766

Data Collection and Refinement Conditions

diffractometer	Bruker D8/APEX II CCD[b]
radiation (λ [Å])	Cu Kα (1.54178) (microfocus source)
temperature (°C)	–100
scan type	ω and ϕ scans (1.0°) (5 s exposures)
data collection 2θ limit (deg)	138.83
total data collected	27297 (-19 ≤ *h* ≤ 19, -18 ≤ *k* ≤ 17, -22 ≤ *l* ≤ 22)

independent reflections	7941 (R_{int} = 0.0312)
number of observed reflections (*NO*)	7075 [$F_o^2 \geq 2\sigma(F_o^2)$]
structure solution method	intrinsic phasing (*SHELXT-2014*[c])
refinement method	full-matrix least-squares on F^2 [c]
absorption correction method	Gaussian integration (face-indexed)
range of transmission factors	0.8837–0.3487
data/restraints/parameters	7941 / 0 / 478
goodness-of-fit (*S*)[d] [all data]	1.096
final *R* indices[e]	
R_1 [$F_o^2 \geq 2\sigma(F_o^2)$]	0.0280
wR_2 [all data]	0.0704
largest difference peak and hole	1.221 and –0.947 e Å^{-3}

[a]Obtained from least-squares refinement of 9666 reflections with 5.76° < 2θ < 137.28°.

[b]Programs for diffractometer operation, data collection, data reduction and absorption correction were those supplied by Bruker.

[c]Sheldrick, G. M. *Acta Crystallogr.* **2008**, *A64*, 112–122.

[d]$S = [\Sigma w(F_o^2 - F_c^2)^2/(n-p)]^{1/2}$ (n = number of data; p = number of parameters varied; $w = [\sigma^2(F_o^2) + (0.0272P)^2 + 8.5025P]^{-1}$ where $P = [\text{Max}(F_o^2, 0) + 2F_c^2]/3$).

[e]$R_1 = \Sigma||F_o| - |F_c||/\Sigma|F_o|$; $wR_2 = [\Sigma w(F_o^2 - F_c^2)^2/\Sigma w(F_o^4)]^{1/2}$.

(κ^2-P,N)Pt(η^3-benzyl) ***4-1***

Crystal Data

formula	$C_{34}H_{47}N_2PPt$
formula weight	709.79
crystal dimensions (mm)	0.16 × 0.14 × 0.04
crystal system	triclinic
space group	$P\bar{1}$ (No. 2)
unit cell parameters[a]	
a (Å)	11.0127 (4)
b (Å)	17.1890 (7)
c (Å)	17.9331 (7)
α (deg)	102.2899 (5)
β (deg)	98.3473 (5)
γ (deg)	101.9720 (5)
V (Å^3)	3180.5 (2)
Z	4
ρ_{calcd} (g cm^{-3})	1.482
μ (mm^{-1})	4.486

Data Collection and Refinement Conditions

diffractometer	Bruker D8/APEX II CCD[b]
radiation (λ [Å])	graphite-monochromated Mo Kα (0.71073)
temperature (°C)	–100
scan type	ω and ϕ scans (0.3°) (20 s exposures)

data collection 2θ limit (deg)	55.08
total data collected	28996 ($-14 \le h \le 14$, $-22 \le k \le 22$, $-23 \le l \le 23$)
independent reflections	14622 ($R_{int} = 0.0250$)
number of observed reflections (*NO*)	11869 [$F_o^2 \ge 2\sigma(F_o^2)$]
structure solution method	intrinsic phasing (*SHELXT*[c])
refinement method	full-matrix least-squares on F^2 [c]
absorption correction method	Gaussian integration (face-indexed)
range of transmission factors	0.9136–0.6276
data/restraints/parameters	14622 / 0 / 697
goodness-of-fit (*S*)[d] [all data]	1.019
final *R* indices[e]	
R_1 [$F_o^2 \ge 2\sigma(F_o^2)$]	0.0251
wR_2 [all data]	0.0543
largest difference peak and hole	0.900 and –0.768 e Å^{-3}

[a]Obtained from least-squares refinement of 9996 reflections with $4.62° < 2\theta < 47.58°$.

[b]Programs for diffractometer operation, data collection, data reduction and absorption correction were those supplied by Bruker.

[c]Sheldrick, G. M. *Acta Crystallogr.* **2008**, *A64*, 112–122.

[d]$S = [\Sigma w(F_o^2 - F_c^2)^2/(n-p)]^{1/2}$ (n = number of data; p = number of parameters varied; $w = [\sigma^2(F_o^2) + (0.0237P)^2 + 0.0385P]^{-1}$ where $P = [\text{Max}(F_o^2, 0) + 2F_c^2]/3$).

[e]$R_1 = \Sigma||F_o| - |F_c||/\Sigma|F_o|$; $wR_2 = [\Sigma w(F_o^2 - F_c^2)^2/\Sigma w(F_o^4)]^{1/2}$.

[(κ²-P,N)NiCl]₂ ***4-2***

Crystal Data

formula	$C_{54}H_{80}Cl_2N_4Ni_2P_2$
formula weight	1035.48
crystal dimensions (mm)	0.27 × 0.27 × 0.16
crystal system	monoclinic
space group	$P2_1/n$ (an alternate setting of $P2_1/c$ [No. 14])
unit cell parameters[a]	
a (Å)	12.8910 (6)
b (Å)	14.2430 (6)
c (Å)	15.3503 (7)
β (deg)	92.1098 (6)
V (Å^3)	2816.5 (2)
Z	2
ρ_{calcd} (g cm^{-3})	1.221
μ (mm^{-1})	0.857

Data Collection and Refinement Conditions

diffractometer	Bruker PLATFORM/APEX II CCD[b]
radiation (λ [Å])	graphite-monochromated Mo Kα (0.71073)
temperature (°C)	–80

scan type	ω scans (0.3°) (15 s exposures)
data collection 2θ limit (deg)	56.76
total data collected	25992 ($-17 \le h \le 17$, $-19 \le k \le 18$, $-20 \le l \le 19$)
independent reflections	6988 ($R_{int} = 0.0328$)
number of observed reflections (*NO*)	5620 [$F_o^2 \ge 2\sigma(F_o^2)$]
structure solution method	Patterson/structure expansion[c]
refinement method	full-matrix least-squares on F^2 [d]
absorption correction method	Gaussian integration (face-indexed)
range of transmission factors	0.9505–0.8233
data/restraints/parameters	6988 / 0 / 289
goodness-of-fit (*S*)[e] [all data]	1.019
final *R* indices[f]	
R_1 [$F_o^2 \ge 2\sigma(F_o^2)$]	0.0321
wR_2 [all data]	0.0832
largest difference peak and hole	0.433 and –0.404 e Å^{-3}

[a]Obtained from least-squares refinement of 7900 reflections with $4.96° < 2\theta < 46.84°$.

[b]Programs for diffractometer operation, data collection, data reduction and absorption correction were those supplied by Bruker.

[c]Beurskens, P. T.; Beurskens, G.; de Gelder, R.; Smits, J. M. M.; Garcia-Granda, S.; Gould, R. O. (2008). The *DIRDIF-2008* program system. Crystallography Laboratory, Radboud University Nijmegen, The Netherlands.

[d]Sheldrick, G. M. *Acta Crystallogr.* **2008**, *A64*, 112–122.

[e] $S = [\Sigma w(F_o^2 - F_c^2)^2/(n - p)]^{1/2}$ (n = number of data; p = number of parameters varied; w $= [\sigma^2(F_o^2) + (0.0377P)^2 + 0.9805P]^{-1}$ where $P = [\text{Max}(F_o^2, 0) + 2F_c^2]/3)$.

[f] $R_1 = \Sigma||F_o| - |F_c||/\Sigma|F_o|$; $wR_2 = [\Sigma w(F_o^2 - F_c^2)^2/\Sigma w(F_o^4)]^{1/2}$.

[(κ^2-P,N)PdCl]$_2$ ***4-3***

Crystal Data

formula	$C_{54}H_{80}Cl_2N_4P_2Pd_2$
formula weight	1130.86
crystal dimensions (mm)	0.42 × 0.34 × 0.30
crystal system	monoclinic
space group	$P2_1/n$ (an alternate setting of $P2_1/c$ [No. 14])
unit cell parameters[a]	
a (Å)	13.2605 (7)
b (Å)	14.2224 (8)
c (Å)	15.1074 (8)
β (deg)	91.6714 (7)
V (Å^3)	2848.0 (3)
Z	2
ρ_{calcd} (g cm^{-3})	1.319
μ (mm^{-1})	0.818

Data Collection and Refinement Conditions

diffractometer	Bruker D8/APEX II CCD[b]
radiation (λ [Å])	graphite-monochromated Mo Kα (0.71073)
temperature (°C)	–100
scan type	ω scans (0.4°) (10 s exposures)
data collection 2θ limit (deg)	56.57
total data collected	26246 (-17 ≤ *h* ≤ 17, -18 ≤ *k* ≤ 18, -20 ≤ *l* ≤ 19)

independent reflections	6999 (R_{int} = 0.0149)
number of observed reflections (*NO*)	6503 [$F_o^2 \geq 2\sigma(F_o^2)$]
structure solution method	intrinsic phasing (*SHELXT-2013*[c])
refinement method	full-matrix least-squares on F^2 [c]
absorption correction method	Gaussian integration (face-indexed)
range of transmission factors	0.8781–0.7498
data/restraints/parameters	6999 / 0 / 289
goodness-of-fit (*S*)[d] [all data]	1.060
final *R* indices[e]	
R_1 [$F_o^2 \geq 2\sigma(F_o^2)$]	0.0190
wR_2 [all data]	0.0527
largest difference peak and hole	0.375 and –0.384 e Å^{-3}

[a]Obtained from least-squares refinement of 9890 reflections with 4.94° < 2θ < 45.72°.

[b]Programs for diffractometer operation, data collection, data reduction and absorption correction were those supplied by Bruker.

[c]Sheldrick, G. M. *Acta Crystallogr.* **2008**, *A64*, 112–122.

[d]$S = [\Sigma w(F_o^2 - F_c^2)^2/(n-p)]^{1/2}$ (n = number of data; p = number of parameters varied; $w = [\sigma^2(F_o^2) + (0.0238P)^2 + 1.0651P]^{-1}$ where $P = [\text{Max}(F_o^2, 0) + 2F_c^2]/3$).

[e]$R_1 = \Sigma||F_o| - |F_c||/\Sigma|F_o|$; $wR_2 = [\Sigma w(F_o^2 - F_c^2)^2/\Sigma w(F_o^4)]^{1/2}$.

(κ^2-P,N)Ni(η^3-benzyl) ***4-4***

Crystal Data

formula	$C_{36}H_{52}N_2NiO_{0.5}P$
formula weight	610.47
crystal dimensions (mm)	0.36 × 0.13 × 0.13
crystal system	monoclinic
space group	$P2_1/n$ (an alternate setting of $P2_1/c$ [No. 14])
unit cell parameters[a]	
a (Å)	12.1189 (2)
b (Å)	22.0610 (4)
c (Å)	13.0307 (2)
β (deg)	101.7018 (9)
V (Å^3)	3411.42 (10)
Z	4
ρ_{calcd} (g cm^{-3})	1.189
μ (mm^{-1})	1.455

Data Collection and Refinement Conditions

diffractometer	Bruker D8/APEX II CCD[b]
radiation (λ [Å])	Cu Kα (1.54178) (microfocus source)
temperature (°C)	–100
scan type	ω and ϕ scans (1.0°) (5 s exposures)
data collection 2θ limit (deg)	148.02
total data collected	24156 (-15 ≤ *h* ≤ 14, -27 ≤ *k* ≤ 27, -16 ≤ *l* ≤ 16)

independent reflections	6750 (R_{int} = 0.0259)
number of observed reflections (*NO*)	6322 [$F_o^2 \geq 2\sigma(F_o^2)$]
structure solution method	Patterson/structure expansion[c]
refinement method	full-matrix least-squares on F^2 [d]
absorption correction method	Gaussian integration (face-indexed)
range of transmission factors	0.9338–0.6694
data/restraints/parameters	6750 / 0 / 375
goodness-of-fit (*S*)[e] [all data]	1.037
final *R* indices[f]	
R_1 [$F_o^2 \geq 2\sigma(F_o^2)$]	0.0330
wR_2 [all data]	0.0940
largest difference peak and hole	0.402 and –0.384 e Å^{-3}

[a]Obtained from least-squares refinement of 9417 reflections with 8.00° < 2θ < 147.60°.

[b]Programs for diffractometer operation, data collection, data reduction and absorption correction were those supplied by Bruker.

[c]Beurskens, P. T.; Beurskens, G.; de Gelder, R.; Smits, J. M. M.; Garcia-Granda, S.; Gould, R. O. (2008). The *DIRDIF-2008* program system. Crystallography Laboratory, Radboud University Nijmegen, The Netherlands.

[d]Sheldrick, G. M. *Acta Crystallogr.* **2015**, *C71*, 3–8.

[e]$S = [\Sigma w(F_o^2 - F_c^2)^2/(n-p)]^{1/2}$ (n = number of data; p = number of parameters varied; $w = [\sigma^2(F_o^2) + (0.0530P)^2 + 1.3378P]^{-1}$ where $P = [\text{Max}(F_o^2, 0) + 2F_c^2]/3$).

[f]$R_1 = \Sigma||F_o| - |F_c||/\Sigma|F_o|$; $wR_2 = [\Sigma w(F_o^2 - F_c^2)^2/\Sigma w(F_o^4)]^{1/2}$.

(κ^2-P,N)Pd(η^3-benzyl) ***4-5***

Crystal Data

formula	$C_{37.5}H_{51}N_2PPd$
formula weight	667.17
crystal dimensions (mm)	0.26 × 0.21 × 0.14
crystal system	orthorhombic
space group	*Aba*2 (No. 41)
unit cell parameters[a]	
a (Å)	22.632 (3)
b (Å)	19.353 (3)
c (Å)	16.129 (2)
V (Å^3)	7064.3 (16)
Z	8
ρ_{calcd} (g cm^{-3})	1.255
μ (mm^{-1})	0.597

Data Collection and Refinement Conditions

diffractometer	Bruker PLATFORM/APEX II CCD[b]
radiation (λ [Å])	graphite-monochromated Mo Kα (0.71073)
temperature (°C)	–80
scan type	ω scans (0.3°) (15 s exposures)
data collection 2θ limit (deg)	56.68
total data collected	33197 (-29 ≤ *h* ≤ 30, -25 ≤ *k* ≤ 25, -21 ≤ *l* ≤ 21)
independent reflections	8795 (R_{int} = 0.0340)

number of observed reflections (*NO*)	8002 [$F_o^2 \geq 2\sigma(F_o^2)$]
structure solution method	intrinsic phasing[c]
refinement method	full-matrix least-squares on F^2 [d]
absorption correction method	Gaussian integration (face-indexed)
range of transmission factors	0.9748–0.8713
data/restraints/parameters	8795 / 3[e] / 354
Flack absolute structure parameter[f]	-0.028(10)
goodness-of-fit (*S*)[g] [all data]	1.049
final *R* indices[h]	
R_1 [$F_o^2 \geq 2\sigma(F_o^2)$]	0.0324
wR_2 [all data]	0.0875
largest difference peak and hole	0.748 and –0.532 e Å^{-3}

[a]Obtained from least-squares refinement of 9908 reflections with $4.58° < 2\theta < 41.52°$.

[b]Programs for diffractometer operation, data collection, data reduction and absorption correction were those supplied by Bruker.

[c]Sheldrick, G. M. *Acta Crystallogr.* **2015**, *A71*, 3–8.

[d]Sheldrick, G. M. *Acta Crystallogr.* **2015**, *C71*, 3–8.

[e]Distances involving the methyl carbon of the disordered solvent toluene molecule were constrained during refinement: d(C1S–C7S) = 1.52(1) Å, d(C2S...C7S) = d(C6S...C7S) = 2.52(1) Å. The carbon-atom positions for the toluene phenyl ring were refined as an idealized regular hexagon with a C–C bond distance of 1.390 Å.

[f]Flack, H. D. *Acta Crystallogr.* **1983**, *A39*, 876–881; Flack, H. D.; Bernardinelli, G.

Acta Crystallogr. **1999**, *A55*, 908–915; Flack, H. D.; Bernardinelli, G. *J. Appl. Cryst.* **2000**, *33*, 1143–1148. The Flack parameter will refine to a value near zero if the structure is in the correct configuration and will refine to a value near one for the inverted configuration.

[g] $S = [\Sigma w(F_o^2 - F_c^2)^2/(n - p)]^{1/2}$ (n = number of data; p = number of parameters varied; $w = [\sigma^2(F_o^2) + (0.0451P)^2 + 5.9066P]^{-1}$ where $P = [\text{Max}(F_o^2, 0) + 2F_c^2]/3$).

[h] $R_1 = \Sigma||F_o| - |F_c||/\Sigma|F_o|$; $wR_2 = [\Sigma w(F_o^2 - F_c^2)^2/\Sigma w(F_o^4)]^{1/2}$.

(κ^2-P,N-[H])PtH(η^1-benzyl) ***4-6***

Crystal Data

formula	$C_{34}H_{49}N_2PPt$
formula weight	711.81
crystal dimensions (mm)	0.25 × 0.10 × 0.09
crystal system	monoclinic
space group	$P2_1/n$ (an alternate setting of $P2_1/c$ [No. 14])
unit cell parameters[a]	
a (Å)	11.7126 (8)
b (Å)	18.3777 (12)
c (Å)	15.4901 (11)
β (deg)	96.430 (2)
V (Å^3)	3313.3 (4)
Z	4
ρ_{calcd} (g cm^{-3})	1.427
μ (mm^{-1})	8.537

Data Collection and Refinement Conditions

diffractometer	Bruker D8/APEX II CCD[b]
radiation (λ [Å])	Cu Kα (1.54178) (microfocus source)
temperature (°C)	–100
scan type	ω and ϕ scans (1.0°) (5 s exposures)
data collection 2θ limit (deg)	149.29
total data collected	23128 (-14 ≤ h ≤ 14, -22 ≤ k ≤ 22, -18 ≤ l ≤ 16)

independent reflections	6557 (R_{int} = 0.0299)
number of observed reflections (*NO*)	6228 [$F_o^2 \geq 2\sigma(F_o^2)$]
structure solution method	Patterson/structure expansion[c]
refinement method	full-matrix least-squares on F^2 [d]
absorption correction method	Gaussian integration (face-indexed)
range of transmission factors	0.5771–0.2746
data/restraints/parameters	6557 / 0 / 349
goodness-of-fit (*S*)[e] [all data]	1.098
final *R* indices[f]	
R_1 [$F_o^2 \geq 2\sigma(F_o^2)$]	0.0400
wR_2 [all data]	0.1033
largest difference peak and hole	1.791 and –2.541 e Å^{-3}

[a]Obtained from least-squares refinement of 9105 reflections with 7.50° < 2θ < 147.64°.

[b]Programs for diffractometer operation, data collection, data reduction and absorption correction were those supplied by Bruker.

[c]Beurskens, P. T.; Beurskens, G.; de Gelder, R.; Smits, J. M. M.; Garcia-Granda, S.; Gould, R. O. (2008). The *DIRDIF-2008* program system. Crystallography Laboratory, Radboud University Nijmegen, The Netherlands.

[d]Sheldrick, G. M. *Acta Crystallogr.* **2015**, *C71*, 3–8.

[e]$S = [\Sigma w(F_o^2 - F_c^2)^2/(n - p)]^{1/2}$ (n = number of data; p = number of parameters varied; $w = [\sigma^2(F_o^2) + (0.0421P)^2 + 15.5387P]^{-1}$ where $P = [\text{Max}(F_o^2, 0) + 2F_c^2]/3$).

[f]$R_1 = \Sigma||F_o| - |F_c||/\Sigma|F_o|$; $wR_2 = [\Sigma w(F_o^2 - F_c^2)^2/\Sigma w(F_o^4)]^{1/2}$.

(κ^2-P,N)Pt(η^3-PhCH(BPin)) ***4-7***

Crystal Data

formula	$C_{40}H_{58}BN_2O_2PPt$
formula weight	835.75
crystal dimensions (mm)	0.38 × 0.25 × 0.21
crystal system	orthorhombic
space group	$P2_12_12_1$ (No. 19)
unit cell parameters[a]	
a (Å)	12.2071 (5)
b (Å)	17.3230 (7)
c (Å)	18.4194 (8)
V (Å^3)	3895.0 (3)
Z	4
ρ_{calcd} (g cm^{-3})	1.425
μ (mm^{-1})	3.678

Data Collection and Refinement Conditions

diffractometer	Bruker PLATFORM/APEX II CCD[b]
radiation (λ [Å])	graphite-monochromated Mo Kα (0.71073)
temperature (°C)	–80
scan type	ω scans (0.3°) (15 s exposures)
data collection 2θ limit (deg)	56.68
total data collected	34031 ($-16 \le h \le 15$, $-23 \le k \le 23$, $-24 \le l \le 24$)

independent reflections	9535 (R_{int} = 0.0282)
number of observed reflections (*NO*)	9317 [$F_o^2 \geq 2\sigma(F_o^2)$]
structure solution method	intrinsic phasing[c]
refinement method	full-matrix least-squares on F^2 [c]
absorption correction method	Gaussian integration (face-indexed)
range of transmission factors	0.5717–0.3861
data/restraints/parameters	9535 / 0 / 424
Flack absolute structure parameter[d]	0.020(2)
goodness-of-fit (*S*)[e] [all data]	1.023
final *R* indices[f]	
R_1 [$F_o^2 \geq 2\sigma(F_o^2)$]	0.0157
wR_2 [all data]	0.0373
largest difference peak and hole	0.570 and –0.690 e Å^{-3}

[a]Obtained from least-squares refinement of 9953 reflections with 4.64° < 2θ < 46.56°.

[b]Programs for diffractometer operation, data collection, data reduction and absorption correction were those supplied by Bruker.

[c]Sheldrick, G. M. *Acta Crystallogr.* **2008**, *A64*, 112–122.

[d]Flack, H. D. *Acta Crystallogr.* **1983**, *A39*, 876–881; Flack, H. D.; Bernardinelli, G. *Acta Crystallogr.* **1999**, *A55*, 908–915; Flack, H. D.; Bernardinelli, G. *J. Appl. Cryst.* **2000**, *33*, 1143–1148. The Flack parameter will refine to a value near zero if the structure is in the correct configuration and will refine to a value near one for the inverted configuration.

[e]$S = [\Sigma w(F_o^2 - F_c^2)^2/(n - p)]^{1/2}$ (n = number of data; p = number of parameters varied; w $= [\sigma^2(F_o^2) + (0.0048P)^2]^{-1}$ where $P = [\text{Max}(F_o^2, 0) + 2F_c^2]/3)$.

[f]$R_1 = \Sigma||F_o| - |F_c||/\Sigma|F_o|$; $wR_2 = [\Sigma w(F_o^2 - F_c^2)^2/\Sigma w(F_o^4)]^{1/2}$.

(κ^2-P,N)Pt(η^3-PhCH(BCat)) ***4-8***

Crystal Data

formula	$C_{43.50}H_{54}BN_2O_2PP$
formula weight	873.75
crystal dimensions (mm)	0.25 × 0.14 × 0.09
crystal system	triclinic
space group	$P\bar{1}$ (No. 2)
unit cell parameters[a]	
a (Å)	11.0100 (3)
b (Å)	12.3474 (3)
c (Å)	16.6516 (4)
α (deg)	98.5016 (6)
β (deg)	90.2386 (8)
γ (deg)	115.9413 (5)
V (Å^3)	2007.21 (9)
Z	2
ρ_{calcd} (g cm^{-3})	1.446
μ (mm^{-1})	7.196

Data Collection and Refinement Conditions

diffractometer	Bruker D8/APEX II CCD[b]
radiation (λ [Å])	Cu Kα (1.54178) (microfocus source)
temperature (°C)	–100

scan type	ω and ϕ scans (1.0°) (5 s exposures)
data collection 2θ limit (deg)	147.96
total data collected	14424 ($-12 \le h \le 13$, $-15 \le k \le 15$, $-20 \le l \le 20$)
independent reflections	7819 ($R_{int} = 0.0100$)
number of observed reflections (*NO*)	7793 [$F_o^2 \ge 2\sigma(F_o^2)$]
structure solution method	intrinsic phasing[c]
refinement method	full-matrix least-squares on F^2 [d]
absorption correction method	Gaussian integration (face-indexed)
range of transmission factors	0.6408–0.3630
data/restraints/parameters	7819 / 0 / 476
goodness-of-fit (*S*)[e] [all data]	1.096
final *R* indices[f]	
R_1 [$F_o^2 \ge 2\sigma(F_o^2)$]	0.0165
wR_2 [all data]	0.0415
largest difference peak and hole	1.167 and –0.602 e Å^{-3}

[a]Obtained from least-squares refinement of 9631 reflections with $9.02° < 2\theta < 147.36°$.

[b]Programs for diffractometer operation, data collection, data reduction and absorption correction were those supplied by Bruker.

[c]Sheldrick, G. M. *Acta Crystallogr.* **2015**, *A71*, 3–8. (*SHELXT-2014*)

[d]Sheldrick, G. M. *Acta Crystallogr.* **2015**, *C71*, 3–8. (*SHELXL-2014*)

[e]$S = [\Sigma w(F_o^2 - F_c^2)^2/(n - p)]^{1/2}$ (n = number of data; p = number of parameters varied; w

$= [\sigma^2(F_o^2) + (0.0172P)^2 + 1.7455P]^{-1}$ where $P = [\text{Max}(F_o^2, 0) + 2F_c^2]/3)$.

[f]$R_1 = \Sigma||F_o| - |F_c||/\Sigma|F_o|$; $wR_2 = [\Sigma w(F_o^2 - F_c^2)^2/\Sigma w(F_o^4)]^{1/2}$.

(κ^2-P,N)Mn(N(SiMe$_3$)$_2$) ***5-1***

Crystal Data

formula	$C_{33}H_{58}MnN_3PSi_2$
formula weight	638.91
crystal dimensions (mm)	0.36 × 0.33 × 0.28
crystal system	monoclinic
space group	$P2_1/n$ (an alternate setting of $P2_1/c$ [No. 14])
unit cell parameters[a]	
a (Å)	17.7984 (5)
b (Å)	19.5744 (5)
c (Å)	22.7785 (6)
β (deg)	107.4957 (16)
V (Å^3)	7568.8 (4)
Z	8
ρ_{calcd} (g cm^{-3})	1.121
μ (mm^{-1})	4.011

Data Collection and Refinement Conditions

diffractometer	Bruker D8/APEX II CCD[b]
radiation (λ [Å])	Cu Kα (1.54178) (microfocus source)
temperature (°C)	–100
scan type	ω and ϕ scans (1.0°) (5 s exposures)
data collection 2θ limit (deg)	148.51
total data collected	53766 (-22 ≤ h ≤ 21, -24 ≤ k ≤ 24, -28 ≤ l ≤ 28)

independent reflections	14977 (R_{int} = 0.0224)
number of observed reflections (*NO*)	13917 [$F_o^2 \geq 2\sigma(F_o^2)$]
structure solution method	Patterson/structure expansion (*DIRDIF–2008*[c])
refinement method	full-matrix least-squares on F^2 (*SHELXL–2014*[d])
absorption correction method	Gaussian integration (face-indexed)
range of transmission factors	0.5437–0.3578
data/restraints/parameters	14977 / 0 / 733
goodness-of-fit (*S*)[e] [all data]	1.040
final *R* indices[f]	
R_1 [$F_o^2 \geq 2\sigma(F_o^2)$]	0.0314
wR_2 [all data]	0.0863
largest difference peak and hole	0.336 and –0.335 e Å^{-3}

[a]Obtained from least-squares refinement of 9815 reflections with 5.56° < 2θ < 147.88°.

[b]Programs for diffractometer operation, data collection, data reduction and absorption correction were those supplied by Bruker.

[c]Beurskens, P. T.; Beurskens, G.; de Gelder, R.; Smits, J. M. M.; Garcia-Granda, S.; Gould, R. O. (2008). The *DIRDIF-2008* program system. Crystallography Laboratory, Radboud University Nijmegen, The Netherlands.

[d]Sheldrick, G. M. *Acta Crystallogr.* **2015**, *C71*, 3–8.

[e]$S = [\Sigma w(F_o^2 - F_c^2)^2/(n - p)]^{1/2}$ (n = number of data; p = number of parameters varied; w $= [\sigma^2(F_o^2) + (0.0456P)^2 + 2.3650P]^{-1}$ where $P = [\text{Max}(F_o^2, 0) + 2F_c^2]/3$).

[f]$R_1 = \Sigma||F_o| - |F_c||/\Sigma|F_o|$; $wR_2 = [\Sigma w(F_o^2 - F_c^2)^2/\Sigma w(F_o^4)]^{1/2}$.

Appendix B – NMR Spectra of Organic Products

^{1}H NMR (300.1 MHz, $CDCl_3$) 1-Benzylmorpholine, 5-2f

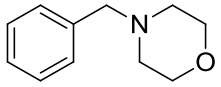

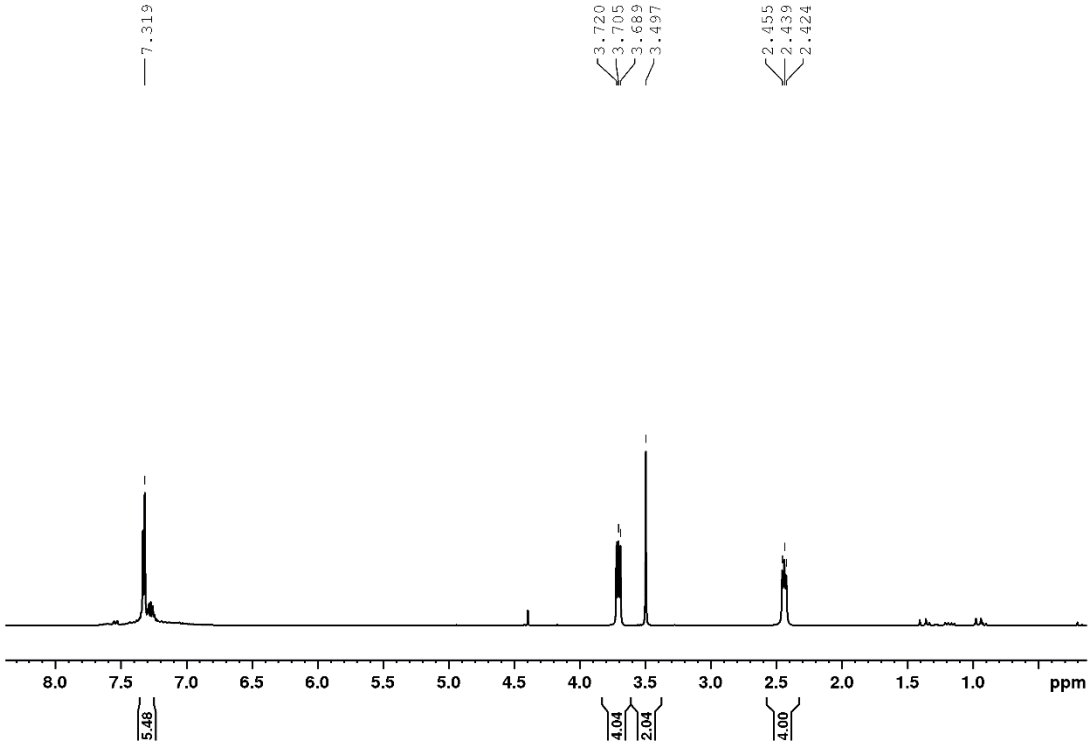

$^{13}C\{^{1}H\}$ NMR (75.5 MHz, $CDCl_3$) 1-Benzylmorpholine, 5-2f

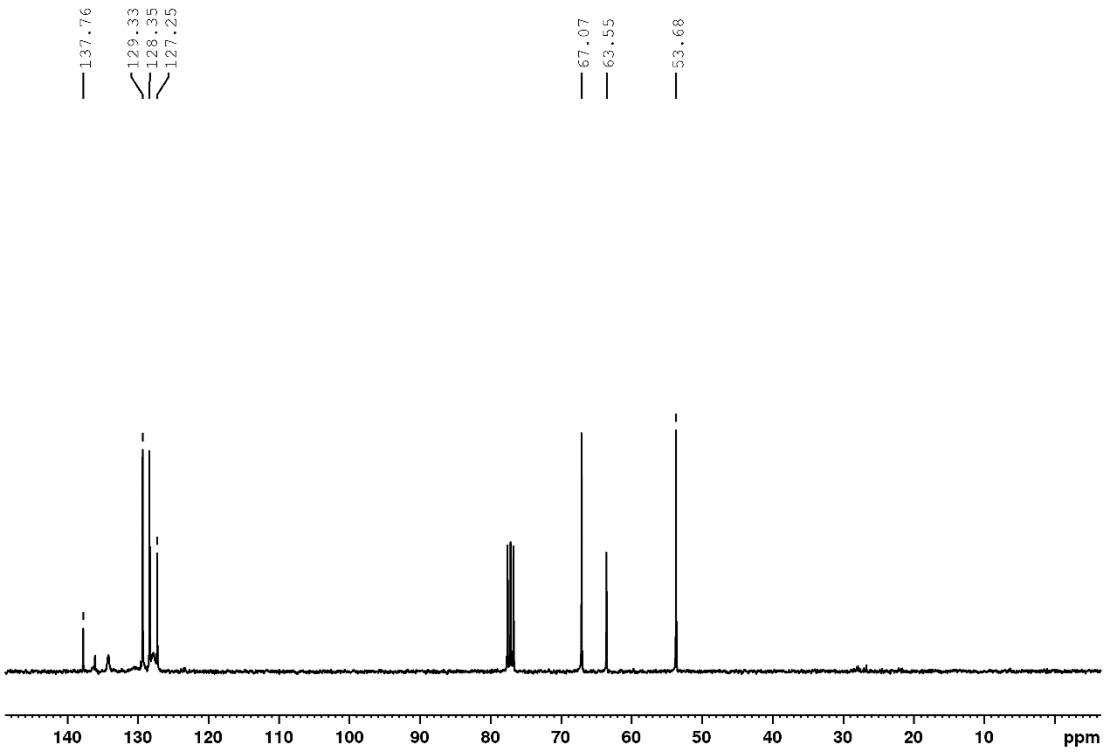

^{1}H NMR (300.1 MHz, $CDCl_3$) *N*,*N*-Dibenzyl-1-(thiophen-2-yl)methanamine, 5-2g

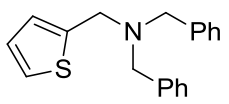

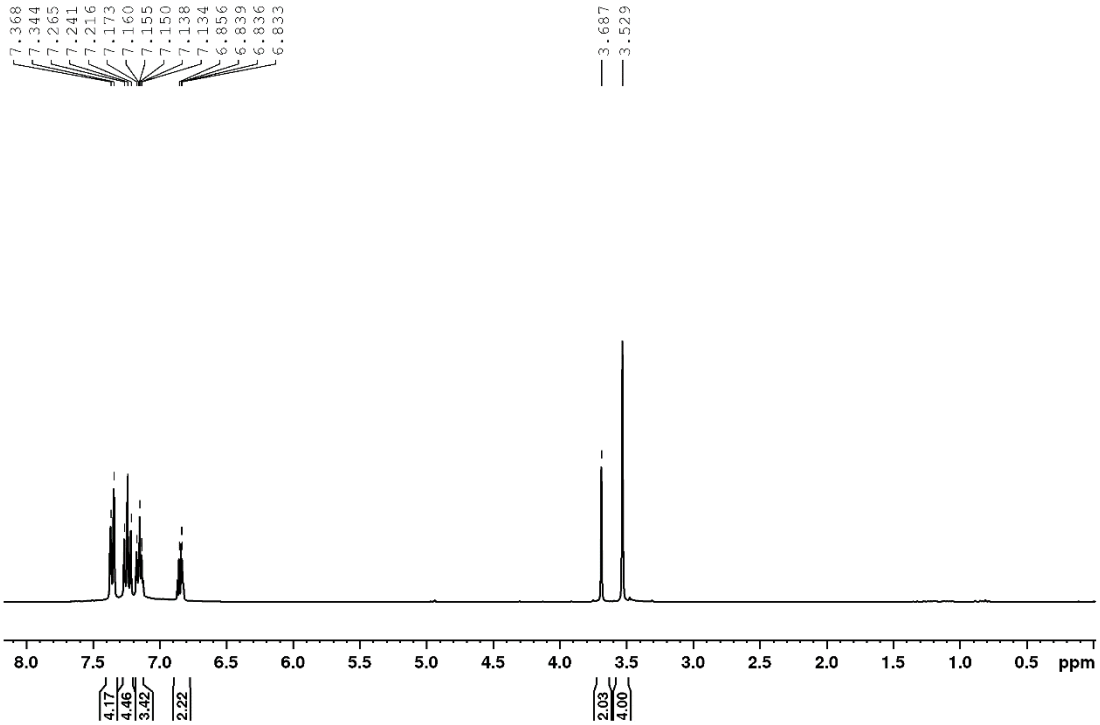

$^{13}C\{^{1}H\}$ NMR (75.5 MHz, $CDCl_3$) *N*,*N*-Dibenzyl-1-(thiophen-2-yl)methanamine, 5-2g

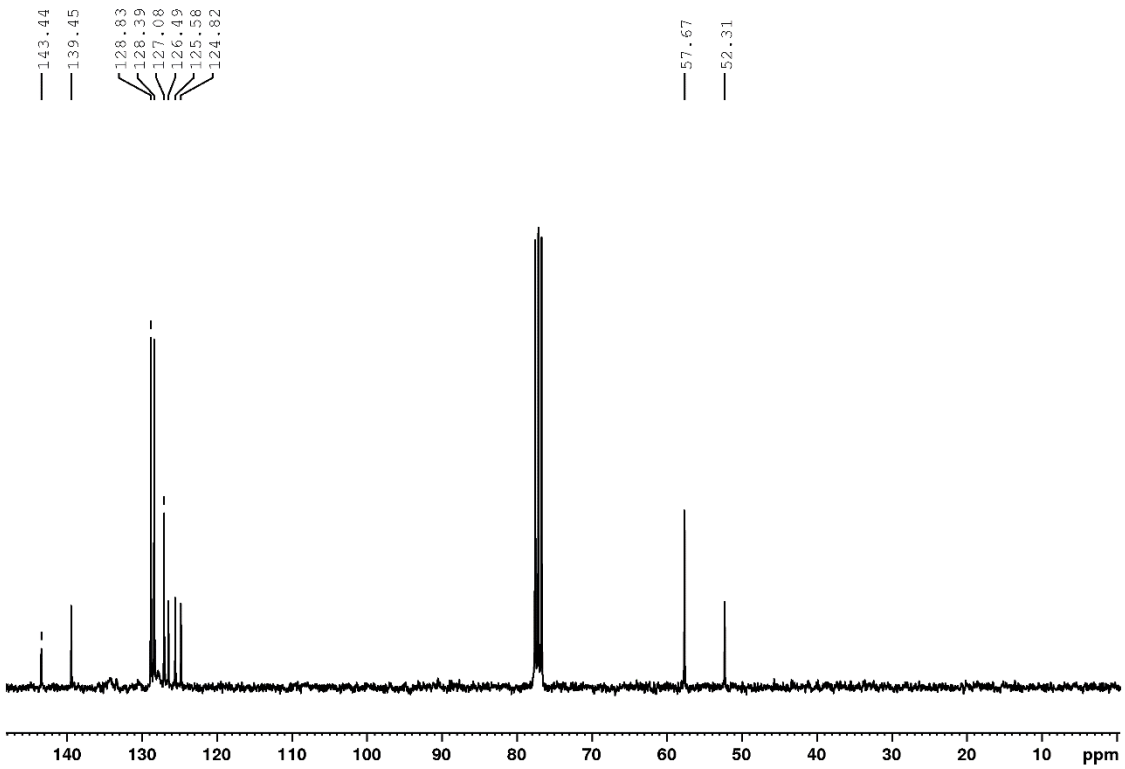

^{1}H NMR (300.1 MHz, $CDCl_3$) Tribenzylamine, 5-2h

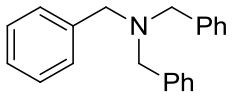

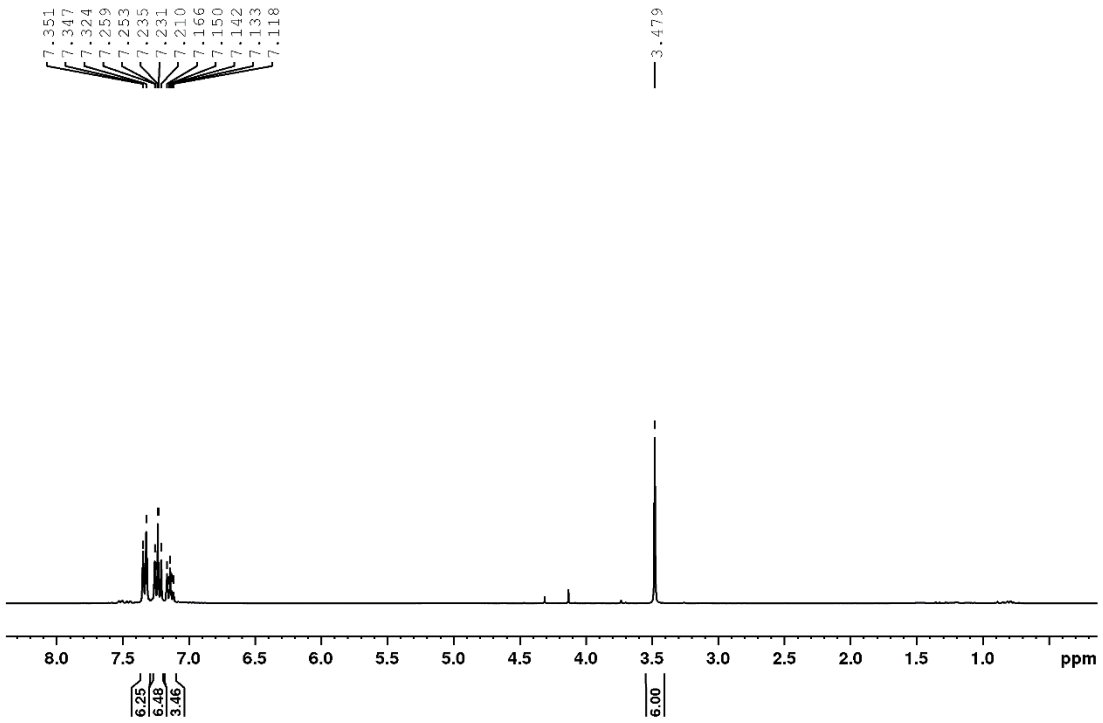

$^{13}C\{^{1}H\}$ NMR (75.5 MHz, $CDCl_3$) Tribenzylamine, 5-2h

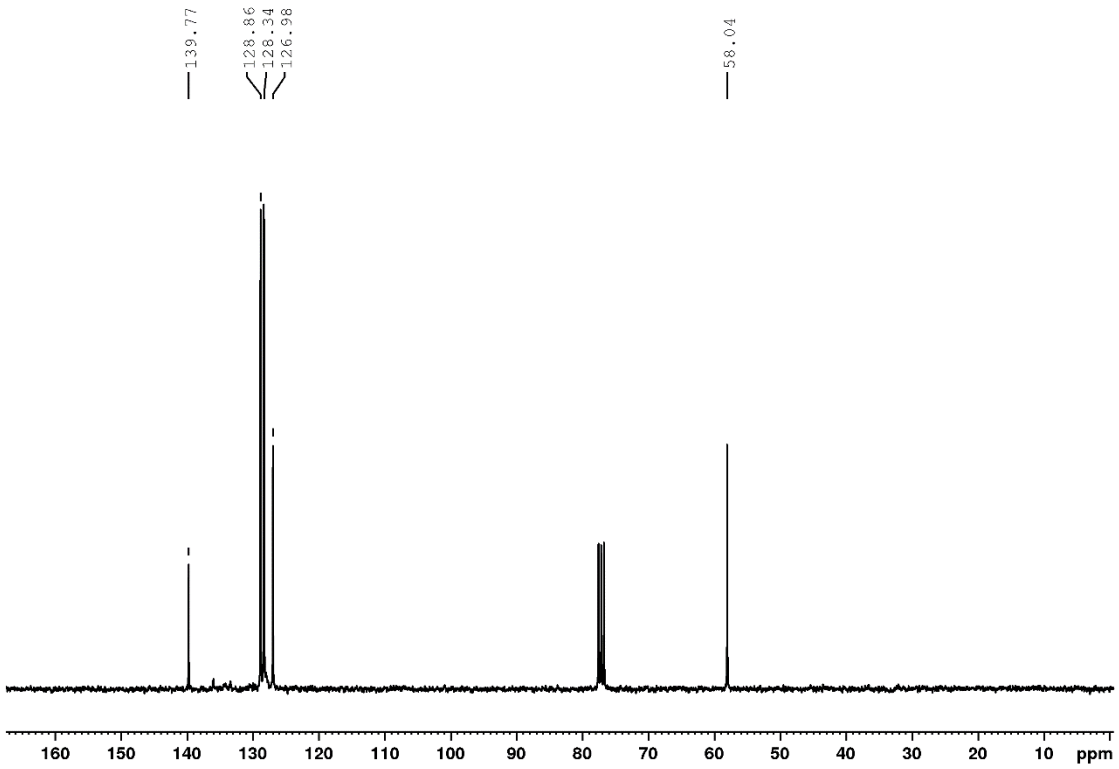

^{1}H NMR (300.1 MHz, $CDCl_3$) *N*,*N*-Dibenzyl-2,2-dimethylpropan-1-amine, 5-2k

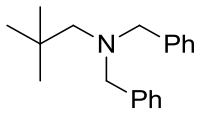

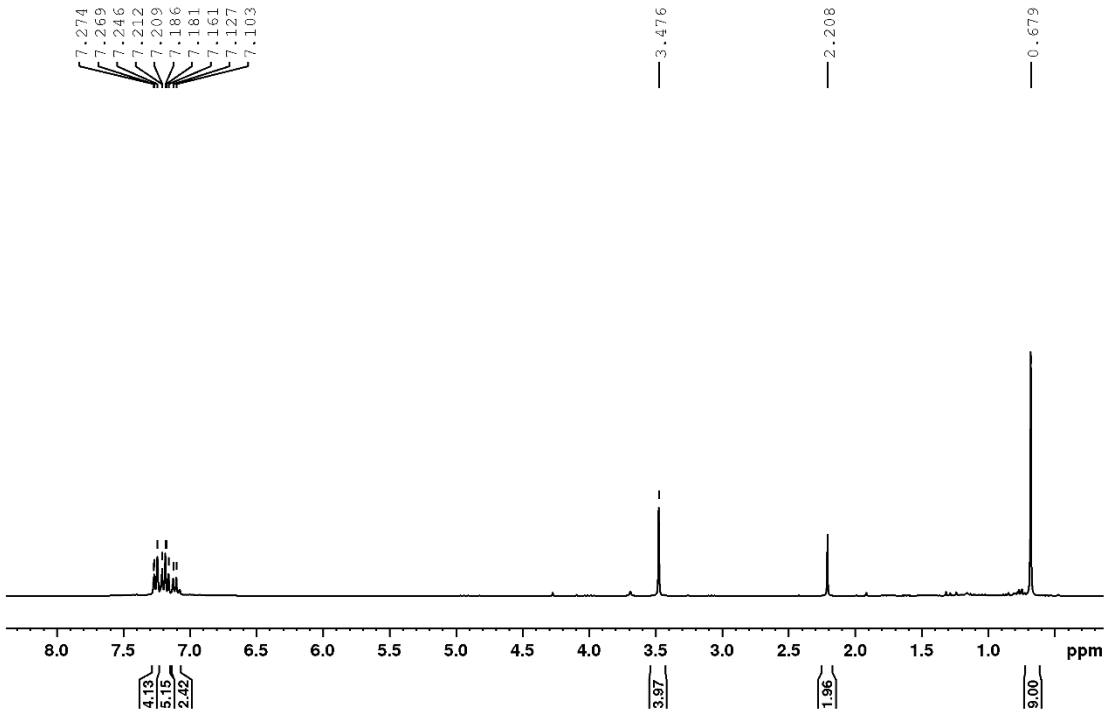

$^{13}C\{^{1}H\}$ NMR (75.5 MHz, $CDCl_3$) *N*,*N*-Dibenzyl-2,2-dimethylpropan-1-amine, 5-2k

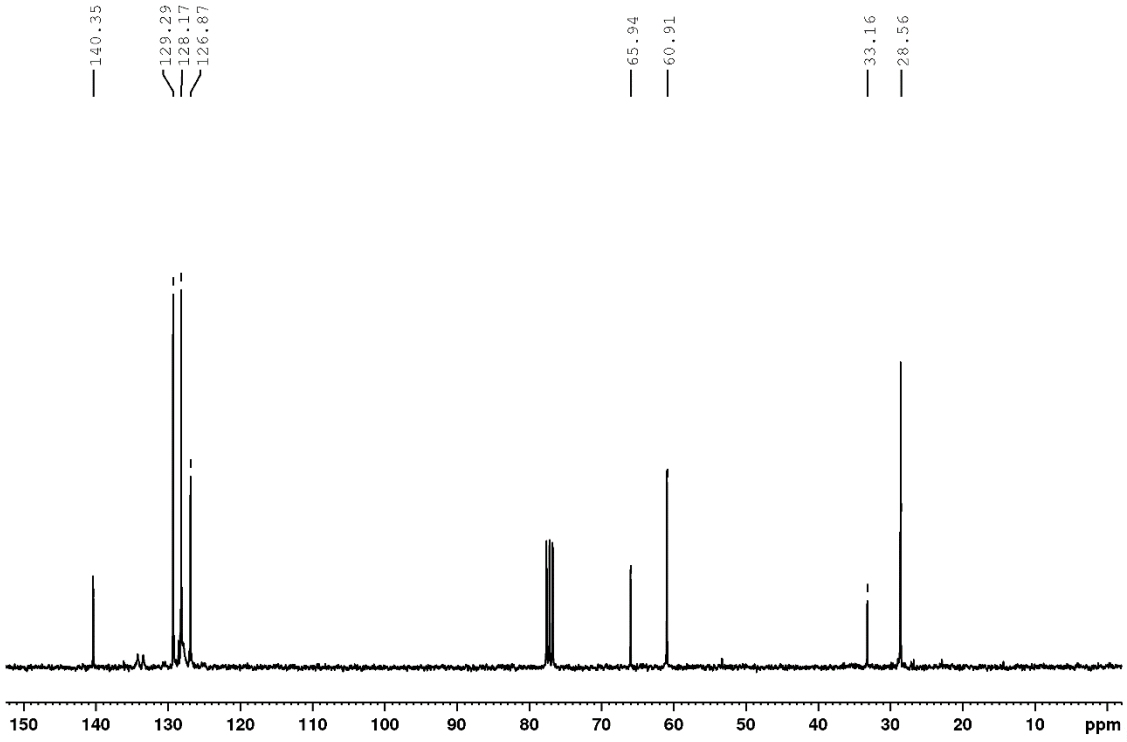

^{1}H NMR (300.1 MHz, $CDCl_3$) 1-Naphthyl ethanol, 5-3d

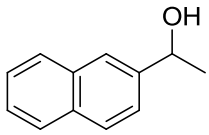

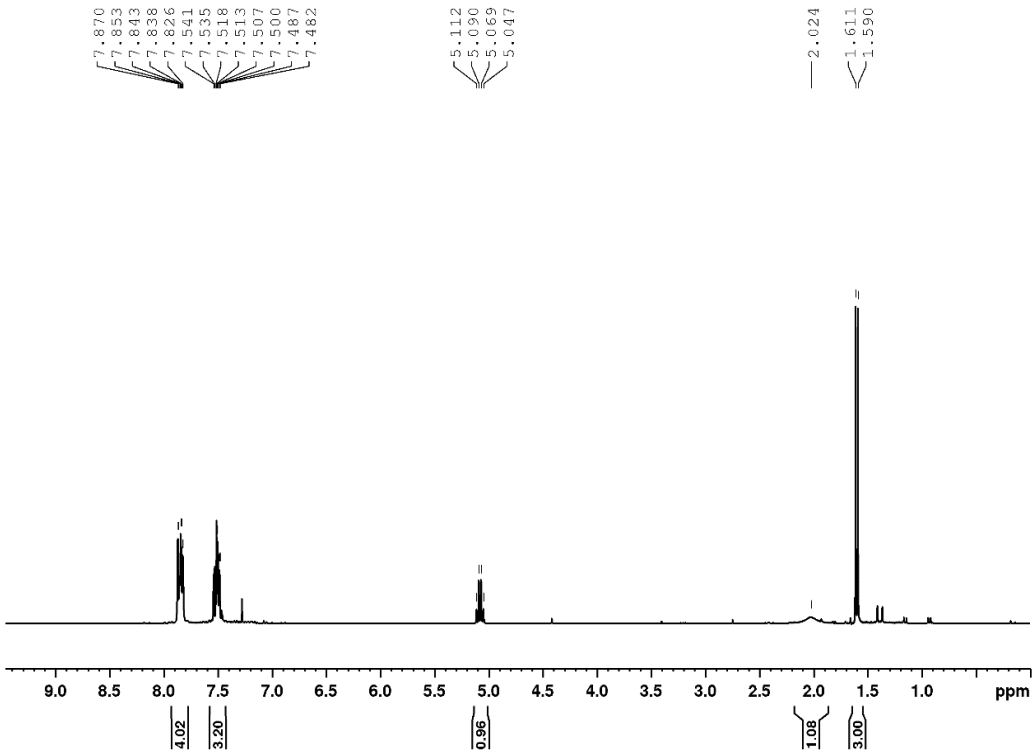

$^{13}C\{^{1}H\}$ NMR (75.5 MHz, $CDCl_3$) 1-Naphthyl ethanol, 5-3d

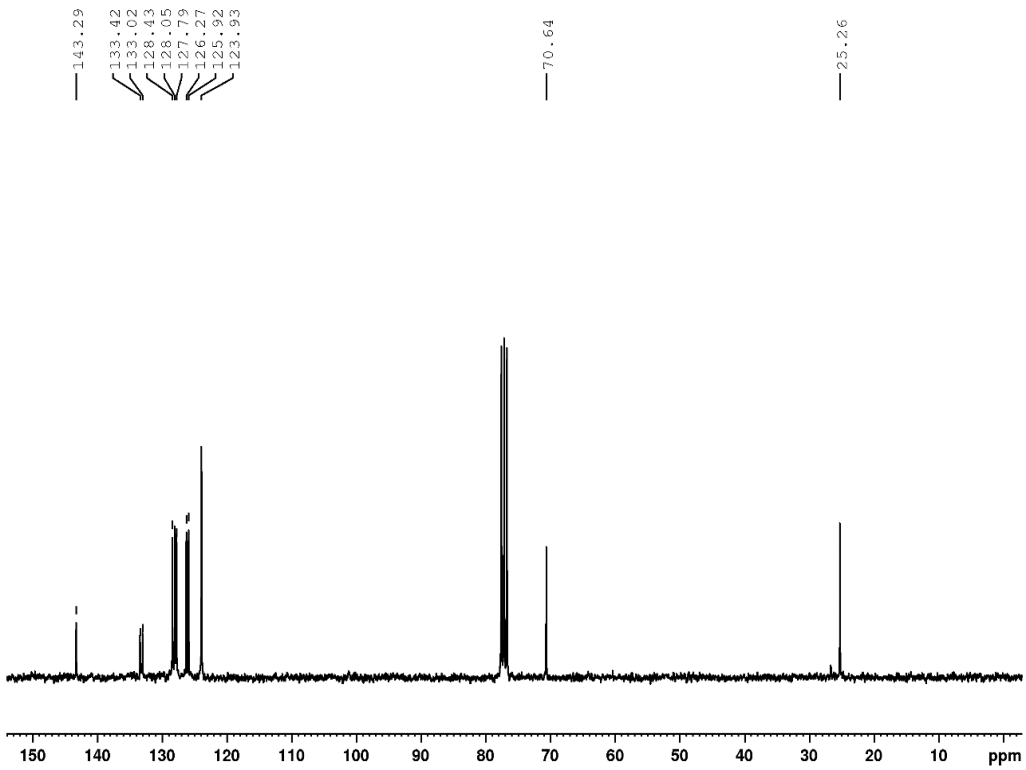

^{1}H NMR (300.1 MHz, $CDCl_3$) 4-Heptanol, 5-3h

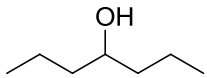

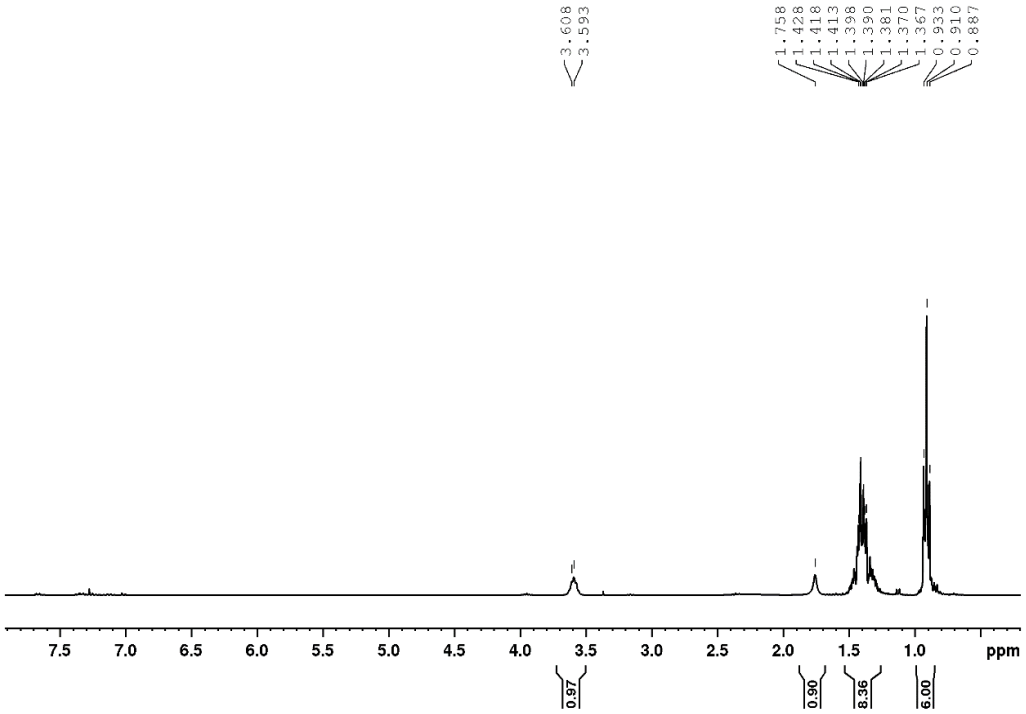

$^{13}C\{^{1}H\}$ NMR (75.5 MHz, $CDCl_3$) 4-Heptanol, 5-3h

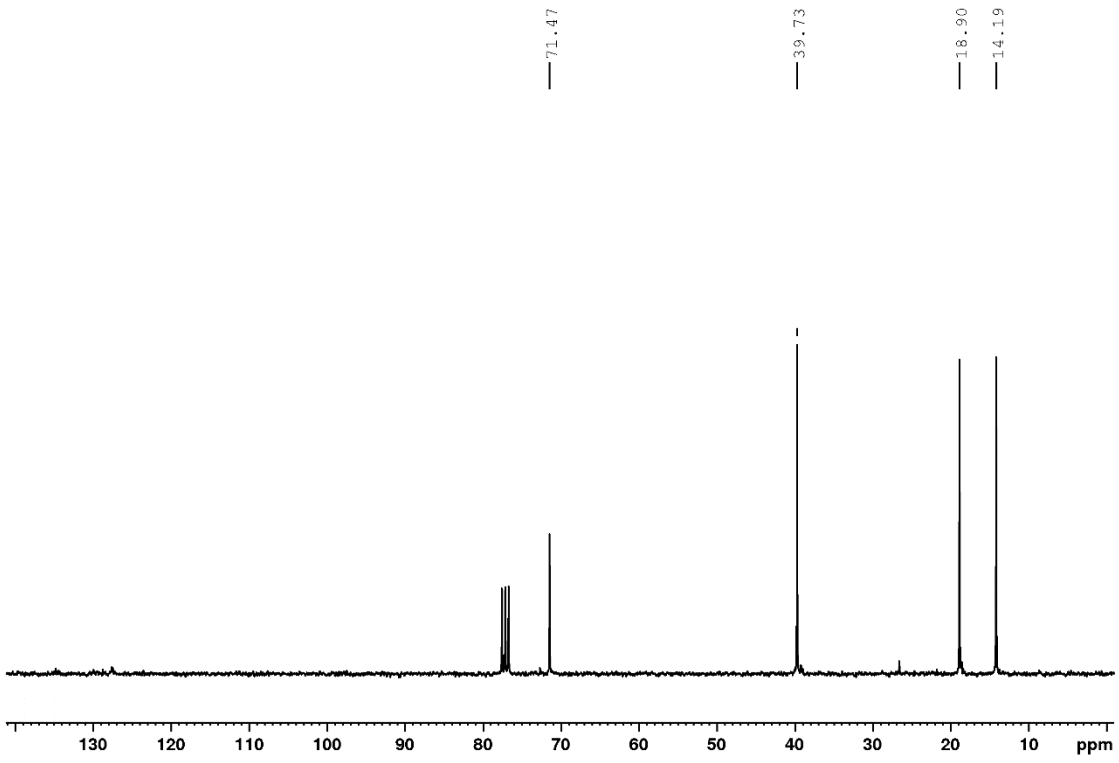

^{1}H NMR (300.1 MHz, $CDCl_3$) Benzyl Alcohol, 5-3i

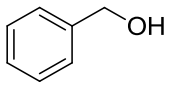

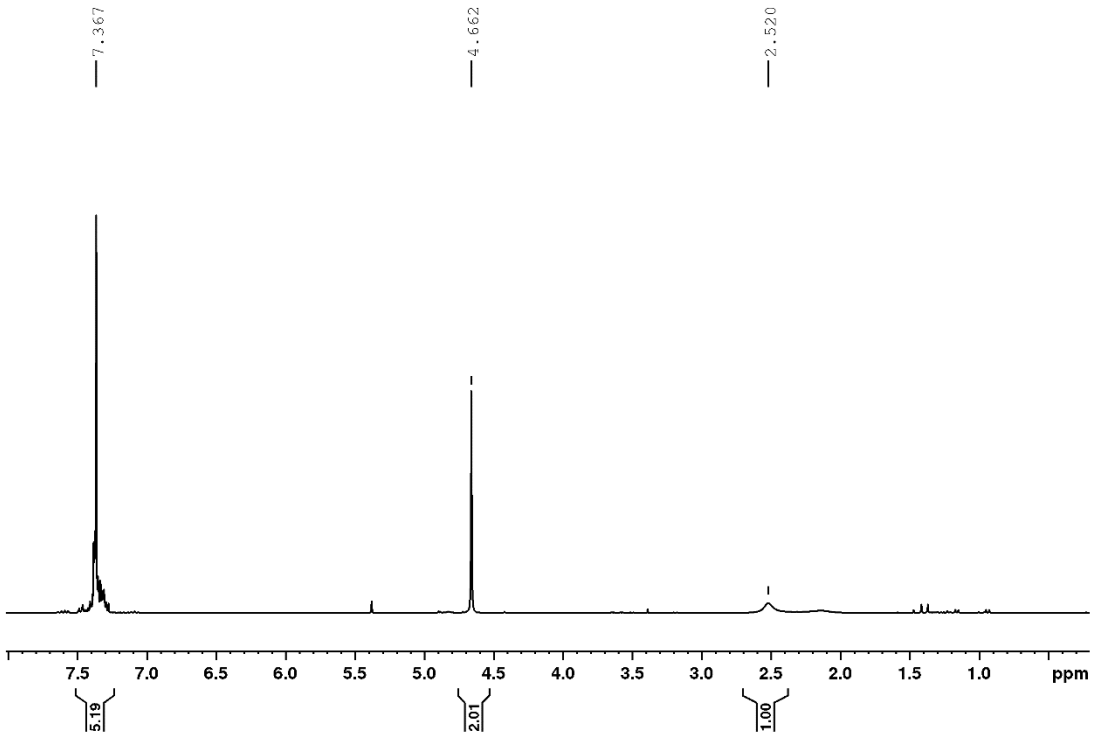

$^{13}C\{^{1}H\}$ NMR (75.5 MHz, $CDCl_3$) Benzyl Alcohol, 5-3i

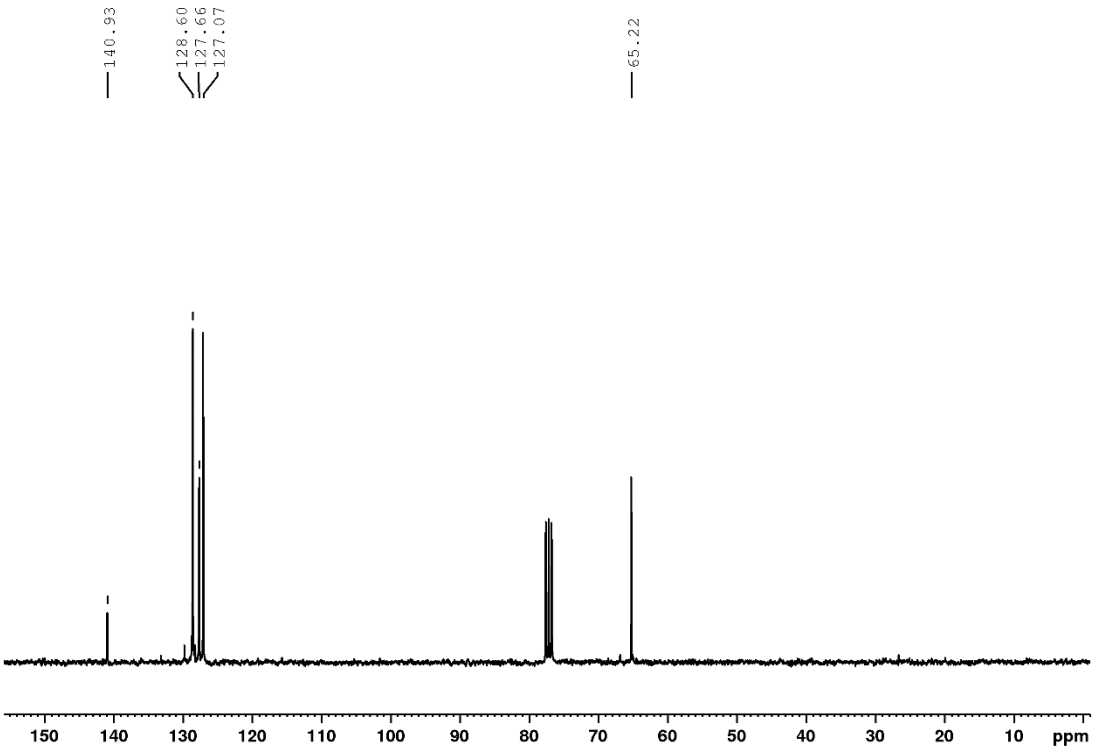

Appendix C: Copyright Agreements

NRC RESEARCH PRESS LICENSE
TERMS AND CONDITIONS

Oct 19, 2017

This Agreement between Mr. Colin Kelly ("You") and NRC Research Press ("NRC Research Press") consists of your license details and the terms and conditions provided by NRC Research Press and Copyright Clearance Center.

License Number	4183820000873
License date	Sep 07, 2017
Licensed Content Publisher	NRC Research Press
Licensed Content Publication	Canadian Journal of Chemistry
Licensed Content Title	Synthesis, structural characterization, and reactivity of Cp*Ru(N-phosphinoamidinate) complexes
Licensed Content Author	Colin M. Kelly, Adam J. Ruddy, Craig A. Wheaton, et al
Licensed Content Date	Mar 1, 2014
Licensed Content Volume	92
Licensed Content Issue	3
Type of Use	Thesis/Dissertation
Requestor type	Author (original work)
Format	Print and electronic
Portion	Full article
Order reference number	
Title of your thesis / dissertation	Synthesis and Study of New Late Metal Complexes Featuring N-Phosphinoamidinate Ligands
Expected completion date	Nov 2017
Estimated size(pages)	200

JOHN WILEY AND SONS LICENSE
TERMS AND CONDITIONS

Oct 19, 2017

This Agreement between Mr. Colin Kelly ("You") and John Wiley and Sons ("John Wiley and Sons") consists of your license details and the terms and conditions provided by John Wiley and Sons and Copyright Clearance Center.

License Number	4183810651981
License date	Sep 07, 2017
Licensed Content Publisher	John Wiley and Sons
Licensed Content Publication	Angewandte Chemie International Edition
Licensed Content Title	Synthesis and Reactivity of a Neutral, Three-Coordinate Platinum(II) Complex Featuring Terminal Amido Ligation
Licensed Content Author	Colin M. Kelly,Doo-Hyun Kwon,Michael J. Ferguson,Steven M. Bischof,Orson L. Sydora,Daniel H. Ess,Mark Stradiotto,Laura Turculet
Licensed Content Date	Oct 8, 2015
Licensed Content Pages	5
Type of use	Dissertation/Thesis
Requestor type	Author of this Wiley article
Format	Print and electronic
Portion	Full article
Will you be translating?	No
Title of your thesis / dissertation	Synthesis and Study of New Late Metal Complexes Featuring N-Phosphinoamidinate Ligands
Expected completion date	Nov 2017
Expected size (number of pages)	200

JOHN WILEY AND SONS LICENSE TERMS AND CONDITIONS

Oct 19, 2017

This Agreement between Mr. Colin Kelly ("You") and John Wiley and Sons ("John Wiley and Sons") consists of your license details and the terms and conditions provided by John Wiley and Sons and Copyright Clearance Center.

License Number	4183810938639
License date	Sep 07, 2017
Licensed Content Publisher	John Wiley and Sons
Licensed Content Publication	Angewandte Chemie
Licensed Content Title	Synthesis and Reactivity of a Neutral, Three-Coordinate Platinum(II) Complex Featuring Terminal Amido Ligation
Licensed Content Author	Colin M. Kelly,Doo-Hyun Kwon,Michael J. Ferguson,Steven M. Bischof,Orson L. Sydora,Daniel H. Ess,Mark Stradiotto,Laura Turculet
Licensed Content Date	Oct 8, 2015
Licensed Content Pages	5
Type of use	Dissertation/Thesis
Requestor type	Author of this Wiley article
Format	Print and electronic
Portion	Full article
Will you be translating?	No
Title of your thesis / dissertation	Synthesis and Study of New Late Metal Complexes Featuring N-Phosphinoamidinate Ligands
Expected completion date	Nov 2017
Expected size (number of pages)	200

JOHN WILEY AND SONS LICENSE
TERMS AND CONDITIONS

Oct 19, 2017

This Agreement between Mr. Colin Kelly ("You") and John Wiley and Sons ("John Wiley and Sons") consists of your license details and the terms and conditions provided by John Wiley and Sons and Copyright Clearance Center.

License Number	4183811127232
License date	Sep 07, 2017
Licensed Content Publisher	John Wiley and Sons
Licensed Content Publication	Angewandte Chemie International Edition
Licensed Content Title	Dehydrogenative B−H/C(sp3)−H Benzylic Borylation within the Coordination Sphere of Platinum(II)
Licensed Content Author	Colin M. Kelly,Jack T. Fuller,Casper M. Macaulay,Robert McDonald,Michael J. Ferguson,Steven M. Bischof,Orson L. Sydora,Daniel H. Ess,Mark Stradiotto,Laura Turculet
Licensed Content Date	Mar 30, 2017
Licensed Content Pages	5
Type of use	Dissertation/Thesis
Requestor type	Author of this Wiley article
Format	Print and electronic
Portion	Full article
Will you be translating?	No
Title of your thesis / dissertation	Synthesis and Study of New Late Metal Complexes Featuring N-Phosphinoamidinate Ligands
Expected completion date	Nov 2017
Expected size (number of pages)	200

JOHN WILEY AND SONS LICENSE TERMS AND CONDITIONS

Oct 19, 2017

This Agreement between Mr. Colin Kelly ("You") and John Wiley and Sons ("John Wiley and Sons") consists of your license details and the terms and conditions provided by John Wiley and Sons and Copyright Clearance Center.

License Number	4183811336747
License date	Sep 07, 2017
Licensed Content Publisher	John Wiley and Sons
Licensed Content Publication	Angewandte Chemie
Licensed Content Title	Dehydrogenative B–H/C(sp3)–H Benzylic Borylation within the Coordination Sphere of Platinum(II)
Licensed Content Author	Colin M. Kelly,Jack T. Fuller,Casper M. Macaulay,Robert McDonald,Michael J. Ferguson,Steven M. Bischof,Orson L. Sydora,Daniel H. Ess,Mark Stradiotto,Laura Turculet
Licensed Content Date	Mar 30, 2017
Licensed Content Pages	5
Type of use	Dissertation/Thesis
Requestor type	Author of this Wiley article
Format	Print and electronic
Portion	Full article
Will you be translating?	No
Title of your thesis / dissertation	Synthesis and Study of New Late Metal Complexes Featuring N-Phosphinoamidinate Ligands
Expected completion date	Nov 2017
Expected size (number of pages)	200

JOHN WILEY AND SONS LICENSE TERMS AND CONDITIONS

Dec 08, 2017

This Agreement between Mr. Colin Kelly ("You") and John Wiley and Sons ("John Wiley and Sons") consists of your license details and the terms and conditions provided by John Wiley and Sons and Copyright Clearance Center.

License Number	4244351500854
License date	Dec 08, 2017
Licensed Content Publisher	John Wiley and Sons
Licensed Content Publication	Angewandte Chemie International Edition
Licensed Content Title	A Manganese Pre-Catalyst: Mild Reduction of Amides, Ketones, Aldehydes, and Esters
Licensed Content Author	Colin M. Kelly,Robert McDonald,Orson L. Sydora,Mark Stradiotto,Laura Turculet
Licensed Content Date	Nov 15, 2017
Licensed Content Pages	4
Type of use	Dissertation/Thesis
Requestor type	Author of this Wiley article
Format	Print and electronic
Portion	Full article
Will you be translating?	No
Title of your thesis / dissertation	Synthesis and Study of New Late Metal Complexes Featuring N-Phosphinoamidinate Ligands
Expected completion date	Nov 2017
Expected size (number of pages)	200